APPENDIX A

REVIEW OF LITERATURE AND IDENTIFICATION OF ISSUES

A comprehensive search was conducted to identify the design and construction issues that have negatively affected the widespread use of DPPCG in long-span bridge construction. The search was divided into a number of main areas. Following is a summary of the areas investigated.

LONGITUDINAL JOINTS AND CONNECTIONS

Longitudinal Joint Details

The ability of the deck to transfer load from one girder to another depends on the strength, stiffness and durability of the joints between them. Various connection details have been tried and used. The use of a match cast tongue and groove joint has been suggested as a connection detail, as shown in Figure A-1. The resulting longitudinal joint requires no grouting or special treatment. The major problems observed were cracking and spalling at the panel joints and leakage of the joints, apparently caused by traffic wear. Also, it was found that it was very difficult to achieve a perfect match in the field after installing the units due to construction tolerances and elevation adjustment of the units.

Because of the problem with the non-grouted match-cast keyway, grouted female-to-female keyway together with a transverse tie are typically used. The primary purpose of shear keys is to transfer vertical wheel loads to adjacent units and to prevent moisture leakage through the deck. Inclined surfaces were provided in the shear key detail to enhance the vertical shear strength capacity of the joint. Therefore, vertical shear forces applied at the joint were resisted by bearing and by bond between the grout and the unit connected. Based on the results reported in the NCHRP Report 287 by Stanton and Mattock (A1) as well as in the final report on the FHWA research project conducted by Martin and Osborn (A2), and others (A3), it appears that the most widely used connection between adjacent precast concrete members is a combination of a continuous grouted shear key and welded connectors at intervals from 4 ft to 8 ft. Size of the plate varies as does the connection detail into the flange of the member. Typical weld plate details which have been used are shown in Figures A-2 to A-7. During construction, after differential camber has been removed by jacking against a transverse steel beam

anchored to the members with less camber, individual welded connectors are used to hold adjacent members in alignment while a keyway between the members is grouted,.

The most frequent problems with connections of DBT bridges relate to grouted shear key connections between adjacent elements. Unsatisfactory performance in shear keys is most often evident by cracking in asphalt surfacing directly over the joint and moisture leakage. This apparently indicates that the grout has cracked or lost bond with the formed sides of the precast element. In extreme cases, a complete deterioration of the keyway material can occur. When this happens, it is probably caused by an initial crack or separation. The pounding from the traffic eventually breaks up the grout material. The consequence of grout key failure is that if girders are designed assuming some load transfer to adjacent units, the girder will be overstressed under the design wheel load. According to Stanton and Mattock (A1), the indicated overstress resulting from a failed shear key is in the range of 50% for narrow slabs on short spans, and less for wider and longer members. The damage that is caused by moisture leakage through the grout keys is relatively minor. However, if water becomes entrapped within the shear key, it sometimes freezes and causes localized spalling. Moisture leakage contributes to corrosion of some bearing devices, and the resulting streaking of the concrete may be unsightly. For an overpass, the dripping water is a nuisance to passing motorists. Problems with obtaining good welded connections due to up to 1.5 in. differential camber between adjacent members have also been reported in Clallam, WA (A1).

After experiencing some cases of poor grout key performance, some states and contractors doing private work have used transverse post-tensioning. A full-depth shear key and transverse post-tensioning were associated with improvement in the bridge performance and prevention of longitudinal cracking (A4).

TxDOT uses the lateral connection detail as shown in Figure A-8 to tie double “T” flanges together. It should be noted that there is no continuous grouted shear key in the detail. In 1997, TxDOT personnel inspected 15 double tee bridges (A5). The inspections revealed no serious structural defects except longitudinal cracks characterized as slight, moderate, and large. In four cases, severity of cracking had already triggered maintenance activities on the bridge riding surface. Cracks tend to run the full length of the span. The results of inspections of Texas bridges suggest that a shear key will eliminate the problem of asphalt in the wearing surface being pushed down into the space between the edges of adjacent flanges, thus reducing (but likely not eliminating) maintenance problems associated with longitudinal reflective

cracking. Based on the review of current available connection details and the inspections of Texas bridges, researchers together with the TxDOT personnel developed a new “simple” connection detail as shown in Figure A-9 after a series of two meetings. In developing this new detail, researchers mainly consider that the ideal lateral connection would possess the following characteristics:

- Inexpensive and quick to install,
- Provide good lateral distribution of wheel loads,
- Eliminate longitudinal cracking.

A scanning tour was sponsored by the Federal Highway Administration (FHWA) and the American Association of State Highway and Transportation Officials (AASHTO) and organized by American Trade Initiatives, Inc. to obtain information about prefabricated bridge systems technologies being used in Japan and Europe (A6). Prefabricated deck systems require that longitudinal and transverse joints be provided to make the deck continuous for live load distribution and seismic resistance. In Japan, this is accomplished by using special loop bar reinforcement details in the joints. Pairs of side-by-side segments on each structure are connected together at the top flanges by a 600-mm (24-in.) wide longitudinal joint to form a continuous top surface for the roadway. Within the joint, hoop bars and J-bars projecting from the top flange of each pair of adjacent boxes overlap each other and are overlapped by a continuous loop bar as shown in Figure A-10a. The bars projecting from the top slab, shown in blue in Figure A-10a are epoxy-coated solely to prevent corrosion while the segments are in storage. Other bars pass through the loops to provide continuity. A cast-in-place concrete closure containing poly-vinyl fibers is used to join adjacent segments. A photograph of the underside of the bridge showing the closure joint between segments is shown in Figure A-10b. A waterproof membrane and asphalt wearing surface will be applied to the deck surface.

A similar detail is also used in Japan to connect precast full depth concrete decks. The transverse joint between panels consists of overlapping hoop bars that project from each edge of the panel. Individual bars are threaded within the loop bars to complete the connections, which are then encased in concrete. A schematic drawing of the deck joint reinforcement is shown in Figure A-11. The decks are not post-tensioned longitudinally. All bridge decks in Japan receive a waterproof membrane and asphalt riding surface. A variation of this detail is

used in France to connect full width, full depth precast concrete deck panels as shown in Figure A-12.

The Poutre Dalle System in France consists of shallow, precast, prestressed concrete inverted tee-beams as shown in Figure A-13. The beams are placed next to each other, connected with a longitudinal joint, and covered with CIP concrete. Continuity along the longitudinal joint is established through the use of 180 degree hooks that protrude from the sides of the webs. The hooks overlap those from the adjacent beam as shown in Figure A-14. The hooked bars are precisely positioned to avoid conflicts at the jobsite. Additional rectangular stirrups may be placed in the space between the webs of adjacent beams. Longitudinal reinforcement is placed inside the stirrups and hooked bars. The scanning team believes that the loop joint detail that is used to join adjacent members in the Poutre Dalle system is expected to provide better continuity than details currently used in the United States. As a result, reflective cracking along the joint will be less and durability will be enhanced.

Grout Material

Grout key materials include: sand-cement grouts; non-shrink grouts; and epoxy grouts. Most grouts used in shear keys connecting bridge elements are a mixture of portland cement, sand, and water. Proportions are usually one part cement to 2.5 to 3 parts sand, with enough water to make the grout easily flowable and completely fill the keyway. When such grouts are used, the water-cement ratio is usually about 0.50. This is a relatively high value, resulting in low strength and high shrinkage. These mortars also exhibit a tendency for the solids to settle, leaving a layer of water on the top. Special ingredients or treatments can improve these characteristics, but add to the cost. There are several proprietary products designed to expand sufficiently during initial hardening and curing to offset subsequent shrinkage of the grout. These mortars are prepared mixtures of cement, fine aggregate and an expansive ingredient. This ingredient may provide expansion by liberating gas, oxidation of metals, formation of gypsum or using expansive cement. It should be kept in mind that the shear key constitutes a very low percentage of the total width of the bridge deck. Thus, while the unit shrinkage of sand-cement grout is much greater than that of the precast units, the total shrinkage of the deck members may actually contribute more to the separation at the joints than the shrinkage of the grout itself. Several railroads (box beam bridges) place a well graded aggregate in the keyway, then pour in a low viscosity epoxy resin. The railroads require that the keyways be sand-blasted

in the casting yard prior to shipment (A2). The pre-placed aggregate method allows the work to be accomplished more quickly than the mixed mortar method.

Cost and Performance

It has been found (A2) that of those shear key construction methods which have been used, the following order of performance (from best to worst) could be expected:

1) Epoxy grout keys with post-tensioned ties (joints properly prepared);

2) Epoxy grout keys with non-prestressed ties (joints properly prepared); non-shrink grout with weld plates; and non-shrink grout with post-tensioned ties;

3) Sand-cement grout with weld plates; and sand-cement grout with post-tensioned ties; and

4) Non-shrink grout with non-prestressed ties; and sand-cement grout with non-prestressed ties.

There is a wide variation in the cost of the grout key materials in a typical shear key. The costs of various types of transverse tie systems will vary somewhat with the experience of the contractor. Based on the study performed by Martin and Osborn in 1980s (A2), the cost comparison among the different connection methods is summarized in Table A-1.

Testing

Little research has been reported on the strength and behavior of connections between the adjoining units. Reports of four tests that were found to be applicable to this are summarized in the succeeding paragraphs.

Tests of Martin and Osborn

Martin and Osborn (A2) made two slab-tests on two types of edge connections between precast, prestressed slab bridge members. In both cases the test specimen consisted of three 8-in. x 36-in. x 18-ft long precast, prestressed solid slabs (f'_c = 6500 psi) placed edge-to-edge, and supported at 16-ft centers on bearing pads resting on steel beams. The two outer slabs were loaded cyclically at midspan, at their centerlines, by equal concentrated loads of 16 kips,

which were intended to simulate HS20 “wheel loads”. In both connections studied, a grout key was provided between the edges of adjoining slabs, as shown in Figure A-15.

In test 1 a high quality, nonshrink grout (f'_c = 6000 psi) was used. The slabs were tied together by tie rods at the third points of the span. The tie rods were in the form of coil rods passing through conduit and anchored at their ends of locknuts. These tie rods were tensioned to 12 kip just before testing. In test 2 a relatively low strength, high shrinkage, sand/cement grout (f'_c = 3500 psi) was used. The slabs were tied together with three welded connectors of the type shown in Figure A-16. In both tests the three slabs were pulled apart by hydraulic rams acting on pull rods, which were anchored in the outer slabs over the slab supports. This was to simulate the forces that might be developed at the supports of a precast concrete bridge due to restraint of lateral shrinkage of the bridge deck. The pull-apart force was maintained by springs during the tests. Figure A-17 shows the test set-up for both tests.

Martin and Osborn only ran two pilot fatigue tests that would try out some methods of simulating the variables, and illustrate the characteristic performance of two types of transverse ties and two different grout key materials. Variables included the magnitude of transverse force caused by shrinkage and temperature change.

It was observed by Martin and Osborn that the low strength grout in the joint had not undergone any significant deterioration as a result of the cyclic loading. The ratio of the measured strains and deflections in the middle and outer slabs at midspan were approximately the same as in high strength grout test. The test did not assess the effects of freeze-thaw cycles and other environmental conditions that can cause severe deterioration of low-strength sand-cement grouts.

Martin and Osborn also observed that the total pull-apart force was not distributed equally between the three welded connectors, as assumed in design of the specimen. The increasing joint separation was causing a greater bending component to be imposed on all the connections. Tests showed the greatly increased strain range that was registered in the midspan connections at higher cycle numbers. It was this combination of tension and bending that failed the connection.

It was pointed out by Martin and Osborn that the constant lateral force induced in these tests did not properly represent field conditions. It is evident that some study of existing bridges is necessary to determine what effects temperature change has on the lateral movements of

bridges. They also stated the complexity of grouted joint behavior. Further research studies should consider: 1) location of the wheel loads on the slab; 2) different joint dimensions and configurations; 3) skewed bridges; 4) the effect of diaphragms; and others.

Tests of Stanton and Mattock

Stanton and Mattock performed pilot tests (a total of six slab-tests) to explore the following variables found in connection details reported in response to their survey: 1) location of connector hardware in the thickness of the slab, i.e., near the top face, near the middle of the slab thickness, or near the bottom face; 2) the weight of the connector hardware; and 3) the size and shape of the grout key; and 4) connectors acting alone and with a grout key.

Each specimen of the six specimens consisted of two 6-in. thick reinforced concrete slabs, joined together at their abutting 60-in. long edges. Three specimens used a type “A” keyway representative of a widely used type of grout key (as shown in Figure A-18). Based on results from type “A” keyway specimens, the shape of type “B” grout key was developed also shown in Figure A-18. Three new specimens with the type “B” keyway were made. Two types of connectors were also used in the tests: 1) a lightweight connector as shown in Figure A-2, and 2) a heavier and stiffer connector located at the bottom of the slab, and is anchored by headed studs rather than rebar as shown in Figure A-6.

In the testing program, concrete design strength was 5000 psi. The grout used was SET nonshrink grout manufactured by Master Builders, Inc. of Cleveland, Ohio. The grout was mixed in the ratio of 7.5 lb of water to 50 lb of the grout mixture. This formed a plastic mixture which was rodded into place in the keyway. Its strength at the time of the test, 2 days after placing, was about 3500 psi (measured on 2-in. diameter x 4 in. long cylinders).

As shown in Figure A-19, the test was setup so that there would be zero moment at the connection. In the tests, the actual shear in the connection was obtained from the readings of load cells A and B. For three of the six specimens, the keyway was not grouted. The other three were grouted. The static loading was applied to all six specimens.

Stanton and Mattock stated that the negligible displacement between opposite sides of the connections and the small connector anchor forces at service load were an indication of why grouted connections of this type had given good service for many years in the great majority of cases. If a wearing surface was placed on the deck, small displacements across the connection

would not cause distress in the wearing surface. Also, the likelihood of fatigue failure of the connector anchors, because of repeated application of service load, was remote due to the small stresses produced in the anchors by service loads.

Test results showed that the primary loads to be carried are shear forces perpendicular to the deck. Loads imposed before grouting by leveling of any differential cambers must be carried by the connectors alone. Those caused by wheel loads are transferred almost entirely through the grout joint, because it is much stiffer than the steel connectors. The shear force per unit length of grout key is localized in the vicinity of the wheel which causes it. It was recommended by Stanton and Mattock that further research be conducted on verification of the local forces in the grouted joint between members caused by wheel loads, both when the load acts next to a connector and when it acts midway between two connectors.

The grouted keyway was found to fail by cracking of the tips of the member flanges where they project above and below the grout key rather than in the grout itself, even when the concrete was 75 percent stronger than the grout. The modified type “B” keyway geometry provided greater cracking strength. Use of this shape of grout key, which has its maximum width at mid-depth of the flange, is strongly recommended (see Figure A-20).

Other Earlier Tests

Ong (A7) reported tests of specimens intended to simulate welded connectors of the type shown in Figure A-21, between adjacent bulb-tee bridge beams. The test specimens consisted of pairs of reinforced concrete beams, 6 x 6 x 36 in. long, placed side-by-side on simple supports which were 30-in. apart. The beams were connected together at mid-span by a welded connector, as shown in Figure A-21.

Two cases were studied. In one case the beams were supported at the same level and the 7/8 – x 7/8 – x 3-in. bar was welded in place transverse to the span. In second case, one of the beams was supported ¼ -in. higher than the other. The same size bar was welded in place parallel to the adjoining beam faces. One of the pair of beams was loaded concentrically at midspan. The connection details used by Ong are not thought to be very representative of actual connections used between adjacent deck bulb tee members. The connector hardware is usually recessed in the slab so that the amount of concrete below the angles does not allow the use of such long vertical studs as are shown. Also, the support provided the connection by the concrete below it will be less in practice than in these tests.

The Cretex Company of Minnesota reported the test of the confined grout key shown in Figure A-22. The length of the test specimen was 36 in. The strength of the grout at test was about 4000 psi. The central block was loaded concentrically. It was reported that "the first visible crack occurred at a load of 42 kips, or 7 kips/ft [length of grout key]." However, it is clear that this testing arrangement would tend to induce compression across the grout key and therefore would be expected to enhance shear strength.

Texas

Before undertaking a full-scale bridge test program incorporating the "simple" connection detail shown in Figure A-9, a series of six load tests was performed on the connection using a beam specimen (A8). Each beam was intended to simulate the connection and an accompanying 12 in. width of tee flange. The mode of failure in all six tests was the same – pullout of the headed studs anchoring the weld plate to the concrete (Figure A-23) with general spalling of the concrete cover on the underside of the beam. The failure of the connection was clearly premature in the sense that with better anchorage, it would have sustained greater loads. Consequently, #4 rebar at least 18 in. long is recommended for anchoring the plates rather than headed studs. The 10 degree slope on the plates offers a recess which receives the 1 in. diameter steel bar. It is believed this arrangement will accommodate variation in the 0.25 in. nominal spacing between adjacent tees resulting from sweep in the members.

These connections were originally spaced longitudinally along the flange edges at 10 ft. centers, and more recently the spacing has been reduced to 5 ft. on center. While the connections seem to have performed as intended, with no particular problems reported in the connections themselves, there remain several issues this research attempts to address, which are summarized below.

The new "simple" connection was incorporated in a 27 ft. span two tee bridge model and tested in the laboratory with the objective of validating the performance of the new connection in a full-scale structure and quantifying the stiffnesses of the connection. Two TxDOT standard 8 ft. wide by 22 in. deep double tees with 6 in. flange thickness were used in the test. As seen in Figure A-24, the two tees were connected at 5 ft. intervals with the lateral connection in Figure A-9, except that the "saw tooth" indentation in the concrete above the embedded plate had to be omitted because of time constraints with the fabricator. The face of each tee flange

was cleaned with a rotary steel brush and then washed with water prior to placing the MasterFlow 928 grout to form the shear key. The average compressive strength of the grout in the shear key was 8,120 psi, based on tests of three standard cubes performed 11 days after casting. Average strength after 92 days was 8,230 psi. The primary instrumentation used in these tests was load cells to measure the reaction forces in the bridge. In addition, 12 displacement transducers were positioned to measure vertical displacements in the structure. After the grouted shear key was installed and cured, electrical resistance strain gages were installed on the upper face of the key at the locations to measure transverse strain induced in the top surface of the key by loads on the bridge.

A series of tests was performed on the individual double tees before they were connected together in order to check the reasonableness of the measured responses. Next a single force of approximately 20 kips was applied at the load positions (8 positions) shown on each of the two double tees in Figure A-25, and the reaction forces recorded. In each load position, the actuator force was slowly increased to the peak value of (approximately) 20 kips, held at that level for several minutes, then offloaded back to zero, reloaded and then brought back to zero again. Very good repeatability of measured reactions between successive loadings was found in every case. The reactions from the first application of load in each load position are recorded to be used for the calibration of the connection stiffness.

After a series of static tests, researchers performed additional load tests to study the response of the connection under cyclic loading, and finally much larger loads were applied in an attempt to cause failure in the connections, given the constraint that the loading system capacity was approximately 100 kips. The ram load was increased to 94.7 kips when the capacity of the hydraulics was reached and the bridge had to be unloaded. Inspection of the tee flange, grout shear key, and the (closest) bar/plate connections showed no signs of distress or any evidence to indicate the loading had reached nearly 100 kips.

Connection Forces and Design Guidelines

Vertical shear forces arise from rectifying differential cambers between beams during construction, from differential temperature effects, and from truckloads. In addition, tension or compression occurs when multi-stemmed members try to twist about their shear centers, which are above the flange. Also, shrinkage and temperature changes will cause forces which tend to separate the precast members. Other parameters to be considered in determining the connection forces are the effect of diaphragms; effect of skews; local lateral forces caused by

vehicles changing lanes, and the “spreading” effects of vertical cyclic loading. In order to develop connection design guidelines, various models have been proposed in the literature.

Martin and Osborn Model (A2)

According to this model, all vertical loads are transferred by the shear key. The transverse ties are only required to provide enough horizontal restraint to keep the grout key closed. Shrinkage and negative temperature change cause the members to decrease in width and pull apart at the joints. In the absence of a positive tie force to pull the members together this would result in a crack at the grout key, or a separation of the grout from the precast member, depending on the bond strength of the grout. To prevent the complete separation of the precast members, there must be a tie force to pull the members together as this decrease in width occurs. This force is resisted at the supports of the members. If the bearing is sufficiently flexible, e.g., with properly designed and performing elastomeric pads, the force will not be great. However, for a variety reasons, these pads may not perform as intended and the forces can build up to the point that the only relief is through slip. Thus, the upper limit of the force would be the friction between the deck member and its support. Coefficients of friction vary considerably, so the magnitude of this force is not precisely determinable. Several studies have indicated that an average value of the coefficient of friction can be assumed at about 1.0. Using this value, the total design tie force should be equal to approximately half the weight of the bridge.

This model should be recognized as idealized. Other factors will contribute to the behavior, such as stiffness of the deck system, transverse connection details at piers and abutments, and the bearing conditions. Certainly, the magnitude of temperature changes and the shrinkage characteristics of the concrete will enter the picture. However, using the “friction model”, weld plate connections resist the forces described by their strength in tension. Through lab tests, a typical connection detail’s capacity can be found out. Then, the number of connectors can be calculated with the “friction” force developed at the joints nearest the center of the bridge. Progressively fewer would be required nearer the outside edges, since less of the bridge needs to be “pulled back”. Using this model, the minimum shear key depth to provide adequate lateral tensile resistance can also be determined.

Design Recommendations from Stanton and Mattock

Stanton and Mattock (A1) performed pilot tests to explore the effects of grout key and connector configuration. The laboratory experiments performed for this study showed that a well-executed grout joint is much stiffer in shear than an embedded steel connector and, prior to cracking, carries virtually all the applied shear. After cracking was initiated, shear appeared to be carried by shear friction between the surfaces of the slab edge and the grout key, with the connector providing the clamping force across the joint. A reasonable approach would be to design the grout key to carry all vertical shears applied after grouting (i.e., truck loading and differential temperature effects). The connectors should then be designed to carry the locked-in shear from leveling during construction, the tension due to restraint of twisting and the tension needed to mobilize the shear resistance of the connection after cracking. The spacing and strength of steel flange connectors should be based on shear forces induced before grouting and tension and moments induced afterwards. Twisting of the girders under live loads is shown to induce tension in the connectors along the joint between the two outer members of a bridge. However, this tension arises largely from compatibility and not equilibrium requirements, and its value is significantly reduced by small deformations of the connectors. It should be noted that the testing program performed by Stanton and Mattock (A1) was limited in scope, and was not intended to produce definitive answers to the many questions raised regarding grout keys and lateral restraint systems.

Stanton and Mattock made the following recommendations for the design of connections (A1):

1. The edge thickness of the precast member flanges should be $6\sqrt{5000 / f_c'}$ in. but not less than 6 in.;
2. The shape of the grout key should be as shown in Figure A-20;
3. The spacing of the welded connectors should not be more than the lesser of 5 ft and the width of the flange of the precast member;
4. Welded connectors should be located within the middle third of the slab thickness;
5. The tensile strength of each connector and of its anchors should be not less than

$$T_n = T_1 + T_2 \quad \text{kip}$$

Where:

$$T_1 = 16(\sin\alpha - \mu_1 \cos\alpha)/(\cos\alpha + \mu_1 \sin\alpha) \text{ kip, but not less than 6 kip}$$

And

$$T_2 = 0.5 s W_m N_m \mu_2 \quad \text{kip}$$

6. If the connector is to be used to resist shears due to the elimination of differential camber before grouting the keyway, both the shear strength of the metal connector and the resistance to shear of the anchors calculated using

$$V_n = N_a(2.5 d_e - 3.5) \quad \text{kip}$$

must not be less than twice the calculated shear per connector due to the leveling operation.

In the above,

f_c' = Compressive strength of concrete;

T_1 = anchor force required to develop a shear resistance of 16 kip, in a length *s* of grouted connection [Note: The shear force of 16 kip is the maximum shear that can be resisted by a 60-in. length precast member flange of thickness $6\sqrt{5000/f_c'}$, using the shape of grout key shown in Figure A-20];

T_2 = maximum probable tension force per connector due to restraint of lateral shrinkage in bridge deck;

α = maximum inclination of sloping faces of grout key (see Figure A-20);

μ_1 = coefficient of friction between grout key and concrete (to be taken as 0.5);

μ_2 = coefficient of friction between precast beams and their bearings (0.80 for concrete on concrete, 0.50 for concrete on elastomeric bearing pad);

s = longitudinal spacing of welded connector, in ft;

W_m = weight per foot length of each precast member and any topping its supports, in kip/ft;

N_m = number of members in width of bridge;

N_a = number of anchor bars or studs attached to connector in each flange; and

d_e = distance from centerline of anchor to nearest face of precast member flange in which it is embedded.

Plate Theory

Bakht et al. (A9) used articulated-plate theory to generate charts of live-load shear force per unit length of joint for the OHBDC, but it should be noted that forces and deformations other than those predicted may also exist. Furthermore, even the vertical shear due to wheel loads is likely to be different in practice from the value predicted by orthotropic (or articulated) plate theory, because it will in fact be influenced by the local geometry and stiffnesses, whereas orthotropic-plate theory uses average properties more suitable for predicting global response. Jones and Boaz (A10) used an analysis based on the force method and singularity functions and included individual connector stiffnesses. They showed that total shear force transferred between any two beams was almost independent of the number of connectors, so that the connectors attract shear force in roughly inverse proportion to their number.

Texas DOT Analysis

The analytical model used by TxDOT treats each double tee beam as a single structural element using elementary beam theory and the flange connections (either discrete connections, or a shear key, or both) are modeled with linear springs (A8). The moments of inertia and area compiled by TxDOT for various standard tees with 6 in. thick flanges were used. The torsional stiffness for the double tee cross section was obtained using a FEM model of the double tee built with 3D solid “brick” elements. Each double tee has four points of support where it rests on

bent caps. The bridge model uses linear springs to simulate the effect of the bearing pad which rests between the underside of the tee stems and the bent cap. The spring stiffnesses represent stiffness of the entire pad and can be computed from known properties and dimensions. Each point of connection between flanges of adjacent tees is modeled with a series of four linear springs which give rise to the set of four forces. In addition to the discrete connections installed on TxDOT bridges, a continuous shear key can be modeled through the addition of closely spaced spring sets along the entire length of the span and defining the stiffnesses appropriately. There is no obvious rational procedure for estimating the four connection stiffnesses nor is there any simple correlation between strains which could be measured in or around the connection and those stiffnesses. Consequently, an indirect approach was developed in which reaction forces in the bridge were measured under various loading conditions and the connection stiffnesses in the analytical model adjusted until reasonable agreement between predicted and measured reactions was obtained.

Analyses with the multi-beam bridge model revealed the interesting fact that the stiffness of the shear key had negligible effect on the reaction forces, even when this parameter was varied over more than four orders of magnitude. The most plausible explanation for this behavior appears to be that the plate/bar components, when spaced at 5 ft. increments, provide sufficient vertical shear transfer between adjacent beams to render the additional transfer provided by the shear key ineffective. This is likely not a general condition but rather one peculiar to the short span (27 ft.) of the laboratory bridge tested.

The lateral connection between the flanges of adjacent tees consists of a welded bar and embedded plate segment, and continuous, grouted shear key. The bar/plate discrete connection, which is spaced at 5 ft. intervals, will develop the four force components (Figure A-26). The continuous shear key portion of the lateral connection lying between the bar/plate locations is also modeled with the springs by lumping the stiffnesses of a 1 ft. length of key into the spring stiffnesses at points spaced at 12 in. intervals along the flange edge. The four force components are displayed in Figure A-27. Forces in the bar/plate connection as well as in the shear key are dependent upon the placement of load, and an important question was what truck(s) positions lead to the largest possible connection forces. Numerical experimentation with various bridges leads to the following observations:

- a 16 kip wheel must be adjacent to the bar/plate (discrete) connection or shear key location where maximum forces are sought,

- discrete connections closest to mid-span of the bridge and shear key zones at midspan develop the largest forces,
- the wider the two beams connected, the greater the connection and shear key forces developed,
- placing two or more trucks on a structure produce connection forces negligibly larger than those resulting from a single well-placed truck, and
- force components F_x and F_y are small in a double tee bridge.

Chaudhury and Ma

The strength of the grouted and ungrouted welded connectors was proposed for the selected shape of the grout key and the selected connector detail by Stanton and Mattock. However, forces in connectors between members caused by wheel loads were not included in their study. These forces are needed for design of shear connectors. Using the calibrated 3D FE models, parametric studies are performed to study the effect of shear connectors and intermediate diaphragms by Chaudhury and Ma (A11). Hinges were used to model weld plate shear connectors. By using the calibrated 3D FE model, connector forces in the three directions can be calculated: two forces in the plane of the bridge deck and one force perpendicular to the deck surface. Two in-plane forces are named as “Horizontal Shear Force” (parallel to the longitudinal joint) and “In-Plane Normal Force” respectively. The force perpendicular to the deck surface is named as “Vertical Shear Force”.

It has been found that connector forces caused by wheel loads are not uniform along the longitudinal joint. The maximum horizontal shear force increases with the increase of the connector spacing. The maximum vertical shear force and in-plane normal tensile-force in connectors do not necessarily increase with the increase of the connector spacing. The summation of connector forces in each direction along the longitudinal joint remains constant irrespective of the number of connectors in the joint.

The PCI Design Handbook Method

PCI Design Handbook (A12) has examples of connections between the flanges of adjacent double-tee members in buildings. Connectors are provided to equalize cambers and deflections between neighboring members, and to resist shears in the plane of the flange if the

double tee deck is to act as a diaphragm resisting lateral forces. No design procedures for shear transverse to the flange could be found. PCI recommends that to resist shears resulting from camber and deflection equalization, the welded connectors be spaced not more than 8 ft apart. A design procedure is provided in PCI for shear in the plane of the flange. PCI Design Handbook also provides design procedures for related problems of anchorages subject to shear, to tension, and to shear and tension in concrete.

Another quantitative recommendation in PCI short-span bridge publication is that the weld plate in the welded connectors should be ¾ in. thick (A13).

AASHTO

The AASHTO LRFD Specifications (A14) presently provides limited guidelines for the design of joints and connections between decked precast prestressed concrete girders. For shear transfer joints, it is recommended that precast longitudinal components may be joined together by a shear key not less than 7.0 in. in depth. The joint shall be filled with nonshrinking grout with a minimum compressive strength of 5.0 ksi at 24 hours (Article 5.14.4.3.2 in LRFD Specifications). It is suggested in Article C5.14.4.3.2 of the LRFD Specifications that long-term performance of the key joint should be investigated for cracking and separation.

According to Articles 5.14.4.3.2 and 5.14.4.3.3 in AASHTO LRFD Specifications (A14), decked bulb tees (DBT) units can be connected together by either “shear transfer (ST) joints” or “shear-flexure transfer (SFT) joints.” The Specifications do not define what a ST-joint is except that it requires the shear key at the longitudinal joint shall be not less than 7.0 inches in depth. For the SFT-joint definition, however, the Specifications indicate that girders “may be joined by transverse post tensioning, cast-in-place closure joints, a structural overlay, or a combination thereof.” Hence, to be “sufficiently connected”, joints must be constructed in this fashion. If post-tensioning is used, the compressed depth shall not be less than 7.0 inches and the effective prestress in the concrete shall not be less than 0.25 ksi. These guidelines are very general in nature. Also, the current flange thickness of DBTs is about 6.0 inches, which is less than 7.0 inches required. In practice, DBT units are connected by ST joints. And grout key sizes and shapes and connector requirements are determined by using rule-of-thumb methods and historical performance, rather than by rational analysis.

SECTION GEOMETRY AND PROPERTIES

One obstacle that will hamper the use of DPPCG bridges nationwide will be the acquisition costs of new forms by precast fabricators. The cost of a new set of forms can run several hundred thousand dollars. Unless a certain minimum volume of work is guaranteed, precasters may be unwilling to make the large capital investment necessary to make the system feasible in their region. Hence, consulting engineers and highway departments will be unwilling or unable to design such systems since their availability will be in question.

Bulb tee girders are perhaps the most common type of girder in current use. Their high degree of structural efficiency as compared to the AASHTO Type I through Type IV series, is the governing factor. Most fabricators have a set of forms to fabricate bulb tees. Significant variations exist in dimensions of the various bulb tee families from region to region. But from an overall standpoint, their structural properties are similar.

Several series of deck bulb tee systems are in use at the present time. The *PCI Bridge Design Manual* details a family of three deck bulb tees. The top and bottom flanges are identical for each girder in the series. The stem height is the variable portion of the section. Total heights for each of the three girders are 35, 53, and 65 inches. The precast concrete fabricators located in the northwest region of the country each have families of deck bulb tee girders that have been in use for many years. Dimensions are similar to the PCI series. The bulb dimensions are nearly identical. Overall top flange dimensions are similar, but with some variation in shear key shape and dimensions. Stem widths are both 6 inches. Stem heights are variable to accommodate overall depth changes.

A strategy that can be employed to help facilitate the use of deck bulb tee girder bridges nationwide is to modify the forming systems that precasters currently have to be able to cast deck bulb tees. The PCI bulb tee series can serve as the basic shape to be used to study the potential for modifications and draw conclusions on their application. The PCI bulb tee series consists of three girder heights. Top and bottom flanges are all identical for each girder. Stem height varies to provide total heights of 54, 63, and 72 inches. A bulb girder based on the PCI series would consist of the same bottom bulb dimensions as the PCI bulb tee series. Stem width would be fixed at six inches and the height would be variable to accommodate a range of total depths. The top flange would be modified to a shape that is similar to the deck bulb tees currently in use as shown in Figures A-28 and A-29.

LIVE LOAD DISTRIBUTION

Distribution of superimposed loads among girders of multi-girder bridges is an essential factor for economic design of bridge structures. In bridges with cast-in-place deck slabs, the slab is capable of transferring the load between adjacent girders and contributes to lateral load distribution. Several investigations have been directed to live load distribution for such bridge structures (A15, A16, A17, A18), but only limited work has been carried out for DPPCG bridges.

Newmark

Based on Newmark's research (A19), the lateral wheel load distribution factors were determined by the expression:

$$g = \frac{S}{D} \tag{A1}$$

Where g = the wheel load distribution factor (DF); S = the center-to-center girder spacing (ft); and D = different constants for different bridge systems (ft).

AASHTO Standard Specifications

Simple "S-over" live-load distribution factors have been used for bridge design since the American Association of State Highway Officials (AASHO) published its first edition of Standard Specifications for Highway Bridges in 1931. These factors allow the designer to uncouple transverse behavior from longitudinal behavior. However, live-load distribution provisions for multibeam precast concrete bridges (such as the decked bulb tee bridges) were not included in the specifications until 1965, when AASHTO published its ninth edition of Standard Specifications. In its ninth edition, the distribution criteria for multibeam bridges were only limited to a brief reference in the slab design section. Specifically, the distribution width per wheel is equal to 4.0+0.06L (L = Span) (ft) with a maximum of 7.0 ft.

In 1977, the distribution criteria for multibeam bridges were incorporated into "Distribution of Loads" section with other bridge systems. The DF formula for multibeam bridges took the same format (of Eq. (1)) as other bridge systems, with the following different definitions:

$$\text{S = effective girder spacing} = \frac{12N_L + 9}{N_g} \tag{A2}$$

$$D = 5 + \frac{N_L}{10} + (3 - \frac{2N_L}{7})(1 - \frac{C}{3})^2 \qquad C \le 3$$
$$= 5 + \frac{N_L}{10} \qquad C > 3 \tag{A3}$$

Where N_L = total number of design traffic lanes; N_g = number of longitudinal beams; and C = a stiffness parameter that depends on the type of bridge, bridge and beam geometry, and material properties, calculated based on the following:

$$C = K\frac{W}{L} \tag{A4}$$

$$K = \sqrt{\frac{E}{2G}\left(\frac{I_1}{J_1 + J_t}\right)} \tag{A5}$$

Where W = the overall width of the bridge (ft); L = span length (ft); EI_1 = flexural stiffness of the transformed beam section per unit width; GJ_1 = torsional stiffness of the transformed beam section per unit width; and GJ_t = torsional stiffness of a unit width of bridge deck slab.

These DF formulas for multibeam bridges were proposed by Sanders and Elleby in NCHRP Report 83 (A16). The multibeam criteria were, as most criteria, based on no reduction in load intensity (i.e., without considering the multiple presence factor). The only stemmed members addressed in NCHRP Report 83 were channels.

For the case of deck bulb tees under the Standard Specifications, all girders—both interior and exterior—are treated the same with regard to live load distribution. These formulae are understood to be conservative. Currently, the only recourse to improving the accuracy of a design is to perform a detailed numerical analysis of the bridge, which, although it can provide more accurate estimates of live load affects, has the significant drawback of being time-consuming and error prone. A more accurate formula-based approach would therefore be highly desirable.

NCHRP 12-24

Considering sections such as double tees, bulb tees, single tees, as well as decked bulb tees have come into common use for bridges; the University of Washington performed the NCHRP 12-24 study on load distribution for precast stemmed multibeam bridges (A1). The

specific objectives of that research were to investigate the distribution of truck wheel loads in the decks of bridges made from single-stem and multi-stemmed precast concrete tee-shaped members, and to make recommendations for their design in a form suitable for inclusion in the AASHTO Standard Specifications. The following DF formulas were proposed in the final NCHRP Report 287 (A1):

S = width of precast member (A6)

$$\begin{aligned} D &= (5.75 - 0.5N_L) + 0.7N_L(1 - 0.2C)^2 \qquad C \le 5 \\ &= (5.75 - 0.5N_L) \qquad C > 5 \end{aligned} \tag{A7}$$

$$C = K\frac{W}{L} \tag{A8}$$

$$K = \sqrt{\frac{EI}{2GJ}} \tag{A9}$$

Where EI = flexural stiffness of each girder; GJ = torsional stiffness of each girder; and others are the same as before.

Comparing Eqs (A6)-(A9) with Eqs (A2)-(A5), the following changes are noted: (1) The former use the effective girder spacing while the later use the actual girder spacing. (2) There is a difference in calculating the stiffness parameter K. (3) The wheel load fractions from both sets of formulas give nearly identical results for small C values (i.e., long narrow bridges made from torsionally stiff members). D increases when C decreases. This is because torsionally stiff members deflect under load but twist little, thereby causing adjacent members to deflect as well, spreading the load into them. However, for large C values (i.e., short wide bridges made from stemmed members), the 1977 AASHTO relationships (Eqs (A2)-(A5)) predict significantly larger D values. Finally, (4) Eqs (A6)-(A9) consider bridges with skew angles up to 45 degrees while Eqs (A2)-(A5) do not take skew into account. For skewed bridges, bridge width W is measured perpendicular to the longitudinal girders and bridge span L is measured parallel to longitudinal girders in Eqs (A6) – (A9).

The current edition of Standard Specifications (A20) has the same DF formulas as Eqs (A6) – (A9). The current specifications state that if the value of $\sqrt{\frac{I}{J}}$ exceeds 5.0, the live load

distribution should be determined using a more precise method, such as the Articulated Plate Theory or Grillage Analysis.

It also states that for non-voided rectangular beams, channels, and tee beams, Saint-Venant torsion constant "J" may be estimated using the following equation:

$$J = \sum \{\frac{bt^3}{3}(1 - 0.630\frac{t}{b})\} \quad \text{(A10)}$$

Where b = the length of each rectangular component within the section; t = the thickness of each rectangular component within the section. The flanges and stems of stemmed or channel sections are considered as separate rectangular components whose values are summed together to calculate "J". The current Standard Specifications also require full-depth rigid end diaphragms to ensure proper load distribution for channel, single- and multi-stemmed tee beams.

AASHTO LRFD

There are two basic approaches taken by the LRFD Specifications to determining live load distribution to girders: refined methods and the approximate method. The refined methods collectively involve modeling the bridge analytically using a grillage, a finite element, or some other refined method of analysis. When such a model is created and calibrated, quite accurate live load analysis results can be obtained. However, this approach is time-consuming and stymies the quality control process and is therefore generally avoided in standard bridge design practice in the United States.

The approximate method of live load distribution is the method favored for the design of deck bulb tee girders. Provisions of its implementation and the limitations on its use are included in Article 4.6.2.2. Deck bulb tee bridges are designated as Type "j" bridges under the LRFD Specifications. The formulae given for Type "j" bridges are the appropriate ones. However, a general determination as to whether the system behaves in a connected or non-connected fashion must first be determined. For the system to be deemed to be "sufficiently connected", it must be capable of transferring both shear and moment laterally between girders. Article 5.14.4.3.3 gives the criteria that must be met to ensure shear-flexure transfer between joints. If any of these criteria are not met, then the system is assumed to behave in a shear only transfer mode and is therefore not "sufficiently connected".

The LRFD Specification (A14) contains the same provisions for load distribution for "multi-beam decks which are not sufficiently interconnected to act as a unit," as appeared in recent editions of the Standard Specifications. Some of the changes are as follows: (1) Instead of using wheel load fraction, as in Standard Specifications, LRFD Specifications use lane load fraction. Thus, "D" value from LRFD is twice as much as the one in Standard Specifications. (2) There is no range of applicability specified in LRFD Specifications other than that the number of beams is not less than four, beams are parallel and have approximately the same stiffness, and the stem spacing of stemmed beams is more than 4 ft or less than 10 ft. (3) The multiple presence factors in LRFD Specifications are different from those in Standard Specifications. (4) The St. Venant torsional inertia, J, may be determined as:

$$J = \frac{1}{3}\sum bt^3 \qquad \text{For thin-walled open beam} \qquad \text{(A11)}$$

$$J = \frac{A^4}{40.0 I_p} \qquad \text{For stocky open sections (such as T-beams)} \qquad \text{(A12)}$$

Where A = area of cross-section; and I_p = polar moment of inertia. (5) The load fraction formulas for the interior and exterior beams are the same in Standard Specifications, while the lane load fraction for exterior beams is based on "Lever Rule" in LRFD Specifications; (6) Similar to Standard Specifications, there is no correction factor available for skewed bridges in LRFD Specifications. (7) Distribution factor method for shear is recommended to use "Lever Rule". Finally, (8) there are no correction factors for load distribution factors for support shear of the obtuse corners of the skewed bridges.

The AASHTO LRFD Specifications recommend using the "Lever Rule" – a method of determining the live-load shear carried by a single girder assuming that the deck acts as a simply supported span between girders. Using the "Lever Rule" results in two perceived problems: (1) The "Lever Rule" is invalid for the Decked Bulb-Tee Girders. The deck formed by these girders has a longitudinal joint midway between adjacent girders. This longitudinal joint acts in a manner similar to a hinge. The assumption of hinges over the girders would result in an instability in the system using the "Lever Rule". And (2) the "Lever Rule" method may be overly conservative for analyzing the Decked Bulb-Tee Girders.

For any bridge deck, the important parameters to model are the plan geometry and the flexural and torsional stiffnesses in two directions. In DPPCG bridges the transverse stiffness is discontinuous, having a finite value within the members and reduced at the joints between them. In fact, some moment may be transferred across the joint, particularly if the members are transversely post-tensioned, but unless the amount is a substantial portion of that which would exist in a beam and slab bridge with a monolithic deck, the effect on the distribution of longitudinal moments is small or at least uncertain. Because the magnitude of the transverse moment is uncertain and depends on the joint details, the live load distribution equations for DPPCGs in the current AASHTO Specifications are based on the assumption of zero moment transfer across the joint.

Because there is a longitudinal joint between girders for this type of bridge, AASHTO lists this bridge under a different category when calculating live load distribution factors (DFs). According to the current AASHTO LRFD Specifications, there are two different live load DF equations for bulb-tee girder bridges other than the DPPCG type. One equation is for single lane loaded, and the other for two or more lane loaded. For the DPPCG bridges with girders that are not sufficiently connected, the AASHTO Specifications provide for one live load DF equation. That equation was based on data from two or more lane loaded bridges. Typically designers use DF equations for single lane loading conditions to rate bridges for permit loads or overload conditions where the bridge will be subjected to only one truck. Hence, it results in a load rating penalty for DPPCG bridges when using AASHTO multiple lane live load distribution factors (A21).

Ma et al

Ma, Millam, Chaudhury and Hulsey of the University of Alaska Fairbanks (UAF) performed field-testing of 8 DBT bridges in 2003 (A22) to determine the distribution factor for single lane loading. Eight decked bulb-tee bridges were instrumented in Alaska. Each bridge was loaded with a single load vehicle to simulate the single lane loaded condition. The experimental data was used to calibrate grillage models of the decked bulb-tee girder system. The calibrated grillage models were used to conduct a parametric study of the bulb-tee girder system subjected to single lane loaded condition. Eight new simplified equations that describe the single lane loaded distribution factor for both shear and moment forces of these bridges are developed (A23). Results from the parametric study showed that girder spacing, bridge length,

and girder moment of inertia had the most influence on the distribution factor. These simplified equations are accurate only when the bridge being modeled is within the following parameters:

- The girders are typical decked bulb tee girders with the deck poured together with the girder as a single unit.
- The girder height is between 36 inches and 66 inches.
- The deck thickness is between 4 and 8 inches.
- The number of girders of the bridge is greater than or equal to four.
- The span length of the bridge is between 40ft and 180ft.
- The girder spacing is between 4ft and 9ft.
- The bridge is only loaded by a single lane of traffic

The variables used in the following simplified equations are defined as follows.

S = Girder Spacing, i.e. the distance between the centerlines of two consecutive girders in units of feet.

L = Span Length of the bridge measured from the centers of each support in units of feet.

I = Area moment of inertia about the horizontal axis of one girder in the bridge system. The moment of inertia used should be calculated from the whole girder including the whole width of the top flange deck portion. The units of this term are in (feet)^4.

Following is a list of recommended equations for the Distribution Factor of the Decked Bulb-Tee bridge girder system when it is subjected to the single lane loaded condition:

Moment over Interior Girder (MI)

$$DF = \frac{S}{12.5} + \frac{I}{300} - \frac{L}{10}\left(\frac{S-3}{200}\right) \quad \text{(A13)}$$

Moment over Exterior Girder (ME)

$$DF = \frac{S}{10} + \frac{I}{300} - \frac{L}{10}\left(\frac{S-1}{300}\right) \quad \text{(A14)}$$

Shear over Interior Girder (SI)

$$DF = \frac{S}{12.5} + \frac{I}{250} - \frac{L}{100}\left(\frac{S}{100}\right) \quad \text{(A15)}$$

Shear over Exterior Girder (SE)

$$DF = \frac{S}{12} + \frac{I}{400} - \frac{L}{100}\left(\frac{S-3}{100}\right) + .07 \quad \text{(A16)}$$

These DFs are compared with current AASHTO Specifications for bridges with not-sufficiently connected girders. Based on analyzed data, the moment DF values from AASHTO LRFD are an average of 66% larger than the experimentally derived values and the shear DF values from AASHTO LRFD are an average of 26% larger than the experimental values. The proposed simplified equations provide a more accurate means of determining the single lane load distribution factor for the decked bulb-tee girder bridge system. It should be noted that the analyses for the proposed simplified equations did not consider the effects of intermediate diaphragms. The use of intermediate diaphragms on a precast decked bulb-tee girder bridge whose girder flanges are connected only enough to prevent relative vertical displacement may cause the bridge to distribute similarly to a bridge with a deck that has full transverse flexural continuity. Also, the proposed simplified equations do not consider the effects of skew.

Pilot Study

The main parameter that differentiates the design of deck bulb tee girders from other types of precast/pretensioned bridge girders is the live load distribution factor. Under the LRFD Specifications, as noted above, deck bulb tee bridges are Type “j” bridges. There are two types of Type “j” bridges: those in which the girders are connected such that they behave as “sufficiently connected” bridges and those that do not behave in this manner. To be “sufficiently connected”, the connections between the flanges of adjacent members must be capable of transmitting both shear and moment. Such a connection would be more complex and costly to construct. But doing so would presumably yield low live load distribution factors. That is, the live load would be shared by more girders and thus the amount of live load to each individual girder

would be smaller, resulting in longer span capabilities. Paradoxically, though, this is not necessarily the case.

A pilot parametric study was carried out in this research to investigate the appropriateness of the distribution factors calculated according to the AASHTO LRFD Specifications. Figure A-30 is a comparison between the sufficiently connected case and the not sufficiently connected case. Deck bulb tees based on the PCI BT-72 girder spaced at 6'-0" on center were used for the comparison. Note that for the span lengths chosen, in each case the distribution factor for the not sufficiently connected system is lower than for the sufficiently connected case. Using the live load distribution factors currently given in the specifications, there appears to be no material benefit to making the system "sufficiently connected."

SUMMARY REVIEW OF SPECIFICATIONS

The main specifications that govern the design of deck bulb tee girders are the *AASHTO Standard Specifications for Highway Bridge Design* and the *AASHTO LRFD Bridge Design Specifications*. The individual states in which deck bulb tee systems have been constructed also potentially contain provisions within their state design and construction specifications that affect this type of construction. The states include Alaska, Idaho, Oregon, and Washington. A review was made of each relevant document to identify the current state of practice as recognized by the governing agencies.

Below are summary reviews of the pertinent specifications. Detailed reviews are contained in Appendix A.

AASHTO Standard Specifications

Little specific mention is made of deck bulb tee girders in the Standard Specifications. This type of construction falls generally under concrete bridges. The design of the girders themselves falls under Chapter 9, Prestressed Concrete. The only chapter in which specific details pertinent to deck bulb tee girders are present is Chapter 3, Loads. That chapter covers loads and load distribution. Both dead and live load distribution are covered.

AASHTO LRFD Specifications

The AASHTO LRFD Specifications also contains few specific references to deck bulb tee girders. As with the Standard Specifications, most of the specifics related to deck bulb tees

contained in the LRFD Specifications is present in the section that deals with load distribution, which is Chapter 4, Structural Analysis and Evaluation.

State Specifications

Little guidance is given in the specifications of those states in which deck bulb tee systems have been built. Washington State specifications contain the most detailed provisions. Many Washington provisions override the corresponding LRFD Specifications, but in a general sense: no provisions are present that specifically address deck bulb tees. Provisions are included regarding girder flange connections, but only in regard to construction.

CONTINUITY FOR LIVE LOAD

Compared with simple-span bridges, continuous span (jointless) precast prestressed concrete bridges are used to improve durability, increase seismic resistance, and increase span capacity. Increased span capacities of precast prestressed concrete girder bridges through the use of continuity and of high strength concrete have made them competitive with structural steel for spans in the 100 to 150 ft range. This span range has become more common in recent years in overpass applications because of safety requirements that dictate elimination of shoulder piers. Continuity also can reduce the lateral resistance demand on piers, definitely improves the riding quality, and can reduce maintenance needs by omitting joints. Many states make precast, prestressed girder bridges continuous using a cast-in-place connection between girders over the piers, e.g., using negative moment reinforcement within the cast-in-place deck slab. For decked precast prestressed concrete girder bridges, however, cast-in-place connection cannot be used. Thus, well-established guidelines for continuity design are becoming more important. Design and construction continuity details need to be studied and recommended for DPPCG bridges as part of this study.

In simple-span non-composite bridges, time-dependent deformations result in little or no change in the distribution of forces and moments within the structure. However, multiple-span composite bridges, made continuous for superimposed dead loads and live loads, become statically indeterminate. As a result, inelastic deformations that occur after the connection has been made will generally induce statically indeterminate forces and restraining moments in the girders. Some sources of inelastic deformations in conventional precast concrete girders with cast-in-place decks are not present in DBTs. Therefore, statically indeterminate forces and

restraining moments in DBTs will differ from those in conventional precast concrete girders, as discussed below.

Conventional Precast Concrete Girders with Cast-In-Place Decks

Sources of inelastic deformation in conventional precast concrete girders with cast-in-place decks include creep and shrinkage, and temperature gradients. Creep of the girder concrete under the net effects of prestressing and self-weight will tend to produce additional upward camber with time. When girders are made continuous at a relatively young age, it is possible that positive moments will develop at the supports over time. These positive restraint moments are caused by continual cambering upwards as a result of ongoing creep strains associated with the prestress. In conventional girders with cast-in-place decks, differential shrinkage between the deck concrete and girder concrete results in downward deflection. Also, loss of prestress due to creep, shrinkage and relaxation results in downward deflection. Therefore, differential shrinkage and loss of prestress has a tendency to reduce this positive moment.

In addition to creep and shrinkage of concrete, temperature gradients can play a major role if the girders are made continuous. Solar heating of the top deck will tend to produce upward camber adding to the positive restraint moment caused by creep. Large restraining positive moment can cause cracking in the bottom flange near the pier locations (A26). Heat of hydration in the cast-in-place deck concrete can have a mitigating effect on the development of positive restraint moment. The cast-in-place deck may be heated to temperature that is higher than the supporting girder temperature by heat of hydration during the initial hydration when the concrete is still plastic. Contraction of the deck concrete with subsequent cooling after the concrete has hardened results in a downward deflection thereby reducing the positive restraint moment caused by creep and solar heating.

Oesterle et al. (A25, A26) presented the results of an experimental and analytical research program, funded by NCHRP, and the Federal Highway Administration, on the behavior of continuous and jointless integral abutment prestressed concrete bridges with cast-in-place deck slab.

Results of the analytical studies showed that the age of the girder when the deck was cast was the most significant factor in determining whether positive or negative restraint moments occurred at the interior transverse joints over the piers due to the interaction of creep

and shrinkage. Results also indicated that the live load continuity of the bridge may be reduced significantly with long-term and time dependent loading effects and with thermal effects.

In the experimental part of the jointless bridge research (23, 24), testing of materials, bridge components, and a full scale girder indicated that:

1. Expected shrinkage of the deck concrete did not occur in the concrete in the outdoor environment of Skokie, Illinois. Thus, the effects of deck shrinkage to mitigate the effects of girder creep did not occur.

2. Heat of hydration effects in the cast-in-place deck concrete can have a mitigating effect on the development of positive restraint moment.

3. Daily temperature effects with heating and cooling of the deck with respect to the girder have a significant effect on restraint moments. Solar heating of the deck causes positive restraint moments of the same order of magnitude as the moments due to girder creep and are additive to the moments caused by creep.

4. Load tests on the full scale girder that was monitored and load tested periodically over an 18 month time frame, demonstrated that cracking due to positive moment at the transverse connection reduced continuity for live-load. When the restraint and dead load moments were added to the live-load moments, effective continuity was negative (i.e., less than 0%). That is, the total midspan positive moment in the tested continuous girder was slightly higher than the anticipated positive moment in a simply supported girder.

5. The positive moment due to combined creep and temperature effects resulted in stresses in the positive moment reinforcement in the connection over the pier that reached or exceeded yield stress.

Results of this research indicated that positive moment reinforcement does not affect the net resultant midspan service level stresses. If positive moment reinforcement is provided and positive restraint moments tend to develop, the need to superimpose the positive restraint moment on the dead and live load moment essentially negates any decrease in service level stresses resulting from the negative moment continuity connection over the piers.

If negative restraint moments develop, positive moment reinforcement is not needed. Therefore, these studies (A25, A26) indicated that there is no net benefit, in terms of service

level stresses in the prestressed girder, by providing positive moment reinforcement in the transverse connections. It is understood, however, that there may be benefit, in terms of structural integrity, for providing the positive moment reinforcement.

The FHWA Jointless bridge project (A26) also included a study of the combined effects of live load and sources of secondary moment for the negative moment response prestressed concrete girders made continuous for live load. Results of this study indicate that the negative moment affecting deck reinforcement stresses can be determined from an elastic, gross section analysis for live load, and the effect of secondary continuity moments can be ignored.

Recently, NCHRP Project 12-53 was completed and results are included in NCHRP Report 519 (A27). This project was carried out to further examine the behavior of simple-span precast/prestressed girders made continuous by connections at the transverse joints over the piers. The focus was on the effectiveness of the positive moment connection and on design criteria for this connection. Results of analytical studies were similar to those reported in the previous study (A25). That is, if positive restraint moments develop, these restraint moments must be added to the positive moments caused by dead and live load, and that the net positive moment at the midspan is essentially independent of the amount of positive moment reinforcement provided in the transverse connection. In addition, analytical studies indicated that cracking in the transverse joint decreases live-load continuity.

NCHRP Project 12-53 also included experimental studies. Live load testing indicated that, contrary to analyses results, the continuity with application of live load was near 100% until the positive moment crack at the connection became very large. The full scale testing result in the NCHRP 12-53 study, with essentially no live-load continuity lost due to positive moment cracking, differed from the result of full-scale testing in the jointless bridge study (A26). However, some results from the NCHRP 12-53 full-scale tests were similar to those observed in the jointless bridge study including:

1. The shrinkage strains in the deck concrete were significantly less than expected.
2. The effects of heat of hydration in the deck concrete were significant.
3. Daily thermal effects were significant.

Based on the analyses and testing, recommendations for the positive moment connection in NCHRP Report 519 included:

1. The positive moment connection should be provided and designed for the calculated moment due to dead, live and restraint moment. However, minimum reinforcement should be provided for a moment equal to $0.6M_{cr}$ where M_{cr} is the cracking moment of the connection. Also, the design moment should not exceed $1.2\ M_{cr}$ because providing more reinforcement is not effective. If the design moment exceeds $1.2\ M_{cr}$, design parameters should be changed. The easiest change to reduce the positive moment is to specify a minimum age of the girder at the time of making the continuity connection.

2. If the contract documents specify that the girders are a minimum age of 90 days when continuity is established, the restraint moment does not have to be calculated. This is based on the observation from surveys and analytical work that, if the girders are more than 90 days old when continuity is formed, it is unlikely that time-dependent positive restraint moments will form.

3. The transverse connection can be considered fully effective if, "… the calculated stress at the bottom of the continuity diaphragm for the combination of super imposed permanent loads, settlement, creep, shrinkage, 50% live load and temperature gradient, if applicable, is compressive."

Decked Girder Bridges

The major difference between the DBT bridges and the type of bridge studied in the NCHRP and jointless bridge projects described above is that, in the DBT bridges, the deck is part of the precast prestressed section. There is no differential shrinkage or heat of hydration strains to help mitigate the effects of the creep in the prestressed section. For DBT girders made continuous, if the camber under sustained dead load is upward after the continuity connection is made, then positive restraint moments will develop from time-dependent effects. Therefore, the criterion for neglecting restraint moments from time-dependent effects if the girders have a specified minimum age of 90 days is questionable for DBT bridges. In addition, restraint moments due to thermal gradients from solar heating may add significant positive moment.

Considering that DBT bridges essentially do not have any differential contraction between the deck and the girder due to differential shrinkage or heat of hydration effects, positive restraint moment from combined creep and temperature effects may be large.

Regardless, however, of all the study and discussion of positive restraint moments and loss of live load continuity in these simple span girders made continuous presented above, this type of bridge girder has generally performed exceptionally well for decades. The only reported serious problems with this type of bridge include a small number of incidences with excessive cracking in the positive moment connection regions near the ends of the girders (A26). The distress observed in these girders was likely due to high positive thermal gradients combined with large capacity of positive moment reinforcement in the connections over the piers. However, if the capacity of the positive moment reinforcement is limited to not exceed 1.2 $M_{cr,}$, as recommended in the NCHRP Report 519, and the positive moment reinforcement is adequately developed in the ends of girders, the positive moment connection will yield before excessive positive moments can develop and the behavior for positive restraint moment will be acceptable

To make decked precast prestressed concrete girders continuous for negative moment at the transverse connection due to live load, the following connection methods can be used: full length post-tensioning method and transverse joint connections between girders over piers (or elsewhere), e.g., using the newly developed high-strength threaded rod continuity method (A24).

Full length post-tensioning requires full length ducts and usually necessitates widening of girder webs. It also requires anchorage blocks to resist stress concentrations at the anchorage zones. These massive anchorage blocks are required to be as wide as one of the two flanges and as long as 3/4 of the beam depth (A20), unless an optimized anchorage block is used (A28). The massive blocks not only add to the beam weight, but also require expensive alteration of the beam formwork. In addition, a specialty contractor is required to perform the post-tensioning and grouting. However, this continuity method provides greater resistance to stresses and allows longer spans for a given beam size than the conventional deck reinforcement continuity method. Cracking in the deck over the piers is virtually eliminated. In addition, beams designed with this method of continuity require fewer pretensioning strands for resisting positive moments. Pretensioning is required only to support self-weight of the beam. This reduced pretensioning results in less camber and less demand for high concrete strength at strand release (A29). Successful cases of application of post-tensioning to DPPCG bridges has been reported (A30).

In one of the newly developed high-strength threaded rod continuity methods, two types of non-prestressed high strength threaded rods were considered: Grade 92 ksi rods and Grade

150 ksi rods. The nominal diameter of these rods is 1.0 in. They are placed in the top flange of the beam to provide for resistance of negative moments at the piers, as shown in Figure A-31. Considering the fact that the post-tensioning is a specialized operation, the continuity method using threaded rods is considered to be the most cost-effective option. The newly developed connection details are constructible. They are proven to give excellent performance and are therefore highly recommended (A24). Other methods can also be utilized for this type of continuity. Some new technical and material concepts have been introduced by Husain and Bagnariol (A31) for design and detailing of jointless bridges. Analytical studies of Washington State Department of Transportation's practice in designing for continuity have recently been presented by McDonagh and Hinkley (A32). They have pointed to an important finding that deeper girders with longer spans do not necessarily develop large positive restraint moment, and that it is possible to design deep girders for full or near-full continuity for superimposed loads. A variety of transverse joints have been addressed specially in the Recommended Practice for Precast, Post Tensioned Segmental Construction (A33), and that need to be studied for possible adaptation and use for DPPCG bridges.

Seismic loading is another source of moment for the transverse connections over the pier. In a seismic event, the longitudinal moment in a typical girder near the pier consists of the sum of the negative dead load moment and a portion of the column seismic moment. On the side of the pier where these moments are additive, the result is a high, rapidly changing moment. While a relatively constant positive moment may be generated on the other side of the pier. This distribution is reversible depending on the direction of the earthquake force. The value of seismic positive moment could become significantly large if the girders are erected as simply supported beams and later made continuous. Therefore, the girders must be designed to carry both a high negative moment near the pier, as well as a smaller positive moment for an extended length on each side of the pier. Additionally, the connection over the pier must be detailed such that strength and ductility requirements are met. The state of Washington has seismic resistance reinforcement details that may significantly exceed volume change demands. However, Washington does not recognize this continuity in its maximum positive moment girder design.

CONNECTION DETAILS FOR NON-CONTINUOUS TRANSVERSE JOINTS

DBT bridges may also have problems over fixed piers where the precast members abut but are not made continuous. Under present practice, there is usually a precast or cast-in-place

end diaphragm. Without continuity, rotation at the end supports of the members causes a constant “working” of the joint. A “semi-expansion” device of some type is required to provide a water tight seal. The problems caused by leakage of this joint are usually not severe, and often the most practical solution is to recognize the problem and detail the end bearings accordingly. Cracking in asphalt surfaces will occur and must be maintained.

Figure A-32 shows a typical transverse deck connection. This bearing employs only elastomeric pads. The deck members are retained transversely by steps cast at the ends of the abutments and piers. The end diaphragm shown may be either cast onto the deck member in the precasting plant or field poured. Figure A-33 shows a transverse connection with dowels. This bearing detail for slab or box units employs smooth bar dowels to retain the deck members transversely.

EXTENDING THE SPAN USING THE SEGMENTAL TECHNIQUE AND SPLICED GIRDERS

Anderson (A34) has discussed extending AASHTO girders to longer spans using post-tensioning of the girder segments at the bridge site. Using AASHTO Type IV girders with higher strength concretes under HS20 loading, he showed that a span of over 180 ft is achievable using the segmental technique. Recommended Practice for Segmental Construction in Prestressed Concrete (A35) and Recommended Practice for Precast Post-tensioned Segmental Construction (A33) present recommendations for design and construction of precast prestressed concrete structures including segments of decked beams that are tied together using post-tensioning. These cover fabrication, transportation, and erection of the component segments, the construction of joints, details of tendons and anchors, and design considerations applicable to segmental construction. Caroland et al. (A36) demonstrate an actual use of segmental prestressed bridge and conclude that segmental I-beams should compete with steel bridges in the span range of 130 to 250 ft. NCHRP project 12-57 is targeting development of recommended load and resistance factor design (LRFD) procedures, standard details, and design examples for achieving longer spans using precast, prestressed concrete bridge girders. This project considers, in not much detail, also the decked girders. The project also studies achieving longer spans with connection of simple spans for continuity and assembling haunched pier segments in the field.

CAMBER AND CROSS SLOPE

It has long been recognized that variation of camber with long-term load effects such as creep is an impediment to the use of longer span DPPCG bridges (A37). Differential camber among adjacent girders can be even more troublesome. Methods of camber control need to be investigated through selection of material properties, age of girder at installation, initial camber, accurate prediction of camber, uniformity of material and casting/installation plan for adjacent girders, methods of and transverse shear transfer through shear longitudinal joints. The issue of camber control will be a major issue especially for longer span DPPCG bridges. It seems that no matter how accurate the camber design and calculation is, there will be a need for balancing the differential camber in the field. In this respect, the matter of camber, in turn, affects the shear connector and longitudinal joints to be discussed in conjunction with camber control.

Among a variety of factors to be considered in determining DPPCG is the cross slope. There are several methods for implementing the cross slope. Among these is placing girders on the same level and use of the wearing surface to provide the slope. The obvious disadvantage of this is the extra weight (A38). To overcome this, the girders can be placed on different levels and use less amount of wearing surface, or to use asymmetrical or tilted girders. Each of these solutions influences the fabrication, design and installation and need to be addressed.

SKEW EFFECTS

To design a bridge, it is essential to determine the maximum reactions and shear. When the bridge is skewed, distribution of reactions and shear, i.e., load distribution, is of course more complicated. Influence of skew on shear and reaction distribution and also on behavior of the bridge in general has been investigated widely for bridges with cast-in-place deck slabs (A39, A40, A41, A42, and A43). The unique design considerations of DPPCG bridges, however, necessitate another look at the skew effects. The research on the latter is limited and there is need for investigation.

DIAPHRAGM EFFECTS

The need for and use of intermediate diaphragms has long been somewhat controversial. When the deck is cast-in-place, diaphragms can often be omitted since the slab is effective in transferring loads to adjacent beams and effect of diaphragms in load distribution is marginal . This has been addressed by several investigations (A44, A45, A46, A47). When a full-thickness integral deck is precast as part of the beam, diaphragms are considered

necessary except for shorter spans or where other means exist for connecting the girder stems (A48). Various types of diaphragms are being used with DPPCG bridges as shown in Figures A-34 to A-36. Cast-in-place (cast through holes left in precast slab) and precast concrete diaphragms have been used. The precast diaphragms are either connected using plates welded to inserts or grouted shear keys and transverse post-tensioning. Steel K type diaphragm and pipe trusses have also been used. End diaphragms tie girders together and also stiffen the slab.

Absence of a monolithic deck structure and presence of joints are parameters that have raised question on the live load distribution and continuity of DBT bridges. The live load distribution equations for DBTs in the current AASHTO Specifications are either based on the assumption that longitudinal joints and intermediate diaphragms do not transfer any transverse moment between girders, or to consider the moment transfer (i.e., “sufficiently connected” bridge) requires calculation of parameters not defined properly for DBTs. Based on limited field tests performed in Alaska (A22, A23), there is a need to reexamine the impact of this assumption. Using the calibrated 3D FE models, parametric studies were performed to study the effect of intermediate diaphragms (A11). It has been found that intermediate diaphragms reduce the maximum horizontal shear force in connectors.

CONSTRUCTION ISSUES

Girder Weight

The most common obstacle cited in the survey to the adoption of deck bulb tees is weight. In the case of the example given above, for an eight-foot girder spacing, a conventional BT-72 girder spanning 145 feet weighs approximately 120 kips. However, the deck bulb tee equivalent spanning its maximum distance of 160 feet would weigh approximately 180 kips. That weight level may prohibit transportation of the girder to the job site on most road systems.

Maximum haul weights will be further researched. Further research into strategies for reducing girder haul weight will also be addressed. For example, a common means of overcoming weight limitations is to cast girders in two or three segments. The individual segments, which are of lighter weight, can then be safely hauled to the job site and reassembled there. NCHRP 12-57 investigated this issue, and the results of that research as well as other bodies of work will be assessed and applied to this project as necessary.

Girder Length

Length is another limiting factor on the use of deck bulb tees. Two- or three-part casting is an effective means of addressing this problem. Much attention has been given to spliced girder techniques in recent years. That research will be reviewed and applied as appropriate to this research project.

MAINTENANCE

Techniques such as welded bar ties and partial depth shear keys for holding decked girders together have been associated with longitudinal cracking along the deck, in most cases resulting in leakage through the joints (A4, A49, A50). Cracking of this form has been observed in similar multi-beam bridges (A51). This has created skepticism among many owners and is seen as major threat to the long-term durability of the structure.

DECK REPLACEMENT

At present, deck bulb tee girders are cast in a similar fashion to that of conventional precast, pretensioned concrete girders. Typically, they are cast in a precast fabrication plant in fixed beds several hundred feet in length. A fixed metal bottom pallet is used with removable metal side forms. A common practice is to cast the deck bulb tee girders in two stages. The portion up to the top of the stem is cast using high-strength concrete. The remaining portion—the fillet and top flange—are cast with an air-entrained concrete mix that is of lower strength. The advantages of this are a more workable top surface that facilitates surface finishing, but provides higher durability. It should be noted that there is no cold joint between the two castings and that the entire section is prestressed as one unit.

Deck replacement of deck bulb tee girder bridges is an issue that has been raised as a possible impediment to their use. If it becomes necessary, the deck replacement will be an issue since deck is integral with the girder. Therefore, casting sequences may need to be altered to allow the removal of the deck and installation of a new deck. Several options are available to enable future deck replacement and are summarized below.

Partial Deck Replacement

Partial deck replacement can take the form of casting a sacrificial layer on top of the top flange to serve as a wearing course. Alternatively, a one-stage casting can be used to construct

a system in which a wearing course is included in the section. The entire system would be prestressed. An allowance would be made in the top flange such that a certain amount of the thickness would be assumed to be worn away. The structural properties would need to reflect this assumption.

Benefits to this approach include ease of fabrication and resistance to transverse cracking. This system would provide maximum durability since it would be completely precast and pretensioned. Future re-decking would consist of grinding down or truing of the surface. A new sacrificial layer would then be recast in the field and ground to true the surface.

Full Deck Replacement

Full deck replacement involves fabricating the girders and incorporating them into a bridge in the conventional manner. In the future, when the deck has deteriorated to the point where replacement is deemed necessary, it is envisioned that the top flange of the girder can be removed using accepted demolition procedures and a new deck installed, either by casting a new deck in the field or installing a full-depth precast deck. A parametric study was conducted to investigate the engineering feasibility of re-decking a conventional deck bulb tee girder bridge by removing and replacing the entire top flanges of all the girders. The study is summarized in two phases as shown below.

Phase 1 is the initial design, which represents the design of a typical girder of a deck bulb tee girder bridge. The bridge cross section consists of four 35 inch deep by 7'-0" wide deck bulb tee girders. Girder concrete strength is 7.00 ksi (6.00 ksi release). This and all subsequent designs are per the LRFD Specifications. All release and final stresses and required flexural strengths are within the required limits. The area of the girder is 895 in^2 and the bottom and top section modulii are 5,118 in^3 and 10,819 in^3, respectively. Thirty ½ in. diameter strands were used in the draped pattern with the upper most level of the drape group kept below the top flange (to facilitate deck removal). Maximum net compression and tension in the girder at release are 3.308 ksi and – 0.158 ksi, respectively, both of which occur at the transfer point of the strands. Maximum net compression and tension in the girder at final conditions are 2.454 ksi and –0.326 ksi, respectively. Net camber at release and at erection are 1.13 in. (+ is upward) and 1.99 in., respectively.

In Phase 2, it is assumed that at some point during the service life of the bridge, the deck is assumed to require replacement. The top flanges are removed down to the top of the

top fillets of the girders. A new deck is formed and cast on-site. CIP deck concrete strength is 4.00 ksi. The area of the cut-back precast section is 303 in^2 and the bottom and top section modulii are 1916 in^3 and 985 in^3, respectively, which are substantially less than those of the gross girder, which is the section upon which the prestress acts. However, the top and bottom section modulii of the girder after new deck is cast are 4,986 in^3 and 26,862 in^3. At final conditions, there is a severe over-stress condition in the girder. This is caused by the beam weight acting on a structurally weak and inefficient section, which generates excessive compressive stresses in the top of the girder. The greatest contributor to the over-stress condition, however, is the weight of the new deck acting on the substantially smaller precast girder than what was originally present (since the flange was removed). At final conditions under all loads, net top compression is 6.591 ksi (versus allowable compression of 4.200 ksi) and net bottom tension is -2.701 ksi (versus allowable tension of –0.503 ksi).

Note that if the girders are shored after deck removal and until the new deck was installed, then the deck weight could be transferred to the composite section properties, which would greatly improve the stress profile. However, even if this step were taken, there would still be a significant amount of over-stress, which means the original design would have to account for this. Under this Phase scenario, assuming no shoring, net camber after the deck is removed would be 0.0 in. Installation of the new deck would cause the system to deflect –2.5 in., resulting in a net camber of –2.5 in. This compares to about a +2.0 of net camber from the Phase 1 scenario, which would likely change the profile grade unacceptably, further suggesting that shoring would be necessary.

With this method of deck replacement, the prestressed girder can safely endure the stress changes resulting from the large top flange of the girder being removed. However, when the new deck is cast, the resulting stresses cause both the maximum net compressive and tensile stresses to exceed their allowable levels by substantial amounts. Further, deflection of the system is unacceptably large. For this approach to be feasible, shoring would have to be installed under the girders until the new deck is installed. This may or may not be feasible at the bridge site. Additionally, temporary diaphragms would likely have to be installed as well to stabilize the girders.

An alternative approach to the shoring would be to design the girder with the anticipation of future deck replacement. For the girder to be able to accommodate the stresses induced by the weight of the new deck until composite action is developed, this may require that part of the

flange not to be removed with the deck in addition to an increase in the required prestressing force. This concept is shown schematically in Figure A-37. The interface between the flange and the deck will need to be detailed to allow for easy deck removal while providing adequate horizontal shear capacity. Tadros and Baishya (A52) and Tadros et al (A53) explored connections between the girder and cast-in-place portion to facilitate re-decking. An innovative shear key interface with a minimal amount of transverse reinforcement crossing the interface was used. Full horizontal shear was able to be developed. However, since much of the horizontal shear was taken by the shear keys, little protruding steel was present, which permitted much easier removal of the deck. For decked bulb tee systems, two-stage casting with a cold joint may be required to allow for easy deck removal. This converts system form a monolithic system to a composite system. This will significantly reduce the efficiency of the system.

Table A-1 Estimated Cost of Grout Keys Plus Transverse Tie

[$ per foot of keyway (Material + Labor)]

Grout Material	Transverse Tie System			
	None	Weld Plate	Tie Rod	Post-tensioned Bars
None		3.56	1.10	1.57
Sand-Cement	1.27	4.83	2.37	2.84
Proprietary Non-shrink	3.01	6.57	4.11	4.58
Epoxy Mortar	5.25	8.81	6.35	6.82

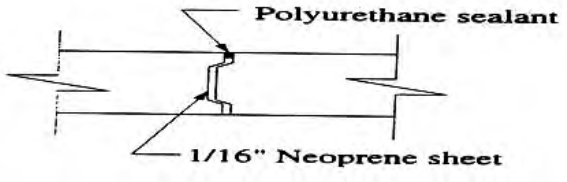

Figure A-1 Non-grouted match-cast joint

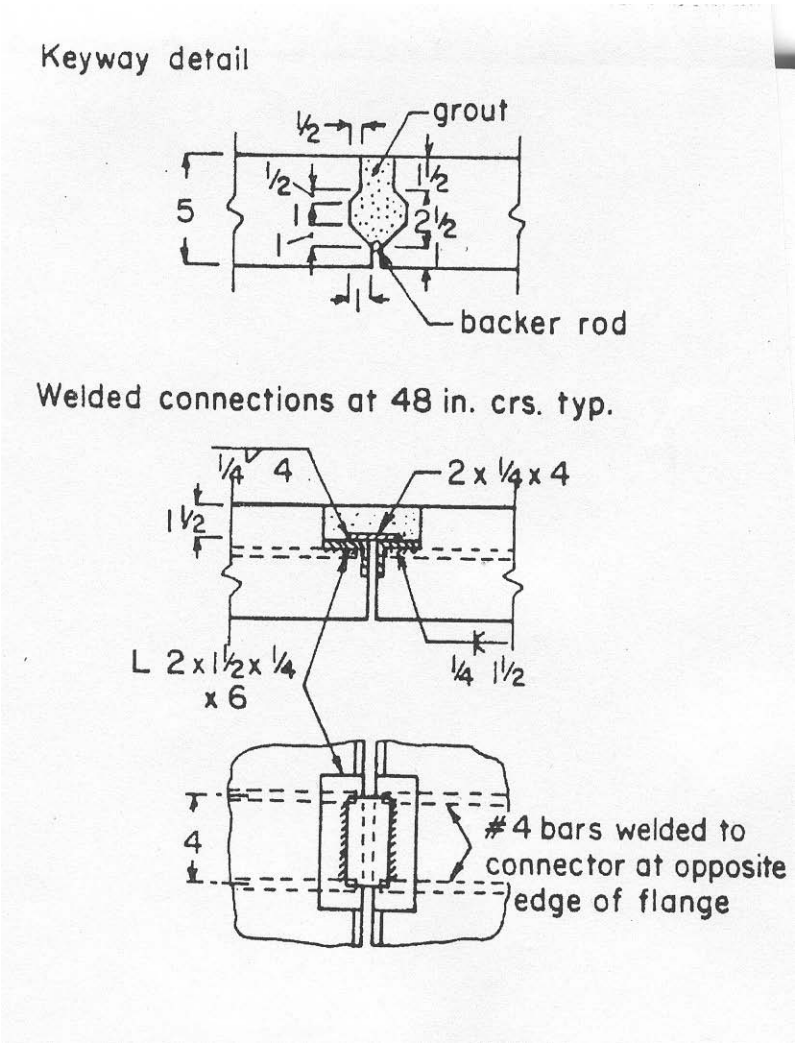

Figure A-2 Typical Connection Detail Used by Concrete Technology Corporation

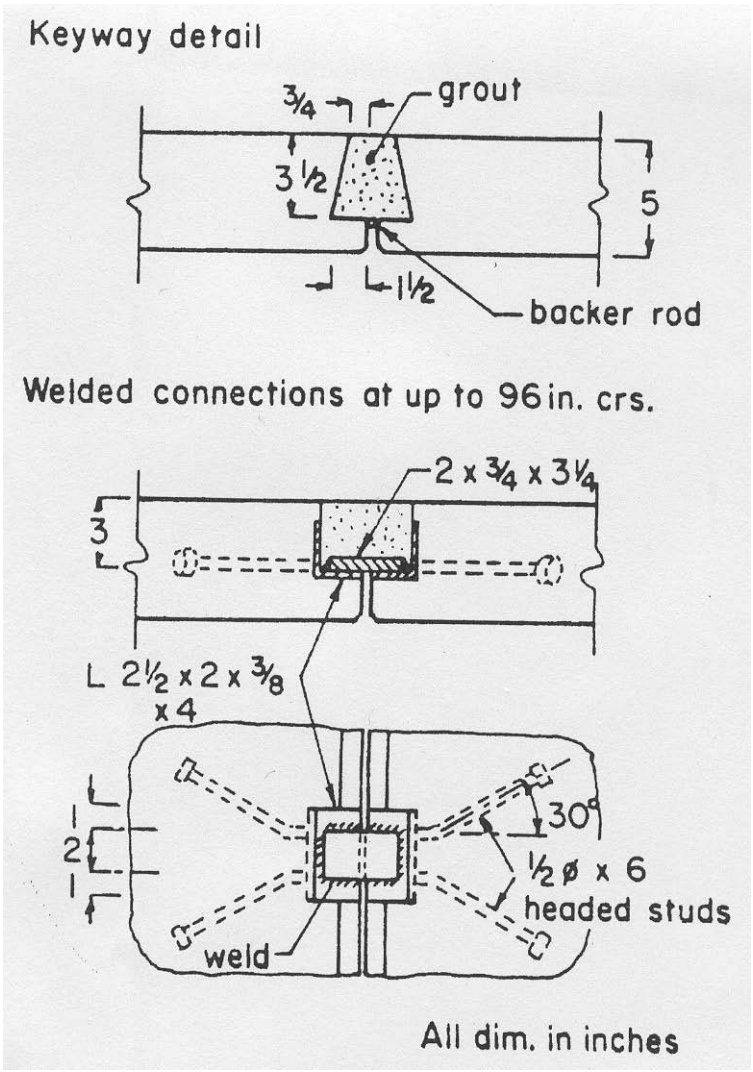

Figure A-3 Typical Connection Detail Used by Central Premix Concrete Co.

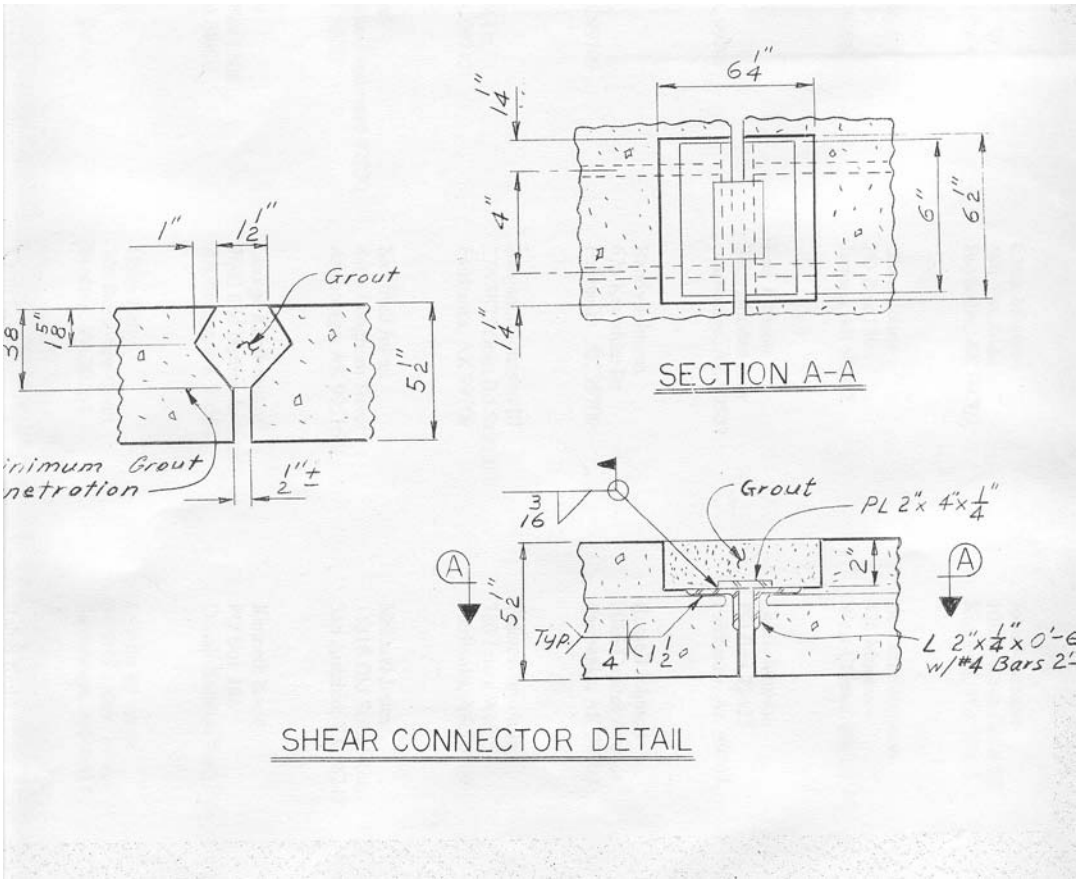

Figure A-4 Typical Connection Detail Used by Alaska DOT

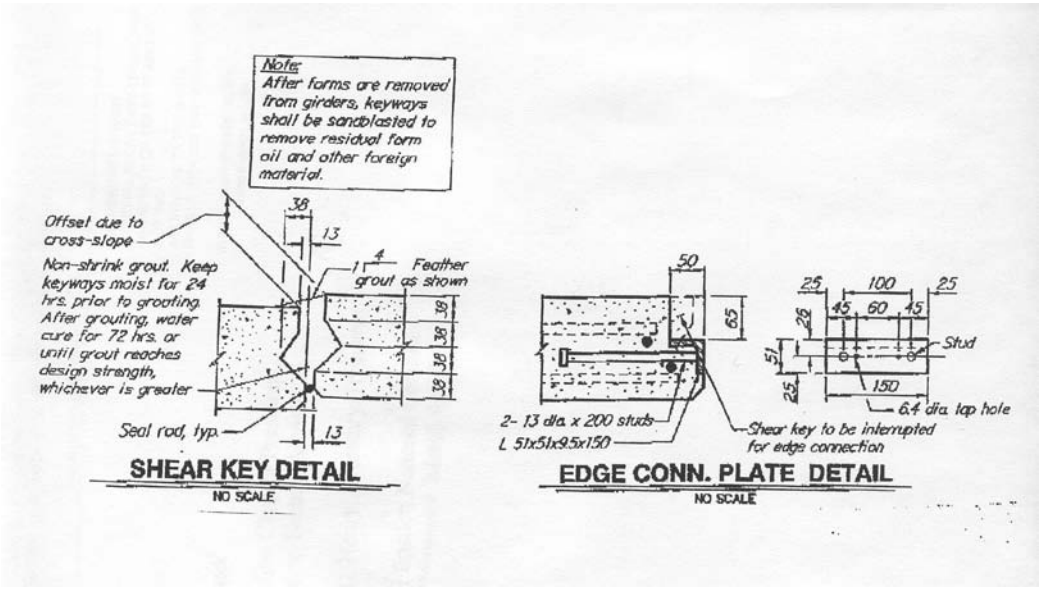

Figure A-5 Typical Connection Detail Used in Oregon

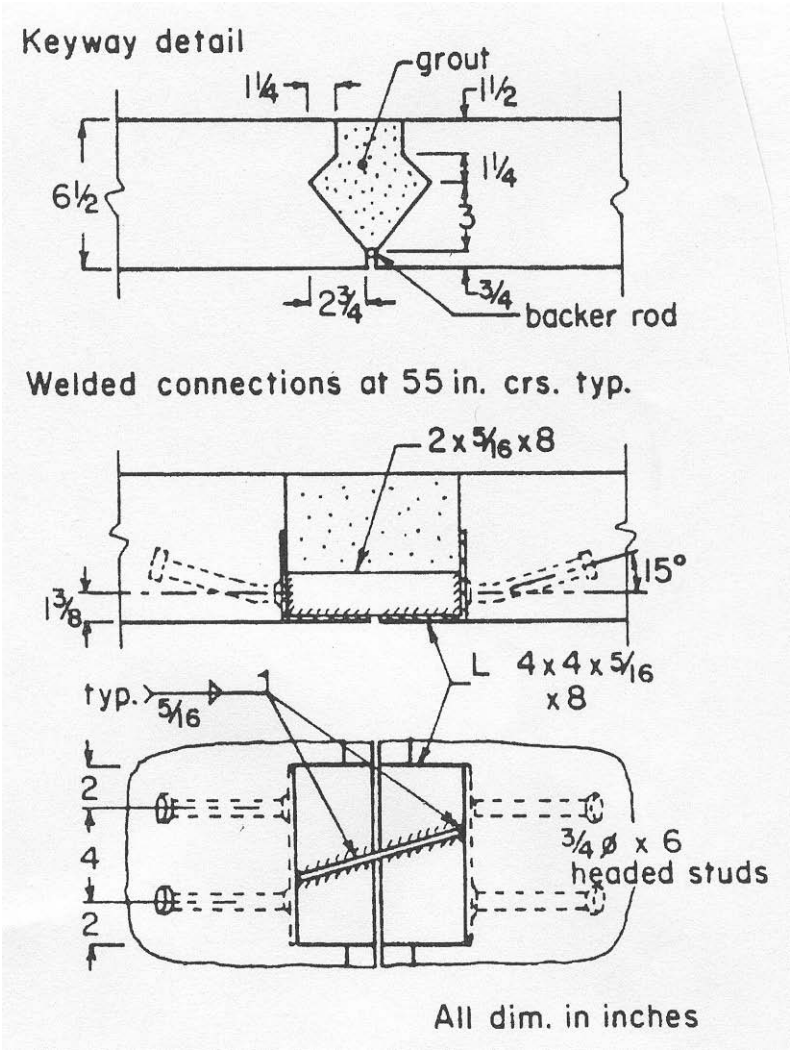

Figure A-6 Typical Connection Detail Used by Genstar Structures & Alberta DOT

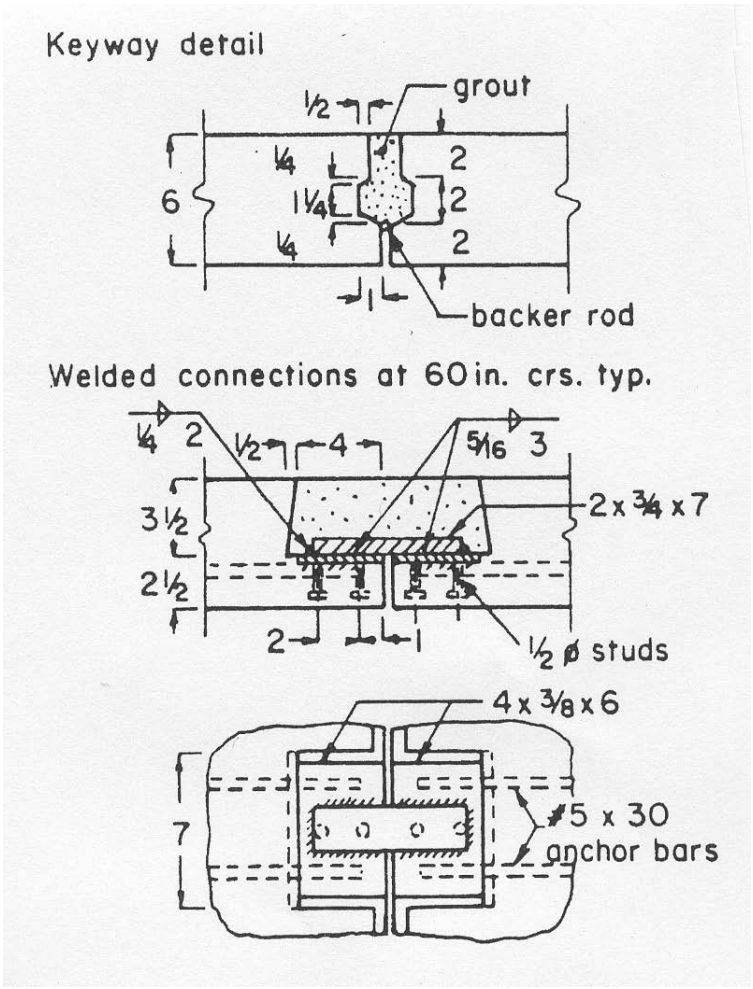

Figure A-7 Typical Connection Detail Used by Stanley Structures, Denver, CO

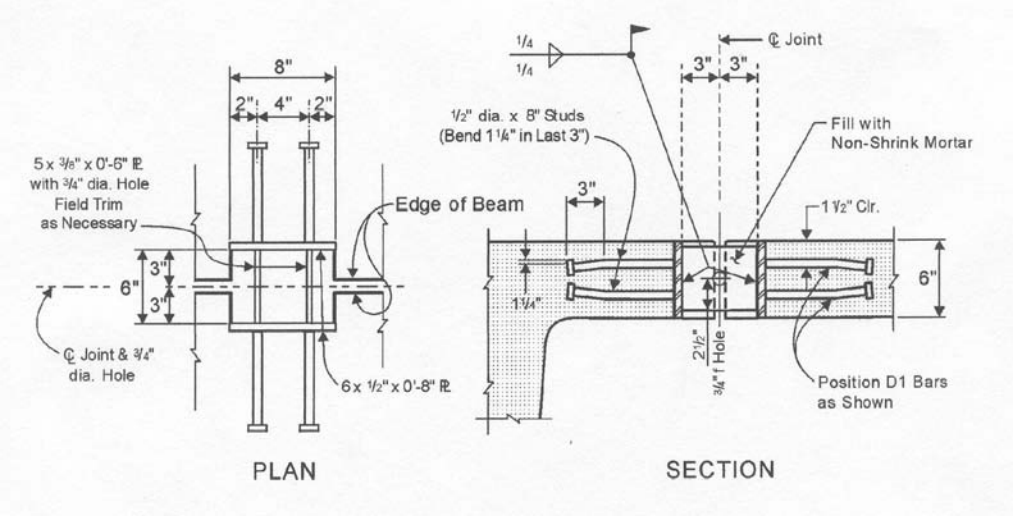

Figure A-8 Original TxDOT Connection Detail

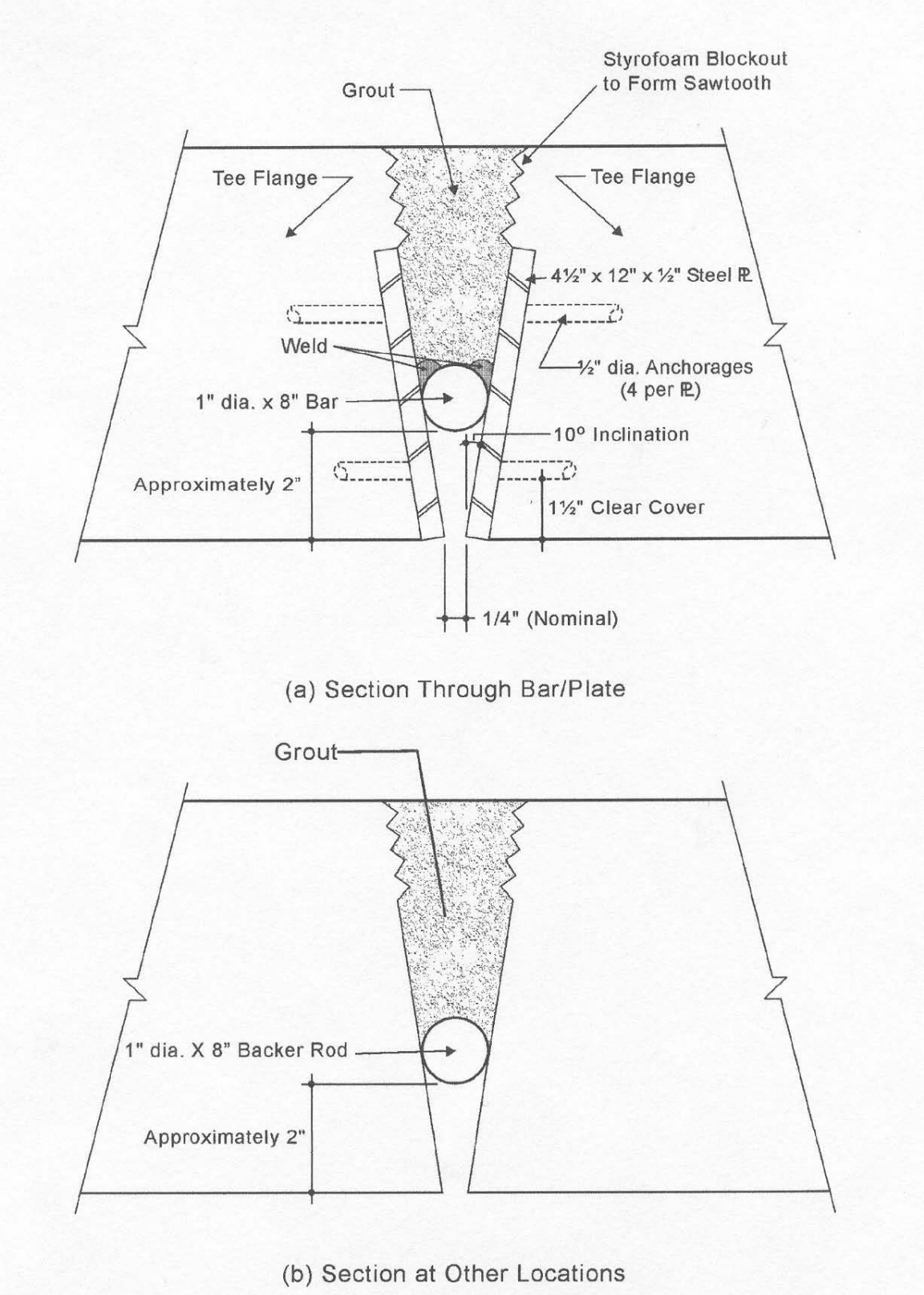

Figure A-9 TxDOT New "Simple" Connection Detail

a. Before Casting *b. Underside after Casting*

Figure A-10 Longitudinal Joint Used in Japan

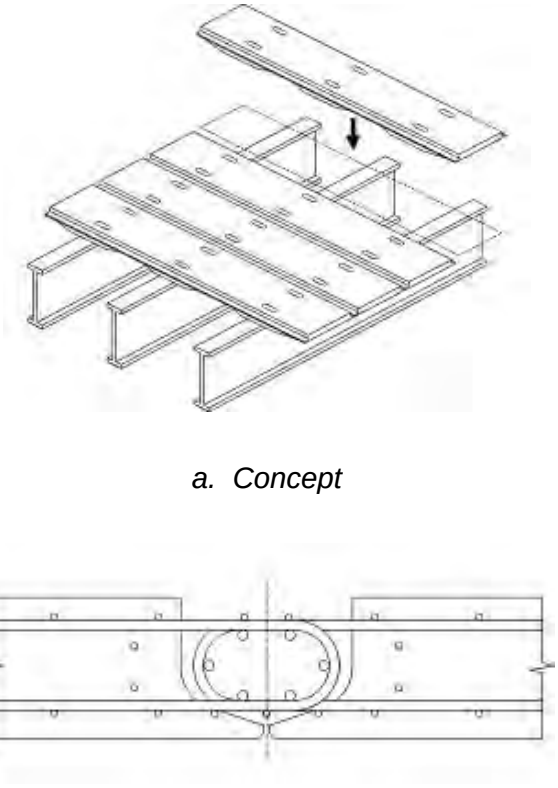

a. Concept

b. Joint Detail

Figure A-11 Full Depth Prefabricated Concrete Deck Used in Japan

a. Deck Panels

b. Transverse Joint

c. Joint Details

d. Finished Bridge

Figure A-12 Full Depth Full Width Precast Deck Panels in France

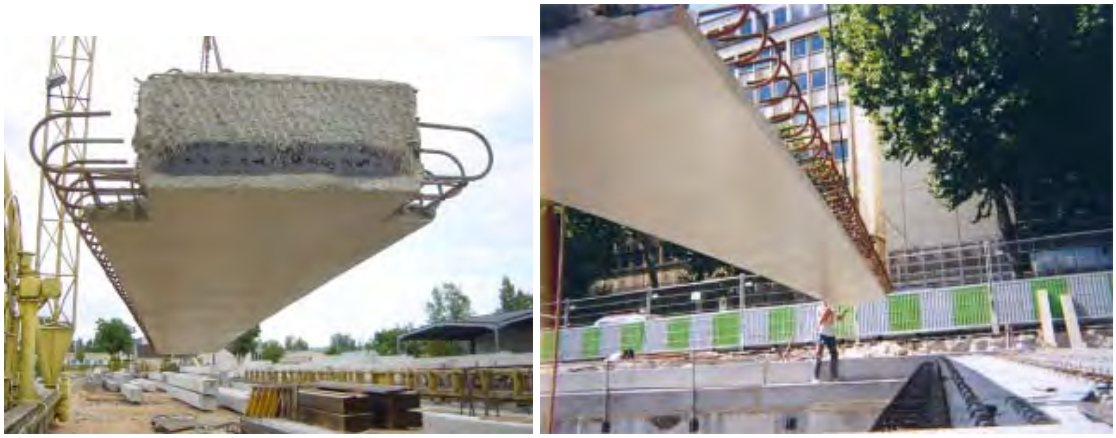

a. At the Fabricators *b. Erection on Site*

Figure A-13 Poutre Dalle System in France

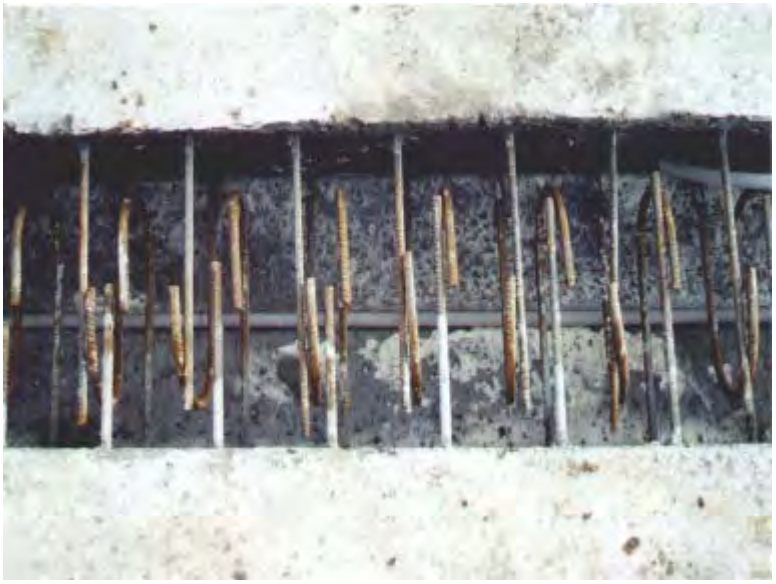

Figure A-14 Overlapping Bars in Longitudinal Joint

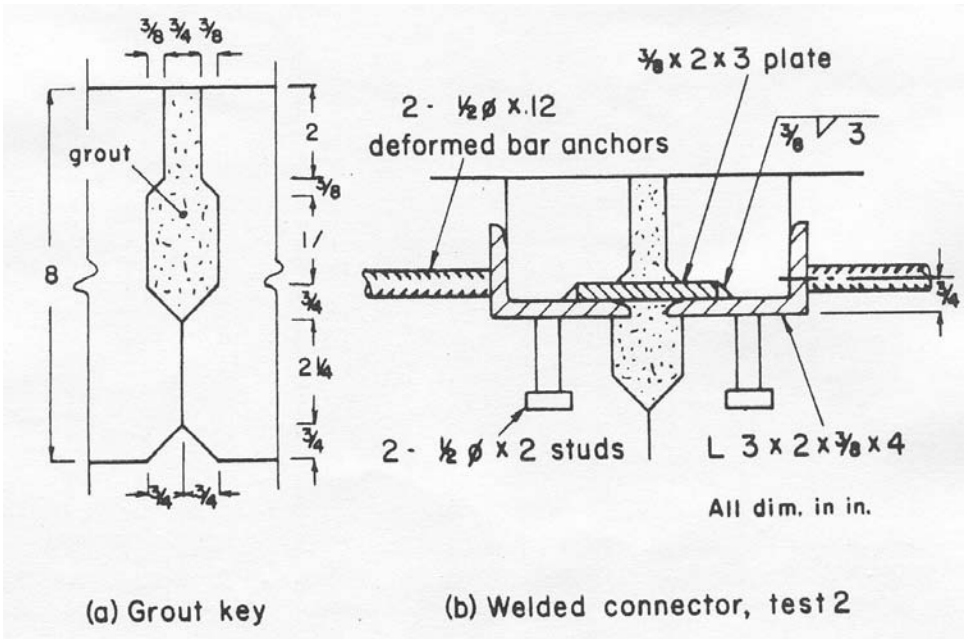

Figure A-15 Connection Details Tested by Martin and Osborn

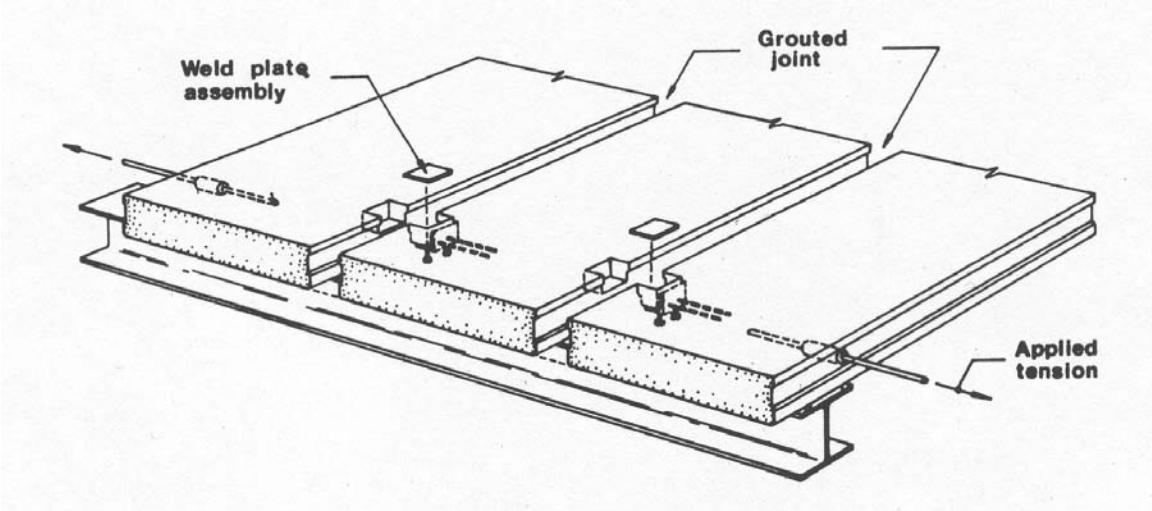

Figure A-16 Schematic of Test 2

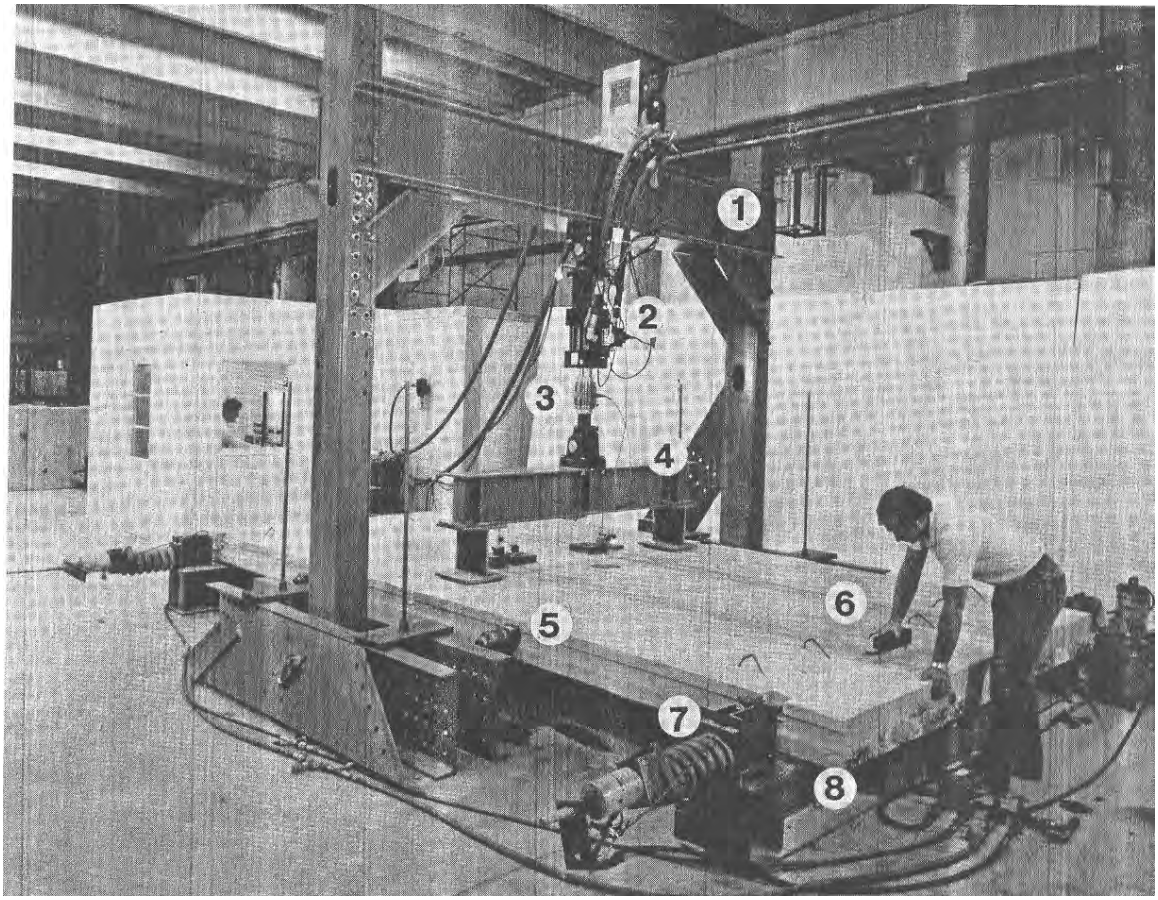

Figure A-17 Test Assembly Used by Martin and Osborn

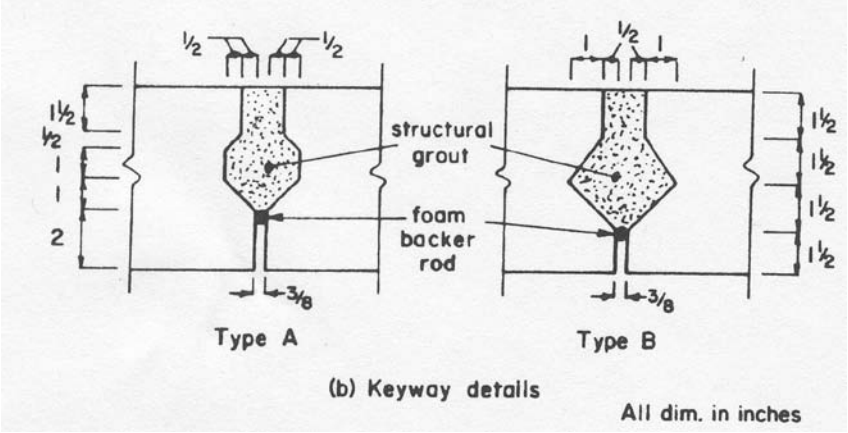

Figure A-18 Keyway Details Used by Stanton and Mattock

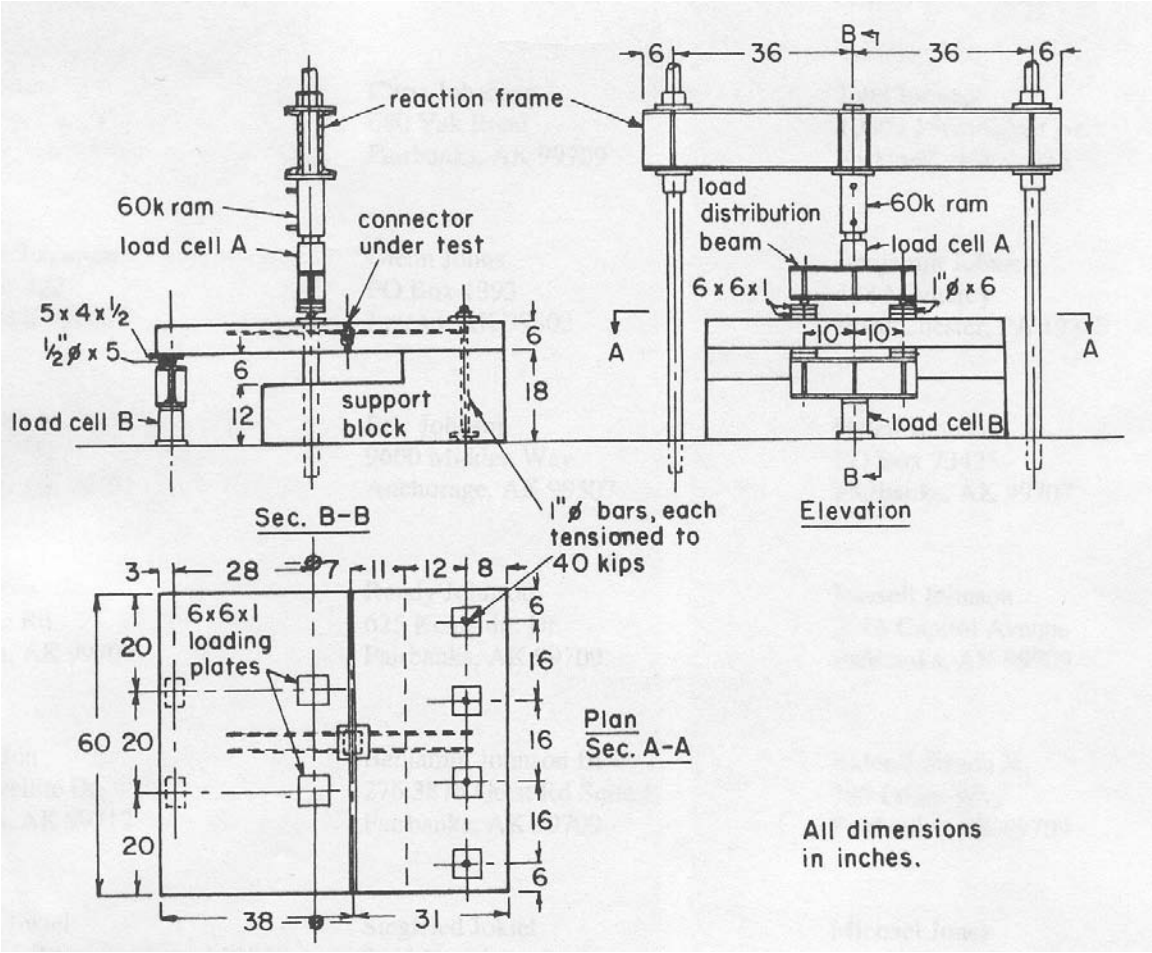

Figure A-19 Test Set-up Used by Stanton and Mattock

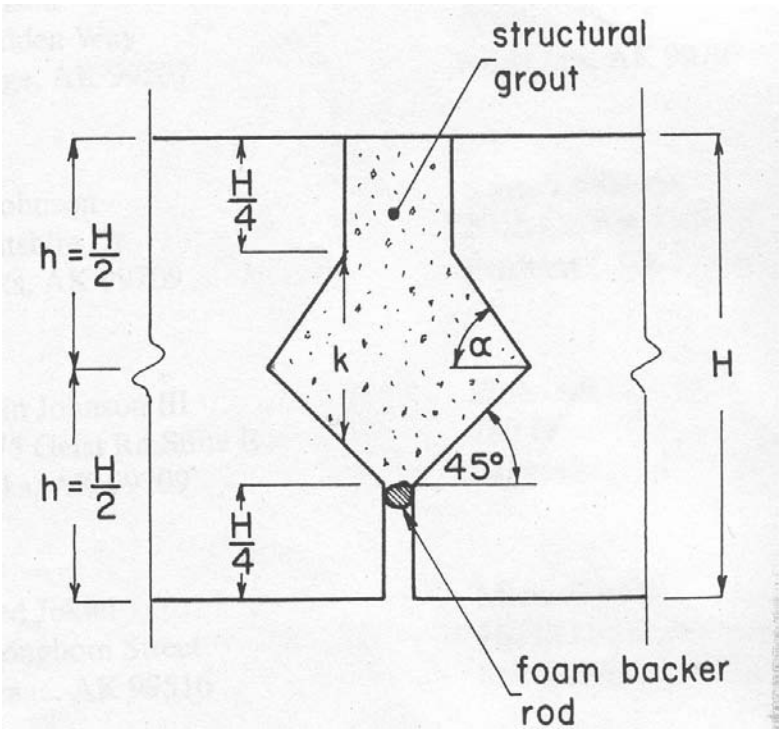

Figure A-20 Shape of Grout Key Recommended by Stanton and Mattock

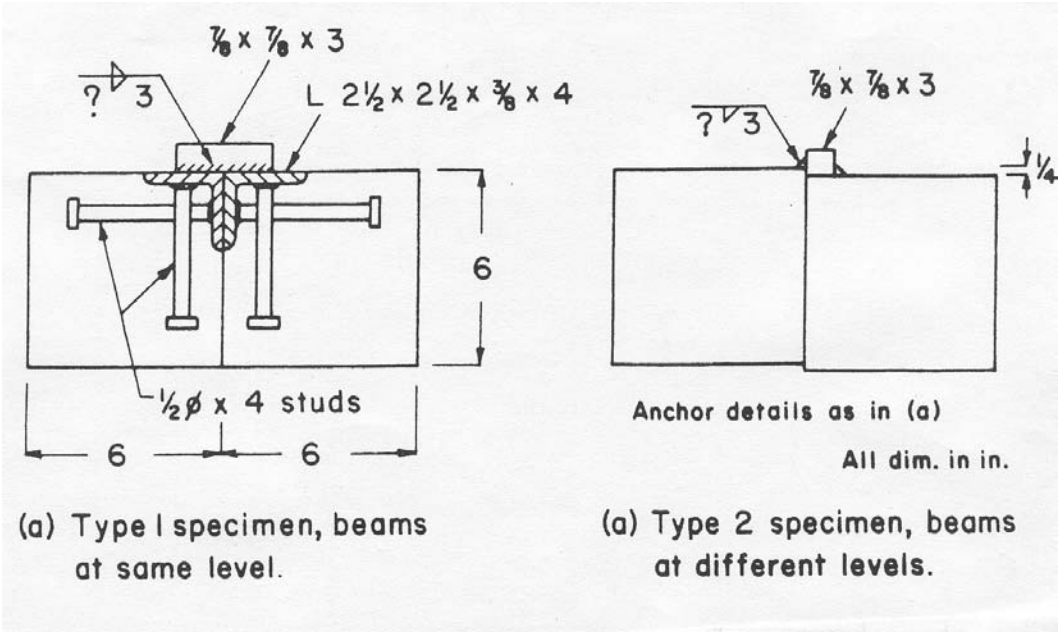

Figure A-21 Details of Specimens Tested by Ong

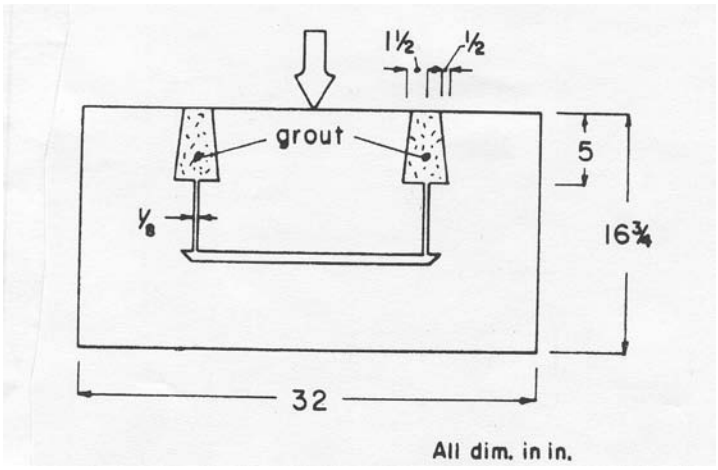

Figure A-22 Cretex Grout Key Test

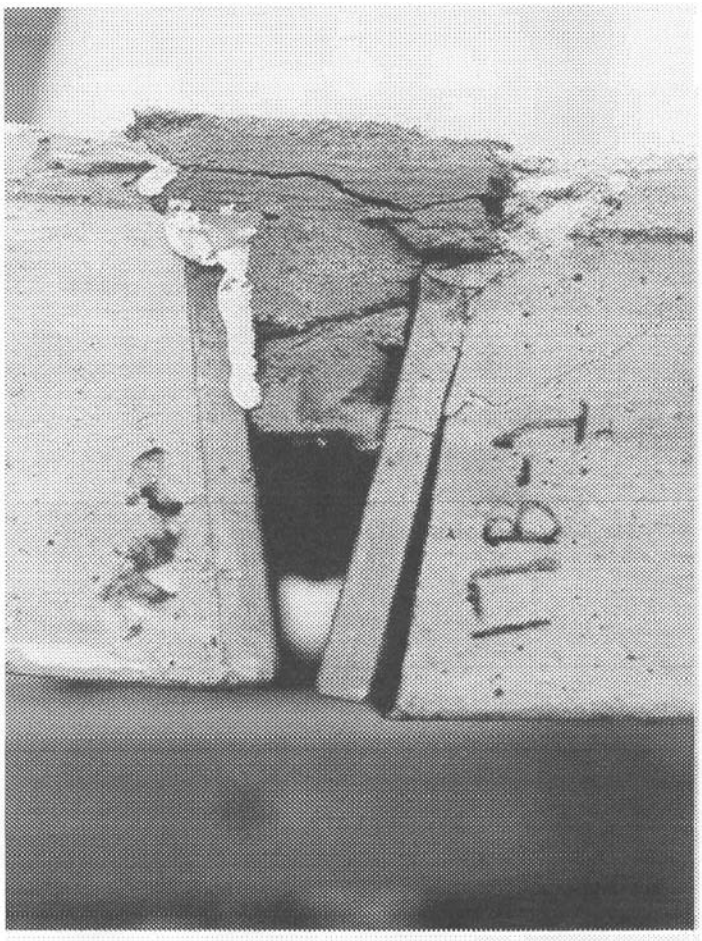

Figure A-23 Pull-Out of Weld Plate in Beam Connection Test

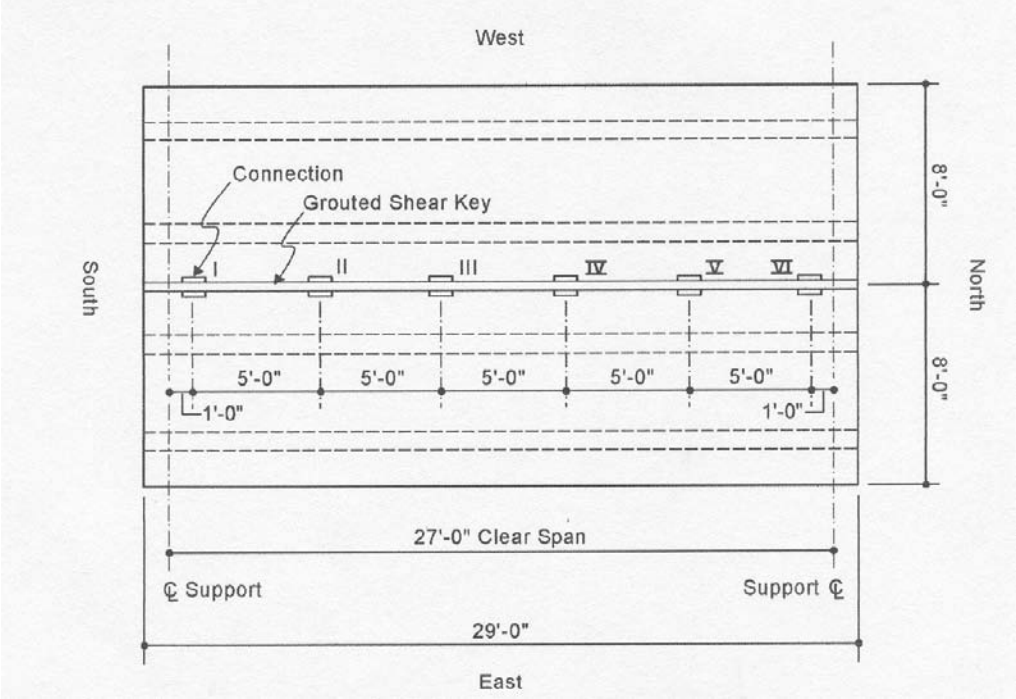

Figure A-24 Plan View of Lab Bridge Model

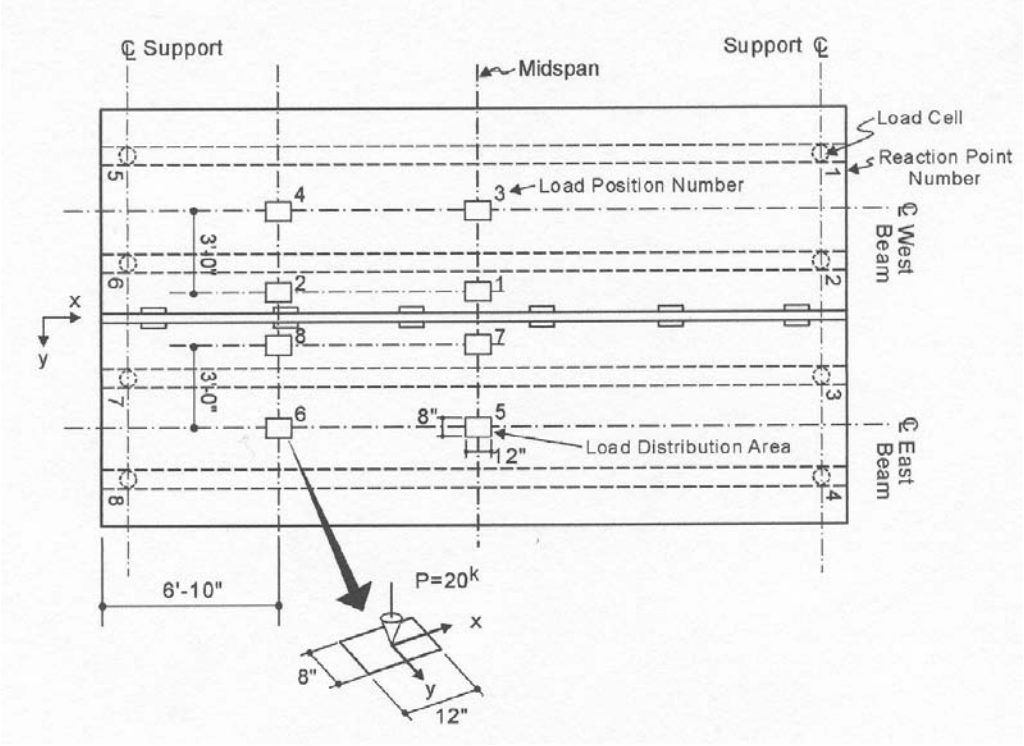

Figure A-25 Loading Positions for Model Tests

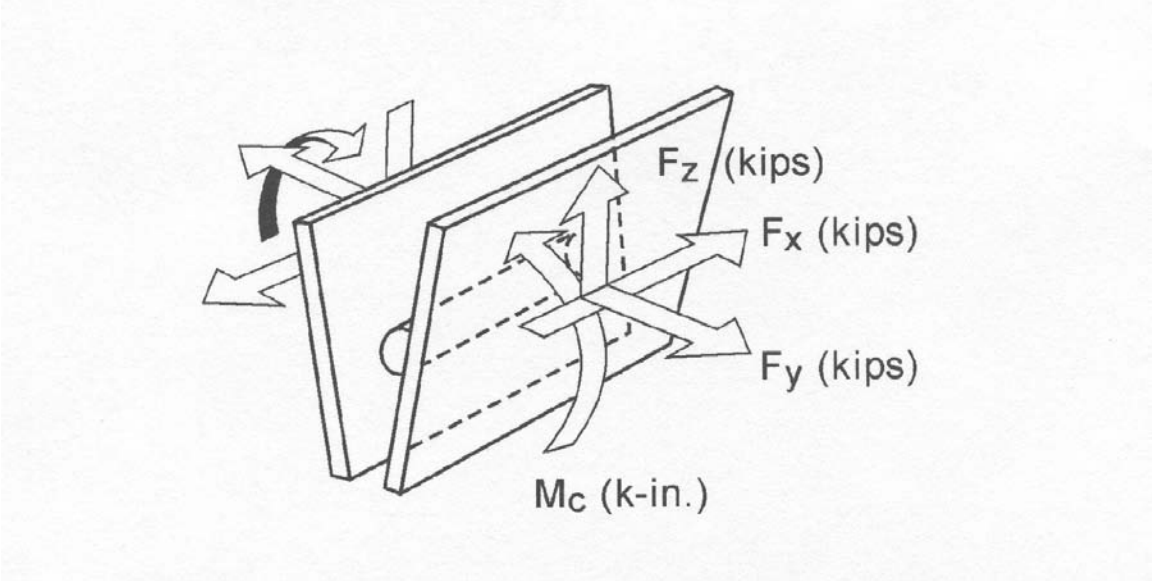

Figure A-26 Force Components in Discrete Connection

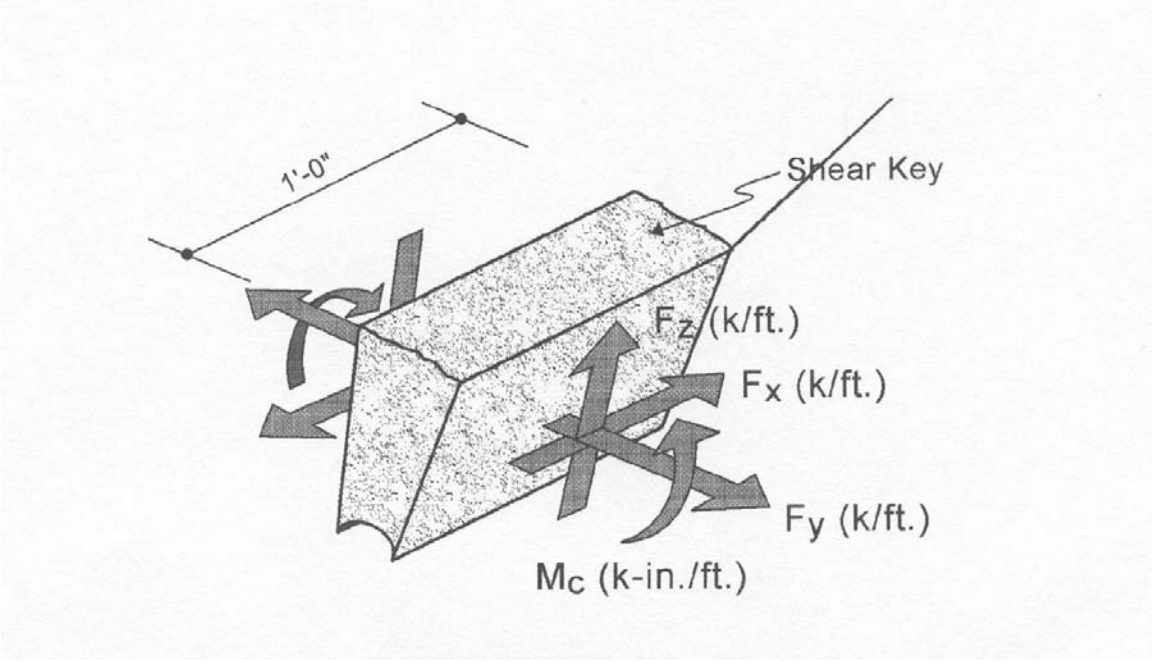

Figure A-27 Force Components in Shear Key

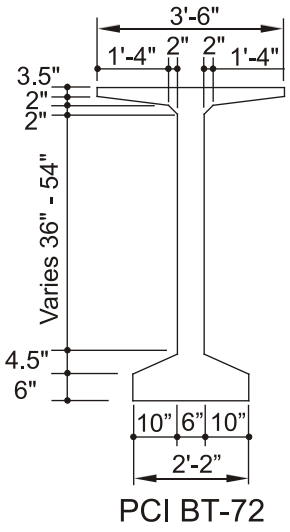

Figure A-28 Section geometry of PCI bulb tee girder series.

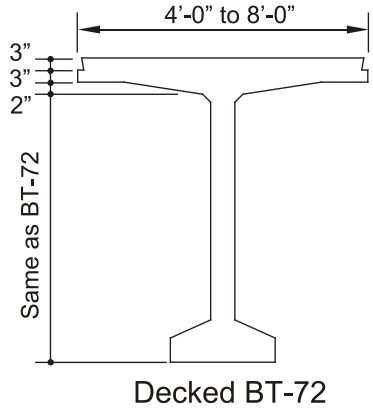

Figure A-29 Section geometry of deck bulb tee series based on PCI bulb tee girder series.

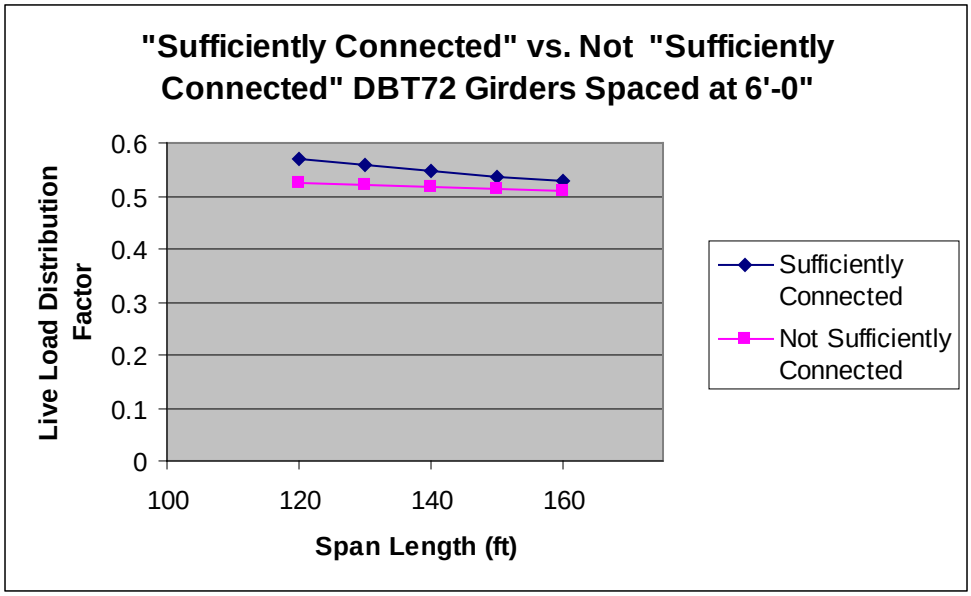

Figure A-30 Live load distribution factors for "sufficiently connected" versus not "sufficiently connected

Figure A-31 Newly Developed High-Strength Threaded Rod Continuity Method

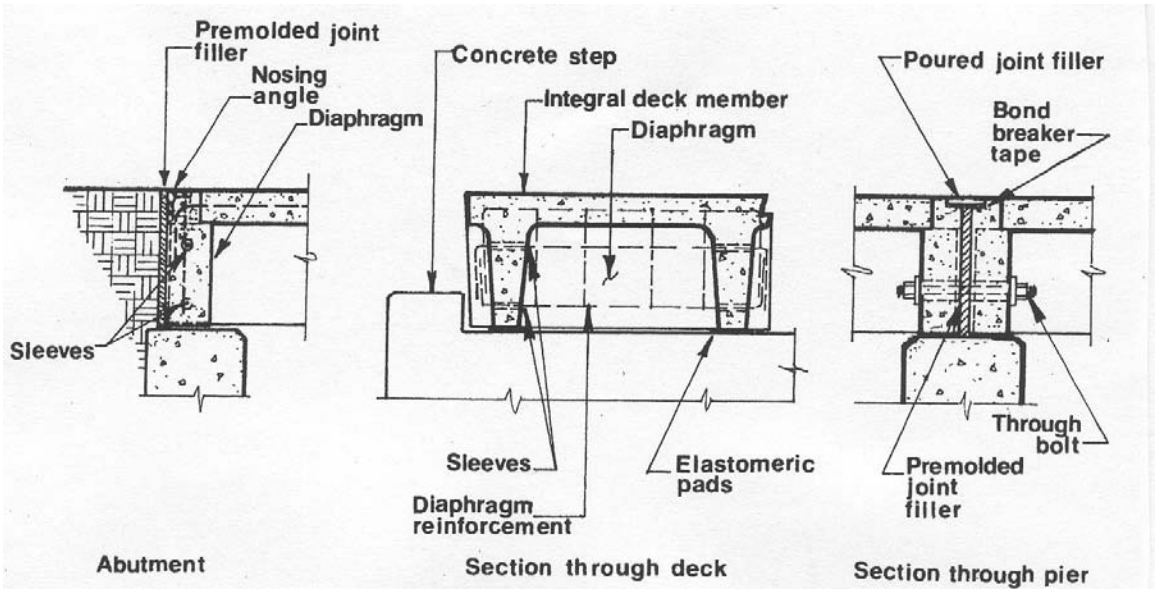

Figure A-32 Typical Transverse Deck Connections

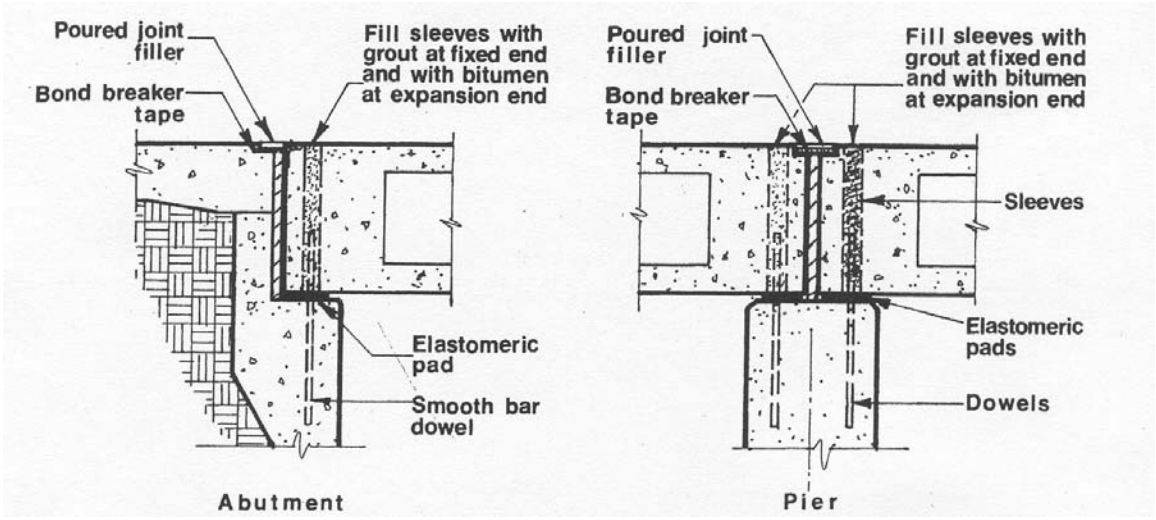

Figure A-33 Typical Transverse Deck Connections with Dowels

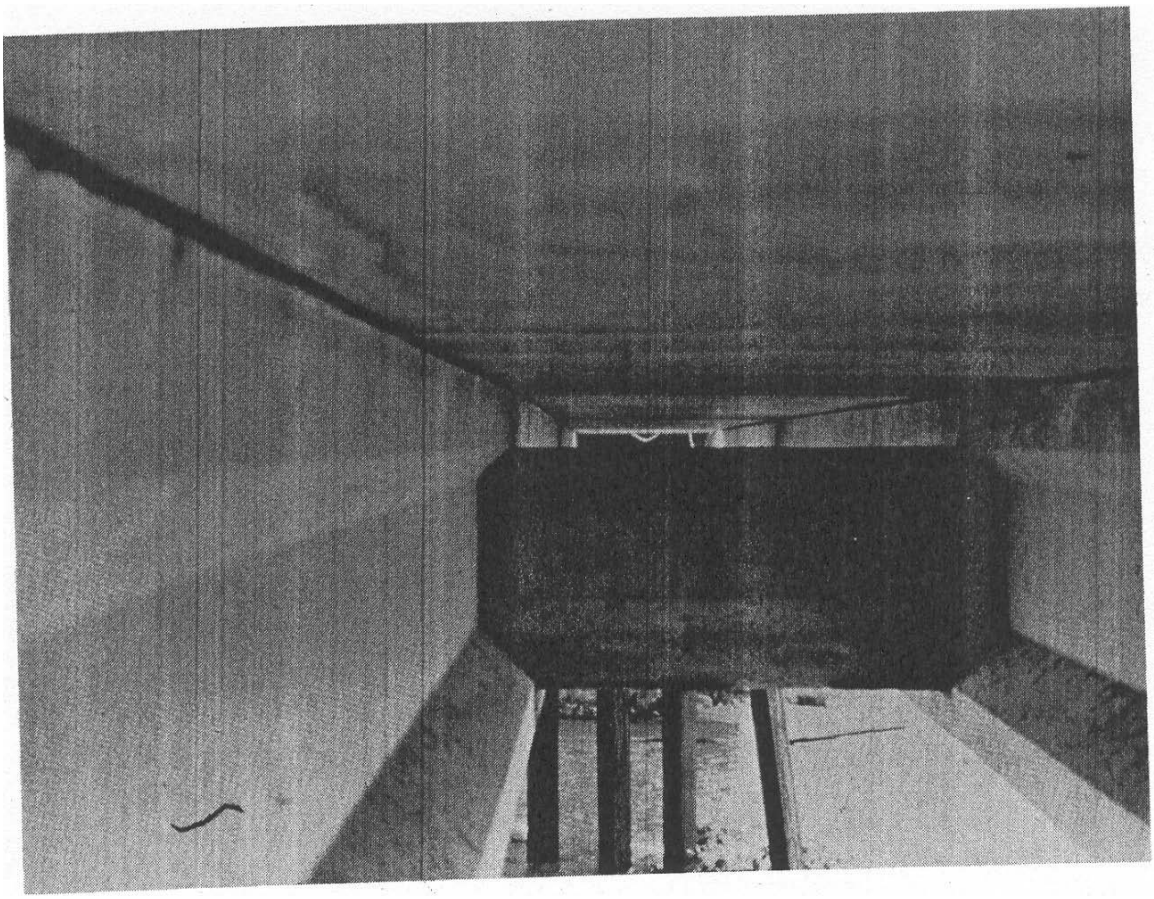

Figure A-34 Precast, field-attached diaphragm

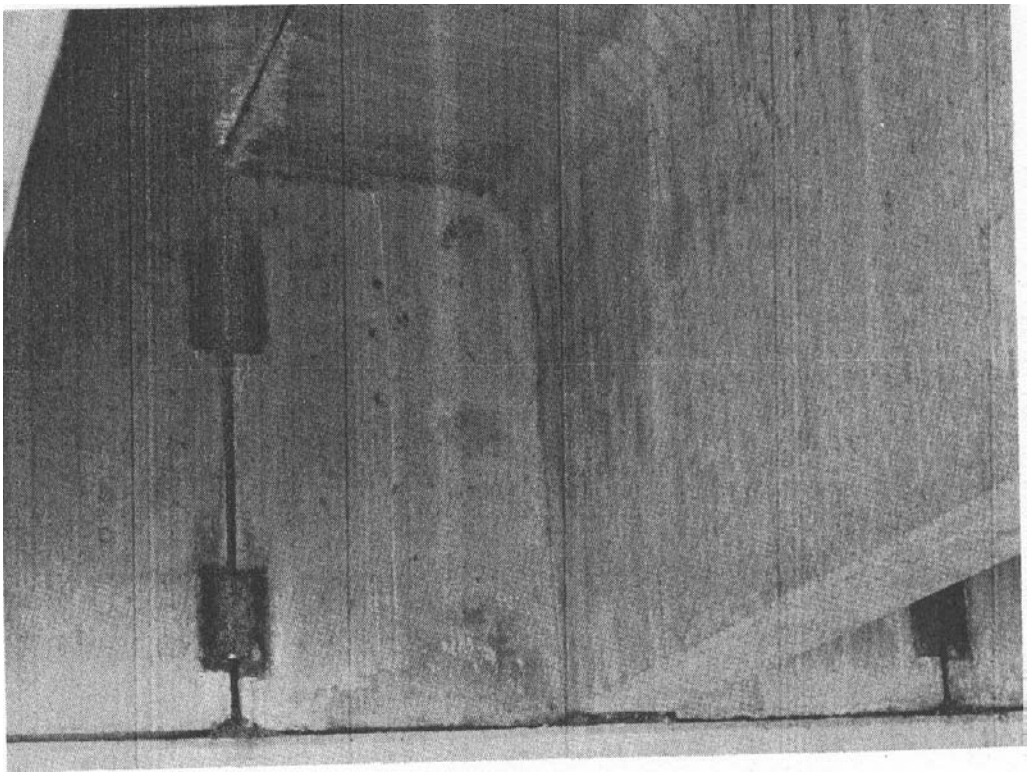

Figure A-35 Monolithic Diaphragm

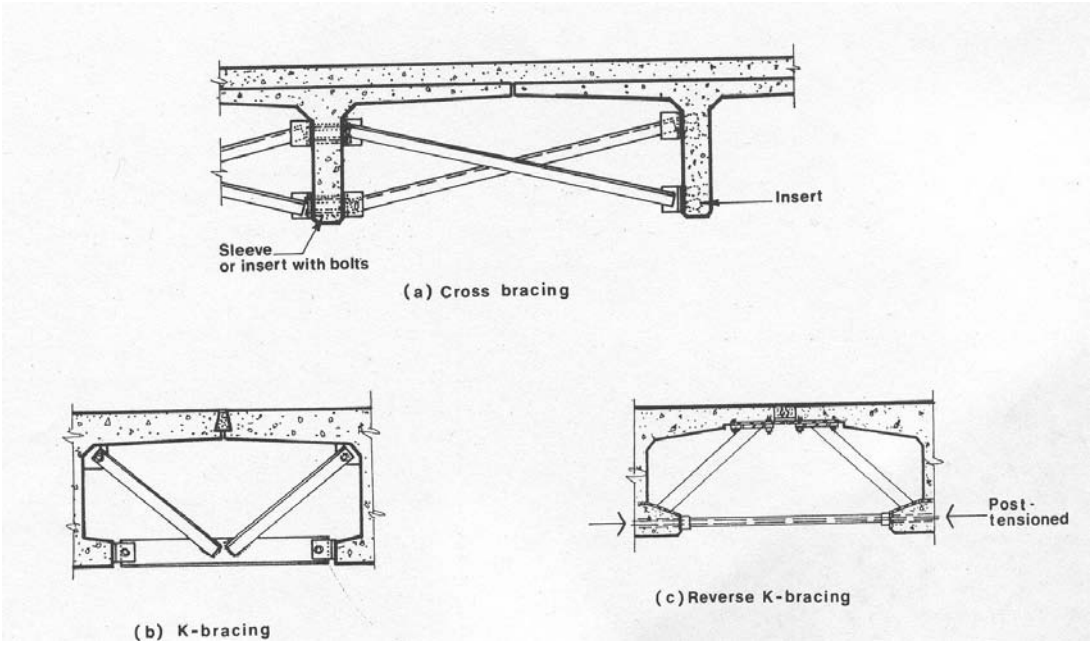

Figure A-36 Steel Diaphragms used in integral deck bridges

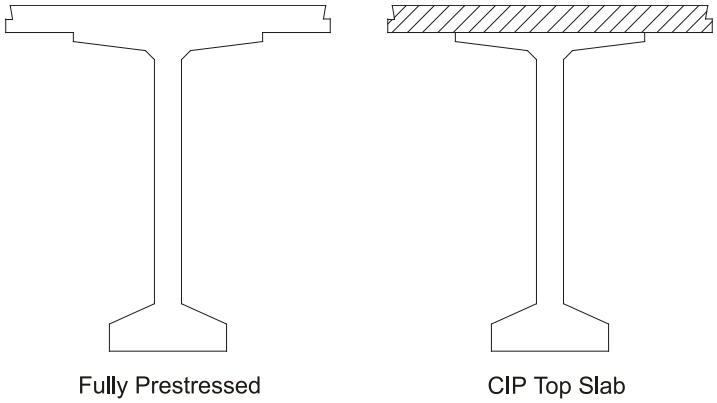

Figure A-37 Comparison between a fully prestressed section and hybrid prestressed concrete girder with integrally cast deck.

APPENDIX A - REFERENCES

A1. Stanton, J.F., and Mattock, A.H., "Load Distribution and Connection Design for Precast Stemmed Multibeam Bridge Superstructures," NCHRP Report No. 287, 1986, 140 pp.

A2. Martin, L.D., and Osborn, A.E.N., "Connections for Modular Precast Concrete Bridge Decks," Report No. FHWA/RD-82/106, US DOT, Federal Highway Administration, August, 1983, 117 pp.

A3. Martin, L.D., and Korkosz, W.J., "Connections for Precast Prestressed Concrete Buildings, Including Earthquake Resistance," Technical Report No. 2, Prestressed Concrete Institute, 1982.

A4. Hill, J.J., McGinnis, L.G., Hughes, W.R., and Shirole, A.M., "Design and Construction of Transversely Post Tensioned Concrete Bulb Tee Beam Bridge," Transportation Research Record 1180, pp. 87-89.

A5. Cotham, J., "Double Tee Field Study," Internal Report, Design Division, TxDOT, 1997.

A6 Russell, H. G., "Prefabricated Bridge Elements and Systems in Japan and Europe," Draft Report No. 3, August, 2004.

A7. Ong, N. N., "An Investigation of Joint Force in Precast and Prestressed Concrete Bulb Tee Multi-Beam Bridges," M.S. thesis, Iowa State University, 1981.

A8. Jones, "Lateral Connections For Double Tee Bridges," Report 1856 – 2, Texas Transportation Institute, April, 2001.

A9. Bakht, B. and Jaeger, L. G., "Bridge Analysis Simplified," McGraw Hill, 1985.

A10. Jones, H. L. and Boaz, I. B., "Skewed Discretely Connected Multi-Beam Bridges," Proc. ASCE, Journal of the Structural Division, Vol. 112, No. 2, 1986.

A11. Chaudhury, S. and Ma, Z., "Effect of Connections between Adjacent Units on Decked Precast, Prestressed Concrete Girder Bridges," Proceedings of PCI NBC 2004, Atlanta, October, 2004.

A12. Prestressed Concrete Institute, "PCI Design Handbook," 5th Edition, Chicago, 1999.

A13. Prestressed Concrete Institute, "Precast Prestressed Concrete Short Span Bridges –Spans to 100 Ft," Chicago, Ill., 1975.

A14. AASHTO, “LRFD Bridge Design Specifications,” Third Edition, American Association of State Highway and Transportation Officials, Inc., 2004.

A15. Hulsbos, C.L., “Lateral Distribution of Load in Multibeam Bridges,” Highway Research Board Bulletin, 1962.

A16. Sanders, W.W., and Elleby, H.A., “Distribution of Wheel Loads on Highway Bridges,” NCHRP Report 83, Highway Research Board, 1970.

A17. Zokaie, T., Osterkamp, T.A., and Imbsen, R.A., “Distribution of Wheel Loads on Highway Bridges,” Final Report, Vol. 1 and 2, Prepared for NCHRP, Transportation Research Board, National Research Council, Washington DC, 1991.

A18. Barr, P., Stanton, J., and Eberhard, M., “Live Load Distribution Factors for Washington State SR 18/SR 516 Overcrossing”, Research Report, WA-RD 477.1, Washington State Department of Transportation, Washington State Transportation Center (TRAC), University of Washington, Seattle, WA, February, 2000.

A19. Newmark, N. M., “Design of I-Beam Bridges,” Journal of the Structural Division, ASCE, V. 74, No. 1, 1948, pp. 305 – 330.

A20. AASHTO, “*Standard Specifications for Highway Bridges*,” 17th Edition, American Association for State Highway and Transportation Officials, Washington, D.C., 2002.

A21. Ma, Z. (J.), Hulsey, J. L., Millam, J., and Chaudhury, S., “A Note on Single Lane Live Load Distribution Factors for the Alaska Style Bulb-Tee Bridges,” Proceedings of the First National Bridge Conference, Nashville, TN, October 6-9, 2002.

A22. Ma, Z., Millam, J., Chaudhury, S., and Hulsey, J. L. “Field Test and 3D FE Modeling of Decked Bulb-Tee Bridges,” Proceedings of 3rd International Symposium on High Performance Concrete and the National Bridge Conference, October, 2003, Florida.

A23. Millam, J. and Ma, Z., “Single Lane Live Load Distribution Factor for Decked Precast/Prestressed Concrete Girder Bridges,” the TRB annual meeting, January, 2005, Washington D.C. (submitted).

A24. Ma, Z., Huo, X., Tadros, M. K., and Baishya, M., “Restraint Moments in Precast/Prestressed Concrete Continuous Bridges,” PCI Journal, Vol. 43, No. 6, Nov-Dec., 1998, pp. 40 – 57.

A25. Oesterle, R.G., Glikin, J.D., and Larson, S.C., “Design of Precast Prestressed Bridge Girders Made Continuous,” NCHRP Report 322, Transportation Research Board, 1989, 97 pp.

A26. Oesterle, R.G., Mehrabi, A.B., Tabatabai, H., Scanlon, A., and Ligozio, C.A., “Continuity Considerations in Prestressed Concrete Jointless Bridges,” Proceedings of the 2004 Structures Congress & Exposition, ASCE Structures Congress, Nashville, TN, May, 2004, pp. 23-26.

A27. Miller, R.A., Castrodale, R., Mirmiran, A., and Hastak, M., “Connection of Simple-Span Precast Concrete Girders for Continuity,” NCHRP Report 519, Transportation Research Board, 2004, 55pp.

A28. Ma, Zhongguo (John), Saleh, M.A., and Tadros, M.K., “Optimized Post-Tensioning Anchorage in Prestressed Concrete I-Beams**,”** PCI Journal, Vol. 44, No. 2, March-April, 1999, pp. 56-73.

A29. bdel-Karim, A. and Tadros, M. K., “State-of-the-art of precast/prestressed concrete spliced - girder bridges,” PCI publications, October, 1992.

A30. Owen, C.R., “Continuity Strengthens South Fork Hoh River Bridge Replacement,” PCI Journal, Vol. 32, No. 1, January-February, 1987, pp. 86-103.

A31. Husain, I, and Bagnariol, D, “Design and Performance of Jointless Bridges in Ontario- New Technical and Material Concepts,” Transportation Research Record 1696, Paper No. 5B0088, Ministry of Transportation of Ontario, Canada, 2000.

A32. McDonagh, M.D., and Hinkly, K.B., “Resolving Restraint Moments: Designing for Continuity in Precast Prestressed Concrete Girder Bridges,” PCI Journal, July-August, 2003, pp. 104-115.

A33. “Recommended Practice for Precast Post-Tensioned Segmental Construction,” PCI Journal, Vol. 27, No. 1, Committee Report, Joint PCI-PTI Committee on Segmental Construction, January-February, 1982, pp. 14-61.

A34. Anderson, A.R., “Stretched-out AASHTO-PCI Beams Types III and IV for Longer Span Highway Bridges,” PCI Journal, Vol. 18, No. 5, September-October, 1973, pp. 32-49.

A35. “Recommended Practice for Segmental Construction in Prestressed Concrete,” PCI Journal, Vol. 20, No. 2.

A36. Caroland, W.B., Depp, D., Janssen, H.H., and Spaans, L., “Spliced Segmental Prestressed Concrete I-Beams for Shelby Creek Bridge’” PCI Journal, Vol. 37, No. 5, September-October, 1992, pp. 22-33.

A37. Kozak, J.J., and Bezouska, T.J., “Twenty-Five Years of Progress in Prestressed Concrete Bridges,” PCI Journal, September-October, 1976, pp. 90- 101.

A38. Libby, J.R., “Long-Span Precast Prestressed Girder Bridges,” PCI Journal, July-August, 1971, pp. 80-98.

A39. Ebeido, T., Kennedy, J.B., “Shear and Reaction Distributions in Continuous Skew Composite Bridges,” Journal of Bridge Engineering, ASCE, Vol. 1, No. 4, 1996, pp. 155-165.

A40. Khaleel, M.A., and Itani, R.Y., “Live Load Moments for Continuous Skew Bridges,” J. Struct. Engrg., ASCE, 116(9),1990, pp. 2361-2373.

A41. Bishara, A.G., Liu, M.C., and El-Ali, N.D., “Wheel Load Distribution on Simply supported Skew I-beam Composite Bridges.” J. Struct. Engrg., ASCE, 119(2), 1993, pp. 399-419.

A42. Bishara, A.G., “Analysis for Design of Bearings at Skew Bridge Support,” Report ODOT 14346, Ohio Department of Transportation, Columbus, OH, 1984.

A43. Marx, H.J., Kachaturian, N., and Gamble, W.L., “Development of Design Criteria for Simply Supported Skew Slab-and-Girder Bridges,”Rep. No. 522, Civ. Engrg. Studies, University of Illinois, Champaign, IL, 1986.

A44. Mattock, A.H., and Kaar, P.H., “Precast Prestressed Concrete Bridges-6, Test of Half Scale Highway Bridge Continuous over Two Spans,” Journal of PCA Research and Development Laboratory, Vol. 3, No. 3, 1961, pp.30-70.

A45. Kostem, C.N., and deCastro, E.S., “Effects of Diaphragms on Lateral Load Distribution in Beam-Slab Bridges,” Transportation Research Record, Report No. 645, 1977.

A46. McCathy, W., White, K.R., and Minor, J., “Interior Diaphragms Omitted on the Gallup East Interchange Bridge- Interstate 40,” Journal of Civil Engineering Design, Vol. 1, No. 1, 1979, pp. 95-112.

A47. Sengupta, S., and Breen, J.E., “The Effects of Diaphragms in Prestressed Concrete Girders and Slab Bridges,” Research Report 158-1F, Center for Highway Research, The University of Texas at Austin, October, 1973.

A48. Tokerud, R., “Precast Prestressed Concrete Bridge for Low-Volume Roads,” PCI Journal, Vol. 24, No.4, 1979.

A49. Lall, J., Alampalli, S., and DiCocco, E.F., “In-Service Performance of Shear-Keys in Adjacent Prestressed-Beam Bridges,” TRB Meeting Publication, January, 1998.

A50. Lall, J., DiCocco, E.F., and Alampalli, S., “Full-Depth Shear-Key Performance in Adjacent Prestressed Beam Bridges,” Special Report 124, New York State Department of Transportation, 1997.

A51. Loo, Y.C., “Cracking of In Situ Connections in Prestressed Concrete Multibeam Bridges, Report No. 77/8, Institution of Engineers, Australia, 1977, pp. 46-50.

A52. Tadros, M. K. and Baishya, M. C., “Rapid Replacement of Bridge Decks,” NCHRP Report 407, Transportation Research Board, National Cooperative Highway Research Program, 1998.

A53. Tadros, Maher K., Badie, Sameh S., and Kamel, Mounir R., “Girder/Deck Connection for Rapid Removal of Bridge Decks”, *PCI Journal*, May/June, 2002, pp. 58-69.

A54. Mehrabi, A.B., “Workplan,” NCHRP Project No. 12-69, Design and Construction Guidelines for Long-span Decked Precast, Prestressed Concrete Girder Bridges, June 15, 2004, 21pp.

APPENDIX A - BIBLIOGRAPHY

Other Publications of interest not included in the list of References.

A1. Alaska DOT and PF, Standard Specifications for Highway Construction, 2004 http://www.dot.state.ak.us/stwddes/dcsspecs/assets/pdf/hwyspecs/english/2004sshc.pdf.

A2. Anderson, A.R., “Systems Concepts for Precast Prestressed Concrete Bridge Construction,” Special Report No. 132, Highway Research Board, 1972, pp. 9-21.

A3. Badie, S. S.; Baishya, M.C, and Tadros, M.K. “NUDECK-An Efficient and Economical Precast Bridge Deck System”, Precast/Prestressed Concrete Institute (PCI) Journal, September-October, Vol. 43, No. 5, 1998, pp. 56-74.

A4. Biswas, M., Osegueda, R.A., and Noel, J.S., “Scale-Model Tests for Full-Depth Precast Concrete Panel-Decked Composite Bridge Span,” Transportation Research Record, Vol. 1, Issue: 950, 1984, pp-163-173.

A5. Discussion by Bassi, and authors, Precast/Prestressed Concrete Institute (PCI) Journal, March-April, Vol. 44, No. 2, 1999, pp. 94-95.

A6. Erdicott, W.A., “‘Instant’ Bridges Keep Traffic on the Move,” PCI’s Ascent Magazine, 1993.

A7. Gulyas, R.J., Wirthlin, G.J., and Champa, J.T., “Evaluation of Keyway Grout Test Methods for Precast Concrete Bridges,” PCI Journal, Vol. 40, No. 1, January-February, 1995, pp. 44-57.

A8. Hays, C.O., Sessions, L.M., and Berry, A.J., “Further Studies on Lateral Load Distribution Using Finite Element Methods.” Transportation Research Record No. 1072, Transportation Research Board, Washington, DC, 1986, pp. 6-14.

A9. Huckelbridge, A.A, El-Esnawi, H, and Moses, F, “An Investigation of Load Transfer in Multi-Beam Prestressed Box Girder Bridges, Report No. FHWA/OH-94/002, Federal Highway Administration, 1993, 109 pp.

A10. Huckelbridge, A.A, Jr., El-Esnawi, H. and Moses, F., “Shear Key Performance in Multibeam Box Girder Bridges,” Journal of Performance of Constructed Facilities, Vol. 9, No. 4, 1995, pp 271-285.

A11. Illinois DOT; “Annual Survey of State Departments of Transportation on Implementation Status of LRFD”; Presentation at the Annual Meeting of the AASHTO Subcommittee on Bridges and Structures; Orlando, Florida; June, 2004.

A12. Issa, M.A., Ribiero do Valle, C.L., Abdalla, H.A., Islam, S., and Issa, M.A., “Performance of Transverse Joint Grout Material in Full-Depth Precast Concrete Bridge Deck Systems,” PCI Journal, July-August, 2003, pp. 92-103.

A13. Issa, M.A., Yousif, A.A., Issa, M.A, Kaspar, I.I., and Khayyat, S.Y., “Field Performance of Full Depth Precast Panels in Bridge Deck Reconstruction,” PCI Journal, Vol. 40, No. 3, May-June, 1995, pp. 82-108.

A14. Mast, R.F., “Lateral Stability of Long Prestressed Concrete Beams,” PCI Journal, Vol. 38, No. 1, January-February, 1993, pp. 70-88.

A15. Ma, Z., ., Tadros, M. K., and Baishya, M., “Shear Behavior of Pretensioned High Strength Concrete Bridge I-Girders,” ACI Structural Journal, Vol. 97, No. 1, Jan. – Feb. 2000, pp. 185 - 192.

A16. Merwin, D.P., “Prestressed Concrete Bridge Built in One Weekend,” PCI’s Ascent Magazine, Summer 2003, pp. 32-34.

A17. Nasser, K. W., “Design Procedure for Lateral Load Distribution in Multi-Beam Bridges,” PCI JOURNAL, V. 10, No. 4, August, 1965.

A18. Slutter, R.G., and Fisher, J.W., “Fatigue Strength of Shear Connectors,” Highway Research Record, No. 147, Highway Research Board, Washington, DC, 1966.

A19. Venuti, W.J., “Diaphragm Shear Connectors Between Flanges of Prestressed Concrete T-Beams,” PCI Journal, Vol. 15, No.1, 1970, pp. 67-78.

A20. Yamane, T., Tadros, M. K., Badie, S. S., and Baishya, M. C., “Full Depth Precast, Prestressed Concrete Bridge Deck System,” Precast/Prestressed Concrete Institute (PCI) JOURNAL, V43, N3, May-June, 1998, pp. 50-66.

APPENDIX B

QUESTIONNAIRE AND SURVEY SUMMARY

Questionnaire Recipients

Questionnaires were sent to transportation officials, designers, fabricators, and others to obtain knowledge on the current state of the practice in design and construction of decked precast prestressed concrete girder bridges. The questionnaire and the accompanying cover letter are included at the end of this appendix. A total of 137 questionnaires were sent out. Questionnaire responses were returned by 36 organizations. Transportation officials from 27 U.S. States, one county engineer, one consulting firm, three design firms, two girder fabricators, and two construction companies responded.

Previous Use of the System (Q1)

Of the 36 respondents, 14 indicated that they had experience with the DPPCG bridge system and returned partial or complete responses to the questionnaire. Of the 14 responses, 6 were from U.S. State transportation officials, one was from county engineer, three were from design firms, two were from girder fabricators, and two were from construction companies. Twenty-two respondents indicated that they have never used, designed, fabricated, or constructed any DPPCG systems. Out of these 22 responses, 21 were from U.S. State transportation officials, and one was from a consulting firm.

Tables B-1 through B-5 summarize the overall response to the questionnaire. Table B-1 summarizes the responses of those who have not used the system before. The name and category of the responding organizations are given in the first two columns. The following columns contain the reasons these organizations indicated for not using the system. Recipients of questionnaire were requested to select all applicable reasons from a given list and to provide any other reasons that are not on the given list. Following is the given list and the number of respondents who selected each reason (in parenthesis):

- Lack of specifications or guidelines (7)
- Unsatisfactory performance of joints between adjacent units (6)
- Difficulty in construction geometry control (6)

- Difficulty in future deck replacement (8)

A variety of other reasons were also indicated by the respondents. These included lack of experience with the system, heavy shipping weight, poor joint performance, greater cost than other alternatives, and satisfaction with cast-in-place decks.

Tables B-2 to B-5 summarize the responses of those who have used the system before. The following sections contain a summary of these responses.

Bridge Configuration (Q2)

The first two columns in Table B-2 provide the name and category of the responding organizations. Questionnaire recipients were requested to provide information on the commonly used span length, section shape, and cross-section dimensions. The next six columns summarize this information. The responses indicated that sections commonly used for DPPCG are either bulb-tees, double-tees, or tri-decks. The span ranges from 30 ft to 200 ft, with double-tees and tri-decks commonly used for shorter spans and bulb-tees used for longer spans. Only one respondent indicated the use 200 ft span, which was a spliced girder. Also one respondent indicated the use of 160 ft span. Several respondents indicated the use of 150 ft span. The depth of the bulb-tee section varies from 35 in. to 66 in., while the depth for the double-tee section varies from 20 in. to 36 in., and the depth for the tri-deck section is typically 27 in. The width of the top flange varies from 4 ft up to 9 ft.

Longitudinal Connection Between Adjacent Units (Q3, Q4)

The questionnaire requested information regarding the types and design of connections between adjacent units. This information is summarized in the following two columns in Table B-2. Thirteen organizations provided information on the type of the connection. All thirteen respondents indicated the typical use of a combination of steel shear connectors, spaced at intervals of 4 ft to 5 ft on center, and a grouted longitudinal shear key. Figures B-1 to B-8 show the details provided by respondents. Different organization indicated different details for the shear connector as well as variations in the shape of the shear key. Eight organizations provided information regarding the design procedure for the connection. Three respondents indicated that they used

standard details with no design involved. The remaining five respondents named different design sources that varied from one organization to the other.

Skew (Q5)

Table B-3 summarizes the information regarding skew for DPPCG bridges, intermediate diaphragms, and wheel load distribution. The first column provides the name of the respondent organization. The next three columns summarize the information regarding the skew. Thirteen organizations provided information on the commonness of skewed bridges and the range of skew angles. The commonness varied form not common to very common. Skew angles of up to 60^o are used. One respondent indicated the use of 10^o skew angle; six respondents indicated skew angles of up to 30^o; one respondent indicated skew angles of up to 40^o; two respondents indicated skew angles of up to 45^o; one respondent indicated skew angles of up to 50^o; and two respondents indicated skew angles of up to 60^o.

Seven respondents provided information regarding how skew is taken into account in design. The answers varied from one organization to the other. Sample answers included design as non-skewed, the use of AASHTO LRFD reduction of load distribution factors for moment in longitudinal beams on skewed supports, shear distribution increase, flaring deck rebars on the skew, and setting bearing elevations so that edges of girders line up.

Intermediate Diaphragms (Q6)

Questionnaire recipients were requested to provide information on the use and type of intermediate diaphragms. This information was returned by fourteen organizations and is given in the next column in Table B-3. Typical intermediate diaphragm details used by different organizations are shown in Figures B-9 to B-11. One respondent indicated none use of intermediate diaphragms. The reaming thirteen respondents indicated the use of concrete diaphragms, with three respondents indicating steel diaphragms as an alternative. Two respondents indicated a maximum spacing of 40 ft for concrete diaphragms and one respondent indicated a maximum spacing of 25 ft for steel diaphragms. For cast in place concrete diaphragms, concrete is typically deposited into diaphragms through holes in flanges.

Load Distribution (Q7)

The next column in Table B-3 contains information regarding the wheel load distribution. Eleven respondents provided such information. All eleven responses referred to different parts of AASHTO Standard or LRFD as the method used to calculate the load distribution.

Span-to-Span Connection Over the Pier (Q8)

Table B-4 summarizes the information regarding the span-to-span connection, the issue of deck replacement, grout specifications, and use of an overlay. The first column in Table B- 4 provides the name of the respondent organization. The next column provides information regarding design and detail of span-to-span connection on the pier. Ten respondents provided this information. Typical details provided by respondents are shown in B-s 12 to 14. Two respondents indicated that they have only used single spans. Four respondents indicated that the girders are designed as simply supported either with expansion joint or ignoring the flexure of the slab at the joint. Two respondents used pier diaphragm and extended the deck reinforcing and the prestressing strands into the diaphragm (B- 14). Another respondent made the girders continuous by welding or mechanically connecting rebars projecting from top flange. Another respondent indicated a monolithic connection.

Deck Replacement (Q9)

The next two columns in Table B-4 provide information on the deck replacement issue. Twelve respondents provided information regarding accommodation for future deck replacement. One respondent indicated that they accommodate for future deck replacement by use of a 4 in. ACP and grinding off 2 in. Eleven respondents indicated that they do not accommodate for future deck replacement. The reasons included that the deck concrete is of same high quality concrete as girder with thirty years of success without any need to replace deck, use of overlays, no use of salts in some parts of the country, deck replacement requires shoring or point supports and the integrity of the finished girder may not be as expected, decked girders are used for roads with low volume of traffic, use of air entrained and epoxy bars, and that the girder and the deck are considered as one unit since they are prestressed as one unit.

Ten respondents answered the question whether they would use deck replacement if it was technically feasible. Five respondents indicated that they would use deck replacement and five respondents indicated that they would not use it. The reasons for not using deck replacement included that deck replacement is not needed in places that do not use salts, difficulty, and preferring to overlay the bridge.

Grouting of the Longitudinal Joints (Q10)

Questionnaire recipients were asked whether or not they have developed specification for the grout properties and the grouting process. This information was returned by twelve respondents and is given in the following column in B- 4. Five respondents have not developed specifications for the grout. Three respondents use Washington State DOT standard specifications. One respondent uses standard non-metallic non-shrink grout. The remaining three respondents did not provide details regarding what specifications they use.

Use of Overlay (Q11)

The next four columns in Table B-4 provide information regarding the use of overlays and treatment of the top surface of the deck. Most DPPCG bridges use overlay. The most common overlay is the asphalt overlay with thickness from 2 in. to 4 in. Three respondents indicated they use concrete overlay with 2 in. to 5 in. thickness for 10% to 25% of their bridges. When overlay is not use, the surface treatment methods included heavy broom finish, grinding in the field after construction, and grooving in the precast plant.

Problems In Service (Q12)

Table B-5 provides information related to the problems encountered in service, overall evaluation of the DPPCG bridges, developments of guidelines or specification for design, fabrication, or construction of DPPCG bridges, and the major difficulties for extending the span length beyond what is being used. The first column provides the name of the respondent organization. The next column provides information regarding the encountered problems. Ten respondents provided this question. Three of them indicated no problems encountered. Six respondents indicated problems with the longitudinal joints, mainly in the form of longitudinal cracks. One respondent indicated

problems with hairline cracking between top of web and bottom of top flange and cracking in end diaphragms at girder bottom flange interface. Another respondent indicated also problems with web and bottom flange cracking at intermediate support due to restraint moment.

Overall Evaluation and Future Use (Q13)

Questionnaire recipients were requested to provide an overall evaluation of the DPPCG system and to indicate whether or not they will use such system in future projects. The overall evaluation of the bridge was returned by thirteen organizations and is given in the next column in Table B-5. Three respondents gave a rating of excellent, seven gave a rating of good, and three gave a rating of fair. The next column provides information regarding the use of DPPCG bridges in future projects. All seven respondents who answered this question indicated that they would continue to use the system in the future. However, some respondents commented that the use of the system is confined to the local road system with low ADT.

Design Guidelines (Q14)

The next column in Table B-5 provides information regarding the development of guidelines or specifications for design, fabrication, or construction of DPPCG systems. Twelve organizations returned this information. Five respondents indicated that they have developed some design guidelines for this type of bridge, while six respondents indicated that they have not. One respondent indicated that they used some information from Washington State Department of Transportation Bridge Design Manual.

Major Difficulties for Extending Span Length (Q15)

The questionnaire requested information regarding the major difficulties for extending span length for DPPCG bridges beyond what is being used. Recipients of questionnaire were requested to select all applicable reasons from a given list and to provide any other reasons that are not on the given list. The next six columns in Table B-5 provide this information. Following is the given list and the number of respondents who selected each reason (in parenthesis):

- Weight (11)

- Length (3)
- Lack of demand for product (3)
- Cost of forms (0)
- Lack of availability of design and construction guidelines (2)

Other reasons given by respondents included camper disparities between beams, lack of spliced girder guidelines for decked members, fabrication yard limitations, stability, and height to depth ratio of the girder.

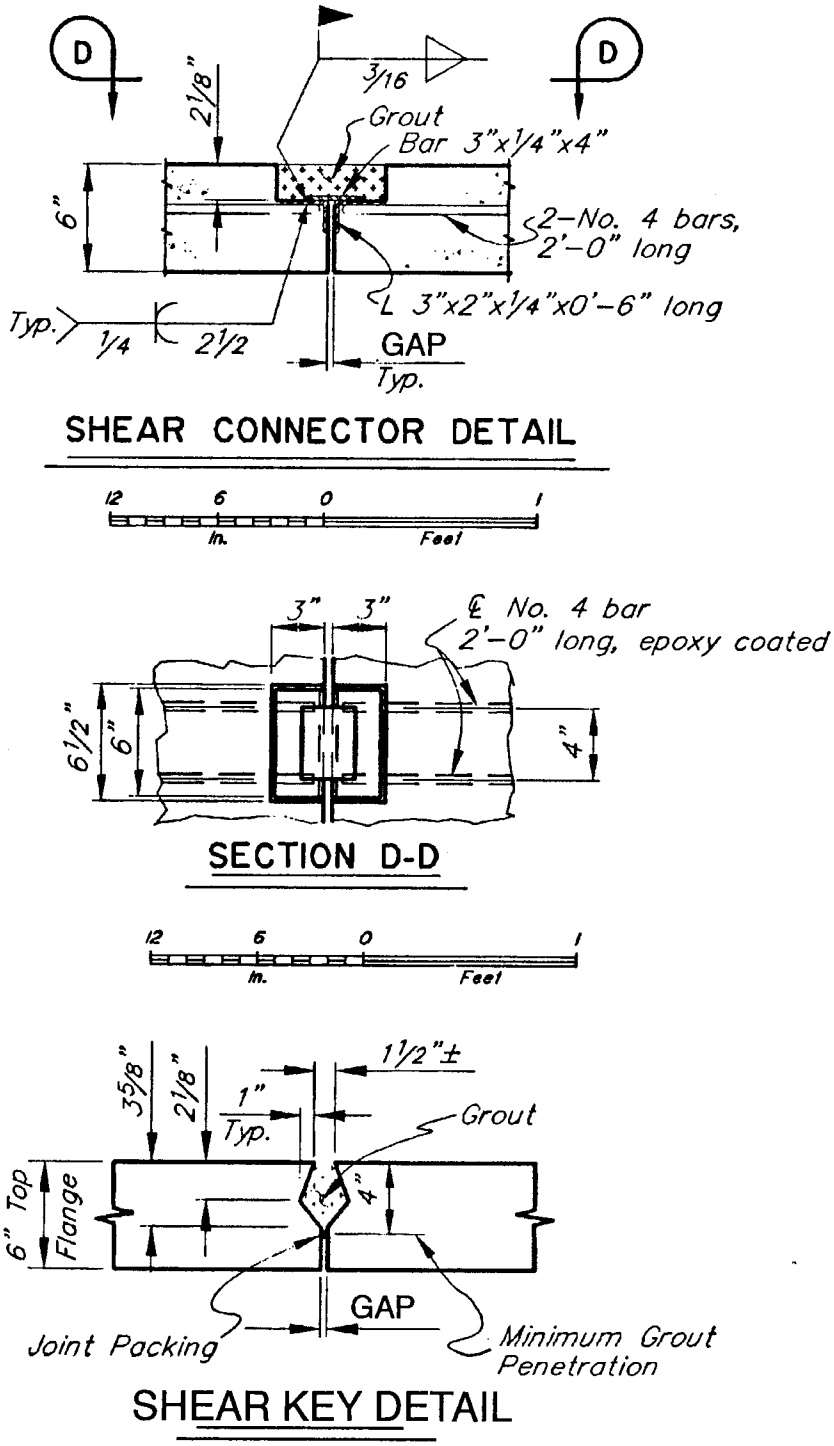

Figure B-1 Typical connection detail used by Alaska DOT

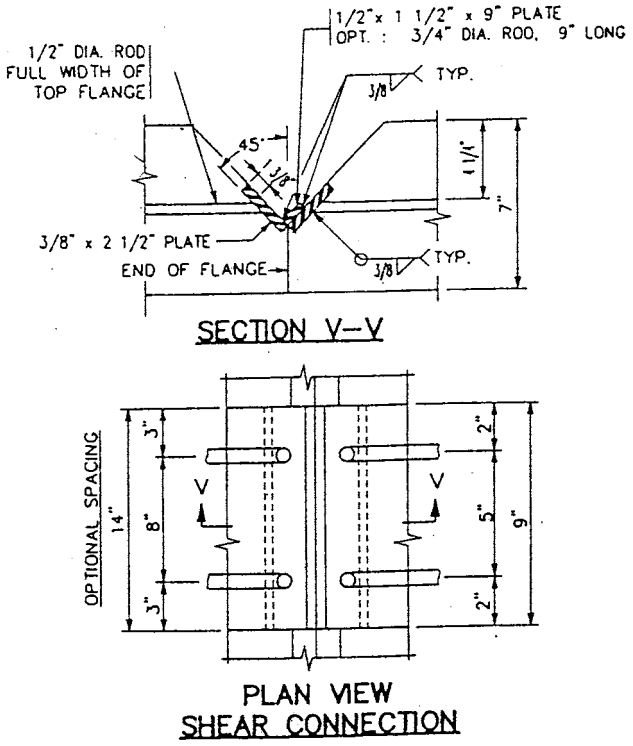

Figure B-2 Typical connection detail used by Minnesota DOT

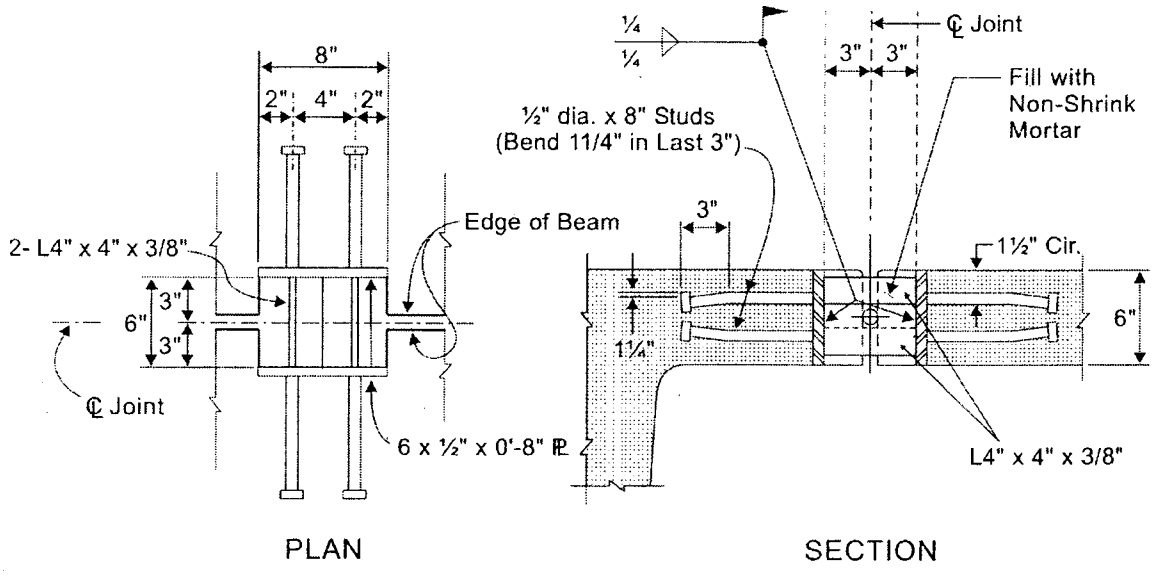

Figure B-3 Typical connection detail used by Texas DOT

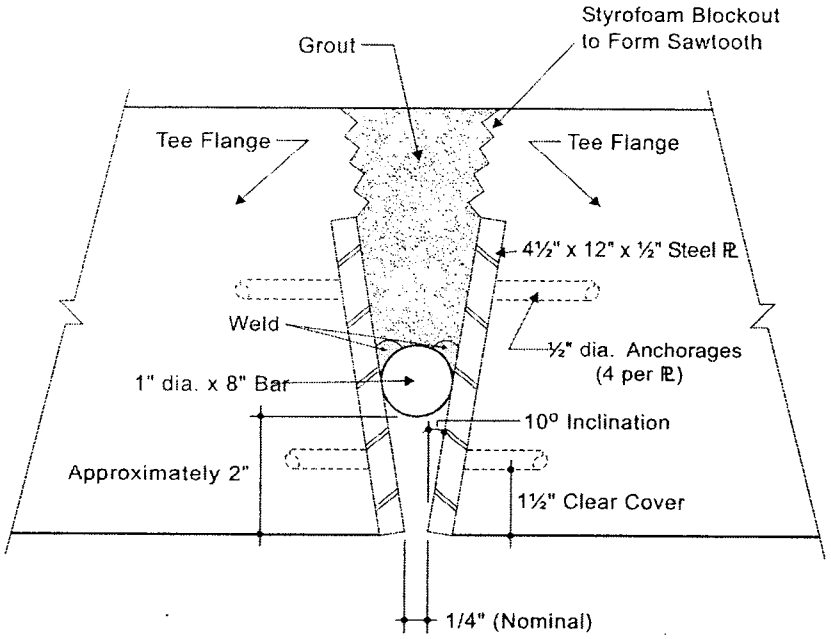

(a) Section Through Bar/Plate

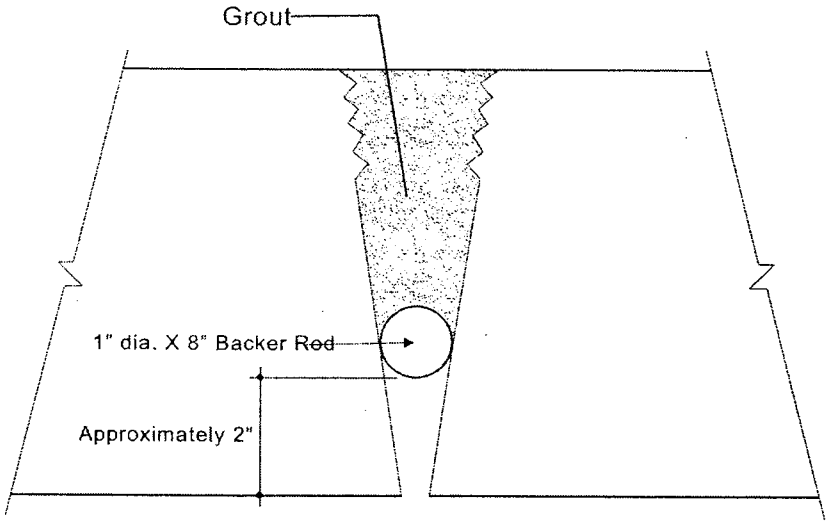

(b) Section at Other Locations

Figure B-4 Connection detail proposed by Texas DOT

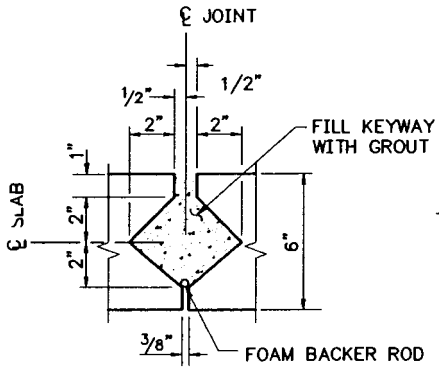

Keyway

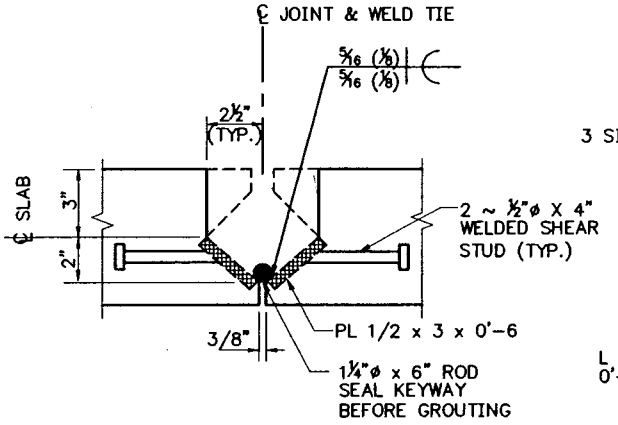

Weld Tie, Alternative #1

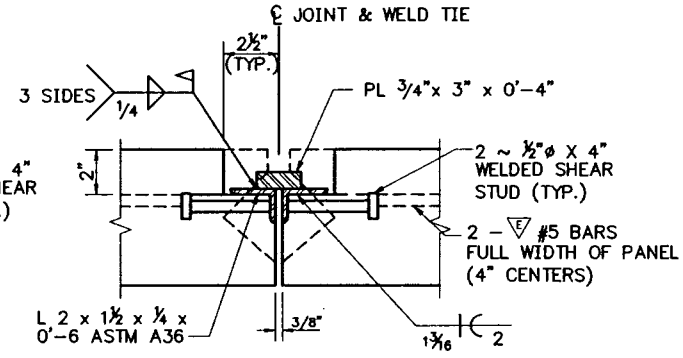

Weld Tie, Alternative #2

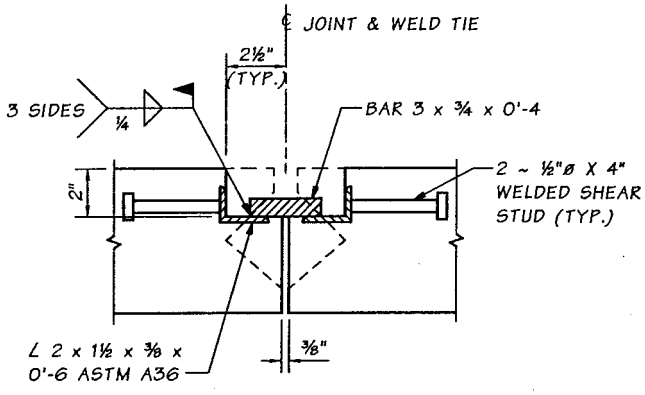

Weld Tie, Alternative #3

Figure B-5 Typical connection details used by Washington State DOT

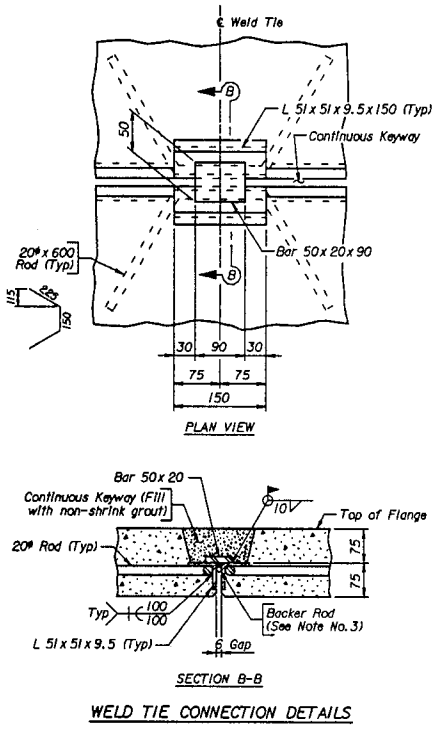

Figure B-6 Typical connection detail used by Wyoming DO

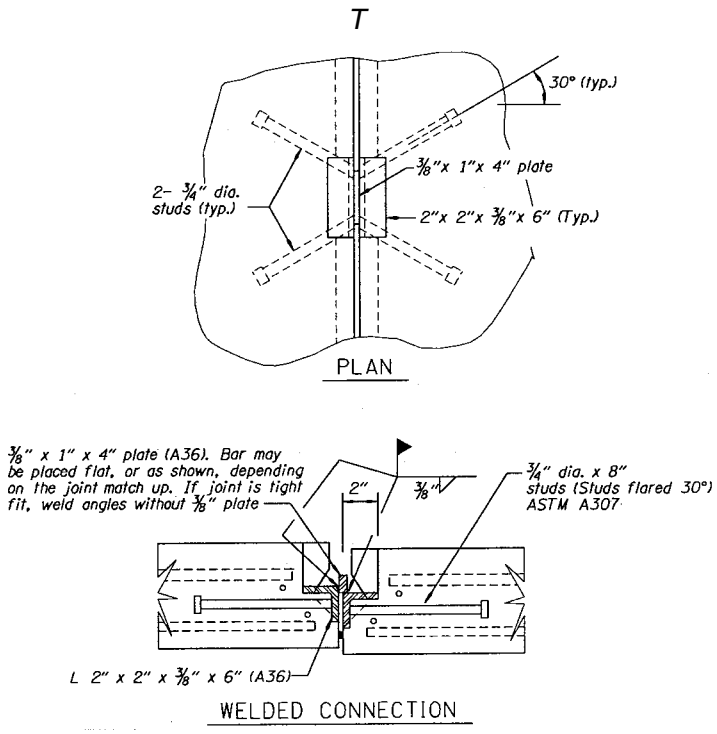

Figure B-7 Typical connection detail used by Oregon DOT

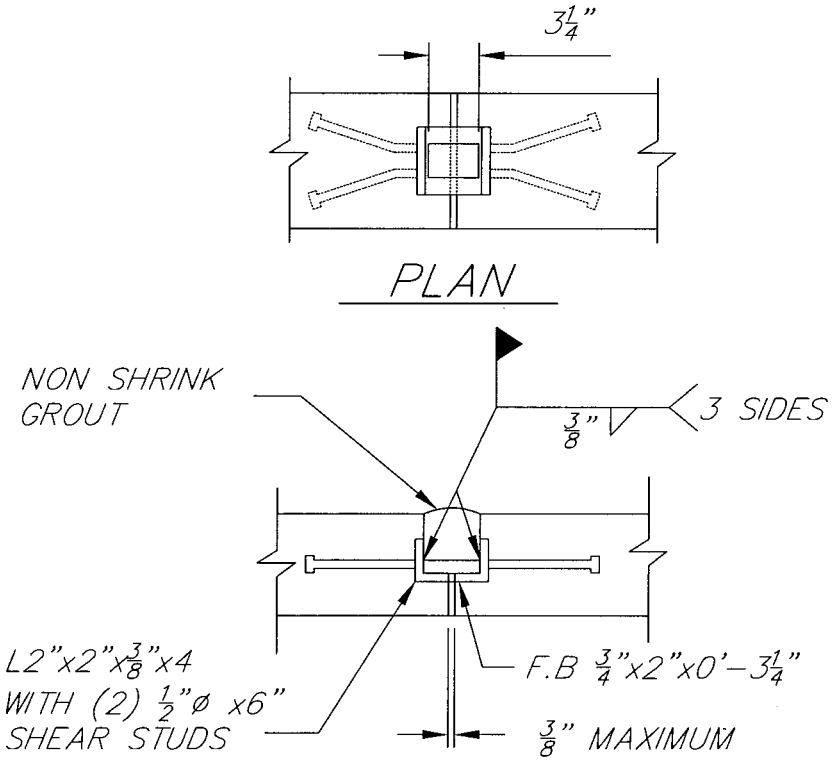

Figure B-8 Typical connection details used by Nicholls Engineering

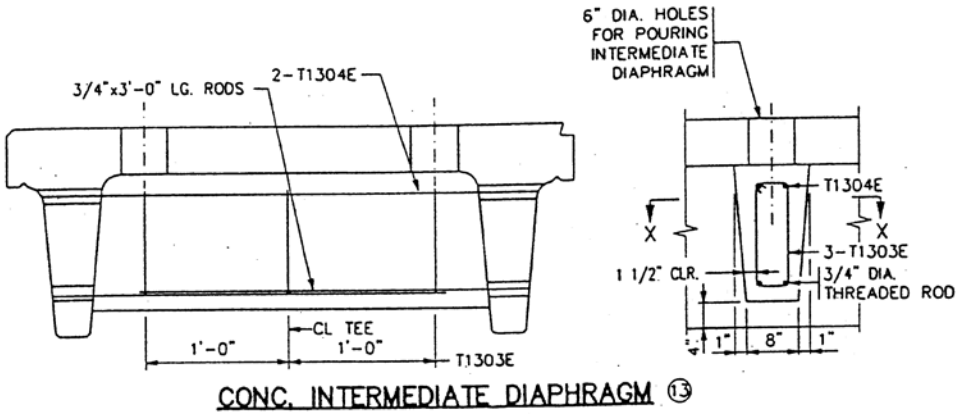

Figure B-9 Typical cast-in-place intermediate concrete diaphragm for Double-Tee girders

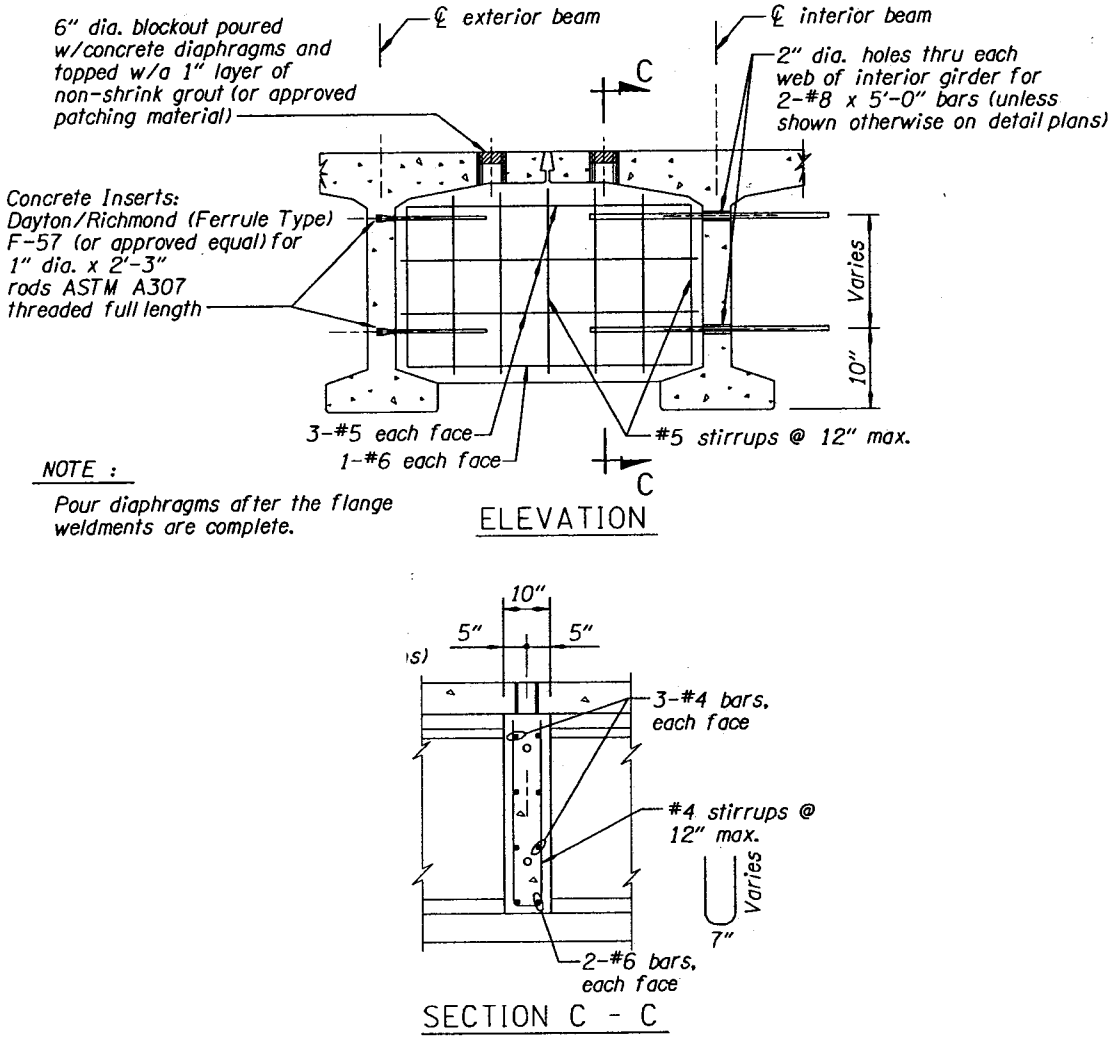

Figure B-10 Typical cast-in-place intermediate concrete diaphragm for Bulb-Tee girders

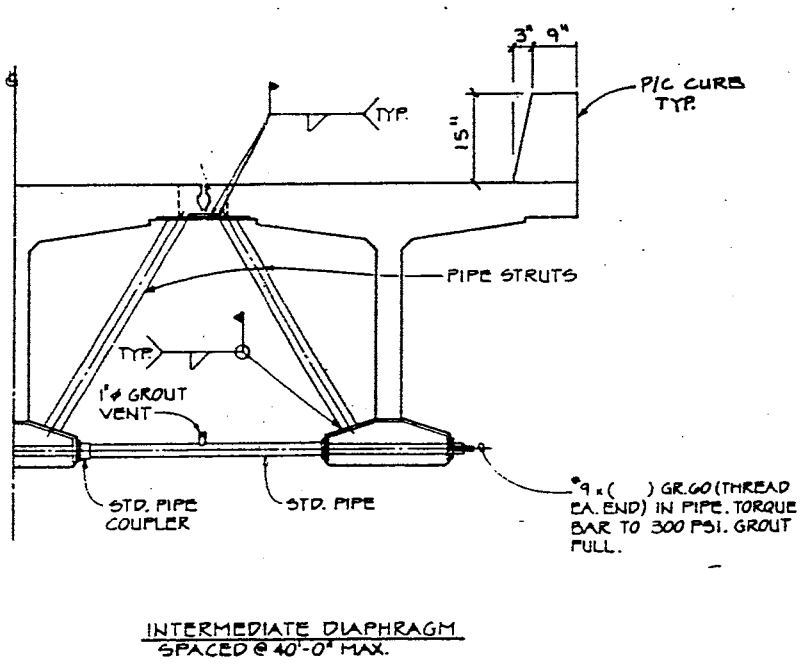

Figure B-11 Example for intermediate steel diaphragm for Bulb-Tee girders

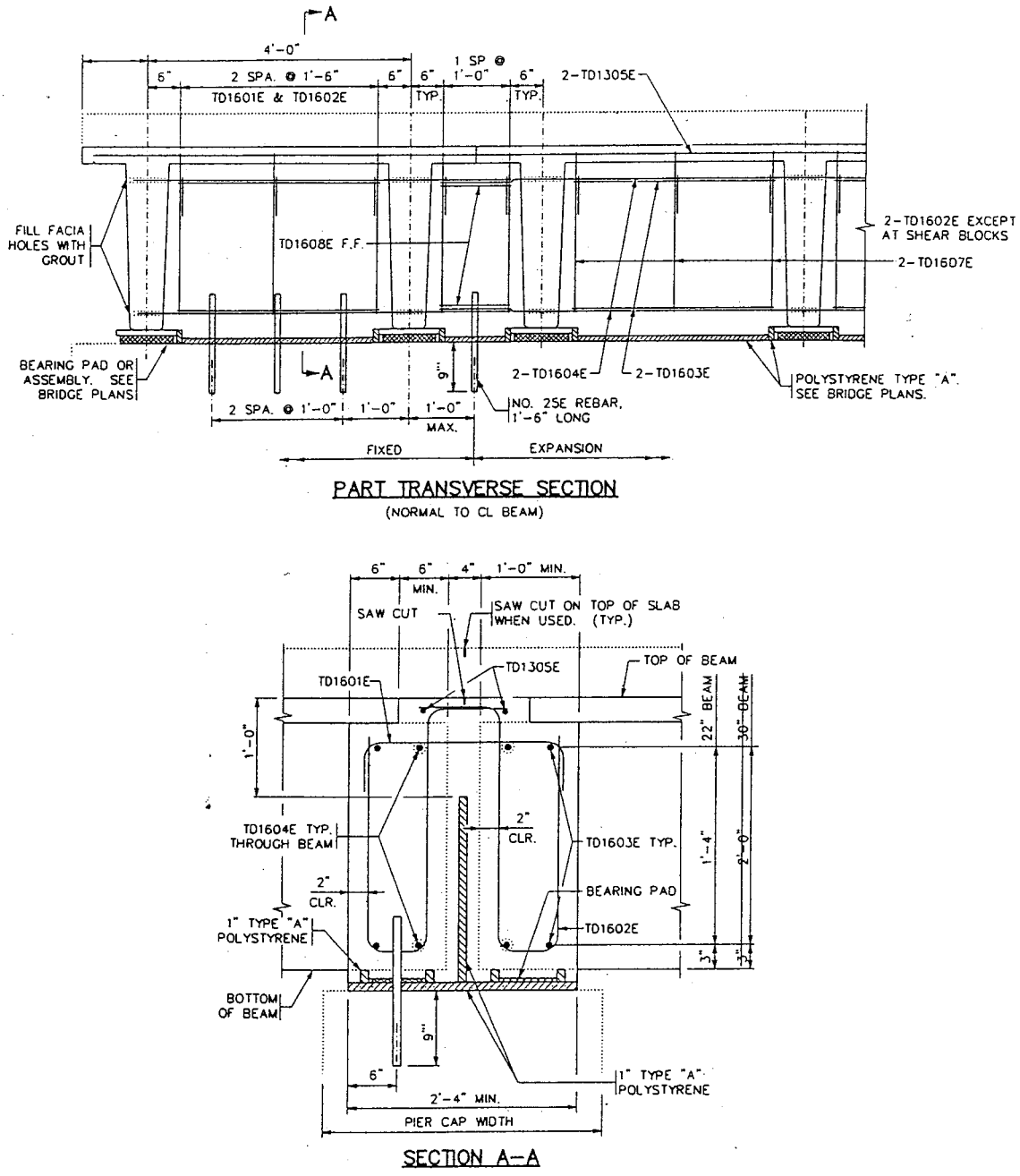

Figure B-12 Concrete pier diaphragm used by Minnesota DOT

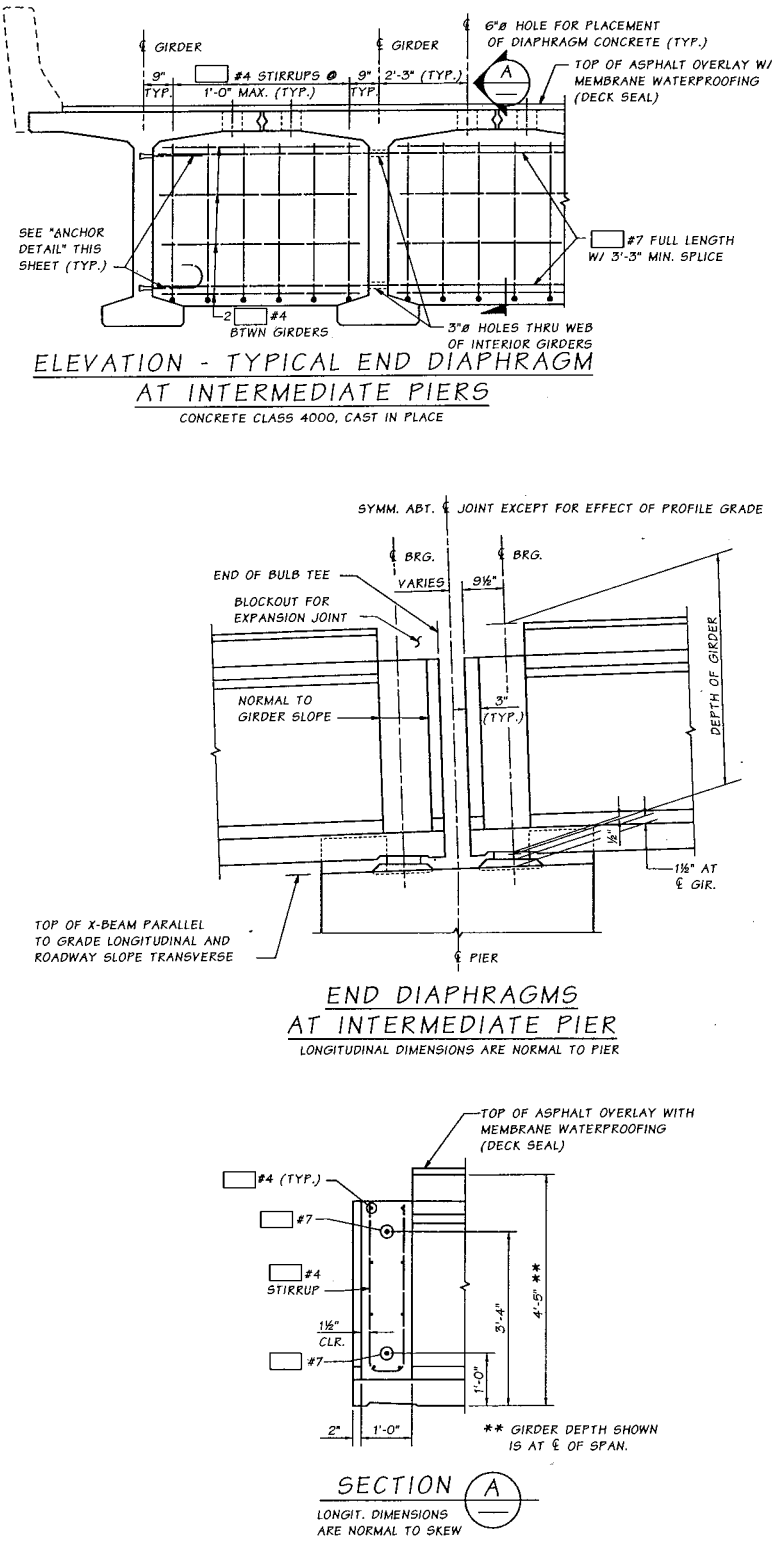

Figure B-13 Concrete pier diaphragm used by Washington State DOT

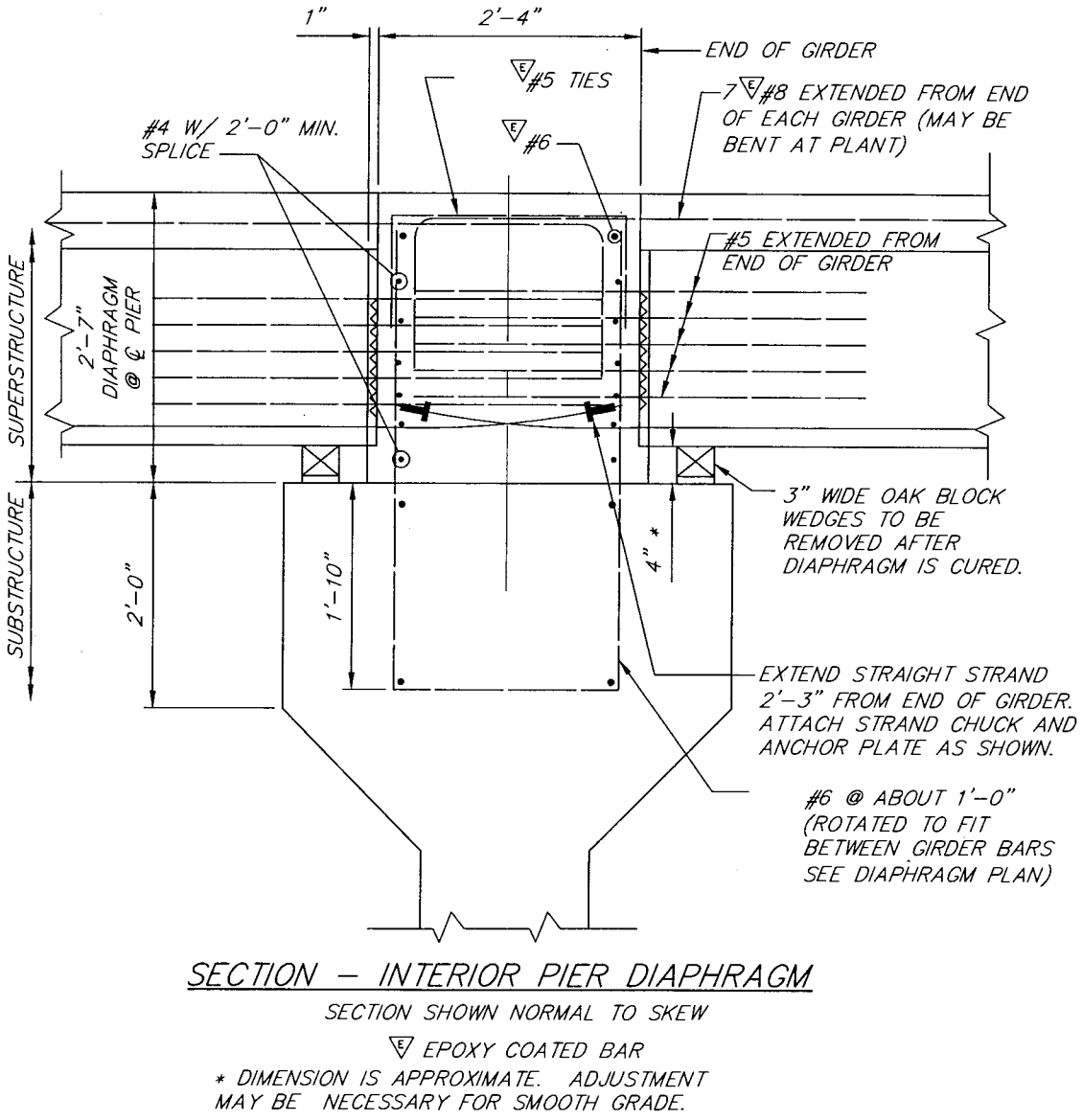

SECTION – INTERIOR PIER DIAPHRAGM

SECTION SHOWN NORMAL TO SKEW

EPOXY COATED BAR

* DIMENSION IS APPROXIMATE. ADJUSTMENT MAY BE NECESSARY FOR SMOOTH GRADE.

Figure B-14 Concrete pier diaphragm used by Nicholls Engineering

Table B-1 Questionnaire summary for respondents who did not use DPPCG

Respondent	Organization Category	Reasons DPPCG not used*				
		a	b	c	d	Other
Georgia DOT	DOT				X	Cast in place decks seem to be satisfactory
Hawaii DOT	DOT	X				---
Indiana DOT	DOT	X				---
Iowa DOT	DOT		X			---
Kansas DOT	DOT					Other options available
Louisiana DOT	DOT					No experience with DPPCG
Massachusetts Highway Department	DOT					Never considered using such system
Missouri DOT	DOT		X		X	---
Nebraska Department of Roads	DOT			X		Simply did not use it
Nevada DOT	DOT	X				---
New Mexico State Highway and Transp. Dept.	DOT		X	X	X	Heavy shipping weight
New York State DOT	DOT		X			Poor joint performance from similar systems
North Carolina DOT	DOT					In planning stages for 1st trial deck bulb-tee bridge
North Dakota DOT	DOT	X		X	X	Not familiar with this type of bridge
Pennsylvania DOT	DOT	X	X		X	Cost of this is greater than other alternatives
South Carolina DOT	DOT					No interest expressed by contractor /fabricator
Tennessee DOT	DOT		X	X	X	---
Utah DOT	DOT			X		Construction issues with heavy lifts, connections between segments
Vermont Agency of Transportation	DOT	X			X	---
Virginia DOT	DOT	X		X	X	---
Wisconsin DOT	DOT					Not economical
Wiss, Janney, Elstner Associates, Inc.	Consulting					Do not design new bridges
	Total No.	7	6	6	8	

*Reasons DPPCG not used
a. Lack of specifications or guidelines
b. Unsatisfactory performance of joints between adjacent units
c. Difficulty in construction geometry control (camber, cross slope, and skew)
d. Difficulty in future deck replacement

Table B-2 Questionnaire summary for configuration and longitudinal connection

Respondent	Organization Category	Configuration						Longitudinal Connection	
		Span	Sec.	Depth	Top Fl	Web	Bot Fl	Detail	Design
Alaska DOT & Public Facilities	DOT	60'-150'	Decked bulb-tee	42", 54", 66"	4'-1" to 8'-6"	6"	25"	Long. shear key with steel shear connectors @ 4' o.c.	Standard key detail
Idaho Transportation Department	DOT	60'-125'	Bulb-tee	Varies	Varies	---	---	Weld tie & grout key between flanges; CIP intermediate & end diaphragms	---
Minnesota DOT	DOT	50'-71' 60'-100'	Double Tee Bulb Tee	22", 30"	6' & 8'	6"	n/a	Long. shear key with steel shear connectors @ 4' o.c.	PCI and AASHTO recommendations
Texas DOT	DOT	30'-60'	Double Tee	20.5" - 36"	6' & 8'	6"-7.75"	n/a	Angles welded to embedded plates and filled with non-shrink grout. 1" diameter steel rod running parallel to the joint and welded to steel plates embedded in beam flanges with gap filled with non-shrink grout.	Research report "Lateral connections for double Tee bridges" by Harry Jones, TTI, 2001
Washington State DOT	DOT	40'-160'	Decked bulb-tee Double-T Tri Rib.	35",41", 53",65" 20"-36" 27"	4'- 6' 7'- 9' 4'- 6'	6" 6.5"-7.5" 5.25"	25" --- ---	Welded tie at 4 to 5 ft spacing and continuous grouted key	NCHRP report 287
Wyoming DOT	DOT	max 36'	Trideck	27"	6'	5.25"	---	Welded tie connection	AASHTO

Table B-2 Questionnaire summary for configuration and longitudinal connection (continued)

Respondent	Organization Category	Configuration						Longitudinal Connection	
		Span	Sec.	Depth	Top Fl	Web	Bot Fl	Detail	Design
Morse Brothers, Inc. (OR)	Fabricator	---	Deck bulb-tee	36",45", 60"	max 8'	6"	24"-26"	Weldments and shear key	---
Concrete Technology Corporation (WA)	Fabricator	max 168'	Bulb-tee	35",41", 53",65"	4'-8'	---	---	Continuous shear key with welded connections at 4-5' on center	Standard connections based on experience
Nicholls Engineering (WA)	Design	20'-200'	Trideck Bulb tee	---	---	---	---	Weld tie with tapered edges, 5' maximum o/c	---
Aggpro (AK)	Construction	up to 150'	Bulb-tee	42",54", 66"	---	6"	25"	Shear connector	---
Shearer Design (WA)	Design	---	Bulb-tee	---	---	---	---	---	Standard detail
Grant County Engineer (WA)	County	80'-120'	Bulb-tee	---	---	---	---	Weld ties, end and intermediate diaphragms	---
Sargent Engineers (WA)	Design	80'-150'	Bulb-tee	---	---	---	---	Welded connections	In house procedure for transfering the wheel load shear between girders
N. A. Degerstrom, Inc. (WA)	Construction	30'-145'	Trideck Bulb tee	---	---	---	---	Weld tie plates at approximately 5' o.c.	---

Table B-3 Questionnaire summary for skew, intermediate diaphragms, and load distribution

Respondent	Skew			Intermediate Diaphragms	Wheel load distribution
	How common	Skew angle	Deign		
Alaska DOT & Public Facilities	50%	0 to 45^{o}	Shear distribution increase, girder camber adjustment, end diaphragm and deck reinforcing	Single CIP	AASHTO equations and "lever rule"
Idaho Transportation Department	---	---	---	CIP concrete diaphragm. Concrete is deposited into diaphragms through holes in flanges.	AASHTO LRFD code
Minnesota DOT	30-35%	5 to 30^{o}	Flare deck bars on skew	Concrete intermediate diaphragms for spans of 40' or more	AASHTO Standard or AASHTO LRFD for multi-beam decks
Texas DOT	Only one bridge	10^{o}	Designed as non-skewed	None	For AASHTO stand. designs, distribution is based on research and in-house studies. For LRFD desings, use LRFD equations for not sufficiently connected.
Washington State DOT	Relatively common	Up to 30^{o}	LRFD Table 4.6.2.2.2e-1 and 3c-1	Concrete diaphragms	LRFD Table 4.6.2.2.2b-1 & 3b-1
Wyoming DOT	Not common	30^{o}	---	Concrete	AASHTO - T beam distribution

Table B-3 Questionnaire summary for skew, intermediate diaphragms, and load distribution (continued)

Respondent	Skew			Intermediate Diaphragms	Wheel load distribution
	How common	Skew angle	Deign		
Morse Brothers, Inc. (OR)	Common	Up to 45^{o}	---	Concrete or steel	AASHTO
Concrete Technology Corporation (WA)	Fairly common	Up to 60^{o}	---	Concrete at 40' o.c. or galvanized steel at 25' o.c.	AASHTO provisions for adjacent precast members
Nicholls Engineering (WA)	Very commom	Up to 60^{o}	By special design program which sets specific pier elevations based on girder spacing, skew, grade, and girder camber at time of set	8' cast in place at maximum 40' o/c	AASHTO 3.23.4.3 multi beam bridges
Aggpro (AK)	50%	0 to 30^{o}	---	Cast in place	---
Shearer Design (WA)	Some	0 to 30^{o}	Design for shear is per AASHTO	Cocrete CIP or steel	AASHTO LRFD formula
Grant County Engineer (WA)	20-30%	10 to 40^{o}	---	Cast in place or precast	---
Sargent Engineers (WA)	20-30%	0 to 30^{o}	Setting bearing elevations so edges of girdres line up	Cast in place concrete	AASHTO procedure for both single and multi-lane bridges; (K) type bridge with connections only enough to prevent relative movement.
N. A. Degerstrom, Inc. (WA)	Common	0 to 50^{o}	---	8" thick reinforced concrete typically cast in place	---

Table B-4 Questionnaire summary for continuity, deck replacement, grout specification, and overlay

Respondent	Span-to-span connection	Deck replacement		Grout specs.	Overlay			Top surface treatment
		Account for	Would use		Type	%	Thick	
Alaska DOT & Public Facilities	Pier diaphragm; extending deck reinforcing and P/S strand into diaphragm	No	Yes	Yes	Asphalt	90	4" max (3" typ)	Heavy broom finish
Idaho Transportation Department	Only single span	No	Yes	Yes (use standard non-metallic, non-shrink grout	Asphalt	~100	4.8"	---
Minnesota DOT	Design assumes beam units as simple spans	No	Yes	Yes	Bitumin. Concrete	75-90 10-25	2" to 4" 2" to 5"	---
Texas DOT	Girders are designed as simply supported. Flexure of slab at joints is ignored.	No	No	No	Asphalt Concrete	90 10	2" 5" min	---
Washington State DOT	Girders are designed as simple spans for both DL&LL. Top flange connection is designed for negative LL&SIDL at piers.	No	No	Yes (per WSDOT standard specifications)	Asphalt	100	3"	---
Wyoming DOT	---	No	No	Yes	Asphalt	100	3"	---

Table B-4 Questionnaire summary for continuity, deck replacement, grout specification, and overlay (continued)

Respondent	Span-to-span connection	Deck replacement		Grout specs.	Overlay			Top surface treatment
		Account for	Would use		Type	%	Thick	
Morse Brothers, Inc. (OR)	---	No	No	No	Asphalt	---	2"-4"	Grinding in the field after construction
Concrete Technology Corporation (WA)	In some cases, they have been made continuous by welding or mechanically connecting rebar projecting from top flange.	No	---	No	Asphalt Concrete	75 25	2" min 2" min	Transverse broom
Nicholls Engineering (WA)	Pier diaphragm; extending deck reinforcing and P/S strand into diaphragm	No	---	Use WSDOT specifications	Asphalt	---	2.4" max	---
Aggpro (AK)	---	---	---	---	---	---	---	---
Shearer Design (WA)	Monolithic	Yes	Yes	No	Asphalt	100	4"	---
Grant County Engineer (WA)	Single span	No	Yes	Yes (WSDOT specifications)	None	---	---	Grooving in the precast plant
Sargent Engineers (WA)	Usually simply supported with joint	No	No	No	Asphalt	50	2"	---
N. A. Degerstrom, Inc. (WA)	---	---	---	---	---	---	---	---

Table B-5 Questionnaire summary for overall DPPCG evaluation, design guidelines, and longer spans

Respondent	Encountered problems	Overall evaluation	Future use	Design guidelines	Difficulties for extending span**					
					a	b	c	d	e	Other
Alaska DOT & Public Facilities	Hair line cracking between top of web and bottom of top flange. Cracking in end diaphragms at girder bottom flange interface	Good	Yes	Yes						Current max span is 150'
Idaho Transportation Department	---	Good	---	Use WA bridge design manual	X	X	X			
Minnesota DOT	Differential movements in the longitudinal joints cause cracking in the rigid bituminous deck overlay above.	Fair	Yes	Yes						Camber disparities between beams
Texas DOT	Cracking of deck near and along longitudinal connection joints.	Good	Yes	Yes	X		X		X	Differential camber and installation of lateral joints
Washington State DOT	Longitudinal cracking along the grouted key. Web & bottom flange cracking at intermediate support. Top flange connection at intermediate pier	Fair	---	Yes	X				X	Spliced girder guidelines for decked members
Wyoming DOT	None	Fair	---	No	X	X				Fabrication yard limitations

Table B-5 Questionnaire summary for overall DPPCG evaluation, design guidelines, and longer spans (continued)

Respondent	Encountered problems	Overall evaluation	Future use	Design guidelines	Difficulties for extending span**					
					a	b	c	d	e	Other
Morse Brothers, Inc. (OR)	None	Good	Yes	No	X					Stability, Site access
Concrete Technology Corporation (WA)	If the joints are not properly grouted, they may leak and the grout may deteriorate.	Good	---	No	X					
Nicholls Engineering (WA)	If weld ties are not designed properly, deicing salts will cause problems with weld ties and precast diaphragm weld.	Excellent	Yes	Yes	X	X				Did 200' using deck girder & splice
Aggpro (AK)	---	---	---	---			X			
Shearer Design (WA)	---	Good	---	No	X					
Grant County Engineer (WA)	Longitudinal cracks on light weight concrete construction.	Excellent	Yes	No	X					Height/Depth of the girder
Sargent Engineers (WA)	None	Excellent	Yes	No	X					
N. A. Degerstrom, Inc. (WA)	---	Good	---	---	X					

**Reasons for difficulties for extending span

a. Weight
b. Length
c. Lack of demand for product
d. Cost of forms
e. Lack of availability of design and construction guidelines

CTL
Construction Technology Laboratories, Inc.

5400 Old Orchard Road
Skokie, Illinois 60077
847.965.7500
Fax 847.965.6541
www.CTLGroup.com

July 8, 2004

Dear Sir:

Construction Technology Laboratories, Inc., in association with the University of Alaska, Fairbanks, and Eriksson Technologies, Inc. under the AASHTO-sponsored National Cooperative Research Program (NCHRP), is conducting Project 12-69, "Design and Construction Guidelines for Long-Span Decked Precast, Prestressed Concrete Girder Bridges." The overall objective of the research is to develop design and construction guidelines for long-span decked precast, prestressed concrete girder bridges in a format suitable for consideration and adoption by AASHTO as part of AASHTO LRFD Bridge Design Specifications.

In spite of their benefits, the use of decked precast, prestressed concrete girders has been limited because of concerns about certain design and construction issues that are perceived to influence the structural integrity of the bridge system. Research is needed to address the issues that significantly influence the performance of these bridges and to develop guidelines for their design and construction.

The attached questionnaire is intended to generate much needed information on distribution, population, and type of bridges using decked girders in the US, problems for construction and maintenance, performance of bridges in service, and available guidelines and specifications. This information is essential for the conduct of our research. In this questionnaire, a "decked" concrete girder is defined as a precast, prestressed concrete I, bulb-tee, double-tee, or single-tee girder with an integral deck that is cast and prestressed with the girder for bridge applications.

We realize that our inquiry will take some of your valuable time, and therefore, we sincerely appreciate your efforts in responding to this questionnaire and sharing your experiences with others who can profit from it. Thank you for your assistance.

Sincerely,

Armin B. Mehrabi, Ph.D., P.E.
Senior Principal Engineer

attachment

SURVEY

National Cooperative Highway Research Program (NCHRP)
Project No. 12-69

"Design and Construction Guidelines for Long-Span Decked Precast, Prestressed Concrete Girder Bridges"

Name of the respondent: _____
Title: _____
Address: _____
_____

Phone number: _____
Fax number: _____
E-mail: _____

Please, send all replies and questions to:

Armin B. Mehrabi, Ph.D., P.E.
Senior Principal Engineer
Construction Technology Laboratories, Inc.
5400 Old Orchard Road
Skokie, IL 60077 – 1030
Phone: 847-972-3184, Fax: 847-965-8997, E-mail: AMehrabi@CTLgroup.com

Please, respond by August 2, 2004

In this survey, a “decked” concrete girder is defined as a precast, prestressed concrete I, bulb-tee, double-tee, or single-tee girder with an integral deck that is cast and prestressed with the girder for bridge applications. Please note that solid and voided slabs, box beams, channels or other precast units are not considered as part of this study.

Q1: Has your organization used/designed/fabricated/constructed any decked concrete girder systems for spans up to 150 ft in highway bridges?

Yes _____

No _____(please, give reasons and go to the last question in this questionnaire):

Lack of specifications or guidelines _____

Unsatisfactory performance of joints between adjacent units _____

Difficulty in construction geometry control (camber, cross slope, and skew)_____

Difficulty in future deck replacement _____

Other (specify)_____

_____

Q2: What decked concrete bridge configurations are commonly used? For example:

Span lengths _____

Section shape (I, bulb-tee, double-tee, or single-tee) _____

_____

Please provide cross-section dimensions _____

Q3: What types of connections between adjacent units are used? Please attach a typical drawing if possible.

Q4: What procedures are used for the design of these connections? Upon what are these procedures based?

Q5: Questions on skew for decked precast, prestressed concrete girder bridges:

Q5a- How common are skewed bridges?

Q5b- What range of skew angles are commonly used?

Q5c- How is skew taken into account in design?

Q6: What type of intermediate diaphragms do you use (if any)? Please attach a typical drawing if possible.

Q7: What methods are used to determine the distribution between girders for forces caused by wheel loads? What about the single-lane loaded bridges?

Q8: How do you design and detail span-to-span connection on the pier? Please attach typical details if possible.

Q9: Deck replacement for decked precast, prestressed concrete girder bridges:

Q9a: Do you accommodate future deck replacement for this system?

Yes_____(if yes, what details are used? Please attach a typical drawing if possible).

No_____(please give reasons)

Q9b: If the answer to Q9a is no, would you use a deck replacement option if technically feasible?

Q10: Successful grouting of the longitudinal joints is considered one of the key elements of having a durable and high performance decked concrete girder systems. Have you developed specifications for the grout properties and the grouting process?
Yes _____(please, attach a copy of these specifications)
No_____

Q11: Do you use an overlay?

Yes _____ (if Yes, please, provide the overlay type and percent of decks)

Asphalt % _____ Thickness_____

Concrete % _____ Thickness_____

Other (specify) _____% _____ Thickness_____

No ____ (If No, did you provide special treatment to the top surface of the deck to provide for ride-ability?)

Yes_____

What type? Roughening in the precast plant during production

Grooving in the precast plant during production

Grinding in the field after construction

Sand blasting in the field after construction

Other (specify)

No_____

Q12: Have you encountered any problems in service with this type of bridges (if yes, please specify)? If available, please provide any records or inspection reports you may have of in-service behavior of members or connections.

Q13: What is your overall evaluation of the decked concrete girder bridges?

Excellent _____

Good _____

Fair _____

Poor _____

Please comment and indicate whether or not you will use the decked concrete girder systems again in future projects:

Q14: Have you developed guidelines or specifications for design, fabrication or construction of the decked concrete girder systems, and/or conducted any proprietary research on this subject?

Yes ___(please attach a copy of these specifications and/or research results)

No___

Q15: Based on your experience, what would be the major difficulties for extending span length for decked concrete girder bridges beyond what is being used (to up to 150 ft)? (Please check all that apply).

Weight _____
Length _____
Lack of demand for product _____
Cost of forms _____
Lack of availability of design and construction guidelines _____
Other (specify) _____

Q16: Please, provide the name, phone number and e-mail address of one person on your staff who can help in answering questions (or interested) on issues related to design and construction with decked concrete girder systems. [We also appreciate that if you recommend a knowledgeable person who is not on your staff].

Name: _____
Title: _____
Phone: _____
E-mail: _____

Thank you very much for your valuable time.

APPENDIX C

SUBTASK 6.1-A – FULL DECK REPLACEMENT

Background

Based on the work accomplished in Task 2, deck replacement of DPPCG bridges is an important issue that has been raised as a possible impediment to their use. From the questionnaire survey, of the 22 respondents who did not use DPPCG bridges, 8 listed difficulties in future deck replacement as a reason DPPCG is not used.

The need for deck replacement is covered in Section 2.5.2.3 of AASHTO LRFD (C1). This section of the specification states:

> *Structural systems whose maintenance is expected to be difficult should be avoided. Where the climatic and/or traffic environment is such that the bridge deck may need to be replaced before the required service life, either the provisions shall be shown on the contract plans for the replacement of the deck or additional structural resistance shall be provided.*

The questionnaire survey responses indicate that current practice does not consider future deck replacement. Of the 14 respondents who did use DPPCG bridges, 12 provided information regarding accommodation of future deck replacement. Of these, 11 indicated they do not accommodate future deck replacement and one respondent discussed use of a partial deck replacement scheme involving grinding off and replacing 2 in. of the deck. A major reason cited for not considering deck replacement is that the deck concrete is of the same high quality concrete as the girder with 30 years of success without any need to replace the deck. However, since this experience is primarily with DPPCG bridges with low volume traffic, this is not a convincing reason if increased use in higher traffic volume applications is a goal.

Another reason cited for not considering deck replacement is that deck replacement requires shoring and the integrity of the finished girder may not be as expected. However, this reason implies that it is a system whose maintenance is expected to be difficult and perhaps should be avoided. It should be noted that the main strength of the DPPCG system is the speed of construction. Therefore, if the deck of DPPCG bridges deteriorates to a state requiring replacement, it may be more efficient and expeditious to replace the entire girder rather than

replace just the deck. However, there may be situations where replacement of the entire girder is not practical. Therefore, in order to promote the use of the DPPCG system, it is necessary to develop a DPPCG system that would allow for rapid full deck replacement without need for shoring while maintaining the integrity of the girder.

To understand further the difficulties in deck replacement in DPPCG bridges, a parametric study was conducted in Task 2 to investigate the feasibility of re-decking by removing and replacing the entire top flange of the girders. This study indicated that, for conventionally designed decked bulb tee girders, the deck (top flange) could typically be removed without overstressing the girder provided proper support for lateral stability is in place. However, since a new cast-in-place deck or precast deck is not composite for the dead load from the new deck, (whereas the top flange of the original girder is) the re-decked girder will be overstressed unless the bridge is shored during the retrofit work. Therefore, the future deck removal must be considered in the initial design. This requires additional prestressing and part of the deck to be left in place or a two-stage casting procedure.

State-of-the-Art

The NCHRP Report 407 (C2) presents a comprehensive study that was conducted to develop optimum systems for rapid deck replacement of existing CIP reinforced concrete bridge decks on steel or prestressed girders. In that study, the bridge deck system and the bridge girder-to-deck connection were identified as main areas affecting the suitability of the bridge for repaid deck replacement. Five different bridge deck systems were tested. These were two full-depth CIP deck systems, two precast deck sub-panels, and one full-depth precast deck system. One of the full-depth CIP systems tested was reinforced with conventional reinforcement. To reduce the duration of construction, the other full-depth CIP system was reinforced with epoxy-coated welded wire fabric. One of the two precast sub-panel systems tested used 3-in. thick conventional stay-in-place (SIP) precast panels with 6-in. thick CIP topping. The other precast sub-panel system utilized a continuous precast prestressed SIP form system as shown in Figure C-1. The system incorporates a 4.5-in. precast prestressed panel and a 4.5-in. CIP topping. The system extends over the full width of the bridge deck and is continuous both in the transverse and the longitudinal directions to eliminate reflective cracking. The portion over the girder line is kept open to accommodate shear studs, and the overhang form is part of the SIP system. The full-depth precast deck system, shown in Figure C-2, incorporates precast prestressed concrete panels. The panels have non-prismatic stemmed section to optimize the

system in terms of weight and reinforcement. The panels extend the full width of the bridge and are transversally pre-tensioned and longitudinally post-tensioned. The full-depth precast panel system was found to require the least construction time of all systems studied. These systems are appropriate for both new construction and replacement. These systems can be used in both steel and concrete girder bridges. However, steel girders were used in all tests.

The continuous stay-in-place panel system was later evolved to full-depth precast, prestressed system (C3) as shown in Figures C-3 to C-5. The primary feature of this system is the fully open gap in the panel over each girder line. This gap provides an open channel over the girder for the placement of the post-tensioning strands and shear connectors. The pre-tensioning strands run continuous through the whole length of the panel. To preserve the tension in the continuous strands, thus the pre-compression in the concrete, the absent concrete strip in the gap is substituted with 4#7 bars at the location of each pair of strands. The bar size is determined by its ability to resist buckling during prestress release and bending during handling and erection. The end deck panel of the bridge is designed to work as the post-tensioning anchorage block. This system has been implemented in the Skyline Bridge in Omaha, Nebraska (C3

The NCHRP Report 407 (C2) also presents an investigation of the bridge girder-to-deck connection. Demolition of bridge decks that are compositely connected with I-girders is one of the major time-consuming tasks in deck replacement. For new bridge superstructures, the time required for deck demolition can be reduced by constructing bridges with connections that provide composite action and allow for easier deck removal. For precast concrete I-girders, a debonded interface with a shear key placed in the top flange of the concrete girder and shear connectors of reinforcement bars at wide spacing, shown in Figure C-6, was developed. To accomplish the debonded interface, a debonding agent was applied to the hardened concrete using a brush or hand-held sprayer. The primary resistance mechanisms for the shear key are bearing and friction between the top flange and bottom of the deck, including the tensile and shear strength of steel connectors crossing the interface. In addition to extensive laboratory tests on push-off specimens, two full-scale girder tests were performed to compare the performance of the unbonded shear key system with that of a conventional system. Test results showed that this debonded surface in conjunction with extended vertical shear stirrups provided adequate horizontal shear transfer to ensure composite action. The debonded surface with less congestion of reinforcement enhanced the deck removal.

The debonded shear key system was implemented on a demonstration bridge in Nebraska (C4; C5). The bridge consisted of two identical northbound and southbound structures. Each structure consisted of five NU1600 girders spaced at 8 ft 2 ½ in. supporting a 7 ½ in. thick composite cast-in-place slab. The conventional interface system was used on the northbound structure while the debonded interface system was used on the southbound structure. As shown in Figure C-7, the shear keys were recessed below the top flange surface. The reason for recessing the shear keys is to make the system suitable for all types of concrete decks, including precast stay-in-place sub-panels, full-depth precast panels, and cast-in-place deck systems (C5). Deflection measurements have shown that the deflection of the southbound structure was almost the same as that of the northbound structure. This indicated that the new shear key system did not increase the flexibility of the bridge and full composite action between the deck and the girder has been achieved.

Several other bridge deck panel systems have been developed and used in bridge replacement projects in the United States. Versace and Ramirez (C6) conducted a synthesis study in order to facilitate implementation of full-depth precast deck systems in the state of Indiana. Information related to full-depth precast deck systems was collected and analyzed. Nine full-depth precast deck systems were identified in that study. None of the systems, however, has been implemented over concrete or precast girders.

Issa et al. (C7) described the construction procedures for rapid replacement of deteriorated bridge decks. The focus was on the rehabilitation of bridge decks via installation of full-depth precast or precast prestressed concrete bridge deck panels. This system can either be supported on steel stringers or precast concrete. However, the nationwide survey conducted by Issa et al. (C7) did not reveal any applications where precast concrete girders were used as supporting systems for full depth precast panels.

Recommendations

Although, there is considerable amount of work done on full-depth precast deck panels for use in deck replacement projects as well as new construction, and it is mentioned in some literature that this deck system can be used efficiently for concrete girder bridges, in all documented applications, steel girders were used as the supporting system. An investigation conducted by Isaa et al. (C8) did not reveal any applications where precast concrete girders were used as supporting systems for full depth precast panels. Reviewing more recent

literature did not reveal any such application either. Accordingly, it is concluded that the concept of the debonded shear key and the cast-in-place deck as described in NCHRP Report 407 (C2) is the current state-of-art for replacement of decks on concrete girders that has been sufficiently tested and documented. Therefore, it is the appropriate system to be incorporated in the development of optimized family of girder sections.

The following parameters need to be considered in the design:

1. Two stage casting procedure (girder and deck) with a debonded interface between the two castings.

2. The connection between the girder and the deck must be capable of transferring the horizontal shear at the interface, while allowing for easy removal of the deck.

3. The dead load from the replacement deck will act on a non-composite section. Therefore, the girder must be capable to support this load without being overstressed to avoid shoring the structure.

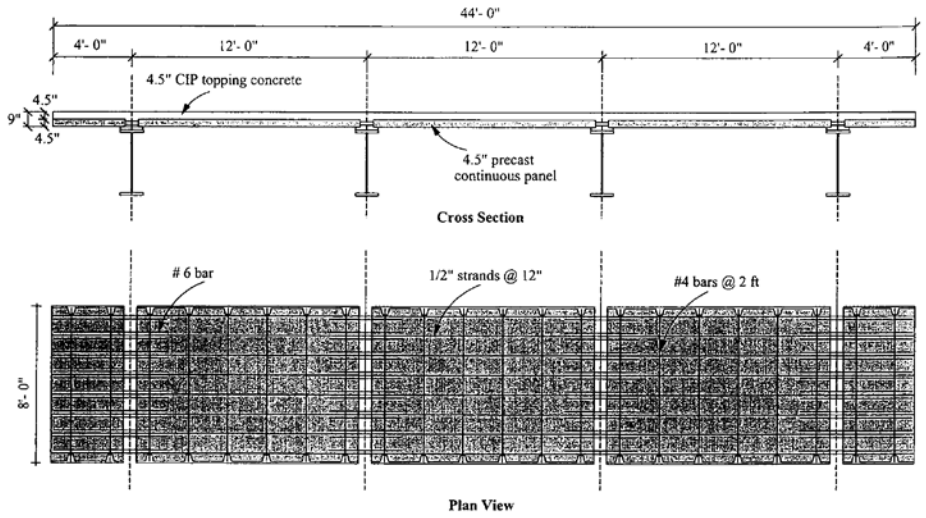

Figure C-1 Continuous SIP Subpanel Bridge Deck System

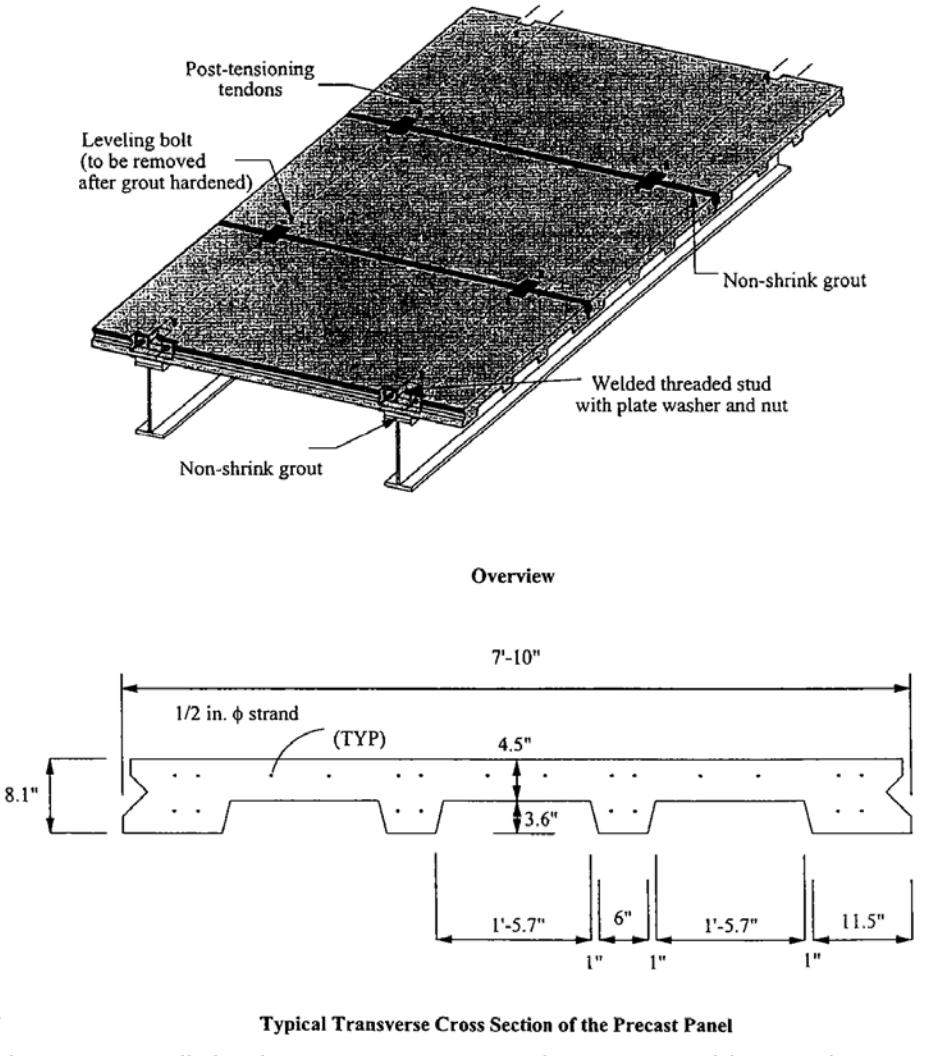

Figure C-2 Full-depth Precast Prestressed Concrete Bridge Deck System

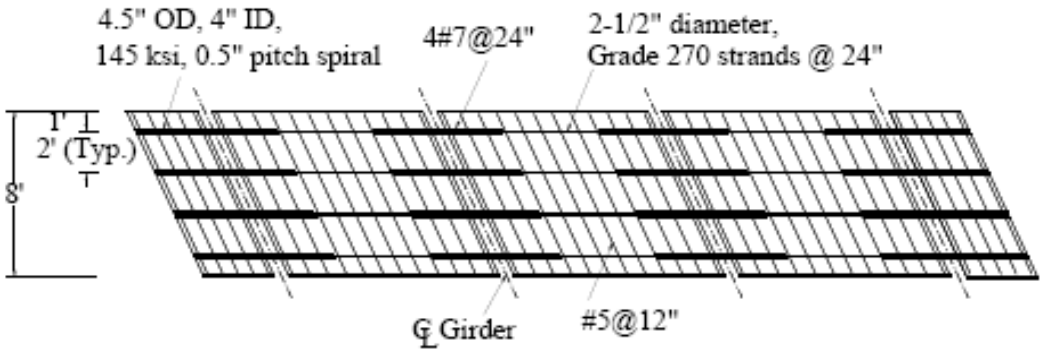

Figure C-3 Plan View of Typical Prestressed NUDECK Panel

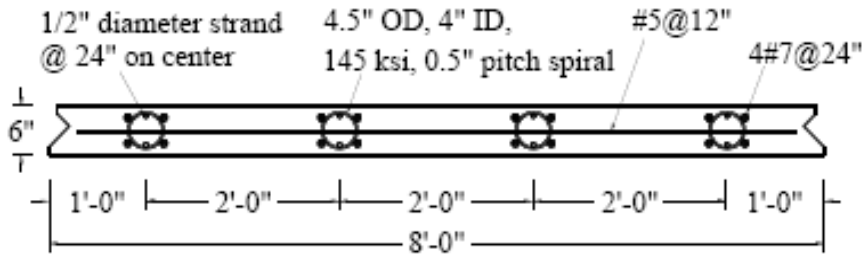

Figure C-4 Cross Section of Typical Prestressed NUDECK Panel

Figure C-5 Plan View of Typical Prestressed NUDECK Panels

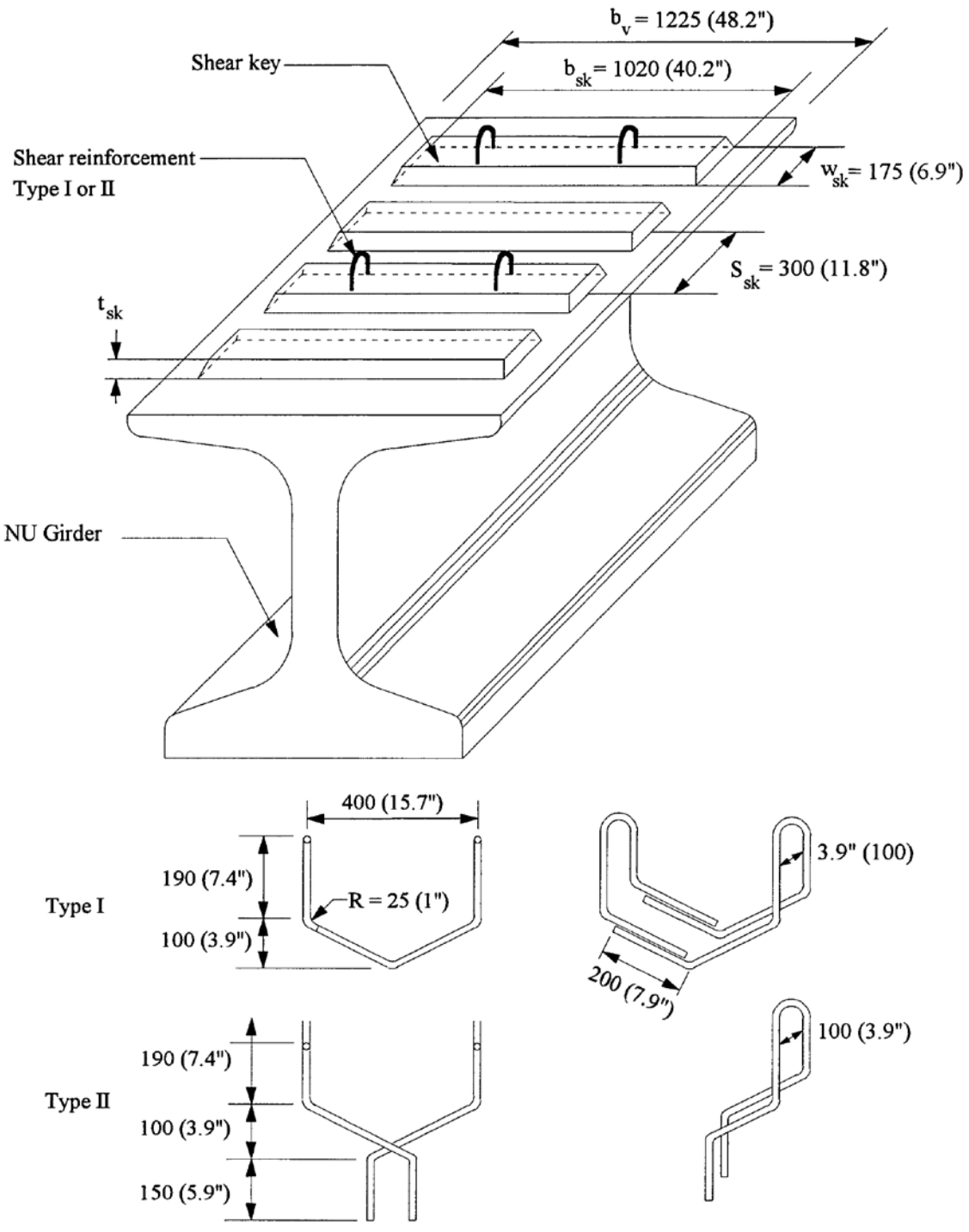

Figure C-6 Girder Shear Key System

Figure C-7 View of the Recessed Shear Key System

APPENDIX C REFERENCES

C1 AASHTO, “LRFD Bridge Design Specifications,” Third Edition, American Association of State Highway and Transportation Officials, Inc., 2004.

C2 Tadros, M. K. and Baishya, M. C., “Rapid Replacement of Bridge Decks,” NCHRP Report 407, Transportation Research Board, National Cooperative Highway Research Program, 1998.

C3 Fallaha, S., Sun, C., Lafferty, M. D., and Tadros, M. K., “High Performance Precast Concrete NUDECK Panel System for Nebraska’s Skyline Bridge,” PCI Journal, Vol. 49, No. 5, Septmber-October, 2004, pp. 58-69.

C4 Badie, S. S., and Tadros, M. K., “I-Girder/Deck Connection for Efficient Deck Replacement,” NDOR Project No. SPR-PL-1(35) P516, Final Report, University of Nebraska-Lincoln, December, 2000.

C5 Tadros, M. K., Badie, S. S., and Kamel, M. R., “Girder/Deck Connection for Rapid Removal of Bridge Decks,” PCI Journal, Vol. 47, No. 3, May-June, 2002, pp. 58-69.

C6 Versace, J. D., and Ramirez, J. A., “Implementation of Full-Width Precast Bridge Deck Panels: A Synthesis Study,” Joint Transportation Research Program, Project No. C-36-56OOO, Purdue University, Indiana, May, 2004.

C7 Issa, M. A., Yousif, A. A., and Issa, M. A., “Construction Procedures for Rapid Replacement of Bridge Decks,” Concrete International, February, 1995, pp. 49-52.

C8 Issa, M. A., Idriss, A. T., Kaspar, I. I., and Khayyat, S. Y., “Full Depth Precast and Precast, Prestressed Concrete Bridge Deck Panels,” PCI Journal, January-February, 1995, pp. 59-80.

APPENDIX D

SUBTASK 6.1-B – OPTIMIZED GIRDER STUDY

Introduction

Decked bulb tees have been used successfully for many years. Their cross sectional shape has evolved to accommodate varying bridge widths and span lengths. A generic shape that closely approximates the decked bulb tees in common use is shown in Figure D-1. Overall girder widths range from approximately 4 ft 0 in. to 8 ft 0 in. Overall depths range from about 2 ft 11 in. to 6 ft 5 in.

A principal requirement of this study is that the system be re-deckable in the future. In Task 6.1 - A, this issued was examined in depth. It was concluded that the shear key system described in NCHRP Report 407 (D1) be adopted and integrated into this girder system to make the system re-deckable.

Assessment of Existing Cross Sections

With minor variations the section family described in Figure D-1 is the primary girder shape used today for most decked bulb tee bridges. Since this basic shape has functioned well and has had a good service history, this shape was used as the basic starting shape of this optimization study. The top flange, web and bottom bulb were each assessed for potential improvement.

Proposed Cross Section

Figures D-2 and D-3 show the dimensions of the two casting stages of the proposed girder shape. The girder shown in Figure D-2 represents Stage 1 casting, which will also be the girder shape when the top portion of the system is removed for future re-decking. The shape in Figure D-3 includes Stage 2 casting, and represents the girder that will initially be used to construct the bridge. Release of prestress occurs after the proper cure of the Stage 2 casting.

Design Criteria

The following design criteria were adopted for this study:

Specifications

AASHTO LRFD Bridge Design Specifications, 3rd edition (2004) (D2).

Bridge Geometry

The overall width of the bridge assumed for the optimized girder study was 48 ft 0 in., and the curb-to-curb width will be 45 ft 0 in. (Figure D-4). The cross section of the bridge consists of six 8 ft 0 in. wide girders. Two standard Jersey-type barriers are assumed.

Section Type

The section family type is decked bulb tees, which will be cast in two stages (Figures D-2 and D-3). Three different overall depths are investigated: 41 in., 53 in., and 65 in. For each of these depths, four different bottom bulbs geometries are investigated: the standard bulb (D3)(i.e., the current industry standard), a "tall" version in which the height of the bottom bulb has been increased by 2 in., a "wide" version in which the width of the bottom bulb has been increased by 4 in. on either side, and a modified NU bulb which has the same dimensions as the Nebraska University (NU) bulb tee girder, but with no transition radii (Figure D-5). Section properties of the girders are provided in Table D-1.

Materials

Girder Concrete: f'_c = 7.00 ksi, f'_{ci} = 5.00 ksi, Normal weight

Deck Concrete: f'c = 4.00 ksi, Normal weight, air entrained

Prestressing Stand: 0.6 in. diameter low-relaxation (Area = 0.215 in^2, f_{pu} = 270 ksi)

Loads

Dead Loads:

Girder self-weight
Barriers: 2 barriers at 300 plf each
Future Wearing Surface (FWS): 25 psf

Live Load:

Construction: Per specifications
Vehicular: HL-93

Allowable Stresses

Allowable tension: $6\sqrt{f'_c}$

Construction Sequence

Stage 1: Cast lower portion (bottom bulb, web, and sub-flange) of girder, cure, and apply debonding agent to top surface of sub-flange (Figure D-2.).
Stage 2: Cast top flange of girder (Figure D-3), cure to 4.00 ksi, and detension strands (check release stresses).
Stage 3: Haul girders to job site (check stability).
Stage 4: Erect girders, place diaphragms, level girders, place steel in joints, grout joints.
Stage 5: Place barriers and protective membrane.
Stage 6: Bridge open to traffic.
Stage 7: Apply future wearing surface (check all code-specified load cases)

Re-Deck Bridge

Stage 8: Remove bridge deck, including barriers (check construction loading).
Stage 9: Install new deck, barriers, and membrane.
Stage 10: Apply future wearing surface (check new structural system).

Optimization Study Parameters

Bottom Bulb

The shape of the bottom bulb of the Washington State DOT standard (Figure D-5) was assumed as a starting point for the optimization study. The width and depth of the bottom bulb were varied to accommodate the required number of strands to determine the most structurally efficient shape of the bulb (D4).

Web Width

The web width was held constant at 6 in.

Flange:

The top portion of the girder consists of two parts: the sub-flange and the top flange (see Figures D-2 and D3). The thickness of the sub-flange is dictated by the shear key depth, reinforcement layout, and concrete cover requirements. Based on these requirements, the edge thickness will be set at 3.5 in. The width of the sub-flange will be dictated by the force demands placed upon the shear key. However, the minimum width is set at 42 in., in order to fully develop transverse reinforcement in the sub-flange. Girder depths and lengths were varied within the specified ranges to determine the maximum forces on the shear key. The sub-flange width was set accordingly. The thickness of the top flange was held constant at 6 in. The width of the top flange was assumed to be 8 ft unless analysis indicates the need for a narrower flange.

Shear Keys:

Top surface of the sub-flange shall have formed shear keys (see Figure D-2). Shear keys shall be the width of the sub-flange of the girder less 2 in. on either side. Depth of shear keys shall be ¾ in. Spacing of shear keys along the longitudinal axis of the girder is dictated by the vertical shear steel requirements and shear friction steel (for composite action).

Girder Concrete:

Two different concretes were used for the lower and upper portions of the girder. For the top portion of the girder, air-entrained concrete was used. The 28-day strength of both concretes will be 7.00 ksi. However, at release of the strands, the top portion is assumed to have reached a strength of 4.00 ksi. At the time the girder is re-decked; two different deck concrete strengths were investigated: 4.00 ksi and 6.00 ksi.

Study Methodology

As discussed above, for a given depth of girder (41 in., 53 in., or 65 in.), four different bottom bulb geometries were investigated: normal, tall, wide, and NU configurations. For each of these bottom bulb geometries, the steps in the investigation were as follows:

1. Generate a load table of span length versus required number of strands at 2-ft span increments for the initial, fully decked, fully prestressed phase of the bridge (Phase 1). Make note of the total long-term losses.

2. Generate a load table of span length versus required number of strands at 2-ft span increments for the phase in the life of the bridge when the top flange is removed and the bridge is re-decked with a 6 in. thick cast-in-place deck (Phase 2). Assume that f'_{ci} of the girders at the time of re-decking is equal to the f'_c. In lieu of calculating the prestress losses, assume that the prestress loss at the "release" stage (i.e., when the top flange is removed) is the lower range of the long-term losses determined in Step 1. For analysis of the re-decked section, assume the long-term losses for this step as the upper bound of the losses computed in Step 1. Preliminarily, assume the "release' and final losses to be 25% and 35%, respectively. Investigate deck concrete strengths of 4.00 ksi and 6.00 ksi.

3. Compare the results of Steps 1 and 2.

4. Adopt the maximum span length for a given girder depth and bottom bulb geometry as the lower of the maximum span for Phases 1 and 2.

5. Check shear key design based on maximum demand placed on shear key and adjust sub-flange width if needed.

6. Check stability of the maximum span for each girder depth (D5, D6).

Summary of Results

Comparison of Bulb Shapes

The efficiency of each of the bottom bulb geometries was investigated by determining the maximum span length for each bulb shape. Two sets of analyses were run, one using a re-decking concrete strength of 4.00 ksi and one with 6.00 ksi. The re-decking concrete strength was varied to determine whether the extra strand locations created by enlarging the bulb could be fully utilized or not.

For the initial bridge construction stage, for the 41 in. deep girder, the maximum span lengths for the normal, tall, wide, and NU bulb shapes were 94 ft, 100 ft, 110 ft, and 118 ft, respectively (Figure D-6). Therefore, the extra strand locations resulted in additional span capabilities. A span increase of approximately 25% was realized from the smallest bulb to the largest bulb. Similar results were observed for the 53 in. and 65 in. deep cases. (Figures D-7 and D-8).

The corresponding maximum span lengths for the 41 in. deep re-decked stage with a deck concrete strength of 4.00 ksi were all less than for the initial stage: 82 ft, 86 ft, 94 ft, and 98 ft. However, as with the initial stage, an increase in span range was realized with increasing bulb size.

For the 41 in. deep girder, by increasing the re-decking concrete strength to 6.00 ksi, the span ranges increased from 0 ft for the smallest bulb to a maximum of 4 ft for the largest bulb (Figure D-9). The increase in span range was due to increased flexural strength that resulted from using a higher strength deck concrete.

For the 53 in. deep and 65 in. deep girders, the increase in span range for the re-decked stage was more pronounced. The increase in span range for the 53 in. deep case varied between 0 ft and 12 ft (Figure D-10). For the 65 in. deep case, the increase in range was 0 to 16 ft (Figure D-11).

Based on the results from varying bulb geometry, it was concluded that the most efficient bulb shape is the NU bulb. Not all strand locations can be utilized for all girder depths and re-decking concrete strengths. However, for girder depths of medium to tall height, significant increases in span capabilities can be realized.

Variation in Girder Spacing

The study of bulb variation was conducted using a girder spacing of 8.00 ft, which is the maximum girder spacing of decked bulb tee girders used in typical practice. To examine the impact of varying girder spacing three girder spacings were investigated: 4.00 ft, 6.00 ft, and 8.00 ft. The NU bulb shape was used for each of these spacings. Figures D-12 through D-14 show the effect of girder spacing on span range for the initial vs. re-decked phases with a re-decked concrete strength of 4.00 ksi.

For the initial case, for each girder depth, the maximum span length was achieved using a girder spacing of 6.00 ft. However, for the re-decking phase, for each girder depth, the maximum span was realized using a girder spacing of 8.00 ft.

Figures D-15 through D-17 show the effect of girder spacing on span range, at the re-decked phase, using deck concrete strengths of 4.00 ksi and 6.00 ksi. The results indicate that for 4.00 ksi deck strength there is a direct relationship between girder spacing and maximum span length. That is, the narrowest girder spacing yields the shortest maximum span length, and the widest girder spacing yields the longest span length. This apparent anomaly is to be due to flexural strength issues. For low deck concrete strengths, flexural strength of the system governs the design. This means that fewer strand locations can be utilized for a narrow girder spacing, which, in effect, amounts to a weight penalty for the system. That is, a larger section is used than what is required, adding unusable concrete to the system. Although the moment of inertia is higher as well, increased section stiffness has no influence on flexural strength of the section.

When the deck strength is increased to about 6.00 ksi, this weight penalty is not as great. For this case, the maximum span length is achieved for each of the three section depths when the girder spacing is 6 ft.

Assessment of Results

Section Shape

Top Flange. A 6 in. top flange thickness was assumed based upon the historical thickness of the top flange of conventional decked bulb tee girders to minimize weight. An 8-ft width of flange was assumed in all cases to cause the highest force demands on the lower portion of the system (i.e., the Stage 1 casting). Design forces for exterior girders require No. 5 bars at 4 in. centers for transverse reinforcement.

Lateral stability checks for an 8-ft wide top flange showed that the system has adequate factors of safety for both hanging and supported conditions for all girder depths (D5, D6). Narrower widths of top flange could be used to extend the span ranges, but would reduce the factor of safety against lateral instability.

At the re-decking phase, f'_c was assumed to be 4.00 ksi and 6.00 ksi, assuming a cast-in-place deck. This was a governing constraint on the span range. Increasing assumed f'_c for re-deck concrete increases the maximum span length.

Sub-flange. The sub-flange width was set based on a study of force demands placed on the flange. The required transverse reinforcement to resist the applied forces was No. 4 bars at 6 in. on center or a pair of No. 4 bars at 12 in. on center. Accounting for web width, cover, and rounding up to the nearest inch, the required total sub-flange width to fully develop the No. 4 bars was 42 in.

Force demands placed on the shear key on the top surface of the sub-flange were checked assuming a minimum 42 in. wide sub-flange. Both horizontal shear capacity and edge bearing were adequate.

Web. A 6 in. web width was maintained for all cases to accommodate two columns of draped strands, transverse reinforcement, and provide adequate cover. Maximum factored shear forces at the critical sections for the 41, 53, and 65 in. cases were 268, 314, and 361 kips. The corresponding maximum nominal shear resistances, V_n, permissible by the LRFD Specifications were 372, 480, and 550 kips, respectively. Therefore, a web width of 6 in. is adequate for all cases.

Bottom Bulb. The extra strand locations provided by making the standard bulb larger resulted in longer span ranges for each depth of girder studied. These extra strand locations enabled more of the concrete in the top portion of the system to be mobilized. Typically, the lowest strand locations in the girder are the most efficient places in which to add strands. Therefore, the wide flange configuration in which eight new strand locations were created at each of the bottom two levels of strands (Figure D-5 c) was more efficient than the tall case, where additional strand locations were also added, but at somewhat higher and therefore less efficient elevations (Figure D-5b). However, the NU bulb shape was the most efficient of all the shapes.

For the 41 in. deep member, the moment of inertia of the initial section (i.e., before re-decking) with the normal bulb width was 191,823 in^4 with a cross-sectional area of 1086 in^2. With the tall bulb, the moment of inertia increased to 206,962 in^4 with an area of 1126 in^2. With the wide bulb, the moment of inertia increased to 226,203 in^4 with an area of 1146 in^2. Therefore, increasing the depth of the bulb resulted in an increase in the moment of inertia of

7.9%, with a corresponding increase in area of 3.7%. Increasing the width of the bulb resulted in an increase in the moment of inertia of 17.9%, with a corresponding increase in area of 5.5%. Similar results were observed for the 53 and 65 in. cases.

For the normal, tall, wide bulb, and NU configurations (Figure 5), the maximum span lengths were achieved in all cases using the NU bulb. For the 41, 53, and 65 in. deep girders, the maximum spans were 118, 148, and 176 ft, respectively for the initial phase of construction. For the re-decked phase using 4.00 ksi deck concrete, the maximum span lengths were 98, 118, and 134 ft, respectively. For the re-decked phase using 6.00 ksi deck concrete, the maximum span lengths were 114, 138, and 160 ft, respectively. Based on the maximum spans achievable, the NU bottom bulb proved to be the most efficient shape.

Deck Replacement

Longer span lengths were possible for the initial phase of the bridge. Therefore, if re-decking capabilities are to be incorporated into the system, significantly shorter span capabilities will result. Use of higher strength concrete for the future re-decking phase will increase span capabilities. Also, span capabilities increase if total superstructure replacement is considered as the future “deck replacement” scheme in lieu of removal and replacement of the top flange.

Conclusions and Recommendations

Based on this study, it is recommended that the girder shape shown in Figure D-3 be adopted with the modified NU bulb configuration shown in Figure D-5 d) incorporated. This shape is structurally efficient and facilitates future re-decking of the system. But the cost of re-decking the system versus total superstructure replacement should be evaluated.

Table D-1 – Section Properties of Girder Family

Section	**Height** (in)	**Area** (in2)	**MI** (in4)	**y_b** (in)	**Weight** (klf)
DBT41	41.00	1,086	191,823	28.28	1.13
DBT41 deck removed	35.00	550	91,174	18.85	0.57
DBT53	53.00	1,158	371,301	36.60	1.21
DBT53 deck removed	47.00	622	191,595	25.08	0.65
DBT65	65.00	1,230	623,209	44.64	1.28
DBT65 deck removed	59.00	694	336,749	31.26	0.72

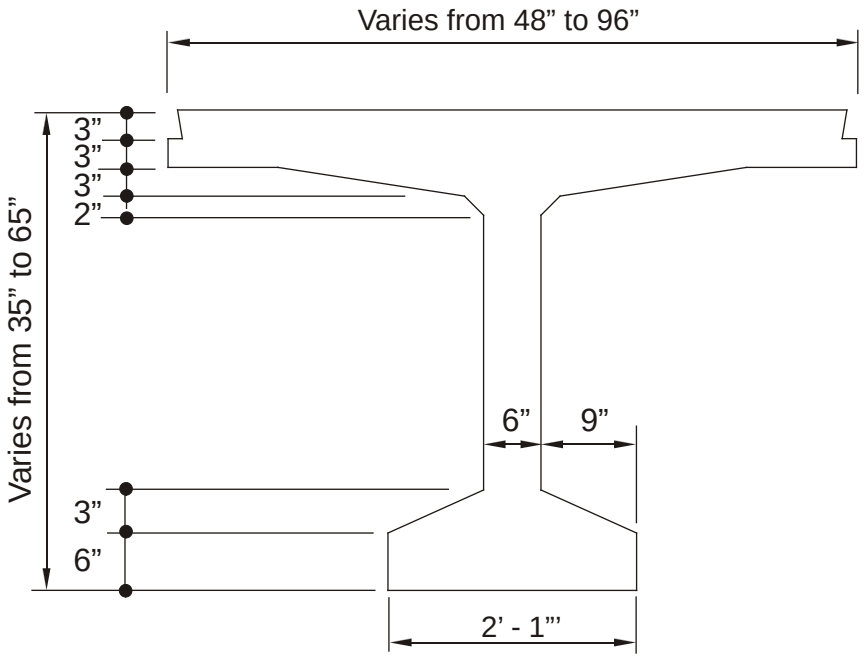

Figure D-1. Conventional Decked Bulb Tee.

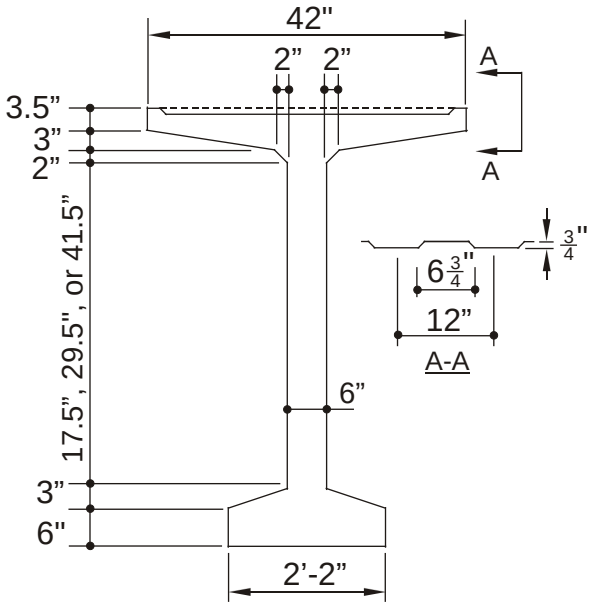

Figure D-2. Proposed Girder: Stage 1 of Casting.

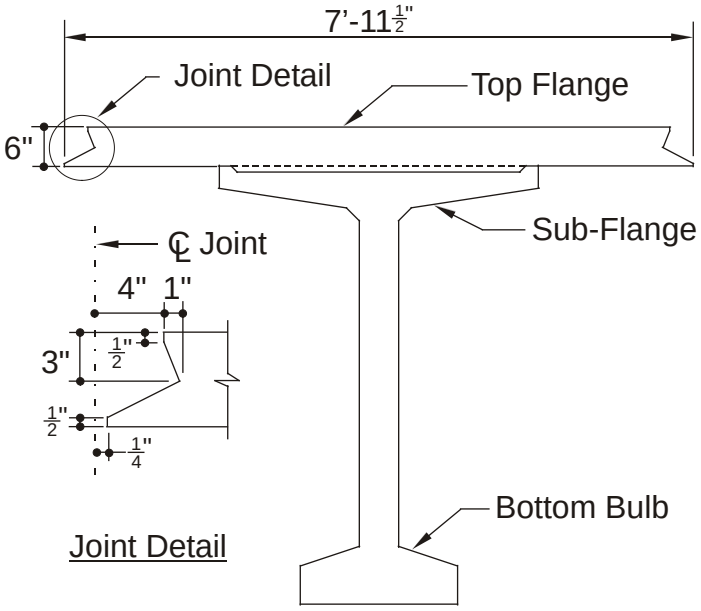

Figure D-3. Proposed Girder: Stage 2 of Casting.

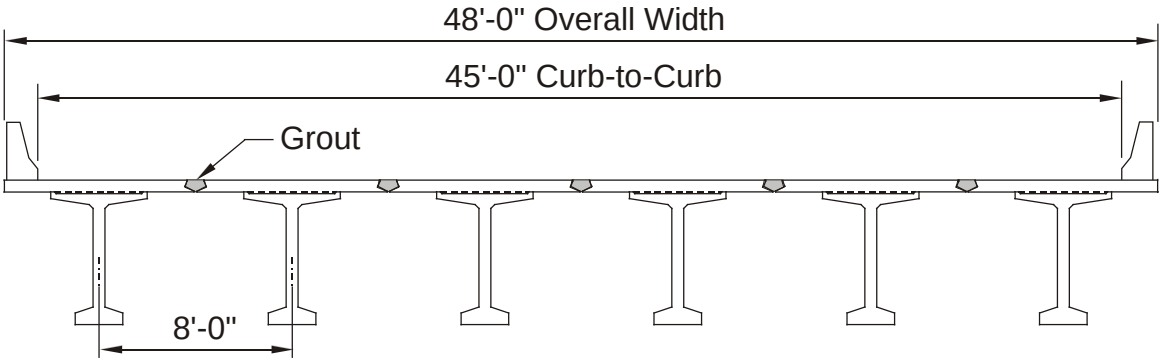

Figure D-4. Bridge Cross Section using Proposed Girder.

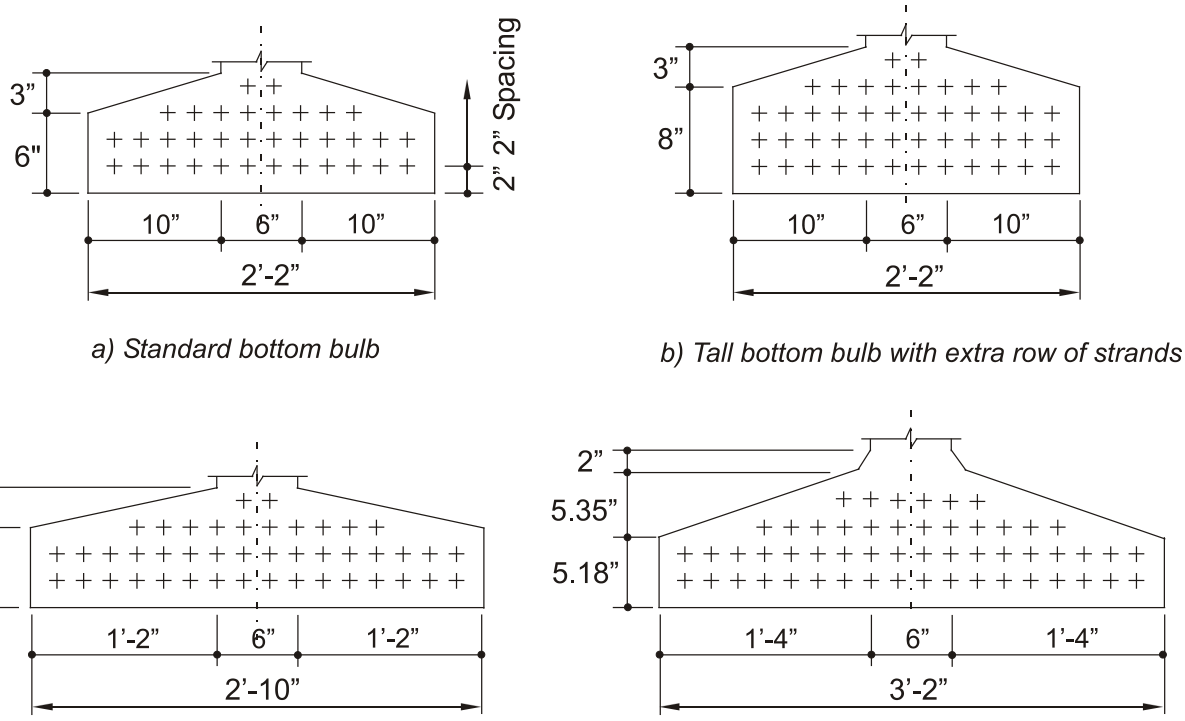

Figure D-5. Bottom Bulb Configurations.

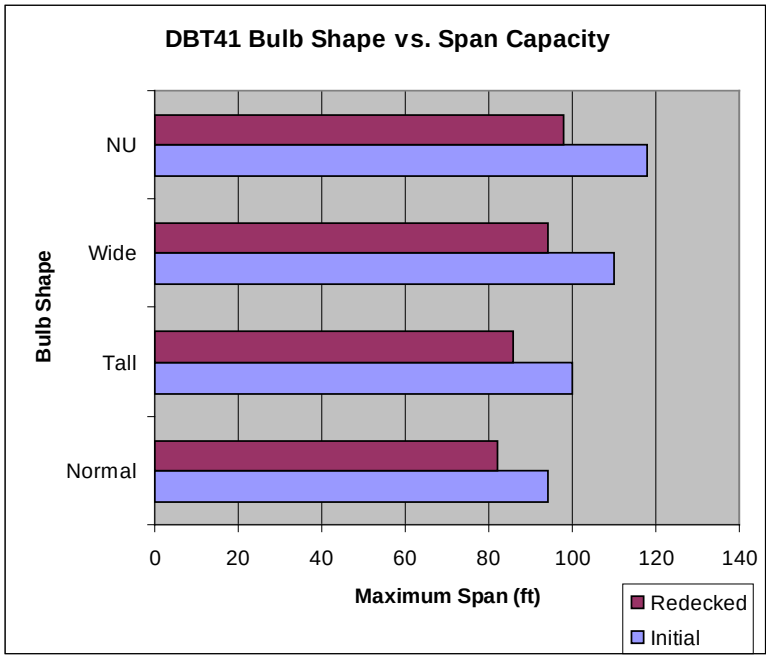

Figure D-6. Span Capabilities of DBT41: Decked vs. Re-decked (deck f'_c = 4.00 ksi).

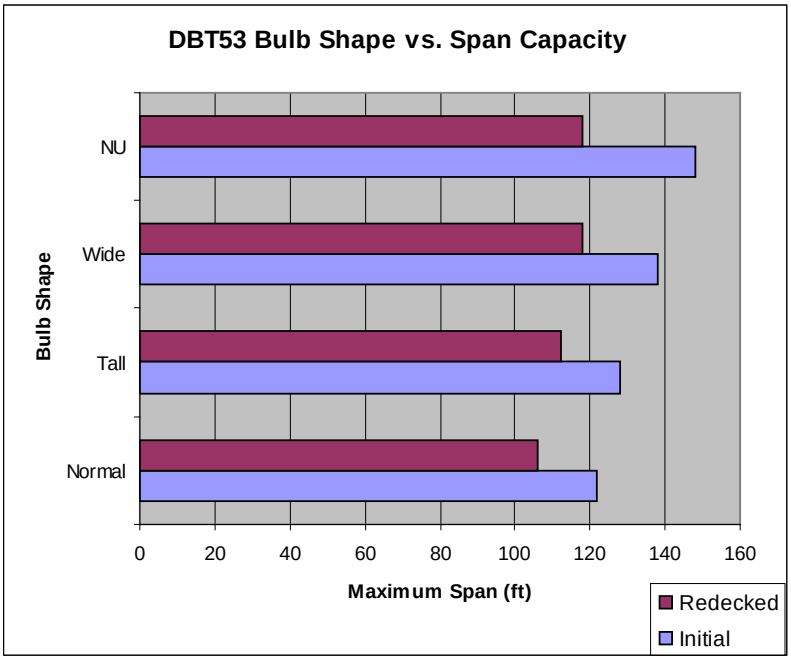

Figure D-7. Span Capabilities of DBT53: Decked vs. Re-decked (deck f'_c = 4.00 ksi).

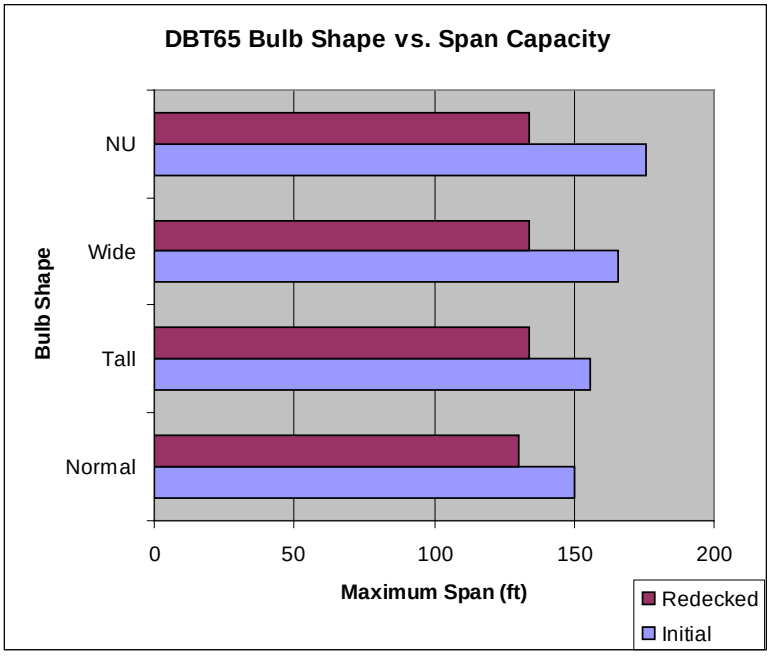

FigureD- 8. Span Capabilities of DBT65: Decked vs. Re-decked (deck f'_c = 4.00 ksi).

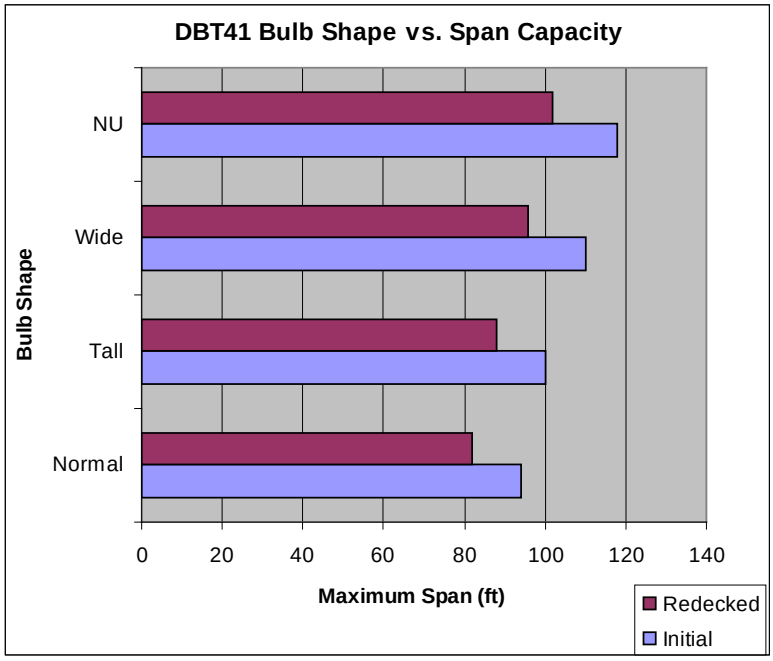

Figure D-9. Span Capabilities of DBT41: Decked vs. Re-decked (deck f'_c =6.00 ksi)

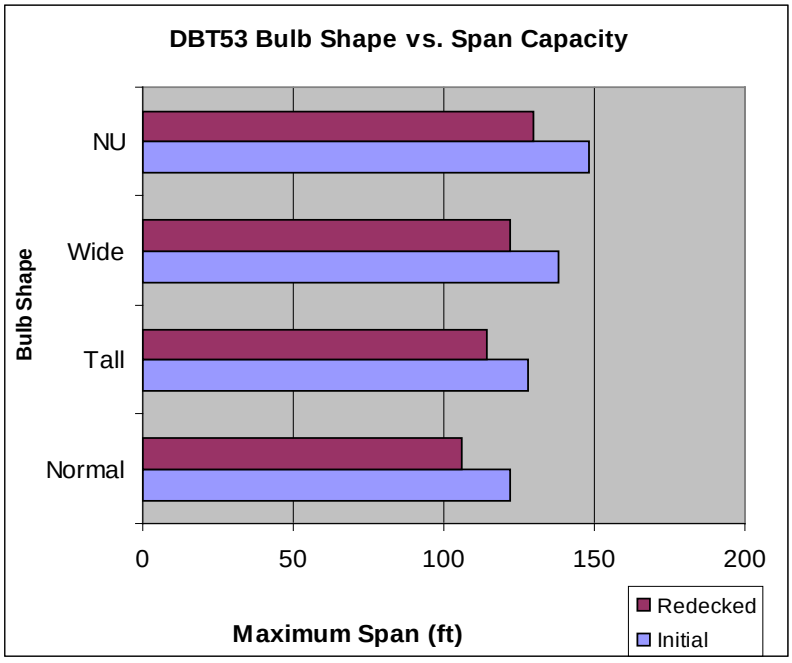

Figure D-10. Span Capabilities of DBT53: Decked vs. Re-decked (deck f'_c = 6.00 ksi).

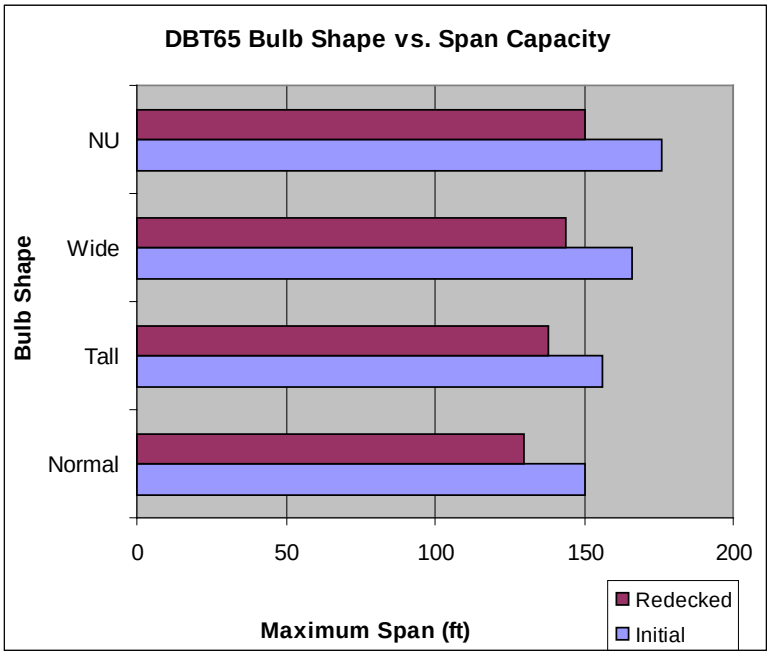

Figure D-11. Span Capabilities of DBT65: Decked vs. Re-decked (deck f'_c = 6.00 ksi).

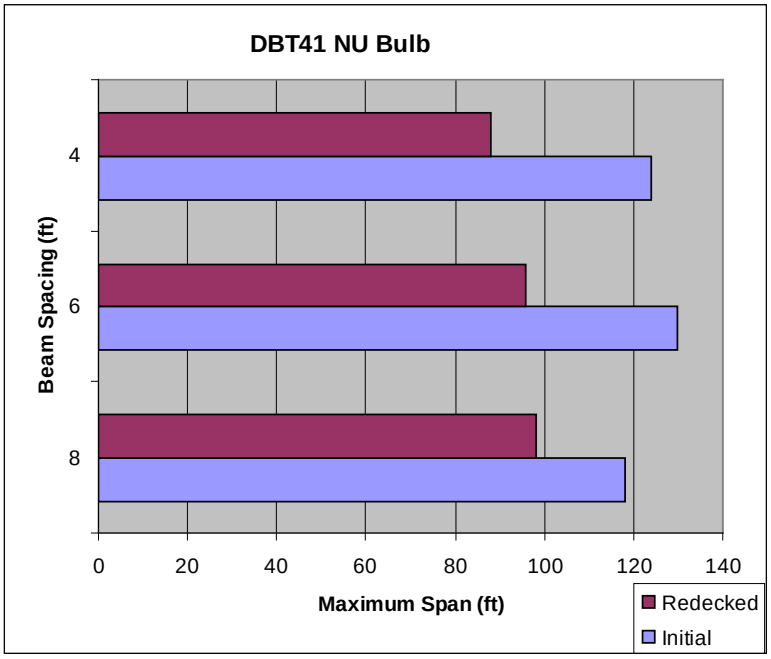

Figure D-12. Span Capabilities of DBT41 with NU Bulb vs. Variable Girder Spacing.

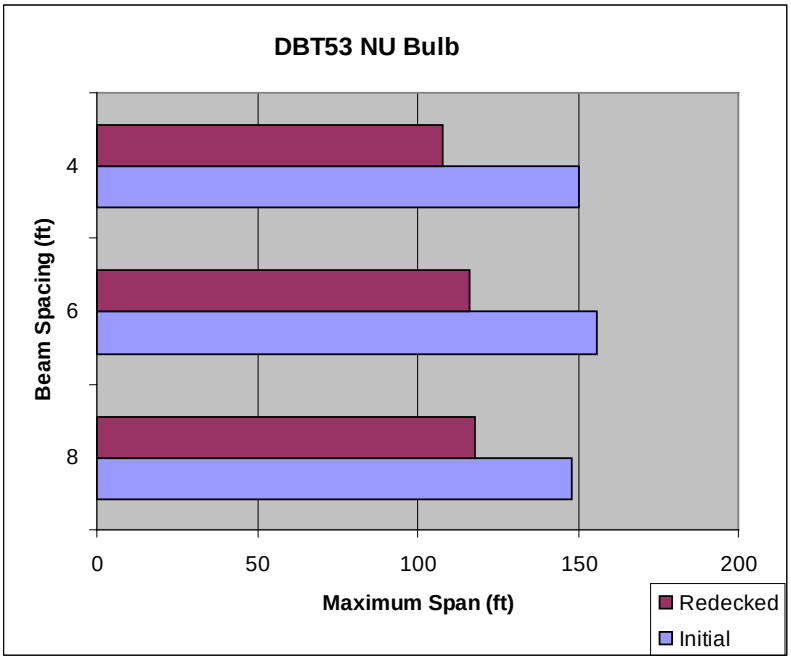

Figure D-13. Span Capabilities of DBT53 with NU Bulb vs. Variable Girder Spacing.

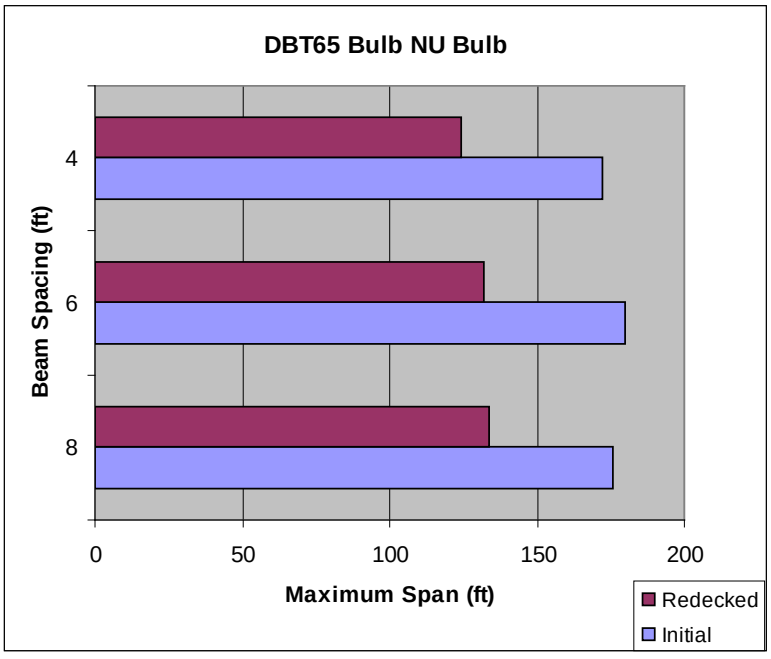

FigureD-14. Span Capabilities of DBT65 with NU Bulb vs. Variable Girder Spacing.

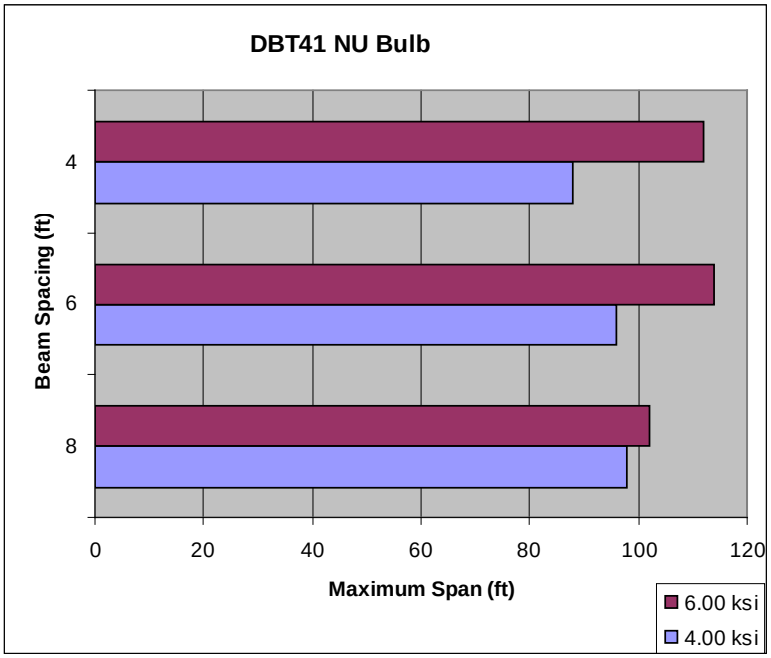

Figure D-15. Span Capabilities of DBT41 with NU Bulb vs. Variable Girder Spacing vs. Variable Deck Concrete Strength.

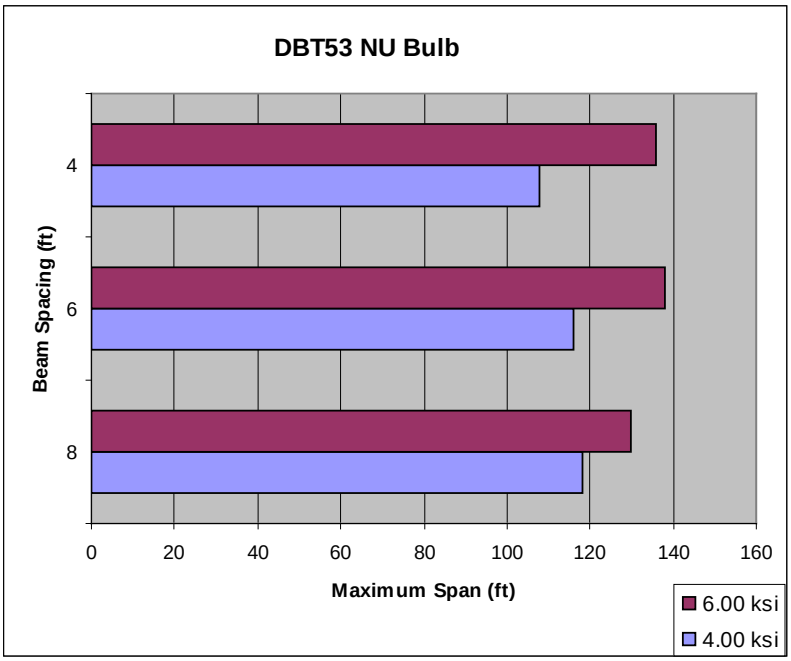

Figure D-16. Span Capabilities of DBT53 with NU Bulb vs. Variable Girder Spacing vs. Variable Deck Concrete Strength.

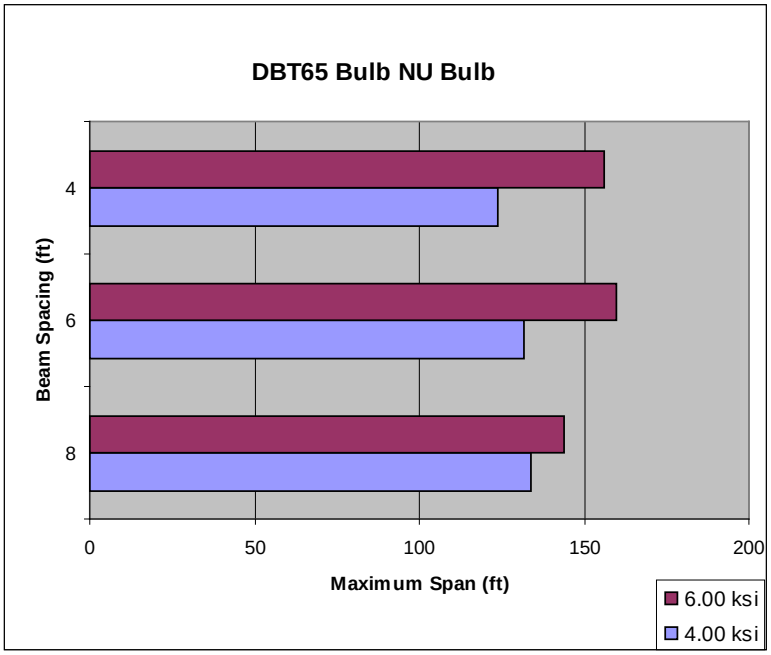

Figure D-17. Span Capabilities of DBT65 with NU Bulb vs. Variable Girder Spacing vs. Variable Deck Concrete Strength.

APPENDIX D REFERENCES

D1. Tadros, M. K. and Baishya, M. C., “Rapid Replacement of Bridge Decks,” NCHRP Report 407, .Transportation Research Board, National Cooperative Highway Research Program, 1998.

D2. .AASHTO, “LRFD Bridge Design Specifications,” Third Edition, American Association of State Highway and Transportation Officials, Inc., 2004.

D3. “PCI Bridge Design Manual”, Prestressed Concrete Institute, Chicago, IL, Oct. 1997.

D4. Russell, H. G., Volz, J. S., and Bruce, R. N., Optimized Sections for High-Strength Concrete Bridge Girders, Report FHWA-RD-95-180, Office of Advanced Research, Federal Highway Administration, Aug. 1997.

D5. Mast, R. F., “Lateral Stability of Long Prestressed Beams – Part 1”, PCI Journal, V. 34, No. 1, Jan. – Feb., 1989, pp. 34-53.

D6. Mast, R. F., “Lateral Stability of Long Prestressed Beams – Part 2”, PCI Journal, V. 38, No. 1, Jan. – Feb., 1993, pp. 70-88.

APPENDIX E

SUBTASK 6.2-A1 –STUDY OF CAMBER LEVELING FORCES

Introduction

The objective of this study is to determine the shear forces transferred across the joint due to leveling of differential camber. Following is a summary of the methodology and findings of this study.

Magnitude of Differential Camber

Alaska DOT specifies a camber tolerance of ± 1/8 in. per 10 ft of length with maximum of 1 in. from approved camber (E1). Alaska DOT also specifies that the camber of any girder shall not differ from that of any other girder by more than 1 in. PCI Design Handbook (E2) reports a typical differential camber tolerance of ¼ in. per 10 ft with a maximum of ¾ in. Washington State DOT (E3) specifies a differential camber tolerance of 1/8 in. per 10 ft of beam length. Based on consultation with experts from the precast-prestressed concrete industry, there seems to be a consensus that with the current industry standards the maximum limits on differential camber are hard to achieve for longer spans. Due to this variation between different specifications, camber measurement data are needed to define the practical limits on differential camber between girders in a span.

In a study conducted by Rosa et al. (E4), camber measurement data were collected for 146 girders. The information gathered included two camber measurements for each girder, one at release and one before shipping. A summary of these measurements is given in Table E-1. The girders were divided into 13 groups. Each group contained girders from one project with same section and length. The number of girders in a group varied between 4 and 28. Additional camber measurement data were reported by Sethi (E5) for 29 girders. A summary of these measurements is given in Table E-2. The girders are divided into five groups. For three groups camber was measured only at release. For the other two groups, camber was measured at release and at 60 days. Figure E-1 shows a plot of the maximum differential camber as a function of the girder length. It is observed that there is a significant scatter in the measured differential camber.

Based on the data presented above, the research team recommends using a differential camber tolerance of 1/8 in. per 10 ft with no upper limit. This relationship is shown in Figure E-1. Further camber measurement data is needed in order to refine this criterion.

Bridge Geometry

The overall width of the bridge used in the investigation of camber leveling forces is 48 ft. The bridge uses the decked bulb tee shapes developed in Subtask 6.1-B-Optimized Girder Study. Three different overall girder depths are investigated: 41 in., 53 in., and 65 in. The span of the bridge varied based on the girder depth and spacing to produce the maximum expected leveling shear for the girder configuration considered. The study included both right bridges and skewed bridges with a skew angle of up to 45^{o}.

Modeling Techniques

The bridge is modeled using finite element modeling techniques. The SAP2000 software is used for that purpose. The top flange, web, and bottom bulb of all girders are modeled using shell elements as shown in E-2. All girders are fully attached to each other, i.e., full continuity is assumed along the longitudinal joints. Thermal loads are applied to only one girder to simulate leveling the camber of this particular girder against the remainder of the bridge. The girder is selected to generate the highest possible camber leveling shear. The magnitude of the thermal loads is such that if the girder was to deflect freely, i.e., not attached to any other girders, the midpoint of the girder would move upward with a magnitude equal to the assumed camber. Since the girder is attached to the remainder of the bridge along the edges of the top flange, transverse shear stresses are generated in the longitudinal joints between that particular girder and the adjacent girders. These shear stresses are equivalent to those developed due to the camber leveling process.

An example of the transverse shear stresses is shown in Figure E-3. The bridge used in this analysis consisted of six girders with 65 in. depth, 8 ft spacing, and 84 ft span. One of the middle girders is assumed to be leveled against two attached girders on one side and three attached girders on the other side. The camber of the girder to be

leveled was assumed to be 1.05 in. It is observed from Figure E-3 that the sign of the transverse shear force across the joint is reversed near the supports.

The reversal in transverse shear stresses near the supports can be explained by studying the deformed shape of the girders. Figure E-4 shows the vertical displacement along various longitudinal profiles in the deck. The dashed line shows the vertical displacement in the deck along the centerline of the web of the cambered girder. If the girder was to camber freely, the camber at midspan would be 1.05 inches. Since the girder is attached to two neighboring girders, the camber is reduced to 0.36 inches. The solid line in Figure E-4 shows the vertical displacement along the longitudinal joint between the cambered girder and one of the neighboring girders. If the girders were not attached, the point at midspan of the flange edge of the cambered girder would camber upward by 1.05 inches. Since the girders are attached, camber of this point is reduced to 0.33 inches. Within the span, the neighboring girders are pulling down on the flange of the cambered girder. Because of the transverse flexibility of the flange, the reduction in camber along the edge of the flange is larger than along the centerline of the web.

As the neighboring girders are pulling down, the cambered girder is pushing upward on the flange edges of neighboring girders within the span. This causes the neighboring girder to bow upward and also to twist as shown in Figure E-5. The twisting causes the tip of the flange near the end supports to move upward and to push up on the flange tip of the cambered girder. This is evident from Figure E-4 where the solid line is higher than the dashed line near the supports indicating that the tip of the flange is moved upward relative to the web. In other words, near midspan, the neighboring girder is pushing downward on the cambered girder while it is the opposite near the end supports. This leads to the observed reversal in the transverse shear stresses.

Girder to be Leveled

Analyses were conducted to determine whether the leveling of an exterior or interior girder would produce higher shear in the longitudinal joint. Two scenarios were investigated. In both scenarios, the bridge consisted of six girders with 65 in. depth, 8 ft spacing, and 84 ft span. In the first scenario, an exterior cambered girder is assumed to be leveled against five attached girders on one side. In the second scenario, one of the middle girders is assumed to be leveled against two attached girders on one side and

three attached girders on the other side. In both cases, the camber of the girder to be leveled was assumed to be 1.05 in. Figure E-6 shows the transverse shear forces due to leveling for the two scenarios. The results indicate that leveling of the middle girder results in higher shear in the joint within the span while it is the opposite near the supports. This can be explained by the twisting of the exterior girder. Since the shear transferred across the joint due to live load is minimal near the supports, the shear forces developed within the span due to camber leveling are of more importance than those developed near the supports. It should also be noted that the joint was assumed to be rigid in this analysis. The flexibility of the joint as well as creep will significantly reduce the sharp peaks near the supports.

Span length

Analyses were conducted to determine whether higher camber leveling shear would be expected in the shorter or longer span ranges. Two scenarios were investigated. In both scenarios, the bridge consisted of six girders with 65 in. depth and 8 ft spacing. In the first scenario, the span was 84 ft with 1.05 in. differential camber. In the second scenario the span was 176 ft with 2.2 in. differential camber. In both cases, one of the middle girders is assumed to be leveled against two attached girders on one side and three attached girders on the other side. Figure E-7 shows the transverse shear forces due to leveling for the two scenarios. The results indicate that for a particular girder depth and spacing the maximum camber leveling shear will occur in the shorter spans of the span range for that girder configuration.

Parametric Study

Parametric study was conducted to determine the range of expected camber leveling shear for different girder depth, girder spacing, and skew angle. Three different overall girder depths are investigated: 41 in., 53 in., and 65 in. For each girder depth, 4 ft and 8 ft spacing are considered. The study included right bridges as well as bridges with skew angles of 15^o, 30^o, and 45^o. The shortest practical span for each combination of girder depth and spacing was used. For the 4 ft spacing, the bridge consisted of 12 girders, while for the 8 ft spacing the bridge consisted of 6 girders with an overall bridge width of 48 ft. For six girder bridges, one middle girder is leveled against two girders on one side and three girders on the other side. For twelve girder bridges, one middle

girder is leveled against five girders on one side and six girders on the other side. The magnitude of differential camber was based on the criterion discussed above.

The lower bound of the span for a give section was determined based on two criteria: minimum required concrete strength at release, f'_{ci}, and minimum required number of strands. The minimum f'_{ci} was limited to 1.0 ksi, and minimum number of strands was set to 18, which is number of strands in the bottom row of the modified bulb of the optimized section. While there is no hard boundary on the shortest span for a given section, these criteria were selected based on the experience of the research team to determine the practical shortest span for each section.

Table E-3 shows the different combinations for the parameters used in this investigation. The analysis was conducted for right bridges as well as bridges with skew angles of 15^o, 30^o, and 45^o.

Figure E-8 shows the transverse shear forces due to leveling for right bridges for the six scenarios investigated. The maximum joint shear ranges between 0.68 kip/ft to 0.87 kip/ft. Figures E-9 through E-11 show the transverse shear forces due to leveling for skewed bridges. The effect of the skew is such that the leveling shear is increased near one end of the longitudinal joint and reduced near the other end. This effect is more pronounced with the increase of the skew angle. The maximum joint shear ranges between 0.85 kip/ft to 1.01 kip/ft for 15^o skew angle, 1.04 kip/ft to 1.18 kip/ft for 30^o skew angle, and 1.28 kip/ft to 1.45 kip/ft for 45^o skew angle.

The maximum flexural stresses resulting in the girders due to camber leveling are summarized in Table E-4. The maximum observed stress is approximately 890 psi. It should be noted that these are transient stresses and that the final stresses will be significantly reduced due to creep.

Stress Relaxation due to Creep

The stress produced by an imposed deformation will relax overtime due to creep of concrete. ACI 209 Committee (E6) provides a methodology for calculating the stress relaxation after sudden imposed deformation given by the following equations.

$$\frac{S_t}{S_i} = 1 - \frac{\nu_t}{1 + \mathrm{X}\nu_t} \qquad \text{(Eq. 1)}$$

$$\nu_t = \frac{(t - t_{la})^{0.6}}{10 + (t - t_{la})^{0.6}} \nu_u \qquad \text{(Eq. 2)}$$

$$\nu_u = 2.35\gamma_c \qquad \text{(Eq. 3)}$$

Where:

S_i stress, internal force or moment produced by a sudden imposed deformation at time t_{la}

S_t stress, internal force or moment at any time $t > t_{la}$

X aging coefficient, depends on age at the time t_{la}, when the structure begins carrying the load and on the load duration $t - t_{la}$

ν_t creep coefficient at time t

ν_u ultimate creep coefficient

γ_c represents the product of the applicable correction factors

To determine the range of the ratio S_t/S_i, the above equations were solved for a range of variables. The time at which camber leveling is performed, t_{la}, will influence the aging coefficient, X, as well as the ultimate creep coefficient, ν_u. Based on consultation with experts from the industry, the girder age at which camber leveling is performed could vary from 3 days to 3 months. ACI 209 provides X values corresponding to t_{la} of 10, 100, 1000, and 10000 days. For simplification of analysis, t_{la} values of 10 and 100 days were considered. The value of ν_u also depends on ambient relative humidity and volume-surface ratio of the member. An ambient relative humidity of 40% represents an upper bound on the calculated creep coefficient. A maximum ambient relative humidity of 80% covers only a small portion of the US near the west coast while an ambient

relative humidity of 70% represents a great portion of the US territories. Therefore, ambient relative humidity values of 40% and 70% were investigated. The volume-surface ratio was calculated for a 53 inches deep girder with 8 ft girder spacing to represent the midrange of the series of girder sections considered in this investigation. The following equations show the creep correction factors for the conditions described above.

$$\gamma_{la} = 1.13\left(t_{la}\right)^{-0.094} \quad \text{for steam cured concrete} \quad \text{(Eq. 4)}$$

$$\gamma_{\lambda} = 1.27 - .0067\lambda \quad \text{for} \quad \lambda > 40 \quad \text{(Eq. 5)}$$

$$\gamma_{vs} = \frac{2}{3}\left[1 + 1.13\exp(-0.54v/s)\right] \quad \text{(Eq. 6)}$$

Where:

γ_{la} loading age creep correction factor

γ_{λ} ambient humidity creep correction factor

γ_{vs} volume-surface ratio creep correction factor

λ ambient relative humidity

v/s volume-surface ratio of the member in inches

The ratio S_i/S_t was calculated at loading E-12. This figure indicates that the shear forces would be expected to reduce to approximately 50% of the initial shear force after 100 days and 35% of the initial shear force after approximately three years.

Conclusions:

Camber Leveling Shear Forces

The results of the camber leveling study indicate that the maximum camber leveling shear will occur in the shorter spans of the span range for each of the three girder depths of 41 in., 53 in. and 65 in. Based on the analyses, higher camber leveling shear forces occur with leveling of a middle girder against attached girders on both

sides. The maximum camber leveling shear stress increases with the increase of the skew angle.

Analyses indicated the maximum joint shear for non-skewed bridges was 0.87 kip/ft. The effect of the skew is such that the leveling shear is increased near one end of the longitudinal joint and reduced near the other end. This effect is more pronounced with the increase of the skew angle. The maximum calculated joint shear was 1.01 kip/ft for 15^o skew angle, 1.18 kip/ft for 30^o skew angle, and 1.45 kip/ft for 45^o skew angle.

This upper bound magnitude of camber leveling shear force of 1.45 kip/ft results in an initial nominal shear stress of 20 psi on the 6 in. thick deck section. Due to creep, the shear forces would be expected to reduce to approximately 35% of the initial shear force after approximately three years. Therefore, based on these studies, camber leveling shear forces do not result in a high shear demand on the type of longitudinal joint under investigation. However, consideration for the presence of constant shear was included in defining the loading to be used in the joint assembly testing in Subtask 6.2-C2.

Although the maximum initial camber leveling shear force will reduce with time, this initial force needs to be considered in design of the camber leveling procedures. Camber leveling procedures are discussed in the Guidelines for Design and Constructions developed in Task 6.3. As discussed in the Guidelines document , for camber leveling procedures, weld plates or temporary clamps may be used to resist the camber leveling forces until the joints are grouted. The maximum calculated levels of temporary joint shear force described above, dependent on whether the bridge is a non-skewed or skewed bridge, can be used to determine the design shear force for the welded connectors.. An example design for temporary clamps, using 1.5 k/ft. as the maximum camber leveling shear force, is included in the following Appendix E1.

Flexural Stress in Girders Due to Camber Leveling

The calculated maximum change in stresses in the bottom bulb of the girders due to camber leveling forces were nominally high (a maximum calculated of approximately 890 psi). This is likely a conservatively high calculated stress considering that:

- The differential camber used to verify the 1/8 in. per 10 ft. was the maximum camber difference between any two of the girders in a group, it is unlikely that this maximum differential camber would actually occur between an interior girder and the two adjacent girders as modeled in the analyses for this study;

- The analyses assumed that 100% of the deferential camber was removed during the leveling process;

- Creep is expected to reduce camber leveling stresses to approximately 35% of the initial stresses;

- The effect of camber leveling has not been shown to be a problem in decked girder bridges presently in use;

Although the nominally high tensile stresses were calculated using conservative assumptions and creep is expected to reduce the level of these stresses in a short time, further consideration was given to these nominally high stresses.

Additional analyses were therefore performed to investigate the sensitivity of the calculated stresses to span length. A governing condition for maximum calculated camber leveling forces in the prior parametric study was a short span. The maximum forces for each girder depth analyzed were calculated using the shortest span length. The additional analyses were therefore carried out to determine if the calculated tensile stresses decreased significantly as the spans were increased. For each combination of girder depth and spacing, the span was varied from the practical shortest span to the longest possible span for that particular section. Figure E-13 shows the effect of the span length on the maximum tensile stress in the bottom of the girder for straight bridges. The analyses did not indicate a significant drop with increased span length. Calculated maximum tensile stresses, ranging from approximately 400 to 500 psi at the longest possible spans, are still nominally high.

One of the reasons given above to support a conclusion that tensile stresses due to camber leveling should not be a problem is that the effects of camber leveling has not been observed to be a problem in decked girder bridges currently in use. However, it should be noted that an allowable of 0 tensile stress is commonly used in the design of decked girders under service load. This criterion allows a margin of tensile capacity to

help compensate for camber leveling tensile stresses. Based on this observation and the nominally high calculated flexural tensile stresses in this camber leveling study, an allowable of 0 tensile stress is included in the design guidelines developed in this project.

Table E-1 Camber Measurement Data (Ref. E4)

Group	Project	No. of Girders	Section	Length (ft)	Camber at Release (in.)			Camber before Shipping (in.)		
					min	max	Diff	min	max	Diff
1	277th St Bridge	16	W50G	96	1.92	3.36	1.44	3.12	4.56	1.44
2	Black Lake Blvd	11	W74G	66	0.12	0.48	0.36	0.24	0.60	0.36
3	Black Lake Blvd	11	W74G	87	0.24	0.48	0.24	0.48	1.08	0.60
4	Black Lake Blvd	11	W74G	107	0.48	1.08	0.60	1.32	2.04	0.72
5	Black Lake Blvd	11	W74G	126	1.68	2.16	0.48	2.76	4.20	1.44
6	Black Lake Blvd	22	W74G	131	1.80	2.76	0.96	2.64	4.56	1.92
7	Cedar River Bridge	4	WF74	95	0.69	0.75	0.06	1.00	1.00	0.00
8	Cedar River Bridge	4	WF74	120	1.00	1.50	0.50	1.50	1.81	0.31
9	Cedar River Bridge	5	WF74	128	1.13	1.50	0.37	1.31	1.75	0.44
10	Keys Road Bridge	28	W83G	178	2.75	4.38	1.63	3.51	4.67	1.16
11	Snake Lake Bridge	8	W74G	135	1.04	2.36	1.32	1.57	2.95	1.38
12	Yakima River Bridge	7	W83G	171	3.25	3.62	0.37	4.25	5.50	1.25
13	Yakima River Bridge	8	W83G	173	3.26	3.75	0.49	4.25	5.25	1.00

Table E-2 Camber Measurement Data (Ref. E5)

Group	Project	No. of Girders	Section	Length (ft)	Camber at Release (in.)			Camber at 60 days		
					min	max	Diff	min	max	Diff
1	---	4	PCBT	90	1.38	2.50	1.13	---	---	---
2	---	10	PCBT	108	2.56	3.63	1.07	---	---	---
3	---	7	PCBT	94	1.38	1.75	0.38	---	---	---
4	Cooper River Bridge	4	79” BT	128	1.60	2.75	1.15	2.10	3.10	1.00
5	Cooper River Bridge	4	79” BT	136	2.50	2.90	0.40	3.25	3.50	0.25

Table E-3 Parameters for Camber Leveling Study

Girder Depth (in.)	Girder Spacing (ft)	Span (ft)	Diff. Camber (in.)
65	8	84	1.05
65	4	108	1.35
53	8	76	0.95
53	4	98	1.23
41	8	64	0.80
41	4	84	1.05

Table E-4 Girder Flexural Stresses Due to Camber Leveling (psi)

Girder			Skew Angle							
Depth	Spac.	Span	0^o		15^o		30^o		45^o	
(in.)	(ft)	(ft)	Tens.	Com.	Tens.	Com.	Tens.	Com.	Tens.	Com.
65	8	84	800	-551	814	-559	843	-658	889	-785
65	4	108	734	-598	737	-599	744	-620	756	-695
53	8	76	742	-480	756	-483	786	-595	832	-710
53	4	98	663	-538	666	-539	673	-560	686	-625
41	8	64	685	-439	702	-443	734	-557	785	-670
41	4	84	596	-488	600	-489	609	-513	623	-570

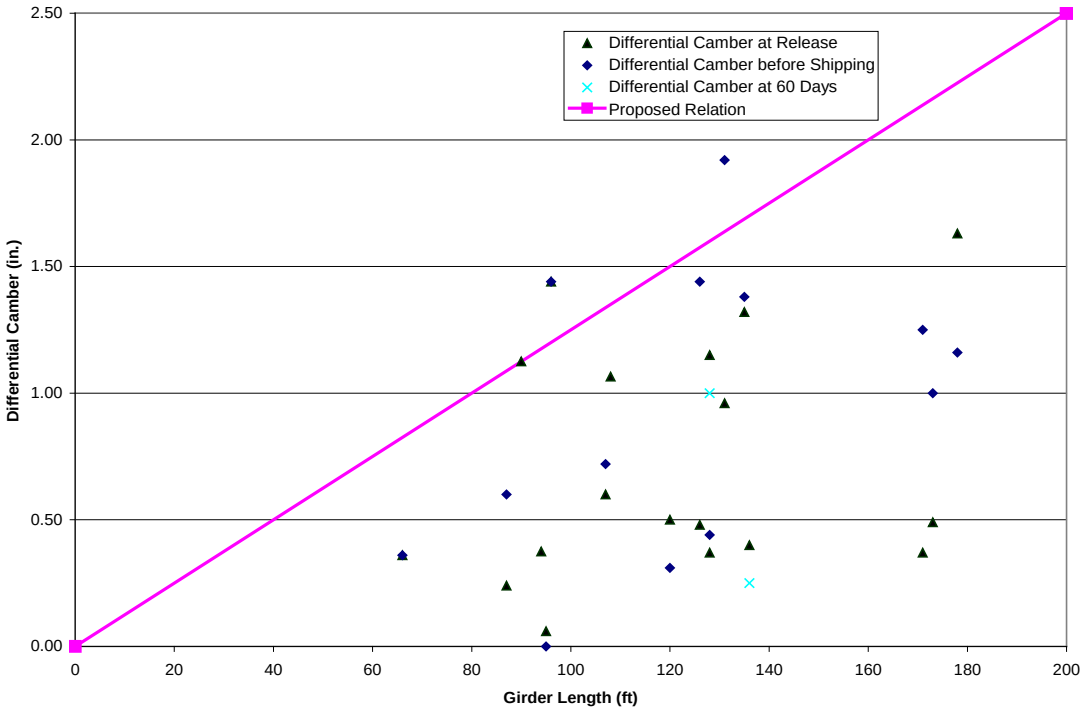

Figure E-1 Differential camber measurements

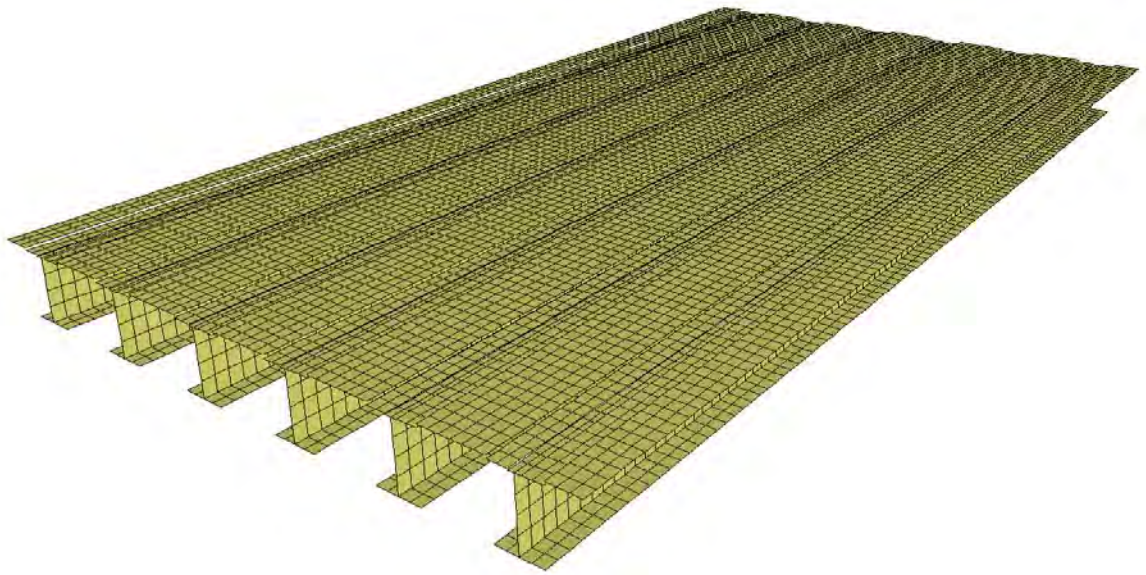

Figure E-2 Finite element model using shell elements

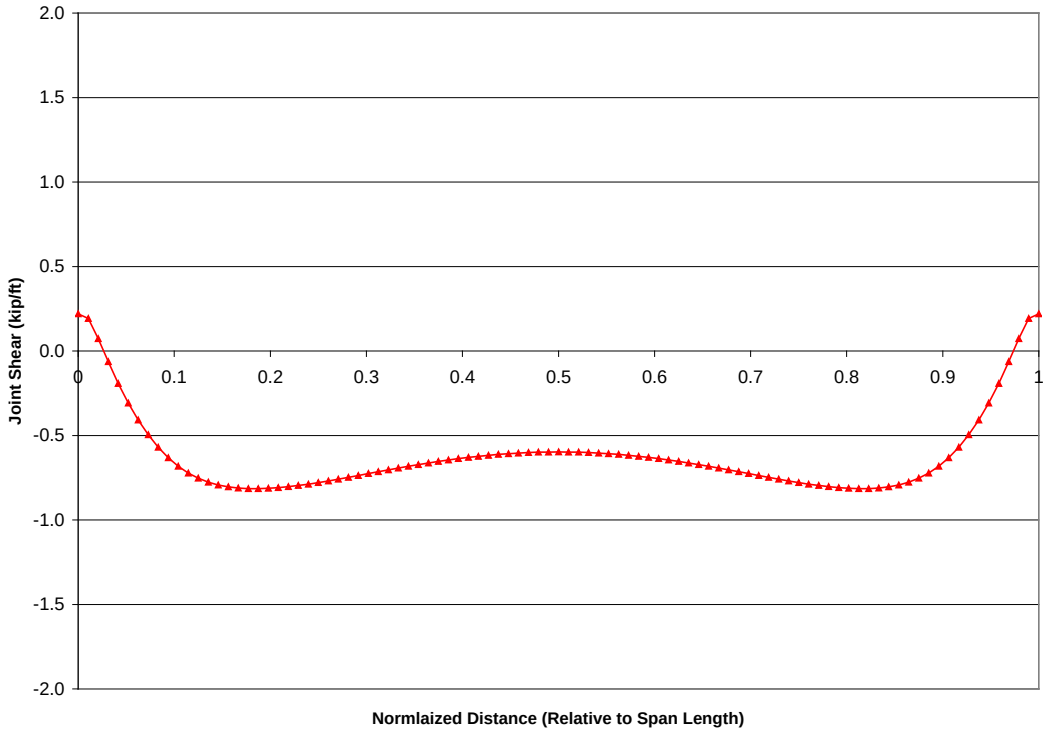

Figure E-3 Transverse shear forces due to leveling of an interior girder

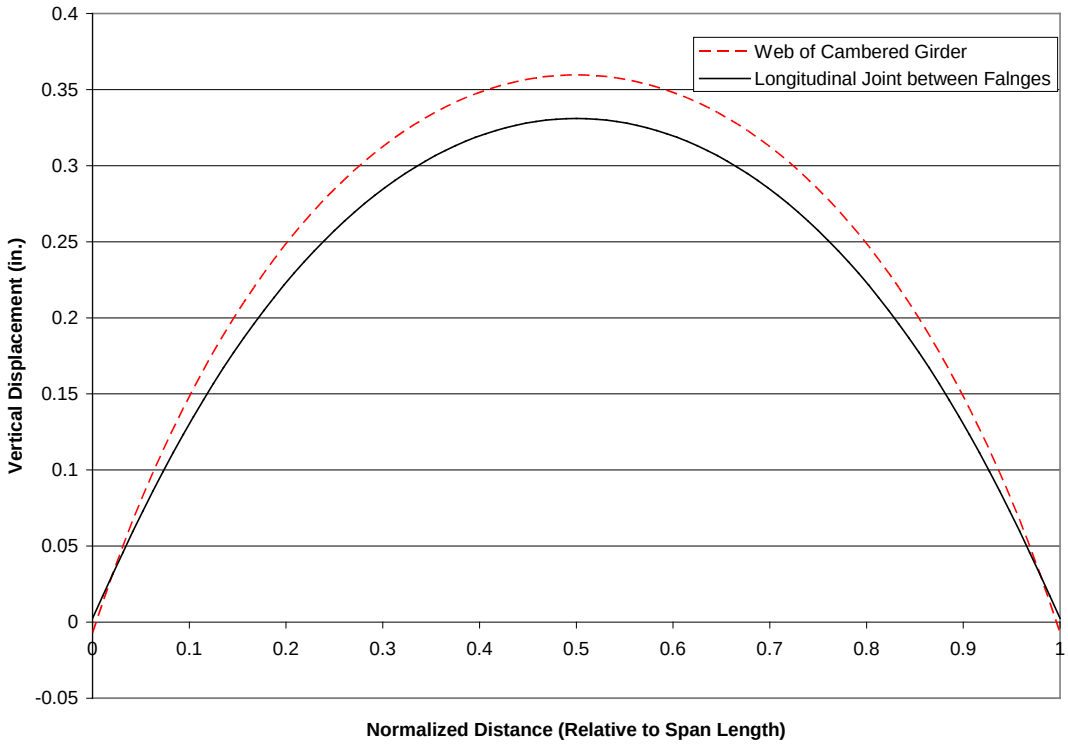

Figure E-4 Vertical displacement along centerline of girder web and longitudinal joint

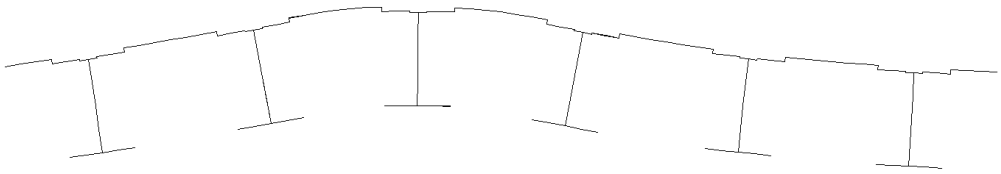

Figure E-5 Twisting of neighboring girders

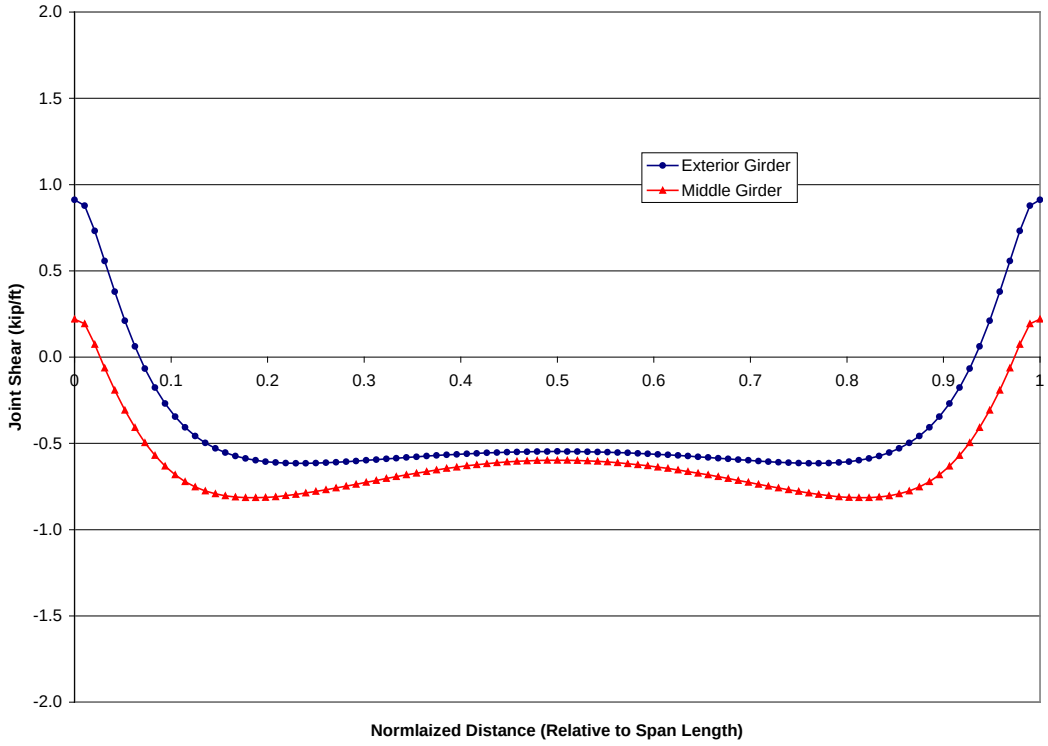

Figure E-6 Comparison of shear forces due to leveling of exterior and interior girders

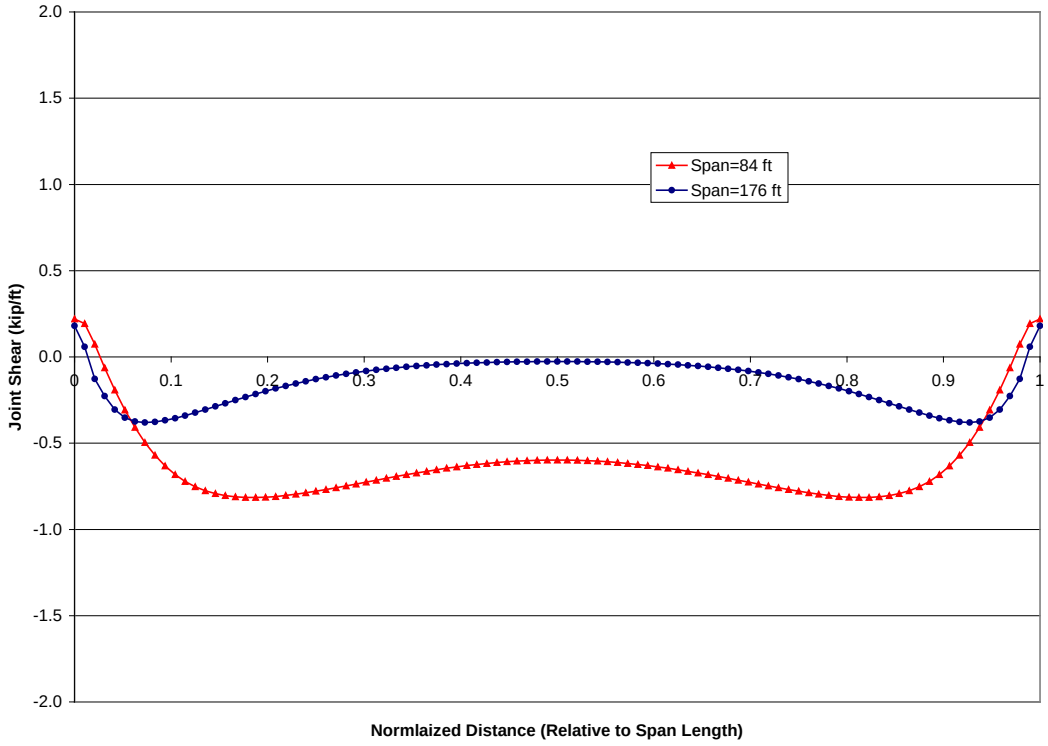

Figure E-7 Comparison of shear forces due to leveling of shorter and longer spans

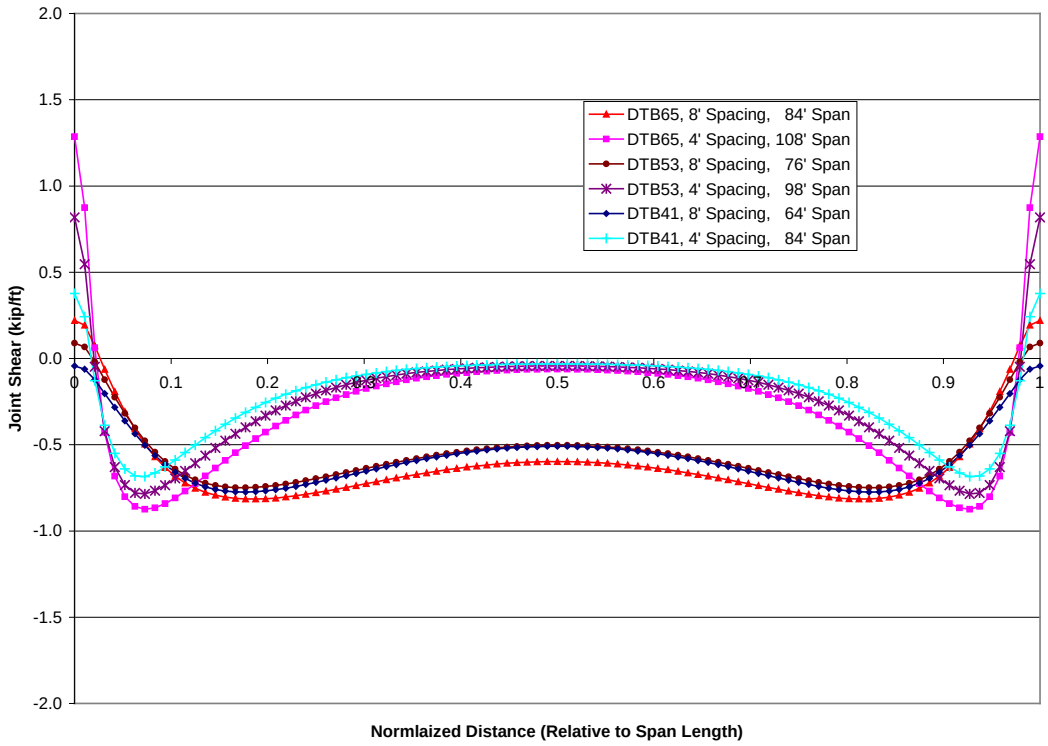

Figure E-8 Shear forces due to camber leveling in right bridges

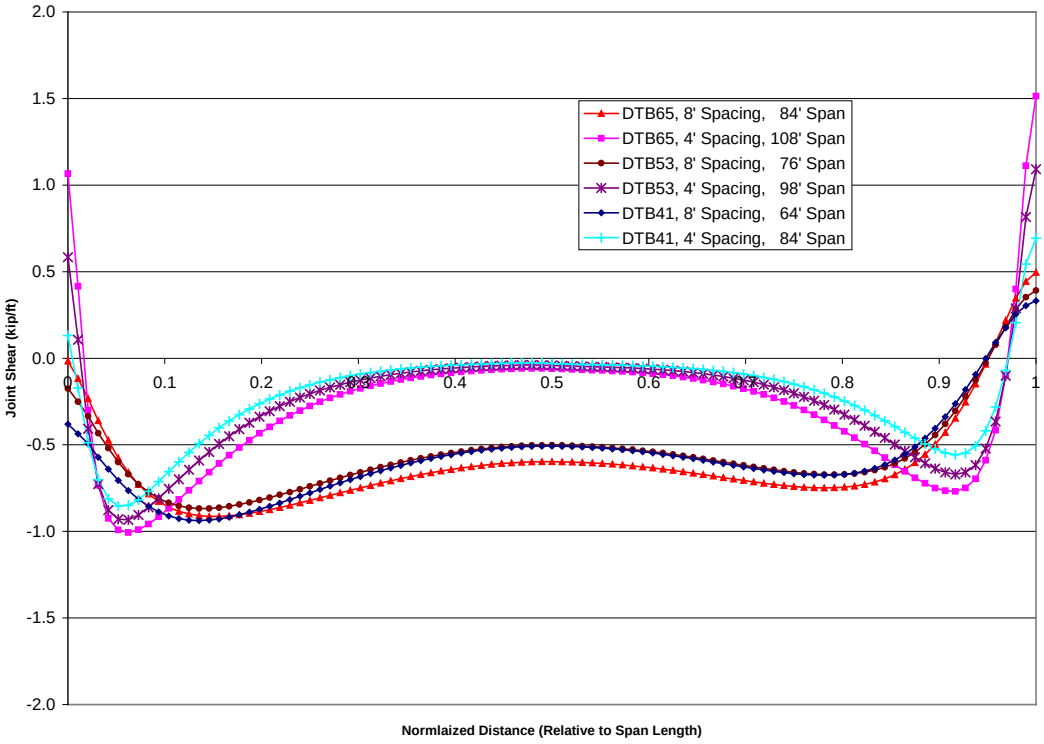

Figure E-9 Shear forces due to camber leveling in 15^o skewed bridges

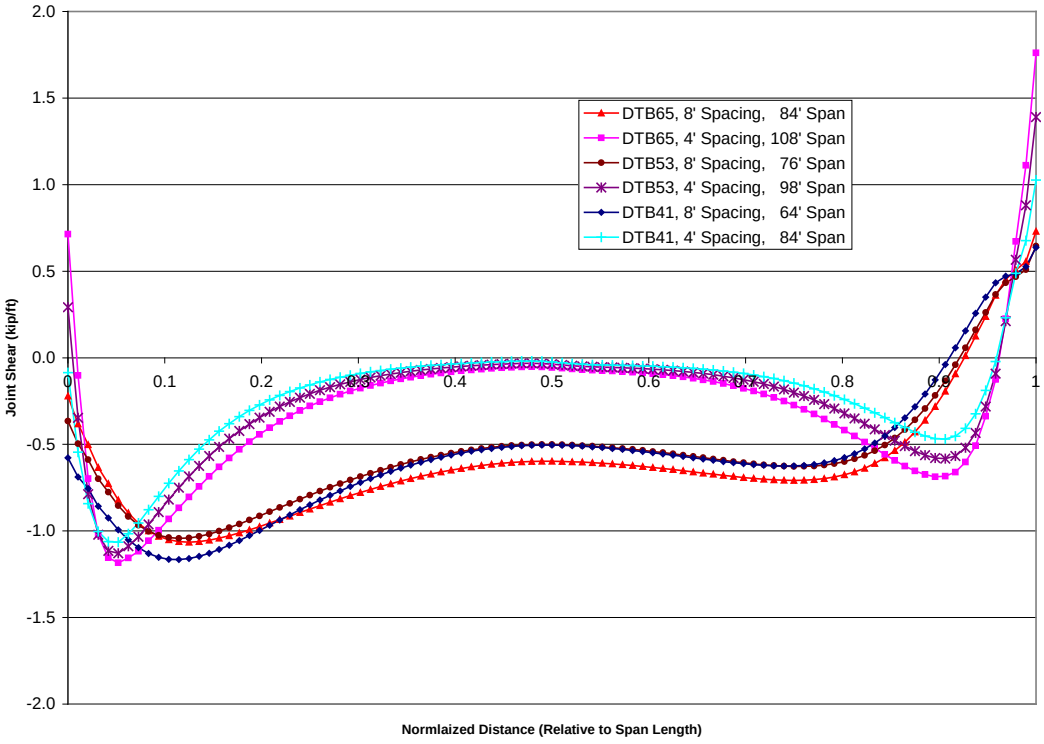

Figure E-10 Shear forces due to camber leveling in 30^o skewed bridges

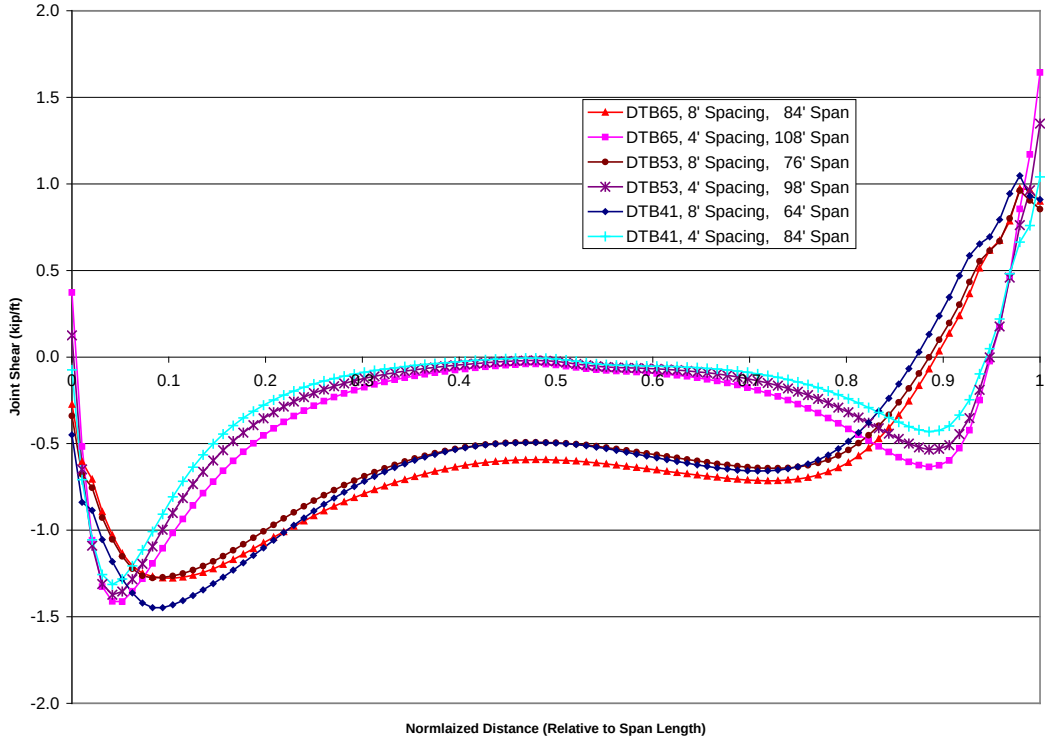

Figure E-11 Shear forces due to camber leveling in 45^o skewed bridges

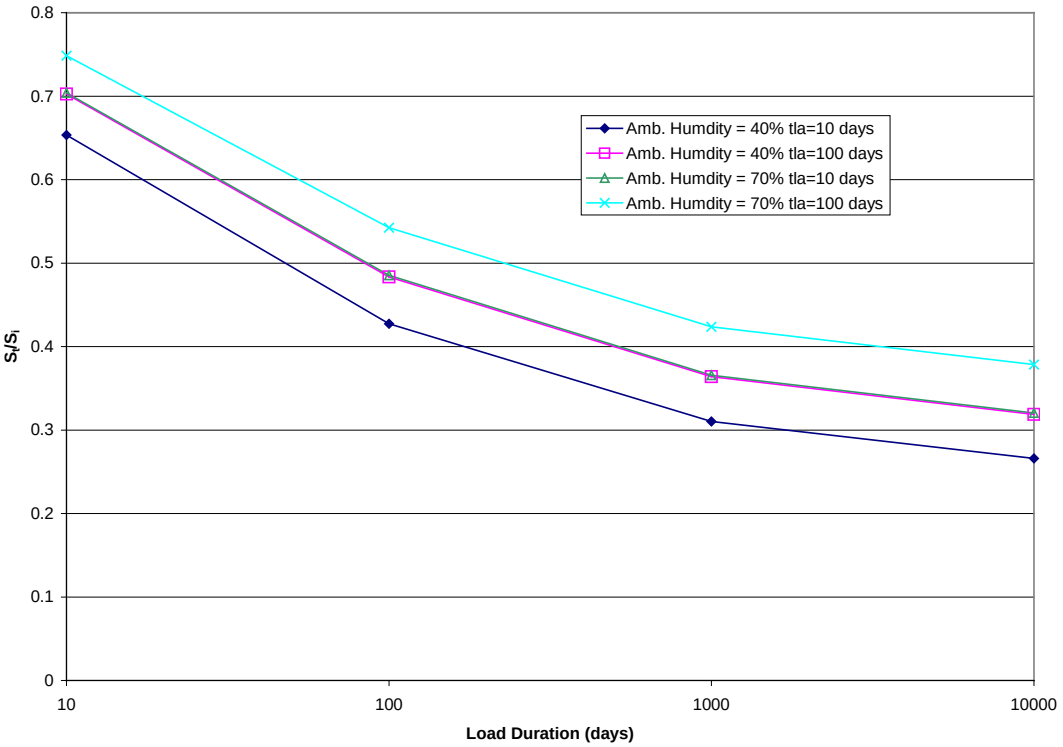

Figure E-12 Stress relaxation due to creep

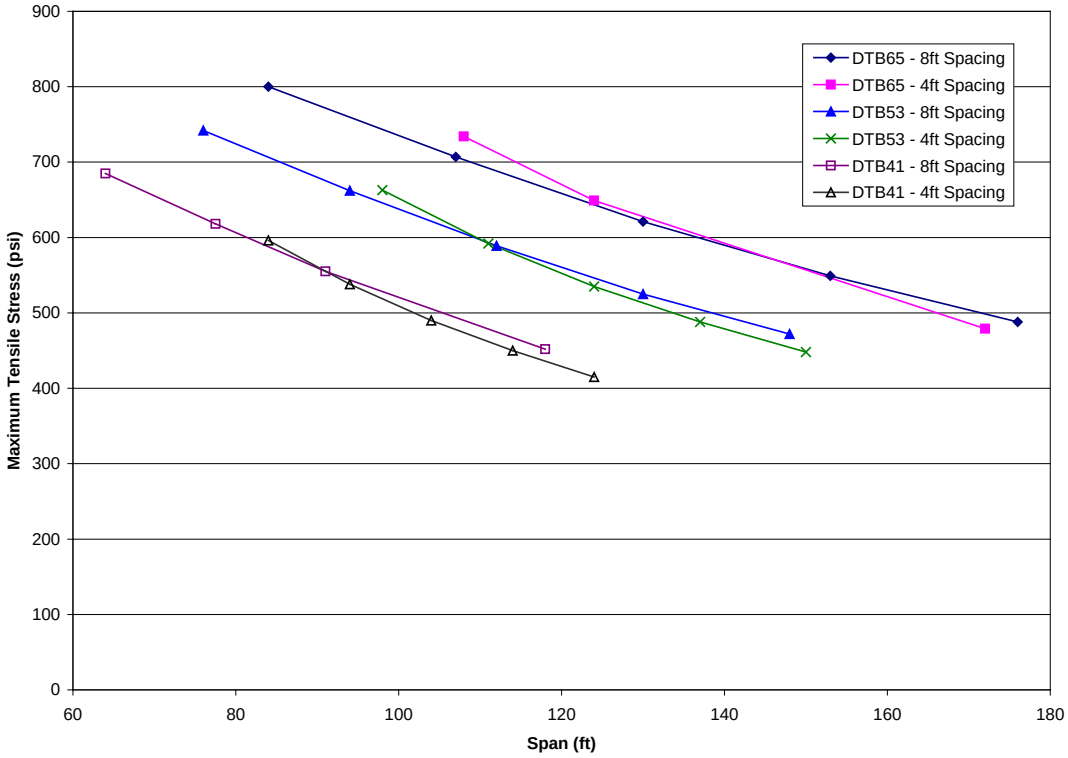

Figure E-13 Effect of Span Length on Camber Leveling Stress

APPENDIX E REFERENCES:

E1 Alaska Department of Transportation and Public Facilities, Standard Specifications for Highway Construction 2004
http://www.dot.state.ak.us/stwddes/dcsspecs/assets/pdf/hwyspecs/english/2004sshc.pdf

E2 Prestressed Concrete Institute, “PCI Design Handbook,” 6th Edition, Chicago, 2004.

E3 Washington State Department of Transportation, Standard Specifications for Road, Bridge, and Municipal Construction, 2006.

E4 Rosa, M., Stanton, J. F., and Eberhard, M. O. “Improving Predictions for Camber in Precast, Prestressed Concrete Bridge Girders,” University of Washington, Seattle, Washington, March, 2007.

E5 Sethi, V., “Unbonded Monostrands for Camber Adjustment,” Master Thesis, Virginia Polytechnic Institute and State University, Blacksburg, Virginia, 2006.

E6 ACI Committee 209, “Prediction of Creep, Shrinkage, and Temperature Effects in Concrete Structures,” ACI Manual of Concrete Practice, 2002.

APPENDIX E1

DESIGN EXAMPLE FOR CAMBER LEVELING CLAMP

- Assume average camber leveling shear = 1.5 kip/ft
- Assume girders are clamped every 5 ft
- Leveling shear force transferred per clamp (V) = (5)(1.5) = 7.5 kip
- Proposed clamp geometry is shown in Figure 1
- Idealization of the force transfer is shown in Figure 2
- From equilibrium

$$P_1 - P_2 = V$$

$$P_1 - P_2 = 7.5$$

$$P_1(7) = P_2(13)$$

$$P_1 = 1.857P_2$$

$$1.857P_2 - P_2 = 7.5$$

$$P_2 = \frac{7.5}{0.857} = 8.75 \quad \text{kips}$$

$$P_1 = 7.5 + 8.75 = 16.25 \quad \text{kips}$$

$$T = P_1 + P_2$$

$$T = 16.25 + 8.75 = 25 \quad \text{kips}$$

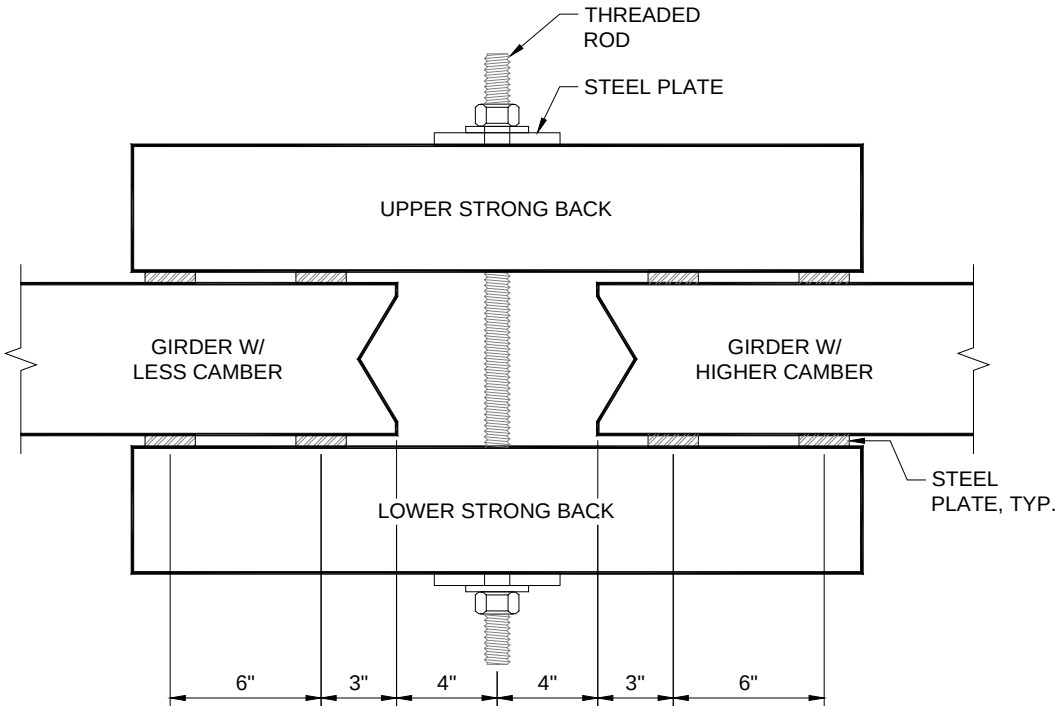

FIGURE 1

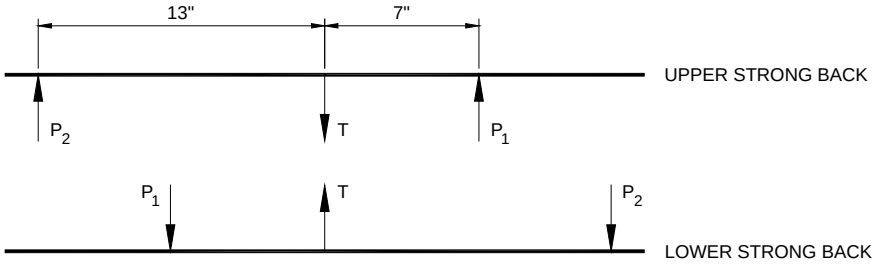

FIGURE 2

Design of strong back

- The reactions and internal forces diagrams for the upper strong back are shown in Figure 3.

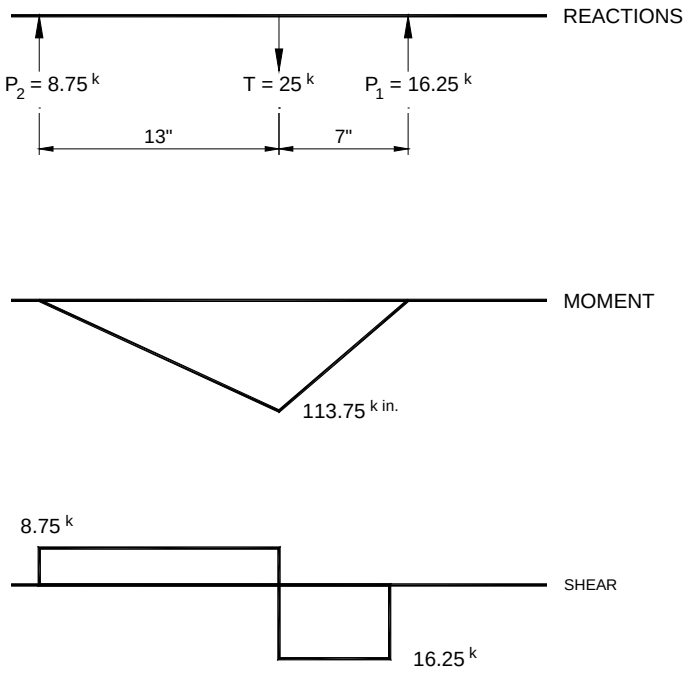

FIGURE 3

- Use a load factor of 1.6 for the design of the steel components of the temporary clamp.

$M_u = (113.75)(1.6) = 182$ kip-in

$V_u = (16.25)(1.6) = 26$ kips

- Use 2C5x9

$\phi V_n = \phi_v (0.6) F_y A_w$

$\phi V_n = 2(0.9)(0.6)(36)(5)(0.325)$

$\phi V_n = 63.18$ kips > V_u (Ok)

$Z = 4.36$ in^3 per channel

$M_p = (4.36)(36) = 156.96$ kip-in per channel

$r_y = 0.489$ in.

$$L_p = \frac{300 r_y}{\sqrt{F_{yf}}}$$

$$L_p = \frac{300(0.489)}{\sqrt{36}} = 24.45 \text{ in.}$$

$L_b = (2)(13) = 26$ in. $\cong L_p$

$\phi M_n = 0.9 M_p$

$\phi M_n = 0.9(2)(156.96) = 282.5$ kip-in > M_u (Ok)

- Check web crippling and local yielding

$T_u = 1.6(25) = 40$ kips

Using LRFD Tables

$\phi R = 2(60) = 120$ kips > T_u (no stiffeners are required)

Threaded rod design

- Use A193, grade B7 all thread rod, 1 in. diameter

$\phi R_n = 0.75(0.75 F_u) A_g$

$\phi R_n = 0.75\big((0.75)(120)\big)(0.7854) = 53.0$ kips > T_u (Ok)

Bearing plate design

- Figure 4 shows a cross section of the strong back.
- Assume reaction is at the center point of the web and plate is acting as simply supported beam.

$$M_u = \frac{40(1.5+0.325)}{4} = 18.25 \qquad \text{kip-in}$$

- Use 5in. x 5in. x 1in. plate

$$Z = \frac{bt^2}{4}$$

$$b = 5 - (1 + 0.125) = 3.875$$

$$Z = \frac{(3.875)(1)^2}{4} = 0.969 \qquad \text{in}^3$$

$$\phi M_n = 0.9(0.969)(36) = 31.39 \qquad \text{kip-in} \quad > M_u \quad \text{(Ok)}$$

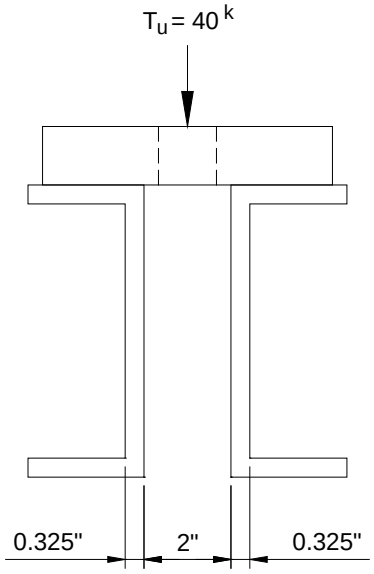

FIGURE 4

Check bearing on concrete

- Load factor for construction loads is 1.5 per LRFD Article 3.4.2.
- Assume support plate is 2in. $\times$ 5in.

$P_u = 1.5(16.25) = 24.375$ kips

$P_n = 0.85 f_c' A_1 m$ LRFD Eq. (5.7.5-2)

$A_1 = 2(5) = 10$ in^2 (see Figure 5)

$A_2 = (2+4)(5+4) = 54$ in^2 (see Figure 5)

$m = \sqrt{\frac{A_1}{A_2}} \le 2$ LRFD Eq. (5.7.5-3)

$\sqrt{\frac{A_1}{A_2}} = \sqrt{\frac{54}{10}} = 2.33$ > 2

Use $m = 2$

$f_c' = 7$ ksi

$P_n = 0.85(7)(10)(2) = 119$ kips

$P_r = \phi P_n$ LRFD Eq. (5.7.5-1)

$P_r = 0.7(119) = 83.3$ kips > P_u (Ok)

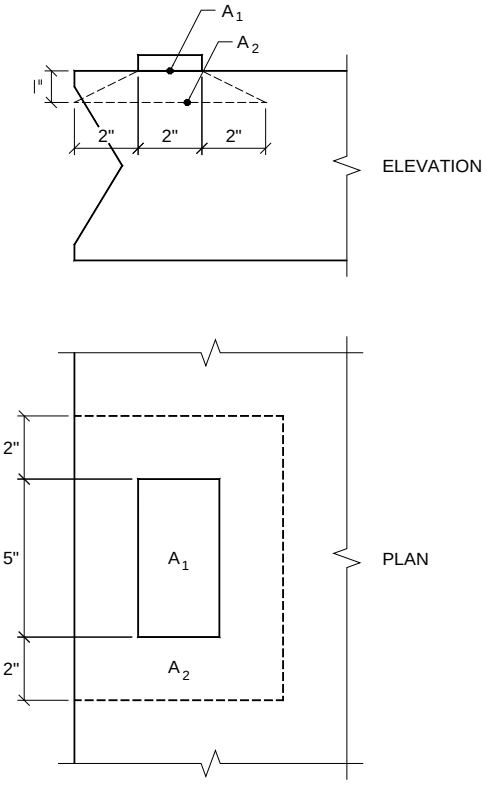

FIGURE 5

Check punching shear

$$V_n = \left(0.063 + \frac{0.126}{\beta_c}\right)\sqrt{f_c'}\,b_o d_v \le 0.126\sqrt{f_c'}\,b_o d_v \qquad \text{LRFD Eq. (5.13.3.6.3-1)}$$

With no. 4 rebars and 1 in. clear cover on the bottom

$$d_v = 6 - 1 - \frac{0.5}{2} = 4.75 \text{ in.}$$

$$b_o = 9.75 + 2(6.375) = 22.5 \quad \text{in. (see Figure 6)}$$

$$\beta_c = \frac{5}{2} = 2.5$$

$$\left(0.063 + \frac{0.126}{\beta_c}\right) = 0.063 + \frac{0.126}{2.5} = 0.113 < 0.126$$

$$V_n = 0.113\sqrt{f_c'}\,b_o d_v = 0.113\sqrt{7}(22.5)(4.75) = 31.95 \text{ kips}$$

$$\phi V_n = 0.9(31.95) = 28.8 \quad \text{kips} \quad > P_u \quad \text{(Ok)}$$

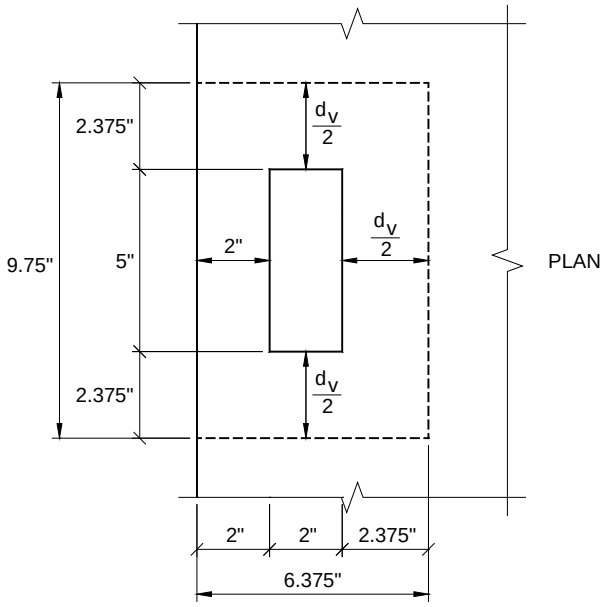

FIGURE 6

Check top flange transverse flexure

- Typical top flange reinforcement is #5 at 4 in. spacing for top reinforcement and #4 at 6 in. spacing for bottom reinforcement.
- Top cover is 2.5 in. and bottom cover is 1 in.

For negative bending of top flange

$$d = 6 - 2.5 - \frac{0.625}{2} = 3.19 \quad \text{in.}$$

$$A_s = 0.31\left(\frac{12}{4}\right) = 0.93 \ \text{in}^2/\text{ft}$$

$$a = \frac{(0.93)(60)}{0.85(7)(12)} = 0.78 \quad \text{in.}$$

$$\phi M_n = 0.9(0.93)(60)\left(3.19 - \frac{0.78}{2}\right) \Big/ 12 = 11.72 \quad \text{kip-ft/ft}$$

For positive bending of top flange

$$d = 6 - 1 - \frac{0.5}{2} = 4.75 \ \text{in.}$$

$$A_s = 0.2\left(\frac{12}{6}\right) = 0.4 \quad \text{in}^2/\text{ft}$$

$$a = \frac{(0.4)(60)}{0.85(7)(12)} = 0.34 \quad \text{in.}$$

$$\phi M_n = 0.9(0.4)(60)\left(4.75 - \frac{0.34}{2}\right) \Big/ 12 = 8.24 \ \text{kip-ft/ft}$$

- Figure 7 shows the leveling forces and the dimensions for 8 ft girder spacing.
- It should be noted that the forces will be reversed on the top flange of the opposite girder.
- Assuming the top flange is acting as an overhang, the width of the design strip is $45.0 + 10.0X$ per LRFD Table (4.6.2.1.3-1)

$$M_{L1} = \pm\frac{16.25(6)}{45+10(6/12)} = \pm 1.95 \qquad \text{kip-ft/ft}$$

$$M_{L2} = \pm\frac{16.25(41)-8.75(35)}{45+10(35/12)} = \pm 4.85 \qquad \text{kip-ft/ft}$$

Section 2 is more critical

$$w_d = 0.15\left(\frac{6}{12}\right) = 0.075 \qquad \text{kip/ft/ft}$$

$$M_{D2} = -\frac{0.075(41/12)^2}{2} = -0.44 \qquad \text{kip-ft/ft}$$

$M_{u2-ve} = 1.25(-0.44)+1.5(-4.85) = -7.83$ kip-ft/ft $< \phi M_n$ (Ok)

$M_{u2+ve} = 1.25(-0.44)+1.5(4.85) = 6.73$ kip-ft/ft $< \phi M_n$ (Ok)

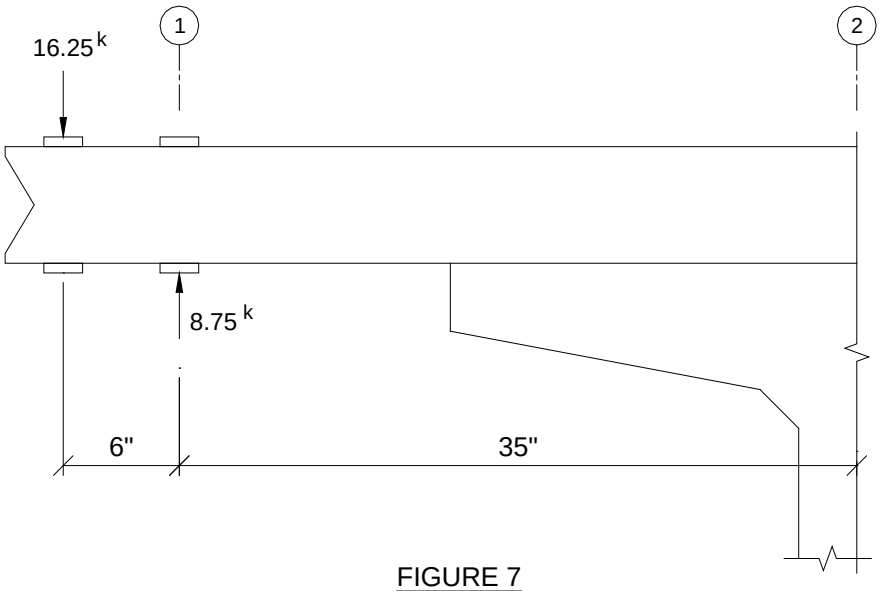

FIGURE 7

Project No. 12-69

DESIGN AND CONSTRUCTION GUIDELINES FOR LONG-SPAN DECKED PRECAST, PRESTRESSED CONCRETE GIRDER BRIDGES

APPENDIX F

FINAL REPORT FOR:
SUBTASK 6.1-A2 STUDY FOR LIVE LOAD FORCES
SUBTASK 6.2-A3 DEVELOPMENT OF LABORATORY TESTING PROTOCOL
SUBTASK 6.2-B SELECTION OF TRIAL ALTERNATE LONGITUDINAL JOINT SYSTEMS
SUBTASK 6.2-C1 LABORATORY TESTING OF TRIAL JOINTS
SUBTASK 6.2 –C2 LABORATORY TESTING OF JOINT ASSEMBLIES

Prepared for
Construction Technology Laboratories, Inc.

Z. John Ma, Ph.D., P.E.
Associate Professor
Department of Civil & Environmental Engineering
University of Tennessee Knoxville (UTK)
223 Perkins Hall
Knoxville, TN 37996 – 2010

May 8, 2009

ACKNOWLEDGMENT OF SPONSORSHIP

This work was sponsored by the American Association of State Highway and Transportation Officials, in cooperation with the Federal Highway Administration, and was conducted in the National Cooperative Highway Research Program, which is administered by the Transportation Research Board of the National Research Council.

DISCLAIMER

This is an uncorrected draft as submitted by the research agency. The opinions and conclusions expressed or implied in the report are those of the research agency. They are not necessarily those of the Transportation Research Board, the National Academies, or other program sponsors.

TABLE OF CONTENTS

TABLE OF CONTENTS (continued)

LIST OF TABLES

LIST OF FIGURES

LIST OF FIGURES (continued)

AUTHOR'S ACKNOWLEGEMENTS

The research reported herein was performed under NCHRP Project 12-69 by the Department of Civil & Environmental Engineering, University of Tennessee Knoxville (UTK). Construction Technology Laboratories, Inc. (CTLGroup) was the contractor for the study with UTK as Subcontractor. Dr. Ralph G. Oesterle, Senior Principal Structural Engineer of CTLGroup was Principal Investigator.

The author would also like to acknowledge Lungui Li, Mary Griffey, Austin Bateman, Ken Thomas and Larry Roberts at UTK for their assistance with the testing. Ross Prestressed Concrete, Inc. donated the concrete materials and helped with the casting of the specimens. Headed Reinforcement Corporation donated the headed bar reinforcement, and Oklahoma Steel and Wire Co., Inc. provided the welded wire reinforcement (WWR).

CHAPTER 1

IMPROVED LONGITUDINAL JOINT DETAILS IN DECKED BULB TEES FOR ACCELERATED BRIDGE CONSTRUCTION: CONCEPT DEVELOPMENT

1.1 Introduction

Speed of construction, particularly for bridge replacement and repair projects, has become a critical issue to minimize disruption of traffic and commerce. A promising system for rapid construction is a precast bridge system using decked bulb tee (DBT) concrete girders. This type of bridge includes the bridge deck precast and prestressed with the girder, manufactured in the precast plant under closely monitored conditions, transported to the construction site, and erected such that the flanges of adjacent units abut. Load transfer between adjacent units is provided by longitudinal joints (parallel to traffic direction). Figure F-1.1 shows a DBT bridge being constructed.

The system eliminates the time necessary to form, place, and cure a concrete deck at the bridge site. In addition, the wide top flange provided by the deck; improves construction safety due to ease of installations, enhances durability since the deck is fabricated with the girder in a controlled environment, and enhances structural performance with a more efficient contribution of the deck in stress distribution. Because of the rapid construction feature provided by this system, it is especially advantageous in regions with short construction seasons or harsh climate, or in remote regions where use of cast-in-place concrete is prohibitive. This type of bridge is relatively common in the northwestern states of Washington, Oregon, Alaska and Idaho.

Despite the major benefits of this type of bridge, use has been limited to isolated regions of the U.S. because of concerns about certain design and construction issues. A particularly important issue is the durability of the longitudinal joint between adjacent units that is currently in use.

Figure F-1.2 shows a typical DBT bridge consisting of five DBTs connected by four longitudinal joints with welded steel connectors and grouted shear keys (Stanton and Mattock 1986, Ma et al 2007). In order to reduce the total DBT weight, the thickness of

the deck is typically limited to 6 in. Welded steel connectors are typically spaced at 4 feet. To make the connection, as shown in Figure F-1.2, two steel angles are anchored into the top flange of DBT and a steel plate is welded to steel angles in the field. Between two connectors, a shear key is provided at the vertical edge of the top flange. Grout is filled into the pocket of the connector and voids of the shear key to tie the adjacent girders together. A joint backer bar is placed at the bottom of the shear key to prevent leakage when grouting.

The current longitudinal joint has the strength needed to transfer shear and limited moment from one girder to adjacent girders. The width of the joint zone is small so that it facilitates accelerated construction. However, since welded steel plates are located 4 feet from each other and at mid-depth of the flange, they can not help to control flexural cracks along the longitudinal joint. Although performance of this type of joint was reported as good to excellent in a survey of current users, problems with joint cracking have been reported in the literatures (Stanton and Mattock 1986; Martin and Osborn 1983). This joint cracking along with joint leakage is perceived to be an issue limiting a wider use of this type of bridges. As a result, the State of Washington has set limitation on the use of DBT for roads with high ADT and for continuous bridges. As part of a research project to address issues that influence the performance of DBT bridges, a specific objective was defined to develop improved joint details which allow DBT bridge systems to be more accepted as a viable system for accelerated bridge constructions. This chapter describes the process of selection of trial longitudinal joint system and the laboratory testing of trial selected joints.

Work presented in this appendix, performed by the Department of Civil & Environmental Engineering, University of Tennessee Knoxville (UTK), include results of:

- Subtask 6.1-A2 Study for Live Load Forces described in Chapter 2 of this appendix
- Subtask 6.1-A3 Development of Laboratory Testing Protocol described in Sections 3.2.6 and 3.2.7 of this appendix
- Subtask 6.2-B Selection of Trial Alternate Joint System described in Section 1.2 of this appendix

- Subtask 6.2_C1 Laboratory Testing of Trial Joints described in Section 1.3 of this appendix, and
- Subtask 6.2-C2 Laboratory Testing of Joint Assemblies described in Chapter 3 of this appendix.

1.2 Proposed New Joint Details

To improve the current joint detail, the proposed new details should control joint cracking better, and maintain the accelerated construction features. One concept is to replace the current welded steel connectors with distributed reinforcement to provide moment transfer as well as shear transfer across the joint. Obviously, well distributed reinforcement can control cracks much better than widely spaced welded steel connectors. However, straight lap-spliced reinforcement requires a much wider joint to develop its strength.

The width of the joint for lap spliced reinforcement is determined by the lap length which typically depends on development length L_d of reinforcement. ACI 318 (2005) provides the following equations to calculate the development length L_d for straight bar and hooked bar.

$$\text{Straight bar: } L_d = \frac{f_y \psi_t \psi_e \lambda}{25\sqrt{f_c'}} d_b \qquad \text{(F-1.1)}$$

$$\text{Hooked bar: } L_d = \frac{0.02 \psi_e \lambda f_y}{\sqrt{f_c'}} d_b \qquad \text{(F-1.2)}$$

Where: f_y = specified yield strength of nonprestressed reinforcement, psi;

ψ_t = reinforcement location factor;

ψ_e = coating factor;

λ = lightweight aggregate concrete factor;

$f_c^{'}$ = specified compressive strength of concrete, psi; and

d_b = nominal diameter of bar, in.

For a typical DBT, the compressive strength of the deck flange and the grout is 7000psi. If #5 epoxy coated bar with yielding stress 60 ksi were lapped in the 6 in. deep flange joint, the development length L_d for straight bar and hooked bar are 21.5 in. and 10.7 in. respectively. The lap length should not be less than the development length L_d, which indicates at least the same joint width needs to be provided to accommodate the lap spliced reinforcement. A straight lap-spliced joint would be much wider than the current joint width, which does not facilitate accelerated construction.

It is very important for the proposed joint width to be as narrow as possible. Joint width minimization will reduce the required expensive grout which results in a reduction of cost and faster construction time. As a result, options to reduce the joint width have been explored. Such options include bars with hook (U bar), bars with headed terminations, and bars with spiral.

As discussed earlier, the hooked bar has a much smaller development length compared to the straight bar. However, it is impossible to have a standard hook for #5 bar within the 6 in. deep flange while still satisfying the cover requirements. As a result, a non-standard U bar with a smaller bend radius was considered as shown in Figure F-1.3-a.

U bars are spliced with the transverse deck reinforcement in the top flange of the DBT. They are bent to contact with the opposite U bars in the adjacent girder. Two longitudinal bars were laced through the interlocking U bars. Figure F-1.3-b shows a non-overlapping headed bar connection detail proposed for consideration. Two layers of transverse deck reinforcement project out of the top flange of the girder with a head on the end. The adjacent girders will be placed with the opposing headed bar abutting each other. One welded wire reinforcement (WWR) is spliced with each layer of headed bar for force transfer. Figure F-1.3-c shows a proposed joint detail with spirals confining lapped splices.

Einea et al (1999) performed an experimental program to determine lap length of the rebar confined in spirals. With the concrete compressive strength of 8660psi, they found that the lap length for #4, #6, and #8 bars confined with circular spirals can be as short as 4in., 5in., and 7in. respectively. In this proposed detail, two layers of transverse deck reinforcement project out of the top flange of the girder and abut with the opposite projecting transverse deck reinforcement in the adjacent girder. The two abutting transverse deck reinforcements are spliced with two straight bars confined by the spiral wire.

In order to better understand the rapid constructability of proposed details, a survey was distributed to a variety of bridge professionals in different states. The bridge professionals were asked to comment on constructability, cost and any available performance data. Approximately 80% of the 28 agencies that were questioned responded to the survey. According to the feedback, it would be desirable to minimize or eliminate the joint zone to expedite construction and reduce cost. Field placement of reinforcement within longitudinal joint zone after erection could be tedious. Cumulative fabrication and erection tolerances, particularly differential camber, will result in some degree of vertical flange mismatching. Any connection detail must have sufficient tolerance to account for the mismatch.

The feedback almost universally indicated concerns with the connection using spiral wire. The respondents felt that the complexity of construction would cause difficulties with effective installation. Assembling the splice bars and spiral wire seemed too difficult and time consuming in the limited space of the joint strip. When the joint is very congested, it is very difficult to achieve full grout penetration throughout the assembly. For the 6 in. deep flange, the use of spiral wire will probably result in violation of the cover requirement: 2 in. at top and 1 in. at bottom, and it would be more realistic to use a thicker flange. It also would be very difficult to provide proper alignment of the opposing transverse deck reinforcements when erecting the bridge girders. It is highly unlikely that this connection would work for skewed bridges.

The primary concern with the U bar detail was achieving the desired bend radius within the 6 in. deep flange and still achieving the desired top and bottom cover requirement. The flange must be thickened substantially for a reasonable pin diameter to work, or the bars would have to be rotated sideways to maintain the required cover.

Contact lapping of U bars will present construction problems in both making laps match up and difficulty in the setting operation for the girders. Much labor may be required in the field to bend bars at all contact locations. A joint with spacing completely out of phase by half a space between adjacent girders should be considered. Large amounts of differential camber may complicate lacing the longitudinal bar though the U bar interlocking, and eliminating longitudinal bar is suggested. Also, the thin, un-reinforced part of the flange under the joint would be very vulnerable to damage at all stages of fabrication and construction. Female-to-female shear key details would be preferred.

From a structural and ease of installation point of view, the headed reinforcement option appeared to be the most favorable. However, several respondents expressed concern for a detail with headed bars that do not overlap. This concept is good for setting assemblies but it does not provide a good load path with reliance on WWR for force transfer. Also, field placement of the inner layer of WWR (above lower headed bars) may be difficult. In addition, the heads of the bars appear to violate cover requirement.

Based on the feedback from the survey, a headed bar detail was selected for further investigation. Considering the limited flange depth, it was decided to investigate use one layer of overlapping headed reinforcement (Figure F-1.4-a). Interlocking WWR detail as shown in Figure F-1.4-b was also chosen for further investigation.

Since contact lapping will present construction problems, headed bar spacing completely out of phase by half a space is proposed shown in Figure F-1.4-a, however, the lap length (measured from inside head to inside head) needs to be studied. Research on anchorage behavior of overlapping headed reinforcement was conducted by Thompson et al (2006). The anchorage capacity of headed bar consisted of head bearing and bond. The following equations were proposed to calculate the development length L_d for headed bar.

$$L_d = [1 - 1.4\sqrt{\frac{A_{nh}}{A_b}}\left(\frac{c_1}{d_b}\right)\frac{f_c^{'}}{f_y}\psi]\frac{L_d^*}{\chi} \geq 6d_b \qquad \text{(F-1.3)}$$

$$\psi = 0.6 + 0.4\left(\frac{c_2}{c_1}\right) \leq 2.0 \qquad \text{(F-1.4)}$$

$$\chi = 1 - 0.7\left(\frac{A_{nh} / A_b}{5}\right) \geq 0.3 \qquad \text{(F-1.5)}$$

Where: A_{nh} = net head area, in^2;

A_b = area of bar, in^2;

c_1, c_2 = half spacing of the headed bar or cover dimension;

L_d^* = development length of the straight bar which has the same diameter as the headed bar;

ψ = radial disturbance factor which recognizes an improvement in capacity for headed bars in which the secondary cover dimension,

c_2, is greater than the minimum cover dimension, c_1.; and

χ = head size reduction factor.

For #5 bars with a 2 in. diameter circular head , the development length L_d is 3.75 in. for both 4 in. spacing headed bar and 6 in. spacing headed bar.

As shown in Figure F-1.4-b, the WWR detail includes three sheets of WWR with “Sheet 3” is put on the top of “Sheet 1” and “Sheet 2” which are abutted with each other. Each sheet is spliced to an adjoining sheet with two interlocking cross wires. The spacing between cross wires of the overlap sheets shall be at least 2in. (ACI 318-05). In this case, width of WWR connection (distance between outermost cross wires) should be 16 in. plus the diameter of the wire.

In order to evaluate the proposed new joint details shown in Figure F-1.4, an experimental program was carried out. As discussed below, the spacing of cross wires in WWR detail is reduced from 2 in. to 1 in. in order to reduce width of connection, so it is comparable with that of headed bar detail which is measured from outside head to outside head. The lap length in WWR detail is defined as the distance between the center of the outermost cross wire to the center of middle wire, which is reduced to 4 in.

1.3 Experimental Program

1.3.1 Testing Plan

Figure F-1.5 shows a model specimen in two adjacent DBTs with the dashed line representing the longitudinal joint. Typically, the spacings of the DBT are 4 feet, 6 feet, or 8 feet respectively. The model specimen with 8 feet span was selected to evaluate the behavior of the proposed longitudinal joint details.

Figure F-1.6 shows details of the three types of specimens. Each specimen was 610mm (2 feet) wide, 3048mm (10 feet) long, and 152mm (6 in.) deep with 51mm (2 in.) cover at top and 25mm (1 in.) cover at bottom.

All the specimens had four layers of reinforcement both at the left side and the right side to simulate the deck reinforcement in the top flange of adjacent girders. The headed bar, WWR Sheet 1, WWR Sheet 2, and the continuous bar were spliced with the deck reinforcement long enough to avoid pulling out. The specification of deck reinforcement was as following: #5 bar spaced at 6 in. at top in the “transverse” direction of the bridge deck; #4 bar spaced at 6 in. at bottom in the “transverse” direction of the bridge deck; #5 distribution reinforcement spaced at 8 in. at top in the “longitudinal” direction of the bridge deck; and #4 distribution reinforcement spaced at 8 in. at bottom in the “longitudinal” direction of the bridge deck. All the reinforcement was grade 60 and epoxy coated. The headed reinforcement was #5 bar with a standard 2 in. diameter circular friction welded head. The head thickness was 0.5 in.

Table F-1.1 shows the main variables of the tested specimens. For the headed bar detail (Figure F-1.6-a), the primary variables were the lap length and the spacing of the reinforcement. “H” means headed reinforcement and “W” means WWR. For example, the notation “H-6-4” means headed bar reinforcement with a lap length of 6 in. and a spacing of reinforcement at 4 in. A #5 bar with a 1.375 in. diameter circular head on each end was placed in the “longitudinal” direction both above and below the headed reinforcement at the middle of the lap length. Figure F-1.6-b shows the WWR detail. As discussed earlier, the lap length is reduced to 4 in. The spacing of WWR was the only variable in the second type of specimen. The diameter of WWR reinforcement is 5/8 in.

(#5 bar). A control specimen with a layer of continuous #5 rebar with a spacing of 6 in. across the joint zone shown in Figure F-1.6-c was tested for comparison purpose.

All eight specimens were cast monolithically to remove the grout as a variable so the actual performance of the reinforcement in the joint zone can be focused on. The design concrete strength at 28 days was 7000psi. The concrete strength $f_c^{'}$ at the time of testing is shown in Table F-1.1. Three cylinders were tested to get the compressive strength of each specimen on the testing day. The compressive strength of the control specimen was not available. Since the control specimen and Specimen H-6-6 were cast from the same batch of concrete on the same day and they were tested within five days, the compressive strength of Specimen H-6-6 was used in calculation for the control specimen.

1.3.2 Instrumentation and Test Setup

In order to have a better understanding of the behavior of the proposed joint details, the steel strains in the joint zone were measured. Figure F-1.7-a shows the strain gauge layout in the control specimen. The notation 1-4L is used to label the strain 4 in. away from the centerline on the left at bar 1. Figure F-1.7-b shows the example of strain gauge layout in headed reinforcement specimens. In this diagram, “1-6” means the strain 6 in. away from the inside head of bar 1. The headed bars are numbered from the edge to the middle of the specimen. Three strain gauges were placed at the end, quarter, and middle of the longitudinal headed bar, which labeled as LB1, LB2 and LB3 respectively. The notation “SH66-1-6” is used in headed reinforcement specimen H-6-6 to indicate the strain at “1-6”. The strain gage notation used in WWR specimen was the same as that used in control specimen.

All specimens were simply supported with a 8 feet span (Figure F-1.8). Neoprene pads were placed between the support concrete blocks and steel girders to ensure the boundary condition was achieved. The specimens were loaded with two equal loads spaced at 40 in. about the center of the span using Material Test System (MTS) rams. The joint zone was located in the center of the span and experienced the maximum constant moment without shear. Linear voltage displacement transducers (LVDT) were

employed to measure the specimen deflection and curvature. The dial gauges were used to measure the settlement.

1.3.3 Moment Capacity and Curvature

Table F-1.2 compiles the moment capacity and measured curvatures of each specimen. The curvatures reported include the measured curvature at maximum moment and the maximum curvature prior to failure. Four of the specimens failed suddenly and the maximum curvature could not be reported. A joint with a high moment capacity and a low curvature will be undesirable in the industry application because the failure will be brittle and sudden. Response 2000 (Bentz and Michael 2000) is an easy to use sectional analysis program that will calculate the strength and ductility of a reinforced concrete cross-section subjected to shear, moment, and axial load. This program was used to predict the moment curvature behavior of a continuously reinforced specimen with either 4 in. or 6 in. reinforcement spacing. The measured reinforcement yield stress of 68 ksi and elasticity modulus of 29809 ksi were used in the Response 2000 analysis.

Figure F-1.9 compares the moment curvature response for each of the headed bar specimens and control specimen. It can be clearly seen that the 6 in. lap length specimens (H-6-4, H-6-6 and control specimen) provided much more ductility than the 2.5 in. or 4 in. lap length specimens (H-2.5-4, H-2.5-6 and H-4-6). The maximum curvatures in 6 in. lap length specimens were almost twice as large as those in specimens with 2.5 in. or 4 in. lap length. In the 6 in. lap length specimen moment curvature response curve, there was considerable flattening of the curve followed by a dropping off which meant that the reinforcement yielded after the specimen reached the nominal moment until the compression zone of concrete crushed and the specimen could not take any more load.

The maximum curvatures in specimens with 2.5 in. or 4 in. lap length were very close and had a relatively small value about 3810×10^{-6} rad/in. The curves did not exhibit a flattening part indicating that the steel did not fully develop before concrete crushing.

Also, the 4 in. reinforcement spacing specimens (H-6-4 and H-2.5-4) provided higher moment capacities than the 6 in. reinforcement spacing specimens because the smaller spacing provided more steel in the same cross section, which can increase the nominal moment.

Figure F-1.10 shows the moment curvature curve for 6 in. reinforcement spacing specimens compared with results of analyses with Response 2000. The specimen results were split into two graphs due to the different compressive strength of the concrete. Figure F-1.10-a shows the behaviors of the control specimen and H-6-6 which had a compressive strength of 10,542psi. Both specimens had a higher moment capacity and higher ductility than Response 2000. H-6-6 had a little bit more moment capacity (3%) than control specimen. The control specimen was more ductile than H-6-6 with a maximum curvature which was 36% larger than that of H-6-6. However, the 6 in. lap length had considerable anchorage to provide desirable moment capacity and ductility.

Figure F-1.10-b compares the moment curvature curve between H-2.5-6, H-4-6 and Response 2000 with average compressive strength of 8,355psi. The moment capacities of both specimens were close to each other and slightly smaller than that in Response 2000. Both specimens had only about half ductility capacity compared with Response 2000. Because of the short lap length, there was not enough anchorage between opposing headed reinforcement in the joint. As the load increased, the concrete between the opposing headed bars began to crush and failed to transfer the force between the overlapping headed reinforcement. So the two specimens exhibited relatively brittle failures with small curvatures.

Figure F-1.11 shows the moment curvature data for 4 in. reinforcement spacing specimens (H-2.5-4 and H-6-4) and Response 2000 with average compressive strength of 8,900psi. H-6-4 had a larger moment capacity and ductility compared with Response 2000. It confirmed the discussion above that 6 in. lap length had the desirable anchorage capacity to yield the steel in the joint. H-2.5-4 had enough moment capacity; however, its ductility was only about 60% of that in Response 2000. Based on the review of the failed specimen, it appears that the connection failed suddenly because of the anchorage failure due to the short lap length, which can be recognized by the abrupt stop in the

moment curvature curve.

Figure F-1.12 shows the moment curvature behavior of the WWR specimens. Neither specimens performed like the expected behavior of Response 2000 and failed prematurely. As noted previously, the spacing between cross wires in the joint zone of 1 in. did not meet the requirement in ACI. If WWR connection is used in the joint, it is suspected that the width of joint needs to be increased to accommodate 2 in. spacing cross wires. In addition, as shown in Figure F-1.4-b, the WWR detail includes a significant shift in the location of the transverse wires in Sheet 3 as compared to Sheets l and 2. It is also suspected that providing a fourth sheet below Sheets 1 and 2 would improve behavior but diminish the constructability of the joint.

1.3.4 Strain Comparisons

The results from the strain gauge readings were plotted against the corresponding moment. Figure F-1.13 compared the moment versus steel strain at different location in Specimen H-6-6. Steel within 0 to 2 in. away from the head (Figure F-1.13-a and b) developed strain with initial load indicating the head bearing provided significant anchorage capacity. Strain in the steel 4 in. to 10 in. away from the head (Figure F-1.13-c, d, e) did not indicate significant strain until the applied moment of approximately 7.41 kips-ft. This moment corresponds with first significant cracking following which the reinforcement strains away from the head increased to two to three times the strains measured near the head indicating that a combination of head bearing and bond provided the whole anchorage. Also strains measured away from the head indicated significant yielding before ultimate load.

In Figure F-1.13-d, the strain development in bar 1 and bar 3 was not as rapid as bar 2 and bar 4. This was because in Specimen H-6-6, there were 4 bars (bar 1, bar 3, bar 5 and bar 7) on the right side and 3 bars (bar 2, bar 4 and bar 6) on the left. To balance the total tension force, the bars on the left which had smaller area needed to develop more strain/stress to produce the same force as the steel on the right side. Figure F-1.13-f shows measured strain in the longitudinal bars was relatively low during the test. Therefore the force in the joint in this direction was relatively low.

Figure F-1.14 compares the moment versus strain response at SH66-4-4 in Specimen H-6-6 with 2-4L and 2-4R in the control specimen. The three moment-strain curve matched very well which confirmed steel 4 in. away from the head would fully develop in the 6 in. lap length headed bar connection. The joint detail in Specimen H-6-6 can transfer moment as effectively as a continuously reinforced joint.

Similar to Specimen H-6-6, the steel close to the head in Specimen H-6-4 developed strain at low load indicating the head bearing provided significant anchorage capacity. Steel away from the head indicated higher strain demonstrating that bond also contributed to the anchorage. Measured strain, greater than yield were measured at location as close as 2 in. from the head and indicated the rebar fully developed by the combination of head bearing and bond.

As discussed before, the spacing of the headed reinforcement was one of the variables that had effect on the lap length. The smaller spacing, the smaller lap length was required. Since Specimen H-6-4 had smaller reinforcement spacing than Specimen H-6-6, the steel at 2 in. away from the head yielded in H-6-4 while the steel at 4 in. away from the head yielded in H-6-6.

For Specimen H-2.5-6, strain data indicates the steel did not yield until failure, which confirms this specimen did not reach the full moment and curvature capacity because of the short lap length. Specimens H-2.5-4 and H-4-6 performed better than H-2.5-6 with respect to the more moment capacity; however, both of them had a sudden, brittle failure due to the short lap length. The 2.5 in. or 4 in. lap length was not adequate to develop the steel and could not provide desirable moment capacity and ductility. For WWR specimens, the strain gauge readings in W-4-4 and W-4-6 indicated the steel did not develop any significant strain.

1.3.5 Load-Deflection

Figure F-1.15 compares the load-deflection curves of all the tested specimens. The string connecting LVDT and the control specimen for deflection measurement was broken when the control specimen had a deflection around 1.2 in. Similar to the

moment-curvature data, the deflection data clearly shows that for headed reinforcement, 6 in. lap length specimens (H-6-4 and H-6-6) were more deformable than the 2.5 in. or 4 in. lap length specimens (H-2.5-4, H-2.5-6 and H-4-6). The maximum deflections in 6 in. lap length specimens were almost as twice the deflections measured for specimens with 2.5 in. or 4 in. lap length. In the specimen with the 6 in. lap length load deflection curves show obviously ductile behavior before reaching the ultimate load. The WWR specimens had low load capacity and ductility.

1.3.6 Cracking

The first cracks developed at in the mid-span region when the load was between 1.5kips to 2kips depending on the different specimens. For 2.5 in. lap length specimens (H-2.5-4 and H-2.5-6), cracks usually consisted of flexural cracks in the “longitudinal” direction in the constant moment zone. The numbers on specimens shown in Figures F-1.16 to F-1.19 represent the applied loads with the unit of kips. There was not much transverse cracking (Figure F-1.16-a) which means the concrete cover was sufficient to develop the bond stress that occurred. Prior to failure, a wide crack propagated along the midspan. However, the top concrete was still good until failure (Figure F-1.16-b). This behavior indicates the 2.5 in. lap length was too small to provide enough anchorage (combination of head and bond). Before the top concrete crushed, the concrete between overlapping headed reinforcement failed and the overlapping reinforcement could not transfer force.

Figure F-1.17 shows the cracking behavior for 4 in. lap length specimen H-4-6. Several cracks formed in the “transverse” direction in the constant moment zone indicating a loss of bond stress with load close to failure (FigureF-1.17-a). These results show that a 4 in. lap length could provide some degree of bond in the lap zone prior the failure. Failure occurred with crushing of the top concrete (FigureF-1.17-b) confirming a reasonably large anchorage capacity was provided by combination with head and bond in 4 in. lap length. However, this lap length was not long enough to develop the steel to fully yield.

Crack behavior for 6 in. lap length specimens (H-6-6 and H-6-4) are shown in Figure F-1.18. Longitudinal flexural cracks were well-distributed along the constant

moment zone. Failure occurred with crushing of the top concrete (Figure F-1.18-a). Results indicated anchorage (combination of head and bond) was sufficient for the specimens to behave as continuously reinforced. Figure F-1.18-b shows the maximum crack width in the constant moment zone against the applied load. Under the failure load, the maximum measured crack width is about 0.2 in. However, the measured crack width under estimated service load moment is about 0.004 in.

In WWR specimens, a large crack propagated at the center of the span until a brittle failure occurred (Figure F-1.19).

1.3.7 Failure Types

Typically, the specimens exhibited two different failure types during testing. Figure F-1.20-a and Figure F-1.20-b display the ductile, slow failure and the sudden, brittle failure respectively. The Specimens H-2.5-4, W-4-4, and W-4-6 experienced a sudden, brittle failure and broke into two pieces. The control specimen, H-6-6 and H-6-4 had a ductile failure. H-2.5-6 and H-4-6 experienced a brittle failure with small curvature but it did not break into two pieces. The testing program indicated that both the reinforcement lap length and the spacing had effects on the failure type. 2.5 in. and 4 in. lap lengths could not provide enough anchorage to fully develop the reinforcement. Since the reinforcement did not yield, as the load increased to a certain value, the anchorage was lost and the load could no longer be carried, and failure occurred suddenly. 6 in. lap length could provide desirable anchorage and had a ductile behavior.

1.4 Conclusions

Based on the survey and the experimental program, the following conclusions were made:

1. The headed bar detail can provide a continuous force transfer in the longitudinal joint for DBT bridge system while minimizing the width of the joint to accelerate DBT bridge construction.
2. The lap length for the headed bar detail is recommended to be 6 in. This lap length provided full development of the bars to produce full load capacity and significant ductility.

3. The reinforcement spacing had an effect on the structural behavior. The smaller spacing provided more load resistance with less ductility because more steel was provided in the same cross section.
4. In the tested WWR connection details was used in the joint, the joint width accommodating 1 in. spacing between cross wires failed to provide the required moment capacity. Therefore, a WWR connection detail with the same joint width as the headed bar detail cannot be recommended.
5. According to the moment capacity, curvature, cracking, deflection and steel strain comparison, the headed bar detail with a 6 in. lap length was recommended for replacing the current welded steel connector detail as the improved longitudinal joint detail for DBT bridges.

Table F-1.1. Main Variables of Beam Specimens

Name	Reinforcement	Lap Length in.	Spacing in.	f_c' psi
Control	Straight Bar	Continuous	6	10,542
H-6-6	Headed Bar	6	6	10,542
H-2.5-6	Headed Bar	2.5	6	8,230
H-6-4	Headed Bar	6	4	8,860
H-2.5-4	Headed Bar	2.5	4	8,950
H-4-6	Headed Bar	4	6	8,480
W-4-6	WWR	4	6	7,750
W-4-4	WWR	4	4	8,352

Table F-1.2. Moment Capacity and Curvature of Specimens

Specimens	Moment Capacity M_n (kips-ft)	Curvature (10^6/ in.)	
		Corresponding to M_n	Maximum
Control	25.19	10,802	12,934
H-6-6	25.83	7,653	9,490
H-2.5-6	17.39	2,167	3,715
H-6-4	39.4	6,320	8,848
H-2.5-4	32.13	3,407	Failed Suddenly
H-4-6	18.4	3,509	Failed Suddenly
W-4-4	4.74	942	Failed Suddenly
W-4-6	3.68	2003	Failed Suddenly

Figure. F-1.1. A DBT Concrete Bridge being Constructed

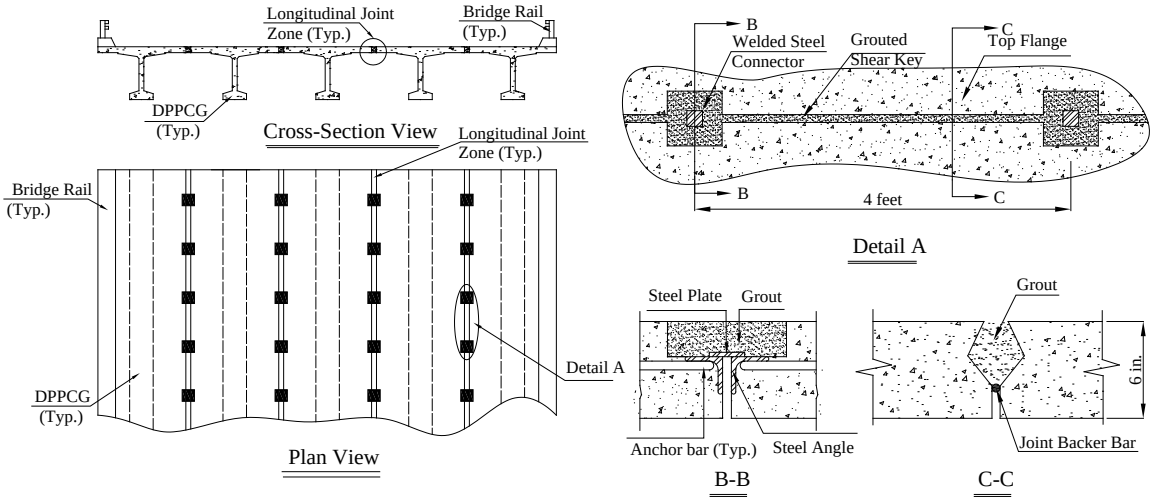

Figure. F-1.2. A Typical DBT Bridge Connected by Longitudinal Joints with Welded Steel Connectors

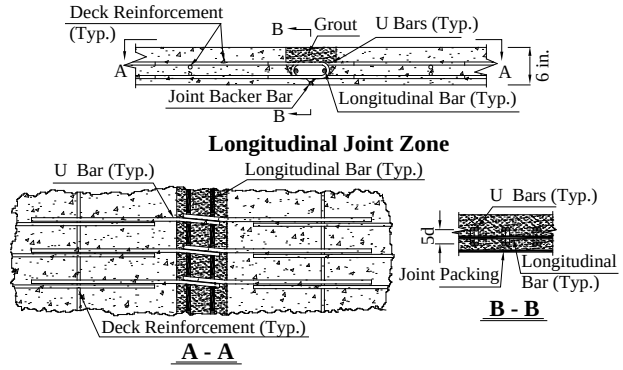

(a): U bar detail

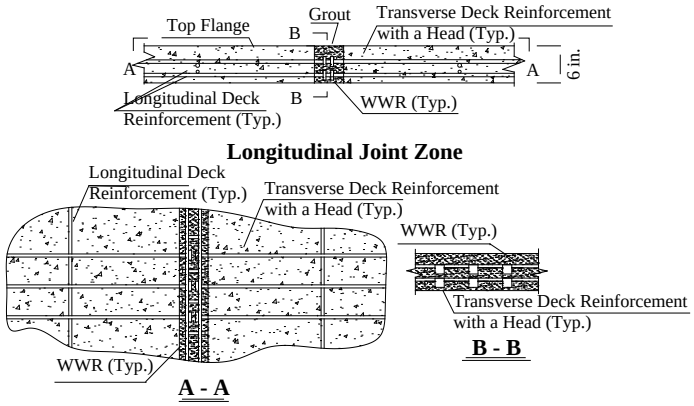

(b): Headed bar detail

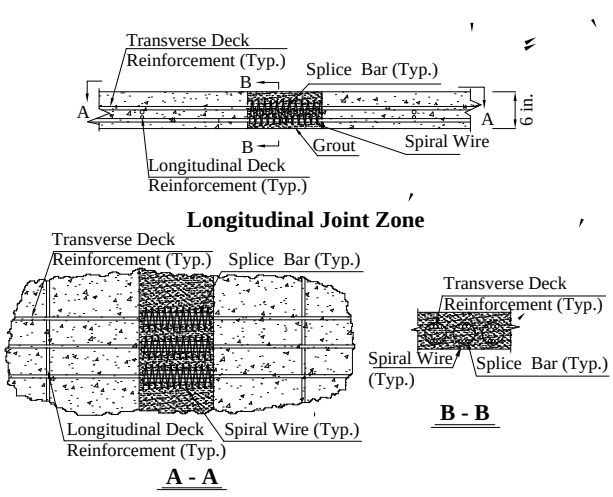

(c): Spiral bar detail

Figure F- 1.3. Proposed New Joint Details

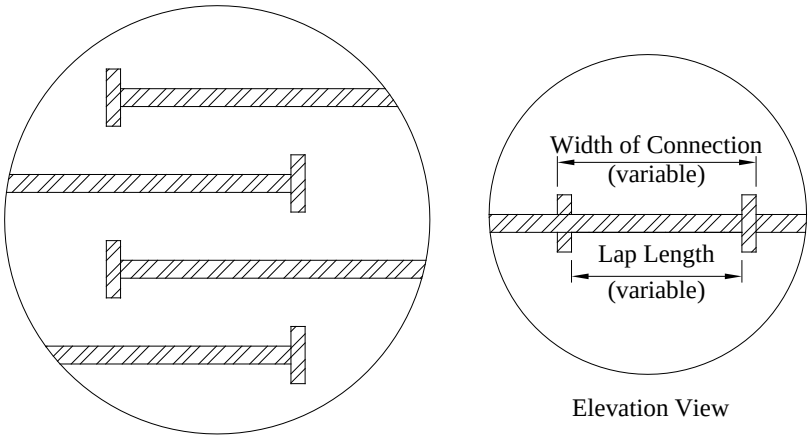

(a): Headed reinforcement connection detail

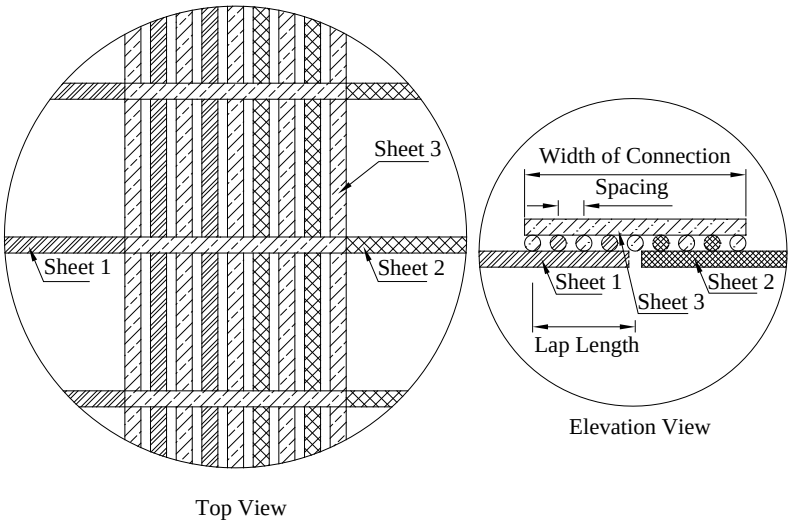

(b): WWR reinforcement connection detail

Figure F-1.4. Improved Joint Details

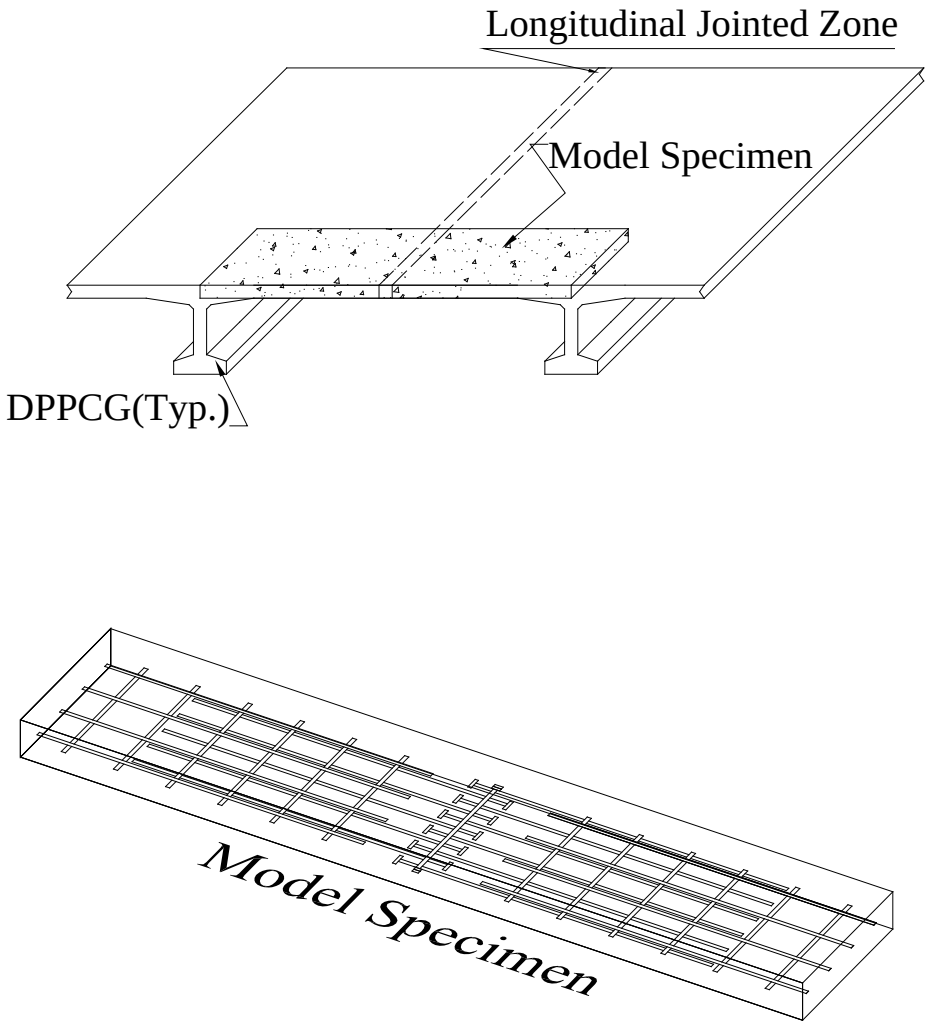

Figure F-1.5. Specimen to Evaluate Joint Behavior

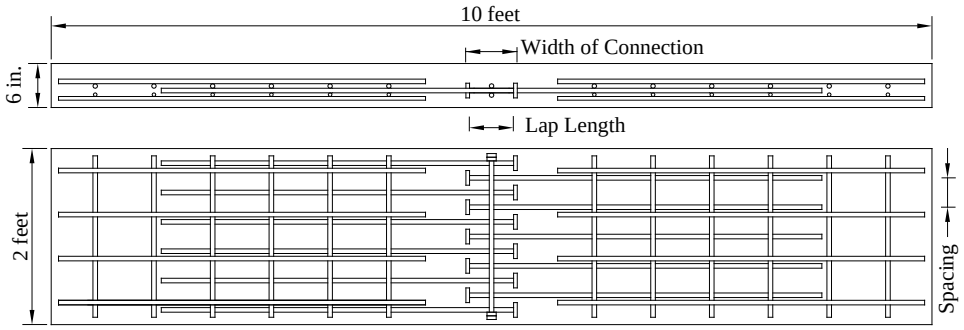

(a): Headed reinforcement connection

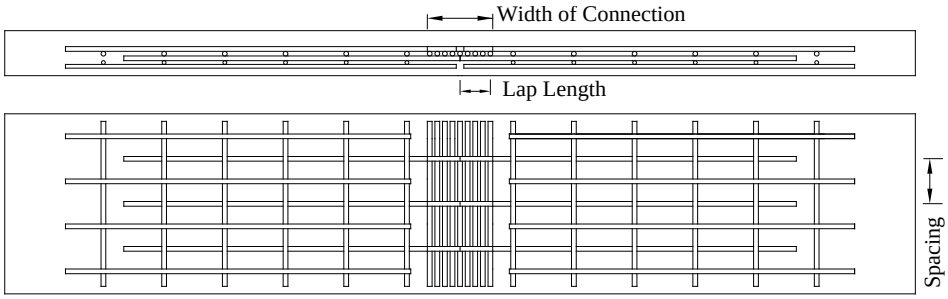

(b): WWR connection

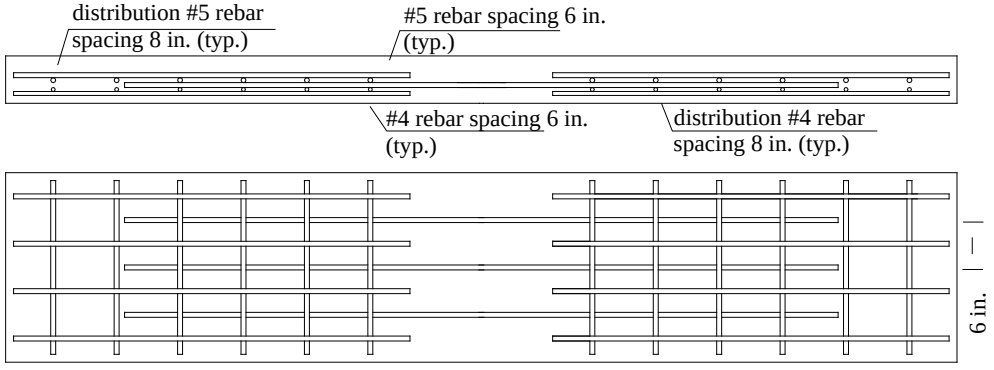

(c): Control beam

Figure F-1.6. Three Types of Specimens

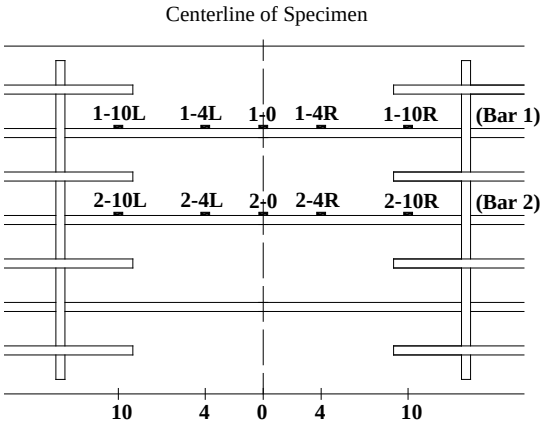

(a): Control specimen

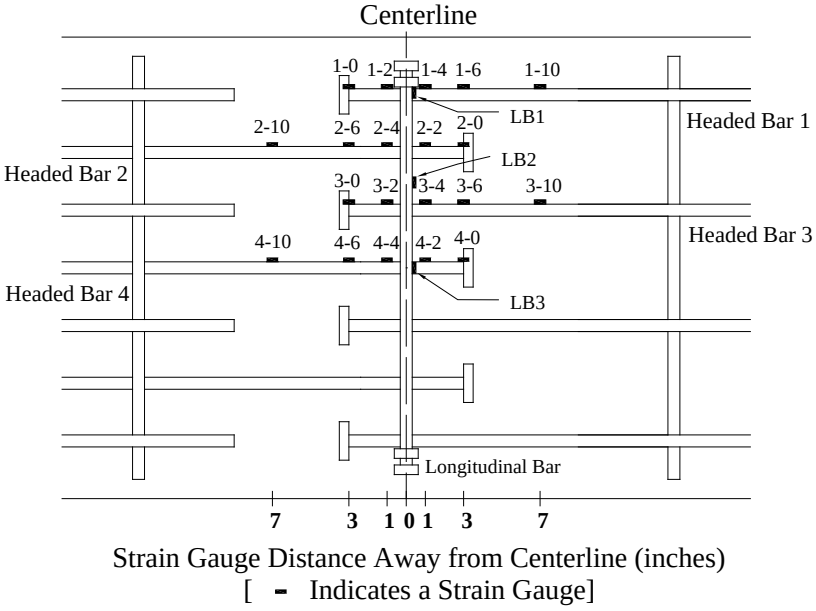

(b): Headed reinforcement specimen

Figure F-1.7. Strain Gauge Layout

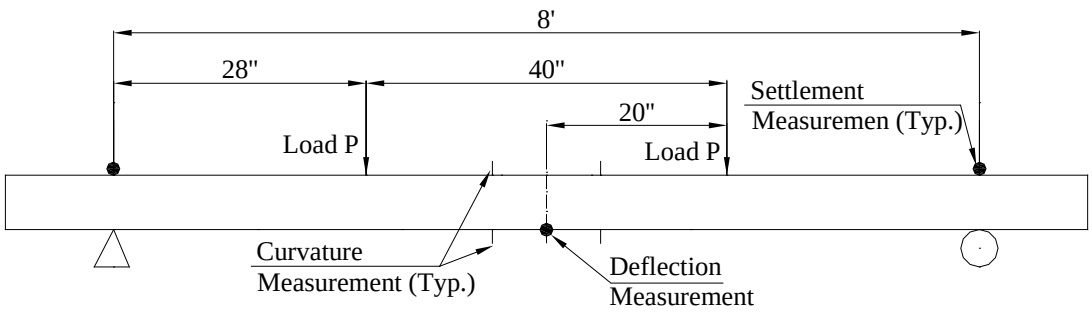

Figure F-1.8. Testing Setup

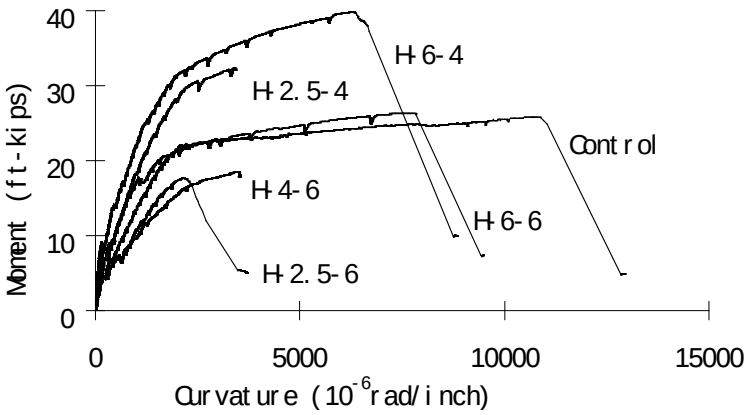

Figure F-1.9. Moment Curvature Diagrams for Headed Bar Specimens

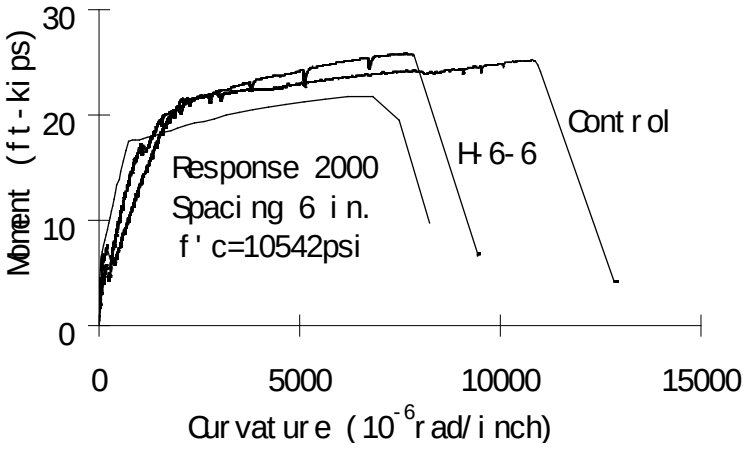

(a): $f_c^{'} = 10{,}542\,psi$

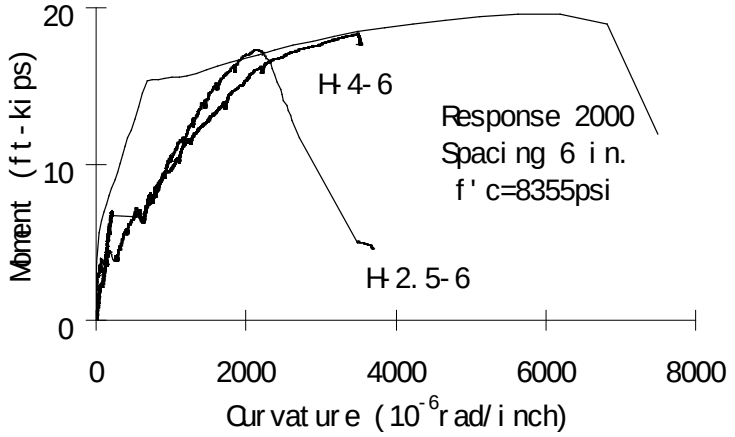

(b): $f_c^{'} = 8{,}355\,psi$

Figure F-1.10 Moment Curvature Diagrams for 6 in. Spacing Specimens with Response 2000

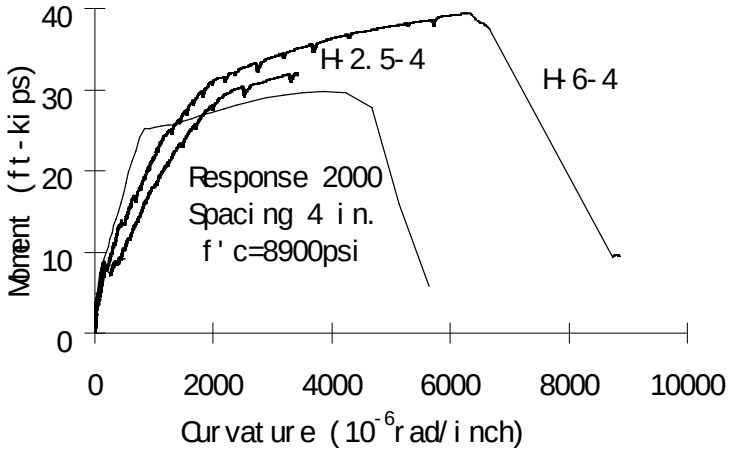

Figure F-1.11. Moment Curvature Diagrams for 4 in. Spacing Specimens with Response

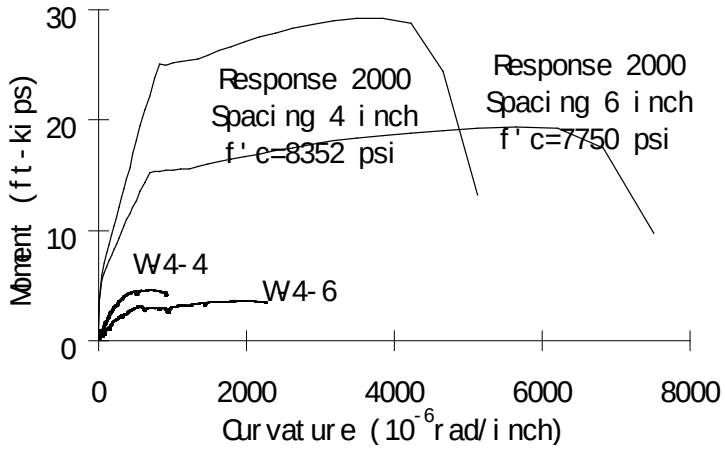

Figure F-1.12. Moment Curvature Diagrams for WWR specimens

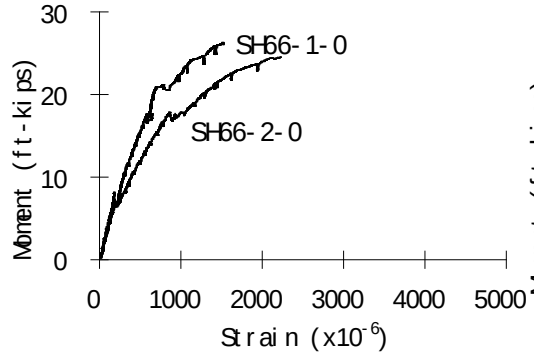

(a): 0 in. from head

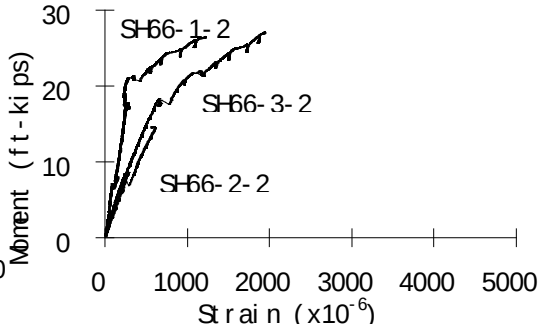

(b): 2 in. from head

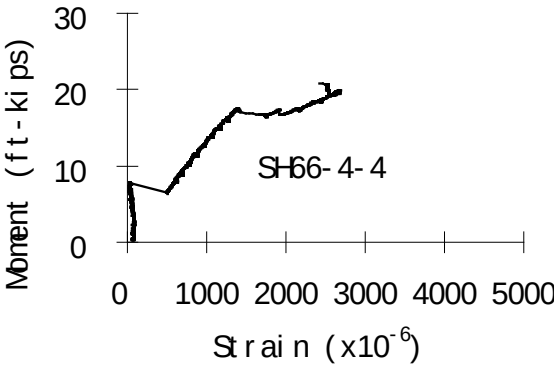

(c): 4 in. from head

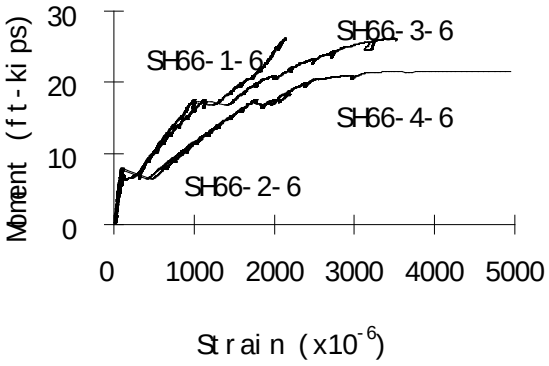

(d): 6 in. from head

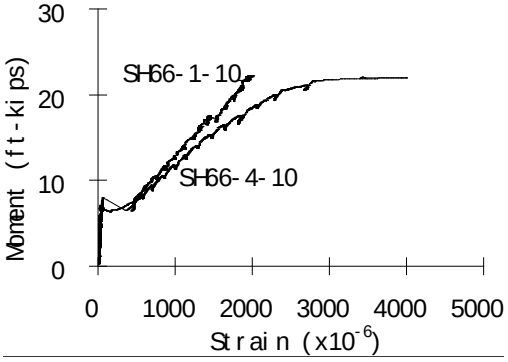

(e): 10 in. from head

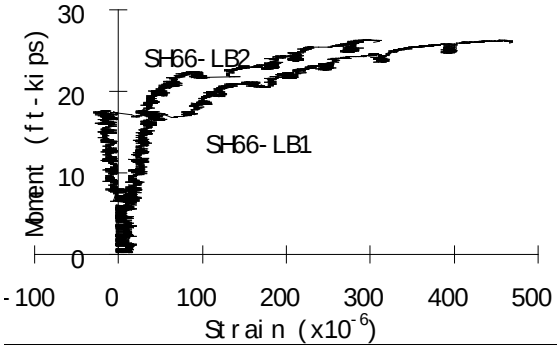

(f): longitudinal bar

Figure F-1.13. Moment vs. Steel Strain Comparison for H-6-6

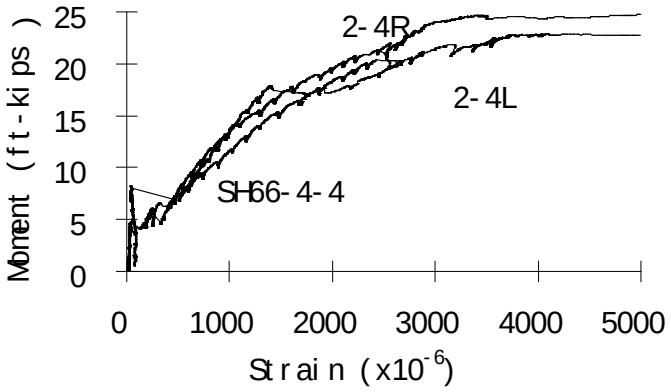

Figure F-1.14. Moment vs. Steel Strain Comparison

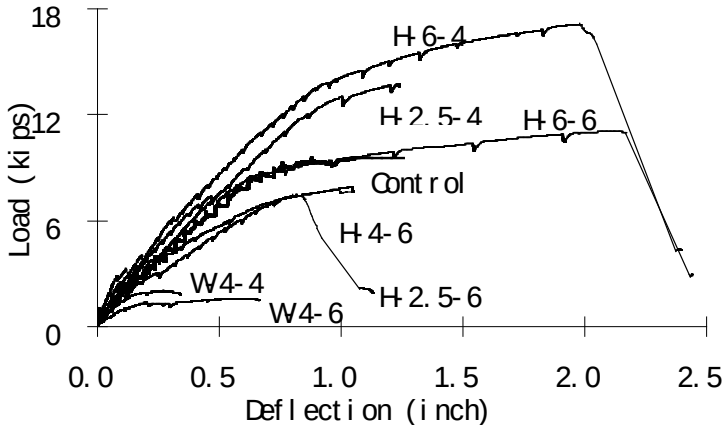

Figure F-1.15. Load vs. Deflection Curve

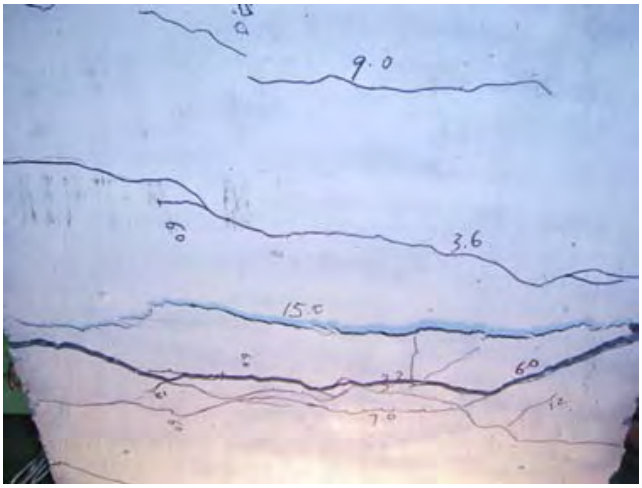

(a): Bottom view

(b): Side view

Figure F-1.16. Crack Behavior for Specimen H-2.5-4 and H-2.5-6

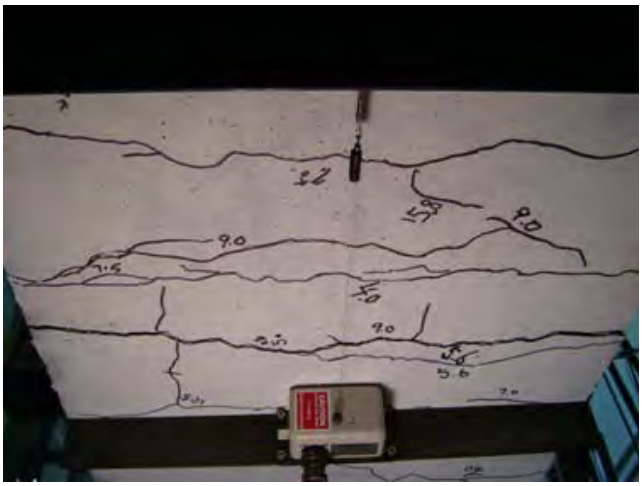

(a): Bottom view

(b): Side view

Figure F-1.17. Crack Behavior for Specimen H-4-6

(a): Bottom view

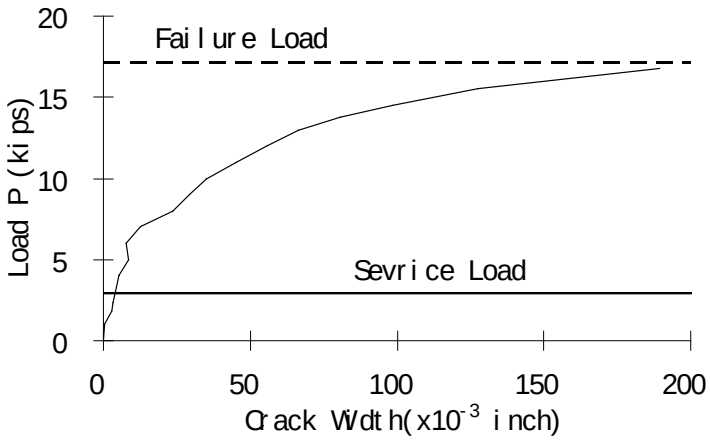

(b): Crack width-load curve

Figure F-1.18. Crack Behavior for 6 in. Lap Length Specimen

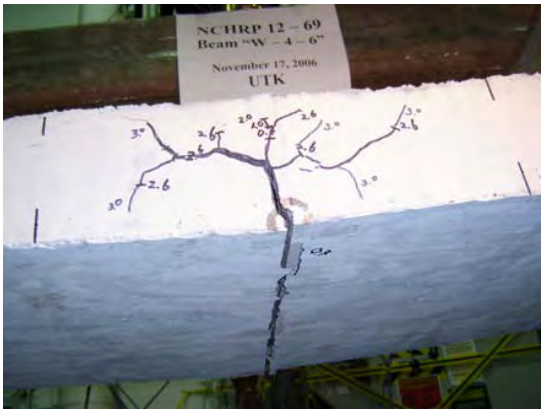

Figure F-1.19. A Large Crack Propagating along Midspan in WWR Specimens

(a): Ductile failure

(b): Brittle Failure

Figure F-20. Failure Types

CHAPTER 2

STUDY OF MAXIMUM FORCES IN THE LONGITUDINAL JOINTS

2.1 Introduction

The objective of the study reported here was to provide the database of maximum forces for determination of loading demand on the longitudinal joints due to service live loads. The effects of individual variables were researched by performing parametric studies using ABAQUS. The following variables were considered:

- Girder geometry including depth, span and spacing
- Single lane loading and multilane loading
- Skewness of the bridge
- Impact of cracking of joints

The decked bulb tee girder was chosen in the study and the development of the girder geometry was discussed in Subtask 6.1: “Develop Optimized Family of Girder Sections”. Based on the Subtask 6.1, Table F-2.1 summarized the practical span ranges for optimized girder sections. Typically, there were three different girder depths: 41 in., 53 in. and 65 in. The girder section is named by the girder depth, such as section “DBT41” referring to a decked bulb tee girder with 41 in. depth. For each girder section, there were three different girder spacings: 4 ft, 6 ft and 8 ft. Figure F-2.1 shows the cross section of the optimized deck bulb tee girder.

2.2 Description of Modeled Bridge Parameters

Table F-2.2 summarizes the seven bridge models with different girder geometry and bridge skewness developed for the parametric study. Bridges A, B, C and D are straight bridges with various girder geometry (depth, spacing and span). Bridges D, E, F and G have the same girder geometry with different bridge skewness.

All seven bridges are simply supported. Use of diaphragms between adjacent girders, as shown in Figure F-2.2, decreases the load transferred across the longitudinal

joint. Therefore, in order to calculate maximum loads on the longitudinal joint, only one intermediate steel diaphragm (ISD) is located at midspan of the bridge to connect the web and bottom flange of the girders. This is considered a minimum of what would be used in practice. Both the inclined member and horizontal member of the ISD use L $3'' \times 3'' \times \frac{3}{8}''$ steels which have a cross area of 2.11 in^2. The deck of the adjacent girders was connected by the proposed continuous longitudinal joint (Figure F-2.3) discussed in Chapter 1.

All the bridge models have the same bridge width of 40 ft. Figure F-2.4 and Figure F-2.5 shows the sketch of each bridge model. Figure F-2.4-(a) to Figure F-2.4-(d) show the cross section views of the four straight bridges and Figure F-2.5-(a) to Figure F-2.5-(c) show the plan views of the three skew bridges. The joints between girders were labeled as “joint 1”, “joint 2” and so on from left to right. Because of the symmetry of each bridge in width direction, the forces in joints locating left half of each bridge were studied. Please note that the metal railing is not shown in these sketches since only live load was considered in the study.

2.3 Description of Loadings

The live load HL-93 according to the AASHTO LRFD Bridge Design Specifications (AASHTO 2007) was used in the study. The live load HL-93 consists of design vehicle load and lane load. The design vehicle is either design truck or design tandem which can produce the larger forces. Figure F-2.6 shows the dimension and wheel weight of the live load HL-93. The tire contact area in design vehicle is 10 in. by 20 in. (AASHTO 2007). The dynamic load allowance should be applied to the design vehicle load but not to the lane load. The length of the lane load is varied to produce the larger forces. The distance between middle wheel and rear wheel of truck load varies from 14 ft to 30 ft to produce the larger force. In the parametric study, multiple presence factors of 1.20 and 1.00 were used for single lane loading and multilane (two lane) loading respectively.

For the fatigue loading, the fatigue truck load is the same as the design truck load specified in Figure F-2.6, but with a constant spacing 30 ft between the middle wheel and the rear wheel. The dynamic load allowance shall be applied to the fatigue load.

2.4 Development of Finite Element Models

The three dimensional (3D) finite element (FE) modeling was completed by using ABAQUS 6.4.1 available at the School of Engineering in the University of Tennessee Knoxville.

The bridge modeling consisted of three main components: intermediate steel diaphragm, decked bulb tee girder, and the continuous longitudinal joint connection between top flanges of adjacent girders (Figure F-2.7). The inclined members of steel diaphragm were modeled using 3D two-node truss elements (T3D2); the horizontal member was modeled using 3D two-node beam elements (B31) as shown in Figure F-2.7-a. The angle between inclined member and horizontal member was depended on the depth and the spacing of the girder. The major portion of the decked bulb tee girder, including the bottom bulb, stem, sub-flange, and the deck directly above the sub-flange, was modeled using 3D twenty-node solid elements (C3D20) as shown in Figure F-2.7-b.

The remainder the deck of the girder contains the longitudinal joint that is located at the outer edges of the deck as shown in Figure F-2.2. This is the main area of interest in this study. It was considered that use of shell elements in lieu of solid elements would facilitate the determination of moments and shear forces in the longitudinal joint. Therefore, sensitivity analyses were carried out to compare results using various modeling approaches for this area of the deck. Results of analyses were compared for moments and shear forces at the longitudinal joints of bridges with only one interior transverse diaphragm at midspan. Analyses were carried out using shell elements for this area of the deck versus more detailed models with solid elements. Based on the results, this area of the deck, including the continuous longitudinal joint connection, was modeled using 3D eight-node thick shell elements (S8R), as shown in Figure F-2.7-c.

Different material properties were assigned to different part of bridge components. The Young's modulus for the stem of girder including bottom bulb and sub-flange, deck of girder and steel diaphragm were 4,769 ksi (based on 7,000 psi compressive strength), 3,605 ksi (based on 4,000 psi compressive strength), and 29,000 ksi respectively. The Poisson's ratios for concrete and steel were 0.18 and 0.3 respectively. A sufficiently

refined mesh was completed to make sure that the results from 3D FE models were adequate.

The bridge models were assumed to be simply supported at the end. In the 3D FE models (Figure F-2.8), one end was applied the roller support by restraining the vertical movement (direction 3) of the bottom flange of the girders. The other end was the pinned support by restraining the movements of girder bottom flanges in both girder length and vertical direction (direction 2 and 3). In the transverse direction (direction 1), both girders' end sections were restrained for modeling concrete end diaphragms. The developed 3D FE models were calibrated and discussed in details by Ma et al. 2007.

2.5 Parametric Study

Based on the bridge models and vehicle loading discussed above, the parametric studies were conducted to find out the maximum forces in the longitudinal joint. The following parameters were considered: different loading locations, effect of bridge width, combination of design truck and lane loading vs. combination of design tandem and lane loading, girder geometry (depth, spacing and span), bridge skewness, single lane loading vs. multilane loading, and impact of cracking of the joints. The purpose of the parametric study was to provide the database of the maximum forces in the longitudinal joints for determination of loadings on the static and fatigue slab tests in Task 6.2-C2: "Laboratory Testing of Joint Assemblies". The maximum bending moment and maximum vertical shear in the longitudinal joints were focused on in the study.

2.5.1 Effect of Loading Locations

2.5.1.1 Lane Loading The sensitivity of the lane loading was studied on joint 1 of the bridge model A. The combination of design truck load and lane load was chosen. To produce the maximum forces in the joint, the extreme condition of design truck load with 14 ft between middle wheel and rear wheel was applied in the following study. Figure F-2.9 shows the loading positions for the study of bending moment in joint 1. The design truck located at the same location in the two cases. In longitudinal direction, the truck was located to produce the maximum moment of the bridge while in transverse direction, the center of left wheels of the truck was located right on the top of the joint 1 to produce the maximum bending moment in the joint according to the influence line

analysis. The length of lane load was varied. In case (a), the lane load was stopped at the center of rear wheel of truck while in case (b), the lane load was fully applied along the bridge in longitudinal direction. The maximum bending moments with the corresponding vertical shear in the joint 1 were shown in Table F-2.3.

As shown in Table F-2.3, the maximum moment in the two cases were very close which means the position of lane load had little effect on the moment in the joint. The values of the corresponding vertical shear were very small and closed to zero indicating that there was almost no shear while the maximum moment was produced in the joint.

Figure F-2.10 was the loading positions for the study of vertical shear. For the design truck load, it located at the same position as the case for moment study in longitudinal direction. In transverse direction, the left edge of left wheels was located right on the top of the joint 1 to produce the maximum vertical shear in the joint according to the influence line analysis. There were three different lane loads. It was applied fully along the bridge; stopped at the center of middle wheels; and stopped at center of rear wheels as shown in case (a) case (b) and case (c) respectively. The maximum shear with corresponding moment in each load case was presented in the Table F-2.4.

From Table F-2.4, it could be seen that case (b) and case (c) produced larger maximum shear than case (a), however, the difference was not significant. As long as the lane load was stopped at the heavy truck wheel (middle wheel or rear wheel), the difference of the maximum shear in the two cases was negligible.

In a summary, the lane load which was fully applied along bridge length direction would produce large moment in the joint while the lane load stopped at center of rear truck wheel would produce large shear in the joint.

2.5.1.2 Truck or Tandem Loading The sensitivity of truck loading was studied on joint 1 of the bridge model A. Figure F-2.11 shows the loading positions for the study of bending moment. In all six cases, the lane load was fully applied along the bridge length direction. For truck load, the center of left wheel was located right on the top of joint 1 (Figure F-2.9-detail A) in transverse direction. In longitudinal direction, the truck positions were different and specified by the distance between the center of front wheel and midspan of the bridge. The results of maximum moment in the joint 1 and the

corresponding shear were shown in the Table F-2.5.

As shown in Table F-2.5, all the six cases produce very closed maximum moment in joint 1. Truck loads with heavy wheel (middle wheel and rear wheel) located around midspan (Case b, Case c, Case d and Case e) produced less 2% more moment than truck loads with heavy wheel located far away midspan (Case a and Case f). However, the influence of truck load position in longitudinal direction on the maximum moment in the joint was negligible while load case (d) produced the largest maximum moment.

Figure F-2.12 shows the loading positions for the study of vertical shear. In all four cases, the lane load was stopped at the center of truck rear wheel. For truck load, the left edge of left wheel located right on the top of joint 1 (Figure F-2.10-detail A) in transverse direction. In longitudinal direction, the truck positions were different and specified by the distance between the center of front wheel and midspan of the bridge. The results of maximum shear and the corresponding moment in the joint 1 were shown in the Table F-2.6.

As shown in Table F-2.6, truck loads with heavy wheel (middle wheel and rear wheel) located around midspan (Case a, Case b, and Case c) produced larger shear than truck loads with heavy wheel located far away midspan (Case d). However, as long as the truck load with heavy wheel locating around midspan, the variation of the maximum shear in the joint was closed to 3%.

In a summary, the influence of truck load position in longitudinal direction on the maximum moment and shear in the joint was not significant while truck loads with heavy wheel located around midspan produced large maximum moment and shear.

The same as the truck loading, the sensitivity of tandem loading was also studied on joint 1 of the bridge model A. Figure F-2.13 shows the locations of tandem load combined with lane load to produce the maximum moment or shear in the joint. In Figure F-2.13-a, the tandem was located to produce the maximum moment of the bridge in longitudinal direction, while in transverse direction, the center of left wheels of the tandem was located right on the top of the joint 1. The lane load was applied fully along the bridge length. In Figure F-2.13-b, the tandem positioned the same location in longitudinal direction, while in transverse direction, the left edge of left wheels was

located right on the top of the joint 1. The lane load stopped at center of rear tandem wheel.

2.5.2 Effect of Bridge Width

Figure F-2.14 shows the study of the maximum negative moment in the joint 2 of the bridge model B. The position of left loading was the same for all the three cases. The left edge of the left lane loading was 2 ft away from the left edge of the bridge. The positions of right loading were varied. The right edge of the right lane loading was 10 ft, 6 ft and 2 ft away from the right edge of the bridge for Case (a), Case (b) and Case (c) respectively. Table F-2.7 summarizes the results of the maximum negative moment under the three loadings.

As shown in Table F-2.7, it appeared that the maximum negative moment increased with the increase of the distance between the two loadings in transverse direction and the larger negative moment would be produced in a wide bridge. In order to study the impact of bridge width on the negative moment, a “modified bridge B” (adding one more girder) was developed in the study. Figure F-2.15 shows the sketch (cross section view) of the modified bridge model B.

Figure F-2.16 shows the multilane loading position on the modified bridge model B to produce the negative moment in joint 2 and joint 3. The left edge of the left lane loading was 2 ft away from the left edge of the bridge while the right edge of the right lane loading was 2 ft away from the right edge of the bridge. The maximum negative moments in the joint 2 and the joint 3 were summarized in Table F-2.8.

As shown in Table F-2.8, the maximum negative moment in modified bridge model B was less than bridge model B.

The maximum positive moment and shear were also studied between bridge B and modified bridge B. The maximum forces under different loading locations were presented in Table F-2.9.

From Table F-2.9, the maximum positive moment and shear in modified bridge model B were also less than ones in bridge model B, however, the difference was not

significant. In summary, increasing the bridge width would decrease the maximum negative moment in some degree. The effect of bridge width on the maximum positive moment and the maximum shear was negligible.

2.5.3 Truck and Lane Loading vs. Tandem and Lane Loading

Live Load HL-93 has two different loading combinations. One combination is truck load plus lane load. The other combination is tandem load plus lane load. Generally, the truck and lane load combination produces larger forces on the long span bridge; while tandem and lane load combination produces larger forces on short span bridge (the span of the bridge is comparable to the distance of the front wheel to the rear wheel of truck). In order to determine the effect of different loading combinations on the maximum forces in the joint on the practical span of the optimized decked bulb tee girders, the maximum forces under two loading combinations both for long span bridge (bridge model A) and short span bridge (bridge model B) were studied.

Figure F-2.17 compares the maximum moment and shear in joint 1 and joint 2 produced by different loading combinations in long span bridge. The label “Truck” means truck and lane load combination while “Tandem” refers to tandem and lane load combination.

Figure F-2.18 compares the maximum moment and shear in joint 1 and joint 2 produced by different loading combinations in short span bridge.

It can be seen that the truck and lane load combination produced larger maximum forces than tandem and lane load combination in both long and short span bridges. It was because the practical span range of the optimized decked bulb tee girders is much longer than the truck length which makes the truck and lane load dominate the loading.

2.5.4 Effect of Girder Span

The effect of girder span on the maximum forces in the joints were studied between bridge model A and bridge model B. Both bridge models had the same girder cross sectional geometry. Bridge model A had long girder span while bridge model B had short girder span. Figure F-2.19 compares the maximum forces in the joint between long span bridge model A and short span bridge model B.

It can be seen that the girder span had some effect on the maximum positive moment in the joint. Longer span produced larger positive moment. However, the influence was not significant. For the shear and negative moment, they were almost the same between two models which means the span had no effect on the maximum shear and negative moment in the joint

2.5.5 Effect of Girder Depth

The optimized decked bulb tee girder family has three different girder depths: 41 in., 53 in. and 65 in. The effect of girder depth on the maximum forces in the joint was studied (Figure F-2.20) between 41 in. girder depth's model (bridge model D) and 65 in. girder depth's model (bridge model A).

The girder depth had the influence on the maximum forces in both joints. Decreasing the girder depth, the positive moment and negative moment (absolute value) increased up to 58% and 120% respectively while the shear decreased 4%. The deck of the girder had the main contribution to resist the moment and the web of the girder had the main contribution to resist the shear. Decreasing the girder depth reduces the height of the web only while the deck and bottom flange of the girder do not change. So the stiffness of the deck was relatively stiffer to produce more moment while the stiffness of the web is relatively weaker to produce fewer shears. However, the impact girder depth had more influence on the moment than the shear.

2.5.6 Effect of Girder Spacing

The optimized decked bulb tee girder family had three different girder spacing: 4 ft, 6 ft and 8 ft. The effect of girder spacing on the maximum forces in the joint was studied (Figure F-2.21) between 4 ft girder spacing' model (bridge model C) and 8 ft girder spacing' model (bridge model A).

From Figure F-2.21, it can be seen that the girder spacing had significant influence on the forces in the joints. Decreasing the girder spacing reduced both the moment and shear. For the bridges with the same width, decreasing the girder spacing means adding more girders to resistant the loading. The bridge with more girder members produced less force but it might cost more.

2.5.7 Effect of Bridge Skewness

The effect of bridge skewness on the maximum forces in the joints was studied between bridge models D, model G, model F and model E (Figure F-2.22). They had the same girder cross sectional geometry while the girder skewness was 0 degree, 15 degree, 30 degree and 45 degree respectively.

It can be seen that the bridge skewness had influence on the maximum moment in the joints while it had no influence on the shear. For bridge models with different skewness, the maximum shear forces were almost the same in each joint. However, the effect of skewness on the maximum moment depended on the loading positions related to the interested joint. To maximize the positive moment in joint 1 and joint 2, the single lane loadings were applied, which made the moment increased with increasing of the skewnwss. To maximize the negative moment (absolute value) in joint 1 and joint 2, the multilane loadings were applied. The multilane loading positioned on the same side of the joint 1 made the negative moment (absolute value) increased with increasing of the skewnwss. However, the multilane loading located on each side of the joint 2 made the negative moment (absolute value) decreased with increasing of the skewnwss.

2.5.8 Single Lane Loading vs. Multilane Loading

Figure F-2.23 compared the effect of number of loaded lanes on the maximum forces in the joints between bridge models. The left column of each model represented single lane loading and the right column of each model represented multilane loading. Note that the data includes a multiple presence factors of 1.20 and 1.00 for single lane loading and multilane (two lane) loading respectively based on the Article 3.6.1.1.2 in AASHTO LRFD.

From Figure F-2.23, it can be concluded that different number of loaded lanes produced different maximum forces in the joint. Both moment and shear under single lane loading were larger than the forces under multilane loading in the two joints. So the single lane loading shall dominate the loading.

Table F-2.10 to Table F-2.14 summarized the maximum forces in the joint in the 7 bridge models under different loading locations. Through Table F-2.10 to Table F-2.13,

the maximum positive moment (M) with corresponding shear (CS) and the maximum shear (S) with corresponding moment (CM) were included.

In a summary, the maximum positive moment, negative moment and shear in the longitudinal joint under live load HL-93 was 7.922kips-ft/ft, -2.152kips-ft/ft and 6.091kips/ft respectively. Based on the DECK SLAB DESIGN TABLE A4-1 in AASHTO, the maximum positive live load moment in the bridge deck supported by 8ft spacing girders was 5.69kips-ft/ft. This table is used in determining the design moments for the bridge deck. Specified assumptions and limitations were used in developing this table and should be considered when using for design.

2.5.9 Impact of Cracking

Based on the results of the analyses discussed above using uncracked sections for the longitudinal joints, it is anticipated that the joints would be cracked under service loading. Therefore, the forces in the joint would be expected to be reduced compared with the forces calculated with uncracked sections. The difference of structural behaviors before and after crack is due to the change in the joint stiffness.

In the FE models where the largest maximum forces in the joint were found, the impact of cracking of the joint was studied by changing the modulus of elasticity (E) while keeping the moment of inertia (I) the same. Figure F-2.24-(a) and Figure F-2.24-(b) show the impact of cracking on the maximum moment (positive moment and negative moment) and maximum shear respectively.

From Figure F-2.24, it can be seen that the cracking has influence on the maximum forces in the joints. With the reduction of the EI, the forces decrease at a different rate. The reduction of the forces becomes faster and faster when the EI reduction increased. The EI reduction has more influence on moment than on shear. When the EI reduction reached up to 95%, the residual moment and residual shear are 35.4% and 75.7% of the values calculated by uncracked section properties respectively.

Based on the beam theory, the EI is the slope of the Moment-Curvature curve. In Task 6.2-C1: “Laboratory Testing of Trial Joints” (Li et al. 2009), 8 beam specimens anchored by different reinforcement details at the joint zone were tested and the 6 in. lap

length headed bar detail was selected for the future study. From the Moment-Curvature curves of the 6 in. lap length headed bar specimen (H-6-6) and continuous reinforcement specimen (Control), the EI reduction after cracking was 88% and 92% respectively. According to the theoretic calculation of the beam, the EI reduction after cracking was 89%.

Considering the force reduction due to the joint cracking, the maximum positive moment, negative moment and shear in the longitudinal joint under live load HL-93 was 4.001kips-ft/ft, -1.137kips-ft/ft and 5.056kips/ft respectively. The corresponding moment (CM) occurring with the maximum shear is 2.887 kips-ft/ft.

2.5.10 Fatigue Loading

The Articles in AASHTO LRFD (2007) referenced to the fatigue loading are listed below:

3.4.1 FATIGUE-Fatigue and fracture load combination relating to repetitive gravitational vehicular live load and dynamic responses under a single design truck having the axle spacing specified in Article 3.6.1.4.1

3.4.1 A load factor of 0.75 (Table 3.4.1-1) shall be applied to fatigue load combination

3.6.1.2.1 Vehicular live loading on the roadways of bridges or incidental structures, designated HL-93, shall consist of a combination of the design truck or design tandem, and design lane load.

3.6.1.4.1 The fatigue load shall be one design truck or axles thereof specified in Article 3.6.1.2.2, but with a constant spacing of 30.0 feet between the 32.0-fip axles.

3.6.2.1 The static effects of the design truck or tandem shall be increased by 15% (fatigue and fracture limit state) for dynamic load allowance (Table 3.6.2.1-1). The dynamic load allowance shall not be applied to pedestrian loads or to the design lane load.

The fatigue loading was determined by the following equation according to the

above Articles:

0.75 [Lane Load + 1.15 (Fatigue Truck Load)]

Using the above equation, the maximum positive moment, negative moment and shear in the longitudinal joint under fatigue live load HL-93 was 2.143 kips-ft/ft, -0.453 kips-ft/ft and 2.326 kips/ft respectively.

It should be noted that the loads above are probably conservatively high in that Lane Load was included. A strict interpretation of the definition of Fatigue in Article 3.4.1 indicated that live load (i.e. Lane Load) be included. A strict interpretation of Article 3.6.1.4.1 indicates however, that fatigue load consists of only load from the fatigue design truck and Lane Load is not included. This second interpretation is more common. Therefore, the loads described above are marginally higher than they need to be.

It should also be noted that, subsequent to completion of the panel fatigue tests described in Section 3.2 of this appendix, revisions to fatigue loading were accepted by AASHTO Bridge Committee, Technical Committees T-5 Loads, and T-14 Steel in May of 2008. The revisions consist of inclusion of two levels of fatigue load in Table 3.4.1-1. These are Fatigue I and Fatigue II. Fatigue II retains the current Load Factor of 0.75 and is to be applied to represent an effective stress range caused by the fatigue truck with respect to a large but finite number of stress range cycles. Fatigue I has a Load Factor of 1.5 (or 2 times 0.75) and is to be applied to the stress range caused by the fatigue truck with respect to an infinite number of stress range cycles.

Using the revised Load Factor of 1.5 for Fatigue I and not including the Lane Load, i.e. 1.5 [1.15 (Fatigue Truck Load)], results in maximum positive moment, negative moment and shear in the longitudinal joint under fatigue live load HL-93 for infinite life of 3.419 kips-ft/ft, -0.568 kips-ft/ft and 4.382 kips/ft respectively. In addition, the corresponding moment (CM) at maximum shear for the fatigue truck load is 1.276 kip-ft/ft. Using this moment with the Load Factor of 1.5 and a dynamic load allowance of 15% results in a factored fatigue moment of 2.201 kips-ft/ft that would be coincidental with the maximum shear of 4.382 kips/ft. The implications of the use of a Load Factor of 1.5 are discussed further in Section 3.2.7 of this appendix.

2.6 Conclusions

A total of seven bridge models with different girder geometry were developed and loaded by HL-93 loading in the parametric study. The purpose of the study was to provide the database of the maximum forces in the longitudinal joints for determination of loadings on the static and fatigue slab tests in Subtask 6.2-C2: “Laboratory Testing of Joint Assemblies”. The following parameters were considered: different loading locations, effect of bridge width, design truck and lane loading vs. design tandem and lane loading, girder geometry (depth, spacing and span), bridge skewness, single lane loading vs. multilane loading, and impact of cracking of the joints. Based on the parametric study discussed above, the following findings are summarized below:

1. The maximum forces in the joint were not sensitive to the length of the lane load. Typically, the lane load fully applied along bridge length direction produced a larger moment while the lane load stopped at the rear wheel of truck load produced a larger shear.

2. In longitudinal direction, the influence of the location of the vehicle load (truck or tandem) on the maximum forces in the joint was not significant. The truck with heavy wheels (middle wheel or rear wheel) or the tandem locating around midspan of the bridge produced a larger moment and shear.

3. The truck plus lane load produced larger forces than the tandem plus lane load and it dominated the loading for the practical span ranges of the optimized decked bulb tee girders.

4. Increasing the bridge width would decrease the maximum negative moment in some degree. However, the effect of bridge width on the maximum positive moment and the maximum shear was negligible.

5. The maximum forces in the joints were not sensitive to the span of the bridge. However, they were influenced significantly by the spacing and the depth of the girder. Girder with a larger spacing and a shallower depth produced a larger moment and shear.

6. The shear was not sensitive to the skewness of the bridge. Increasing the skewness, the maximum positive moment would increase; however, the maximum negative moment would decrease.

7. Single lane loading produced larger forces than multilane loading and it dominated the loading level.

8. The maximum forces in the joints decreased after the joint cracking. However, the impact of cracking had more effect on moment than on shear.

9. Before cracking, the maximum positive moment is 7.922 kips-ft/ft; the maximum negative moment is -2.152 kips-ft/ft; the maximum shear is 6.091 kips/ft. After cracking, the maximum positive moment is 4.001 kips-ft/ft; the maximum negative moment is -1.137 kips-ft/ft; the maximum shear is 5.056 kips/ft. The maximum forces before and after cracking will be used to determine the static loading demand for test specimens in Subtask 6.2-C: “Laboratory Testing”

10. The maximum positive moment, negative moment and shear in the longitudinal joint under fatigue live load HL-93 was 2.143 kips-ft/ft, -0.453 kips-ft/ft and 2.326 kips/ft respectively. The corresponding moment (CM) occurring with the maximum shear is 2.887 kips-ft/ft. These forces will be used to determine the fatigue loading demand for test specimens in Subtask 6.2-C: “Laboratory Testing”

A separate analytical parametric study was carried out using SAP2000 to determine the shear force transferred across the joint due to the leveling of differential camber during construction. Based on that study, a shear force 0.5 kips/ft was determined as a reasonable upper bound to consider in the test specimen.

Table F- 2.1: Practical Span Ranges for Optimized Decked Bulb Tee Girders

Section	Spacing (ft)	Span (ft)	
		Minimum	Maximum
DBT41	4	84	124
	6	72	130
	8	64	118
DBT53	4	98	150
	6	84	156
	8	76	148
DBT65	4	108	172
	6	94	180
	8	84	176

Table F-2.2 Summary of the Seven Bridge Models

Bridge	Girder		Span (ft)	Skewness (degree)
	Depth (inch)	Spacing (ft)		
A	65	8	134	0
B	65	8	84	0
C	65	4	108	0
D	41	8	118	0
E	41	8	118	45
F	41	8	118	30
G	41	8	118	15

Table F-2.3: Forces in Joint 1 due to Loads in Figure F-2.9

Load Positions	Forces in Joint 1	
	Maximum Moment (kips-ft/ft)	Corresponding Shear (kips/ft)
Case (a)	5.341	0.094
Case (b)	5.498	0.114

Table F-2.4: Forces in Joint 1 due to Loads in Figure F-2.10

Load Positions	Forces in Joint 1	
	Corresponding Moment (kips-ft/ft)	Maximum Shear (kips/ft)
Case (a)	3.76	4.932
Case (b)	3.604	5.916
Case (c)	3.716	6.024

Table F-2.5: Forces in the Joint 1 due to Loads in Figure F-2.11

Load Positions	Forces in Joint 1	
	Maximum Moment (kips-ft/ft)	Corresponding Shear (kips/ft)
Case (a)	5.393	0.044
Case (b)	5.497	0.049
Case (c)	5.496	0.091
Case (d)	5.498	0.114
Case (e)	5.494	0.139
Case (f)	5.488	0.067

Table F-2.6: Forces in the Joint 1 due to Loads in Figure F-2.12

Load Cases	Forces in Joint 1	
	Corresponding Moment (kips-ft/ft)	Maximum Shear (kips/ft)
a	3.821	5.814
b	3.716	6.024
c	3.606	5.952
d	2.8	5.388

Table F-2.7: Negative Moment in the Joint 2 due to Loads in Figure F-2.14

Load Positions	Maximum Negative Moment (kips-ft/ft)
Case a	-0.662
Case b	-1.000
Case c	-1.034

Table F-2.8: Negative Moment in the Joint 2 and Joint 3 due to Loads in Figure F-2.16

Modified Bridge B	Maximum Negative Moment (kips-ft/ft)
Joint 2	-0.669
Joint 3	-0.866

Table F-2.9: Maximum Positive and Shear Comparison between Bridge B and Modified Bridge B

	Bridge B		Modified Bridge B	
	Moment (kips-ft/ft)	Shear (kips/ft)	Moment (kips-ft/ft)	Shear (kips/ft)
Joint 1	5.034	5.646	5.030	5.628
Joint 2	5.225	5.899	5.148	5.694
Joint 3			5.099	5.688

Table F-2.10: Maximum Forces in Joint 1 under Single Lane Loading

Bridge Models	Maximum Moment		Maximum Shear	
	M (kips-ft/ft)	CS (kips/ft)	CM (kips-ft/ft)	S (kips/ft)
A	5.498	0.114	3.716	6.024
B	5.034	0.094	3.373	5.646
C	2.242	0.029	1.672	4.745
D	6.304	0.227	4.492	5.768
E	6.713	0.137	5.027	5.703
F	6.512	0.178	4.693	5.718
G	6.404	0.204	4.585	5.746

Table F-2.11: Maximum Forces in Joint 2 under Single Lane Loading

Bridge Models	Maximum Moment		Maximum Shear	
	M (kips-ft/ft)	CS (kips/ft)	CM (kips-ft/ft)	S (kips/ft)
A	6.286	0.112	4.206	5.856
B	5.225	0.048	3.442	5.899
C	3.386	0.299	2.432	4.738
D	7.393	0.347	5.294	5.946
E	7.922	0.421	5.464	6.091
F	7.528	0.364	5.370	6.054
G	7.432	0.348	5.305	6.041

Table F-2.12: Maximum Forces in Joint 1 under Multilane Loading

Bridge Models	Maximum Moment		Maximum Shear	
	M (kips-ft/ft)	CS (kips/ft)	CM (kips-ft/ft)	S (kips/ft)
A	4.376	0.230	2.964	5.070
B	3.933	0.039	2.619	4.672
C	1.715	0.019	1.254	3.956
D	5.056	0.385	3.524	4.956
E	5.785	0.285	4.355	4.911
F	5.369	0.322	3.798	4.926
G	5.185	0.358	3.603	4.939

Table F-2.13: Maximum Forces in Joint 2 under Multilane Loading

Bridge Models	Maximum Moment		Maximum Shear	
	M (kips-ft/ft)	CS (kips/ft)	CM (kips-ft/ft)	S (kips/ft)
A	4.472	0.095	2.830	4.723
B	3.936	0.056	2.525	4.888
C	2.287	0.230	2.195	3.699
D	5.219	0.517	3.492	5.128
E	6.475	0.573	4.074	5.270
F	5.703	0.510	3.760	5.221
G	5.390	0.516	3.578	5.167

Table F-2.14: Maximum Negative Moment

Bridge Models	Joint 1 (kips-ft /ft)	Joint 2 (kips-ft/ft)
A	-0.371	-0.978
B	-0.389	-1.034
C	-0.078	-0.215
D	-0.785	-2.152
E	-1.400	-1.560
F	-0.939	-1.940
G	-0.824	-2.110

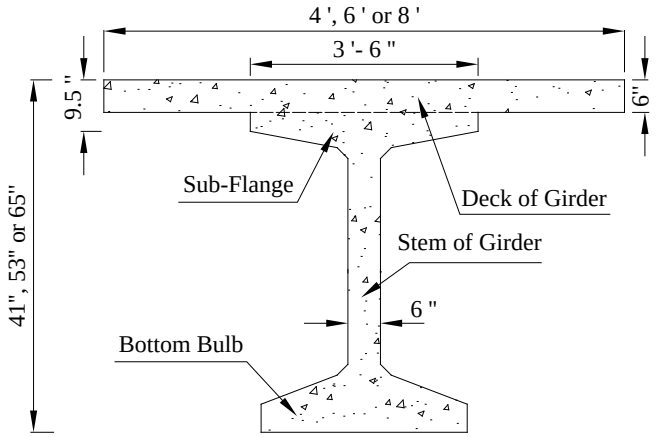

Figure F-2.1: Cross Section of Optimized Decked Bulb Tee Girder

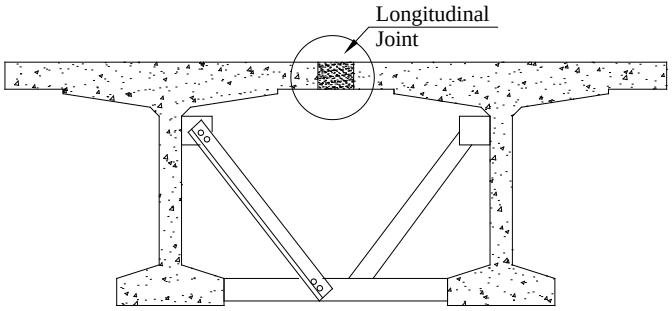

Figure F-2.2: Steel Diaphragm Connecting Adjacent Girders at Midspan

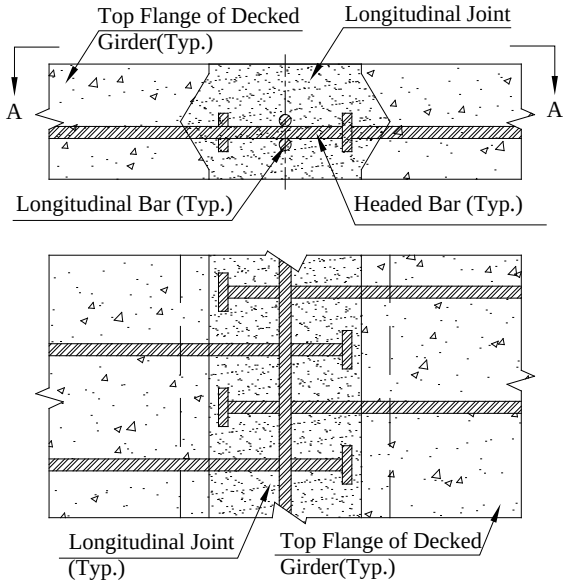

A - A

Figure F-2.3: Proposed Continuous Longitudinal Joint

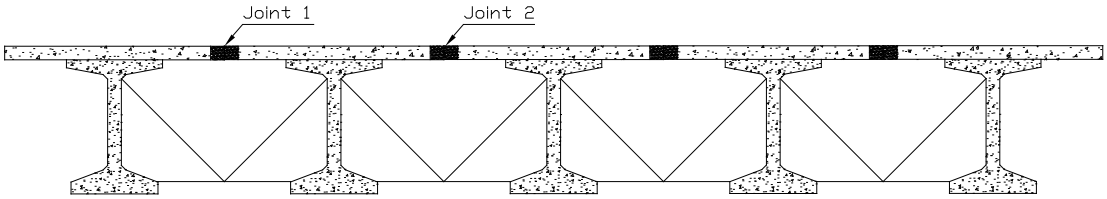

(a) Bridge A

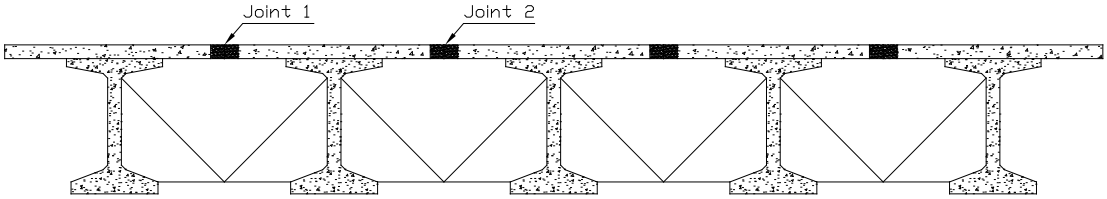

(b) Bridge B

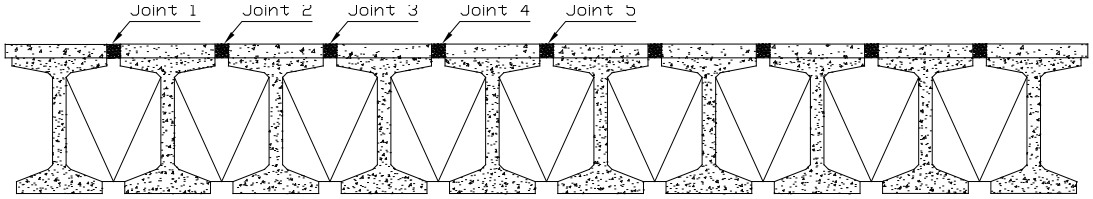

(c) Bridge C

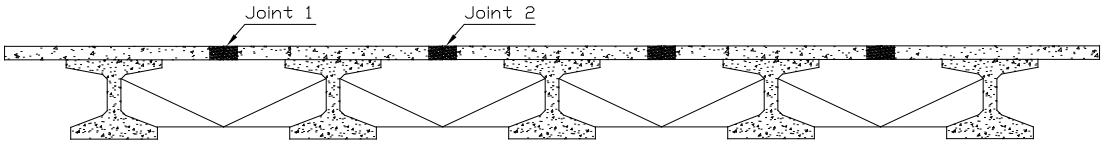

(c) Bridge D

Figure F-2.4: Cross Section Sketch of Bridge Models

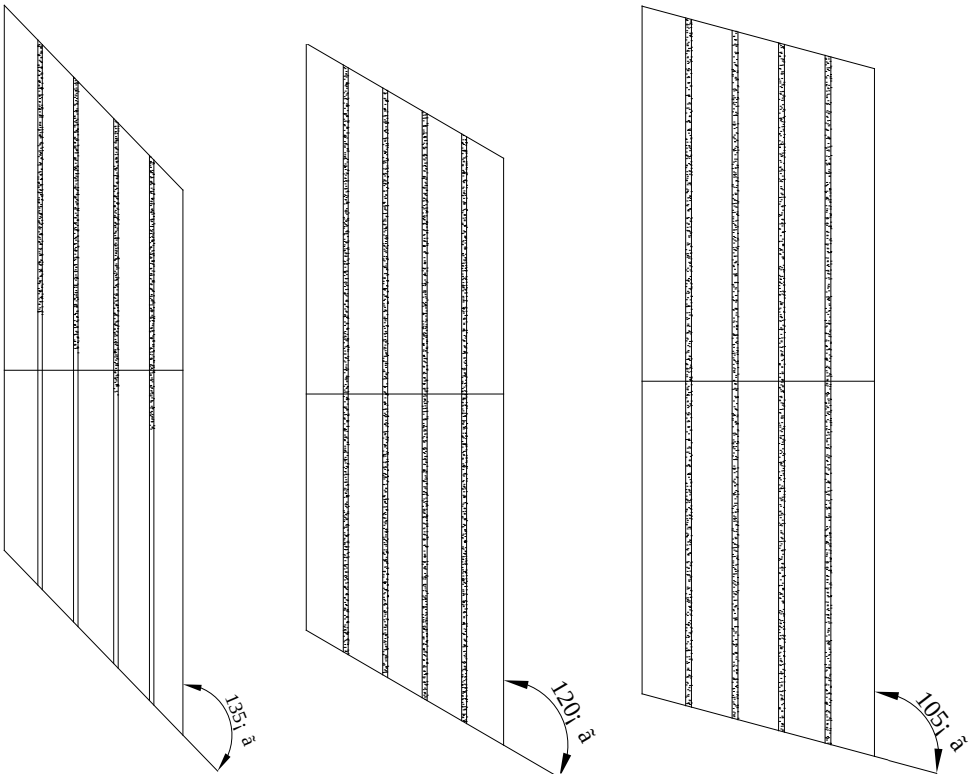

(a) Bridge E (b) Bridge F (c) Bridge G

Figure F-2.5: Plan View Sketch of Bridge Models

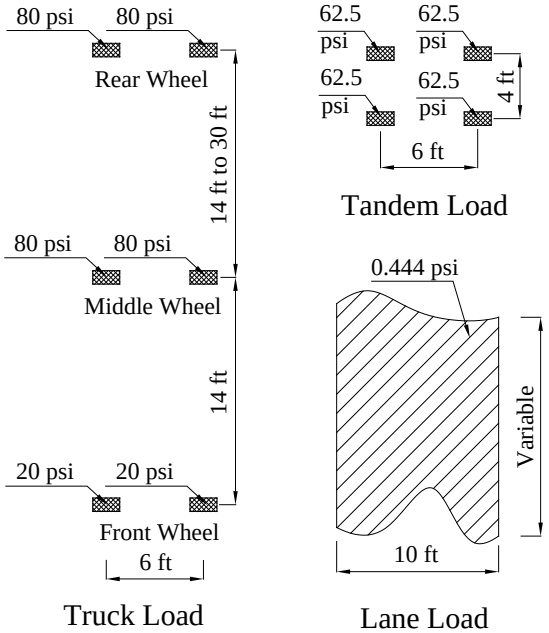

Figure F-2.6: Dimension and Wheel Weigh of the Live Load HL-93

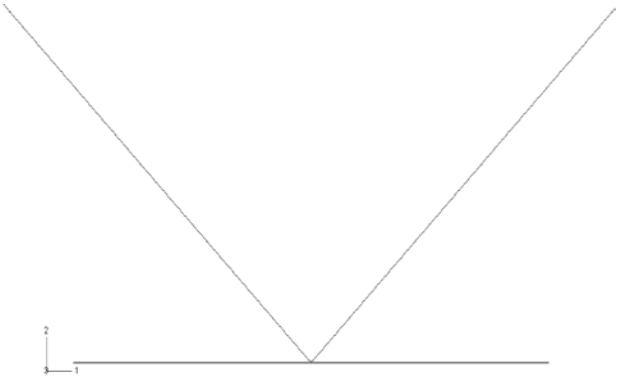

(a) Intermediate Steel Diaphragm

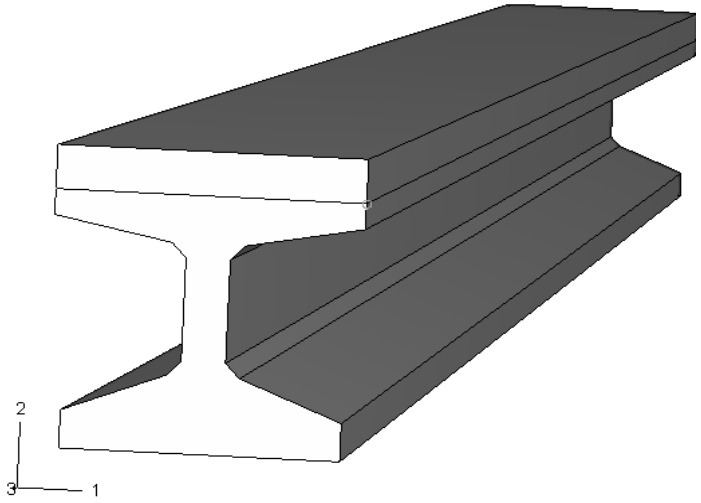

(b) Decked Bulb Tee Girder

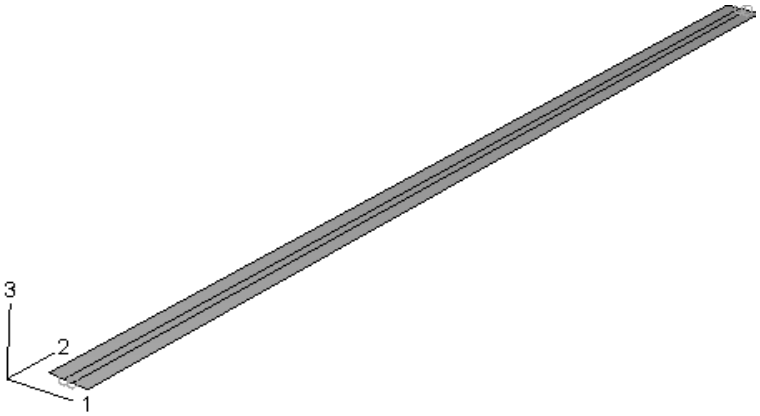

(c) Continuous Longitudinal Joint Connection

Figure F-2.7: Bridge Components Modeled by 3D Finite Elements

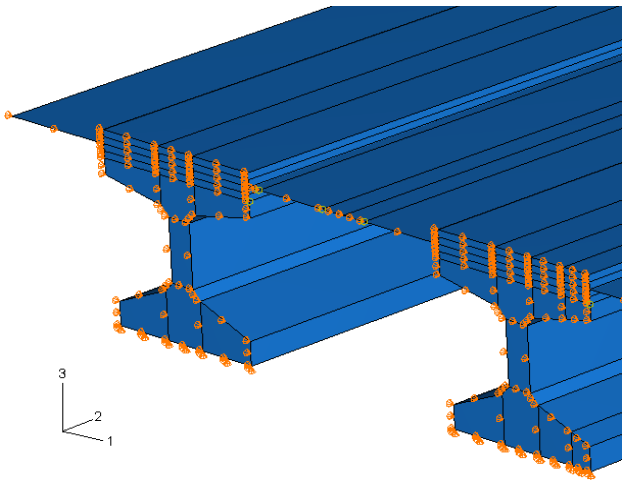

Figure F-2.8: Boundary Conditions

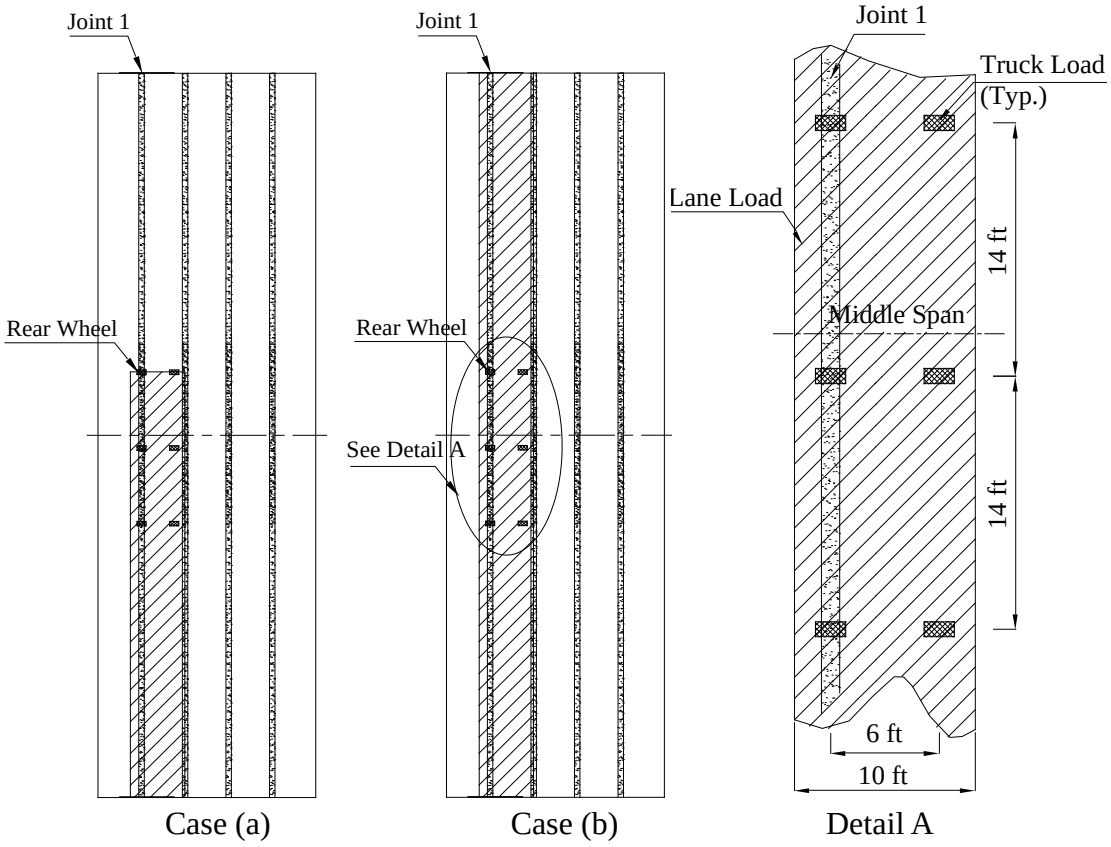

Figure F-2.9: Loading Locations for Moment

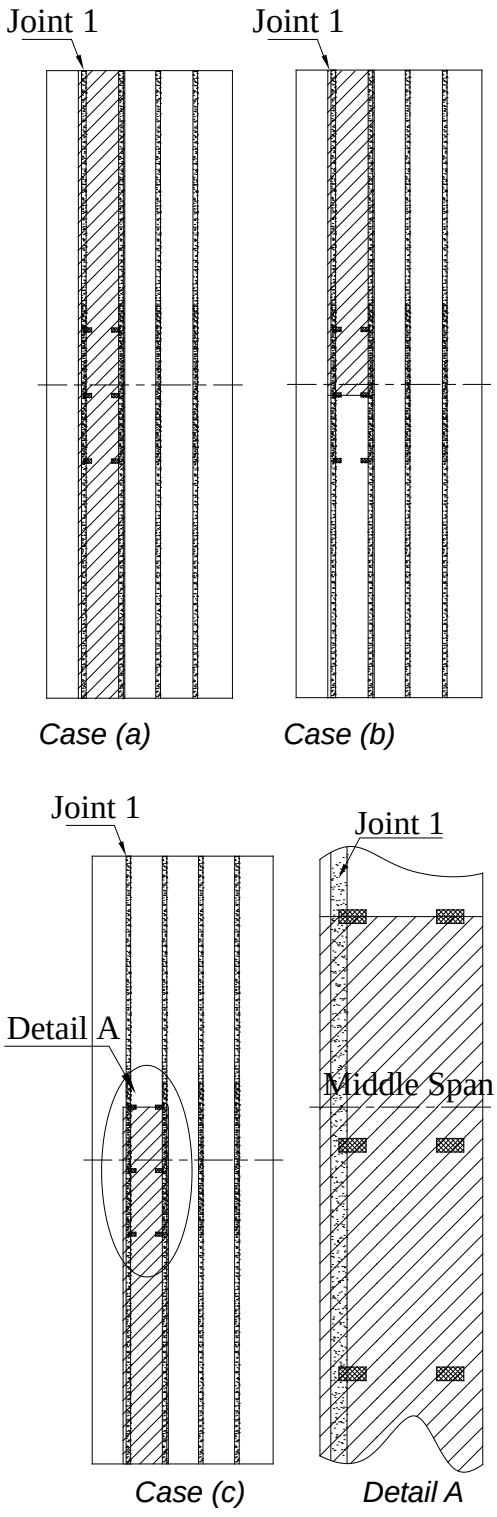

Figure F-2.10: Load Positions for Shear

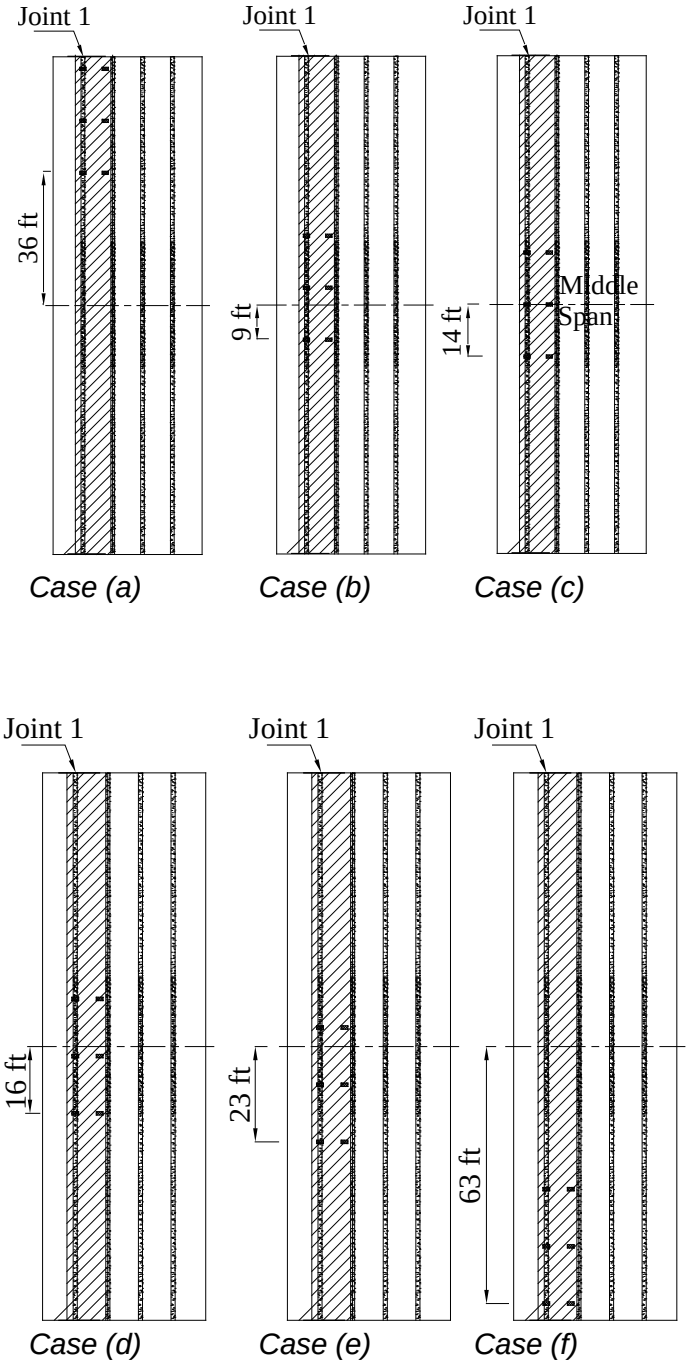

Figure F-2.11: Truck Load Positions for Moment

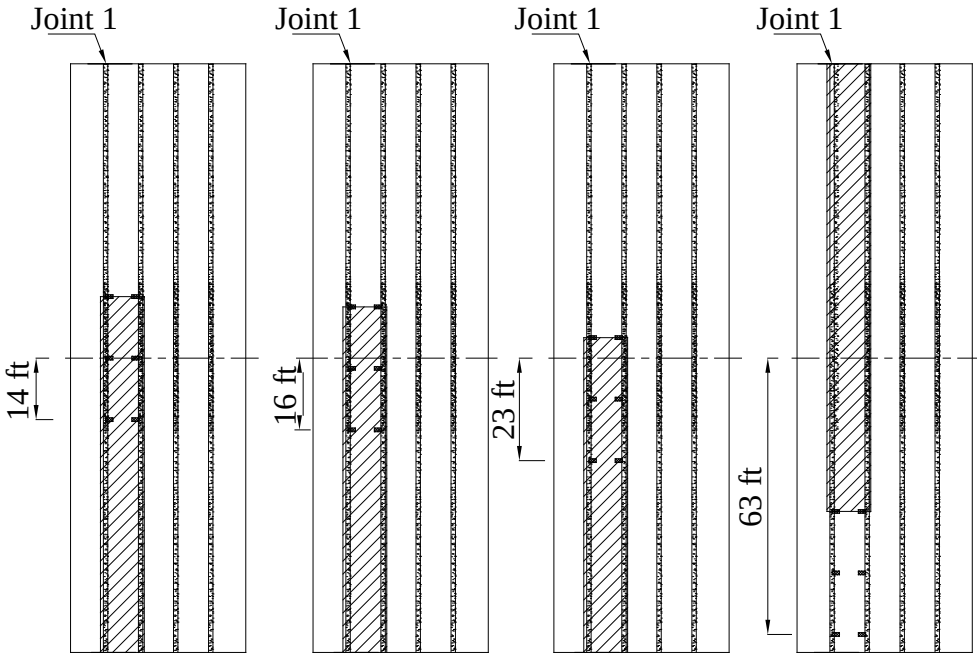

Figure F-2.12: Truck Load Positions for Shear

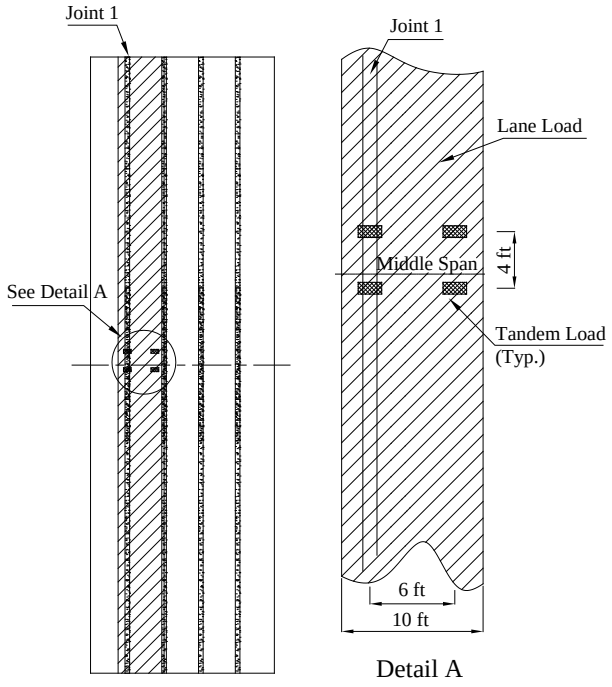

(a): Maximum Moment

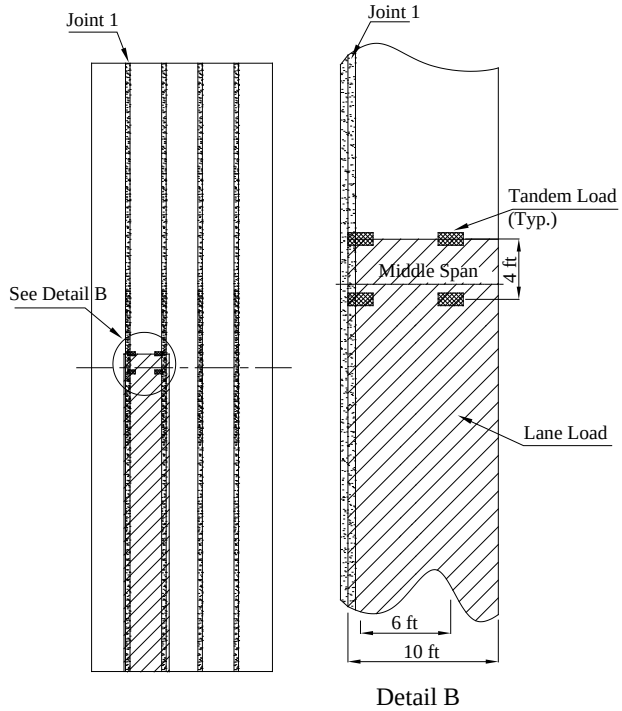

(b): Maximum Shear

Figure F-2.13: Locations of Tandem Load Combined with Lane Load

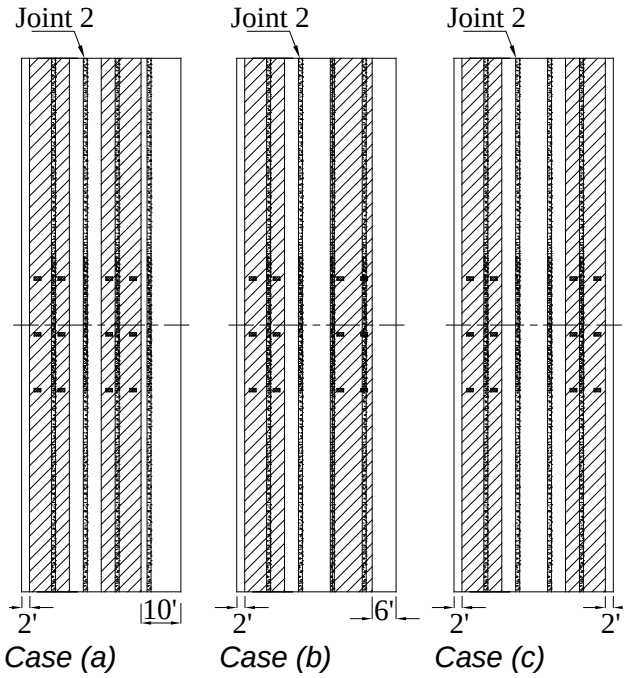

Figure F-2.14: Load Positions for Negative Momen

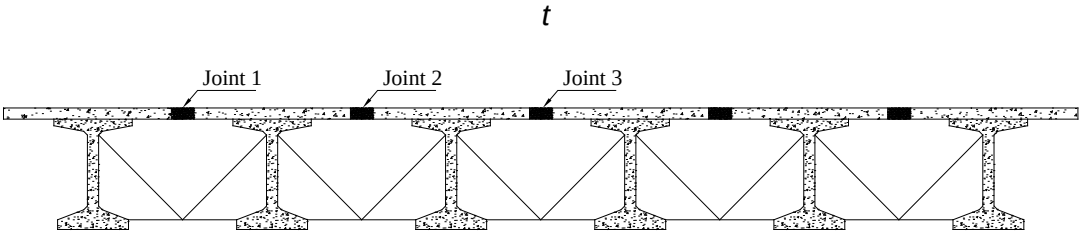

Figure F-2.15: Sketch of Modified Bridge B

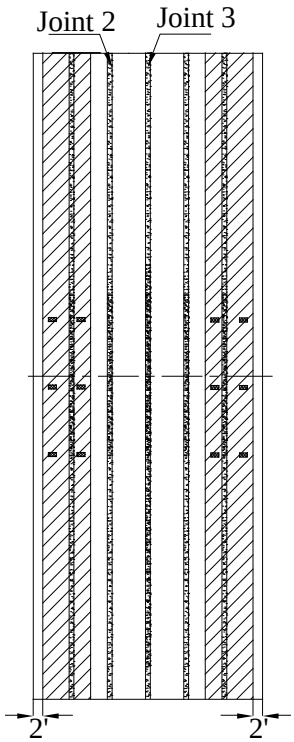

Figure F-2.16: Loading Position on Modified Bridge Model B

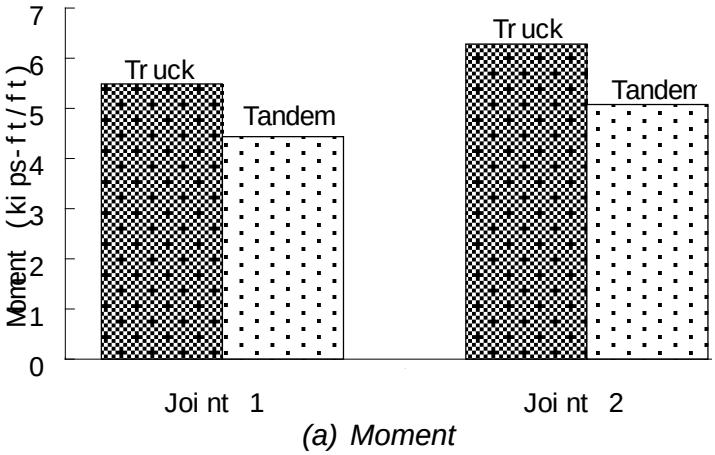

(a) Moment

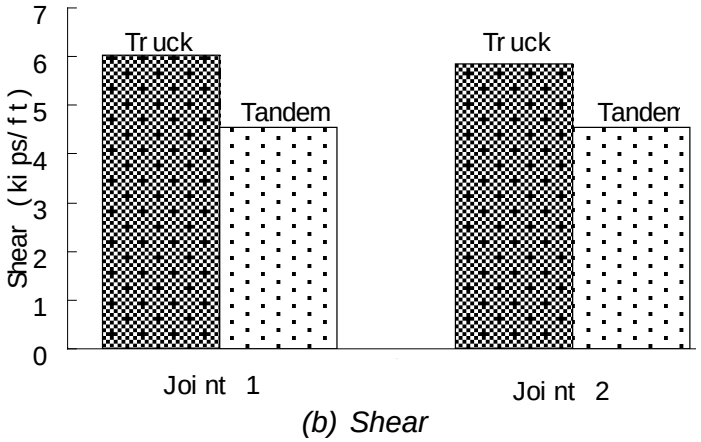

(b) Shear

Figure F-2.17: Forces Comparison in Long Span Bridge

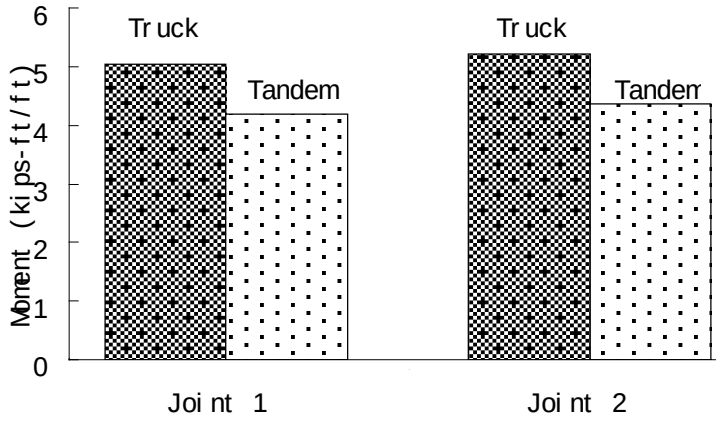

(a) Momen

t

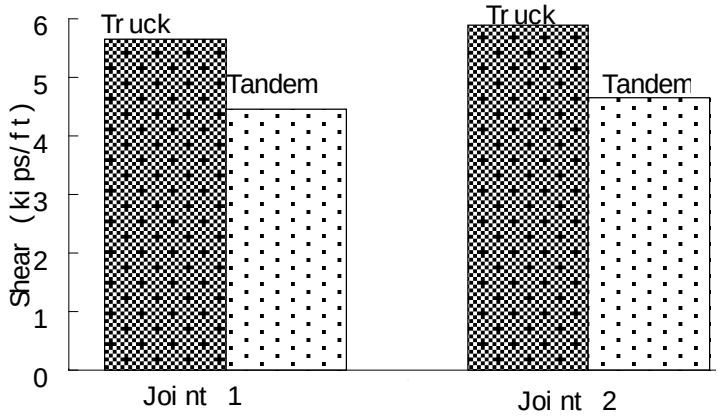

(b) Shear

Figure F-2.18: Forces Comparison in Short Span Bridge

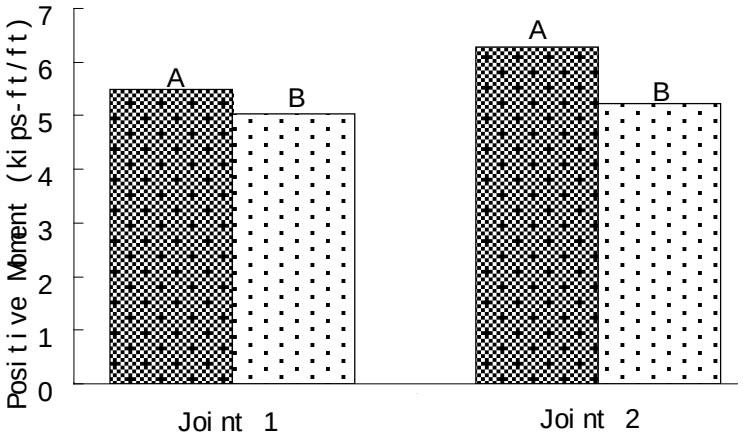

(a) Positive Moment

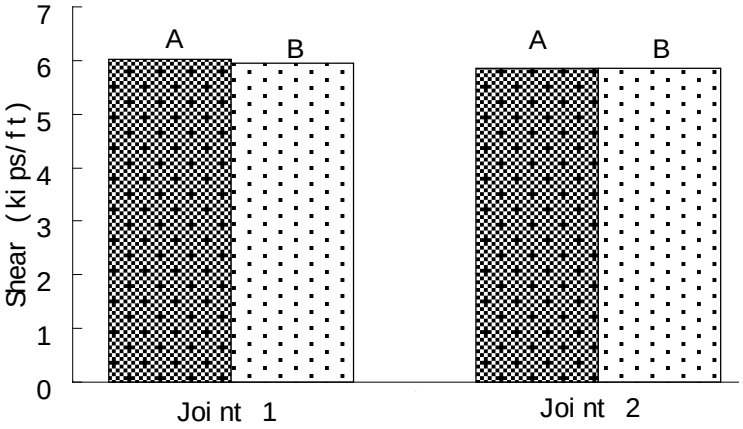

(b) Shear

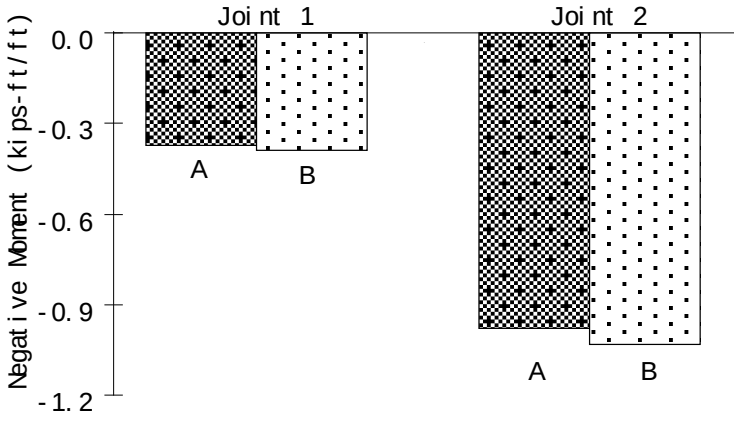

(c) Negative Moment

Figure F-2.19: Span Effect on Forces in Joint

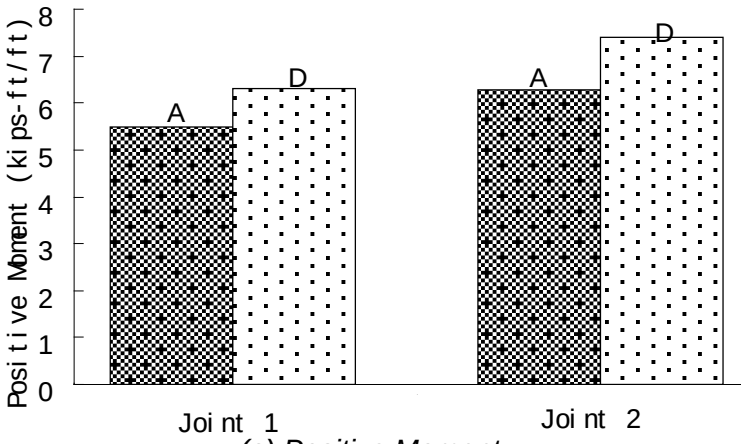

(a) Positive Moment

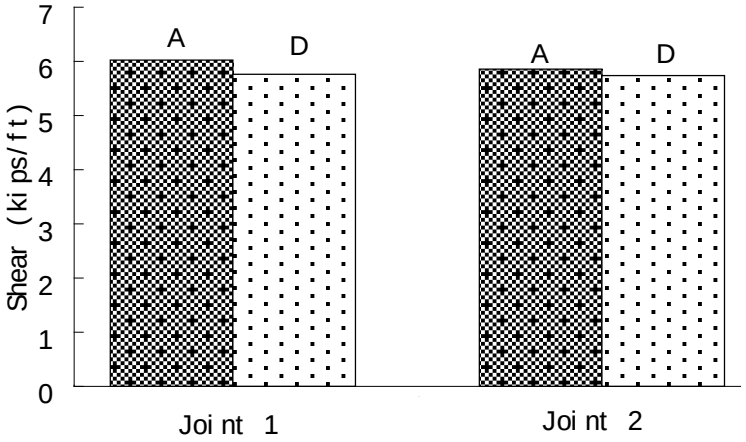

(b) Shear

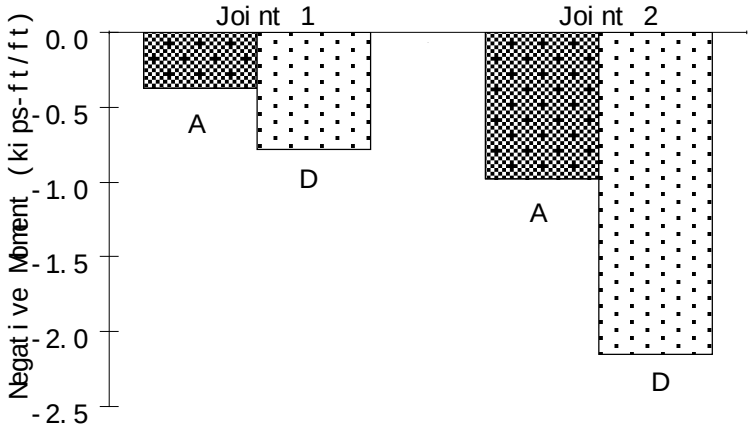

(c) Negative Moment

Figure F- 2.20: Depth Effect on Forces in Joint

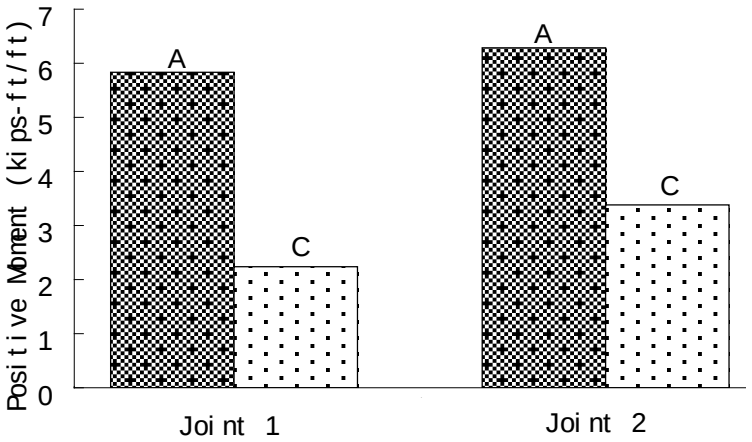

(a) Positive Moment

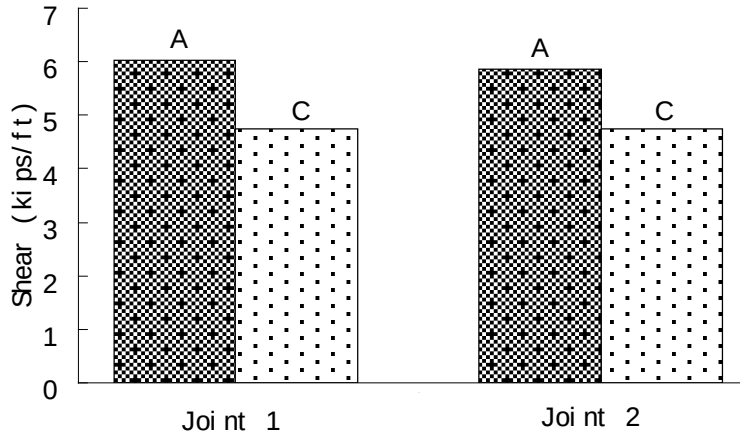

(b) Shear

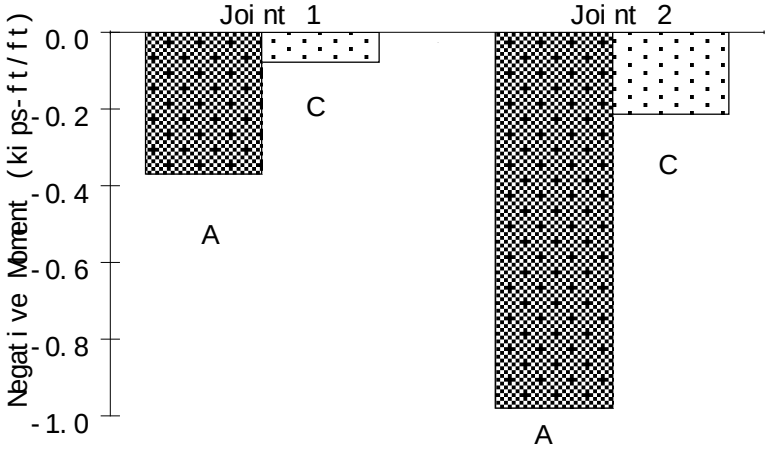

(c) Negative Moment

Figure F-2.21: Spacing Effect on Forces in Joint

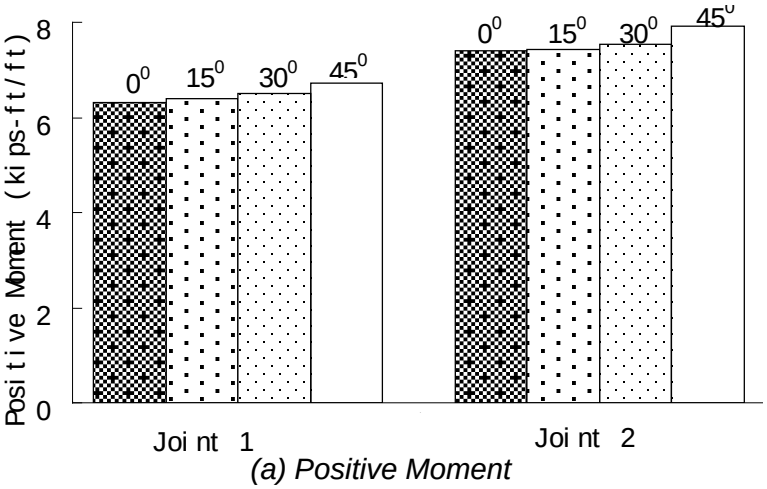

(a) Positive Moment

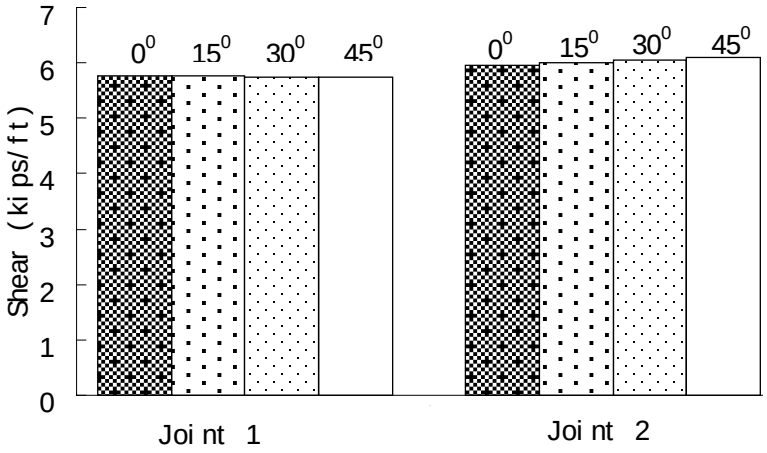

(b) Shear

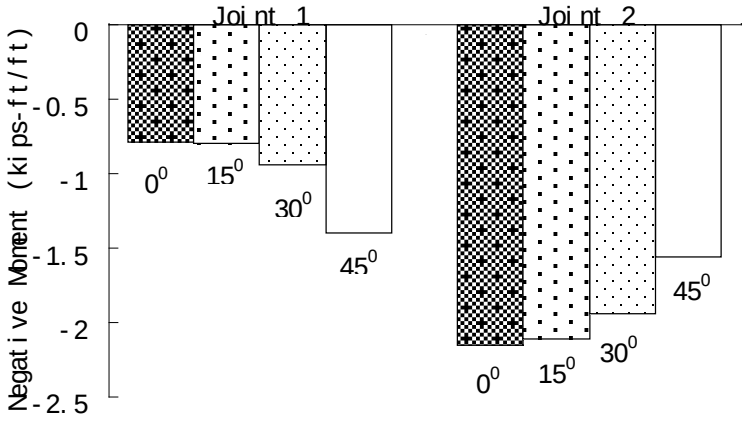

(c) Negative Moment

Figure F-2.22: Skewness Effect on Forces in Joint

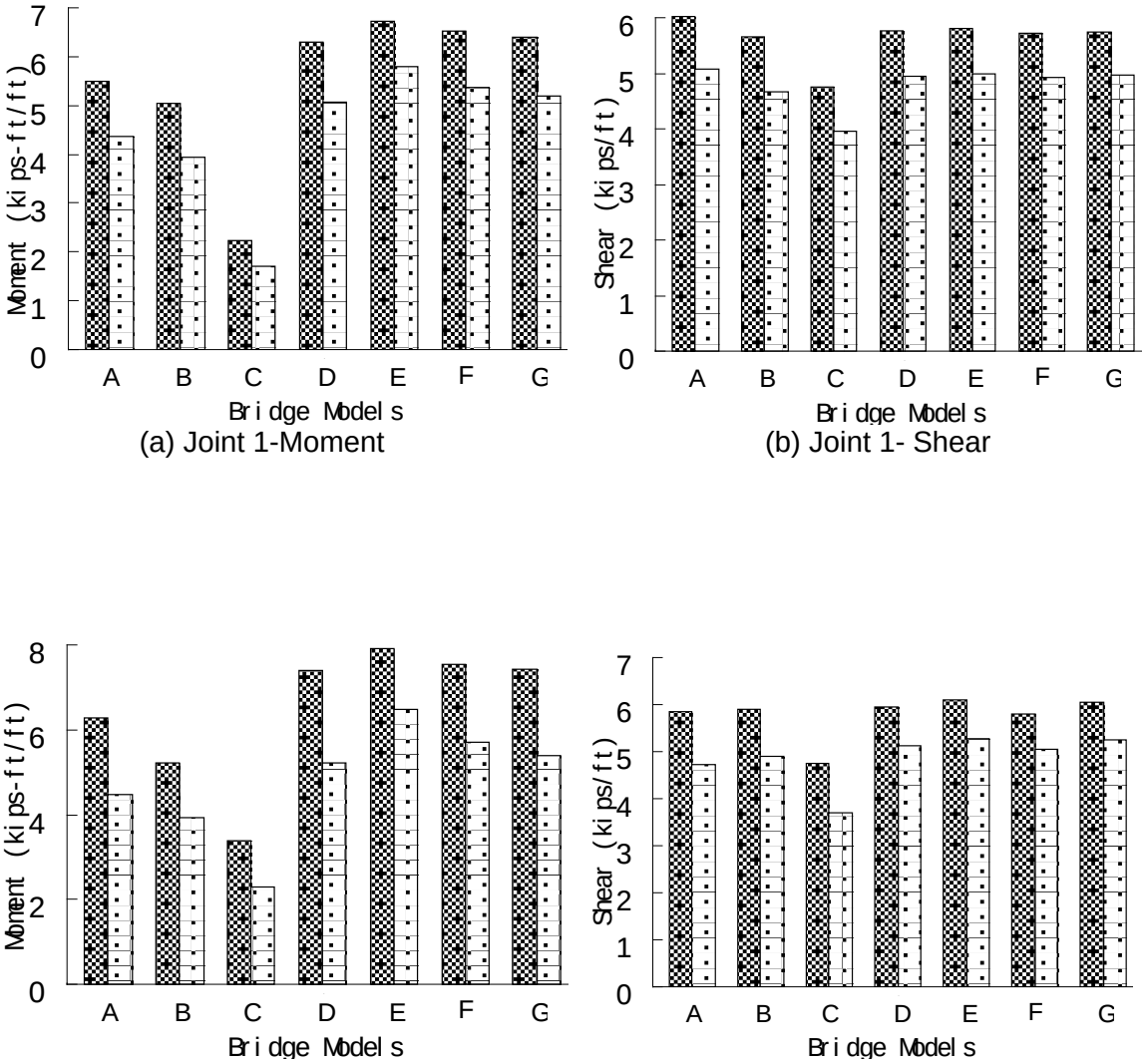

(a) Joint 1-Moment (b) Joint 1- Shear

(c) Joint 2-Moment (d) Joint 2-Shear

Figure F-2.23: Number of Loaded Lane Effect

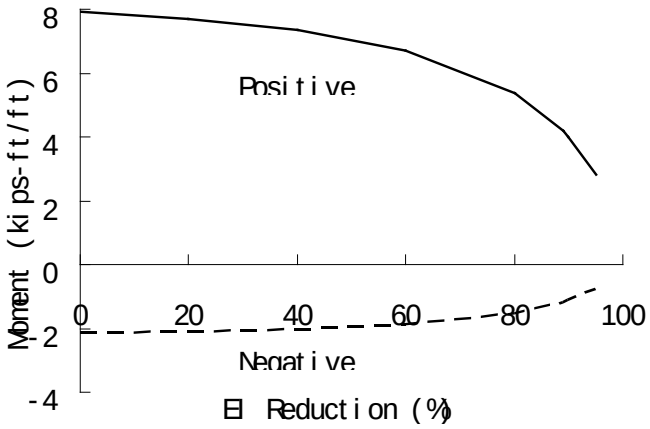

(a) Moment

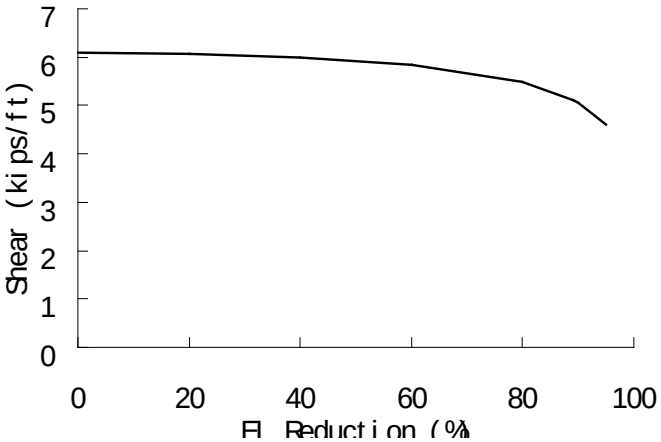

(b) Shear

Figure F-2.24: Impact of Cracking on Forces

CHAPTER 3

IMPROVED LONGITUDINAL JOINT DETAILS IN DECKED BULB TEES FOR ACCELERATED BRIDGE CONSTRUCTION: FATIGUE EVALUATION

3.1 Introduction

Chapter 1 presents the results of a study that assesses potential alternate joint details for decked bulb tee (DBT) bridges based on constructability, followed by testing of selected details. Seven reinforced concrete beam specimens connected with either lapped headed reinforcement or lapped welded wire reinforcement (WWR) were tested along with another specimen reinforced by continuous bars for comparison. Based on that study, a headed bar detail with a 6 in. lap length was recommended for additional testing to further investigate replacing the current welded steel connector detail. This chapter describes the test program and presents results of this additional testing.

In this study, four full-scale slabs connected by a headed reinforcement detail utilizing a 6 in. lap length were fabricated and tested. The analytical parametric study was conducted to provide the database of maximum forces in the longitudinal joint in Chapter 2. These maximum forces are used to determine the loading demand necessary in the slab testing due to the service live load. Static and fatigue tests under four-point pure-flexural loading, as well as three-point flexural-shear loading, were conducted. Test results were evaluated based on flexural capacity, curvature behavior, cracking, deflection and steel strain. Based on these test results, the improved longitudinal joint detail is a viable connection system to transfer the forces between the adjacent DBT girders.

3.2 Experimental Program

3.2.1 Slab Dimension

A total of four slabs with the same dimensions were fabricated for the static and fatigue testing. Each specimen consisted of two panels as shown in Figure F-3.1. Each panel was 72 in. wide, 64 in. long and 6 in. deep. The female-to-female shear key was provided at the vertical edge of both ends in the specimen length direction. This allowed each slab to be used for two tests.

3.2.2 Reinforcement Layout and Strain Gage Instrumentation

Figure F-3.2 displays the reinforcement layout used in the slab specimen. There are five layers of reinforcement in each panel along the specimen depth direction with a 2 in. cover at the top and 1 in. cover at the bottom. The top two layers and bottom two layers of reinforcement simulate the deck reinforcement in the top flange of DBT girders. The specification of this reinforcement is as follows: #5 bar spaced at 6 in. at the top in the slab length direction; #4 bar spaced at 6 in. at the bottom in the slab length direction; #5 distribution reinforcement spaced at 8 in. at the top in the slab width direction; #4 distribution reinforcement spaced at 8 in. at the bottom in the slab width direction. The middle layer of the reinforcement consists of epoxy coated headed bars which project out of the panel to splice with the headed bars in the adjacent panel in the longitudinal joint. All the epoxy coated reinforcement has yielding stress of 60 ksi. The spacing of the headed bar is 6 in. and the splice length (inside head to inside head) is also 6 in. One longitudinal headed bar was placed along the center line of the joint both above and below the spliced headed reinforcement. The headed reinforcement is a #5 bar with a standard 2 in. diameter circular friction welded head. The head thickness is 0.5 in.

The headed reinforcement around the joint zone was instrumented with strain gages to gain a better understanding of the behavior of the slab connected by the longitudinal joint. Figure F-3.3 depicts the strain gauge layout in the slab for the four-point pure-flexure test (the left figure in Figure F-3.3) and the three-point flexure-shear test (the right figure in Figure F-3.3).

There are seven headed bars with installed strain gages. These seven headed bars are numbered from the edge of the slab (number 1) to the middle (number 7) along the slab width direction. Three strain gages are installed on each of the headed bars, which are labeled beginning at the head. For example, strain gage “3-2” means the strain gage #2 on the headed bar #3. Strain gages #1 and #2 on each headed bar intend to measure the strain in the joint. They are positioned 3 in. and 6 in. away from the inside face of the head respectively. Strain gages #3 intends to measure the strain close to the loading zone. They are positioned 21 in. away in the four-point pure-bending slab and 11 in. away in the three-point flexure-shear slab. Three strain gauges are also placed at the end, quarter, and middle of the longitudinal headed bar,

which are labeled as L-1, L-2 and L-3 respectively.

3.2.3 Panel Fabrication

The concrete panels were fabricated locally at Ross Prestressed Concrete Inc. in Knoxville, TN. Figure F-3.4-a shows the panel reinforcement before placement of the concrete. The two ends of the wood form, in the length direction, were slotted at a spacing of 6 in. to fix the headed reinforcement in place. Foam wedges were used to form the configuration of the shear key at the vertical edge of the panel. The design concrete compressive strength at 28 days was 4000 psi. A total of 18 concrete cylinders were made with the pouring of panels (Figure F-3.4-b).

3.2.4 Joint Surface Preparation

The surfaces of the shear key were sandblasted to prepare the joint for the closure pour. The purpose of the surface preparation is to remove all contaminants that can interfere with adhesion and to develop a surface roughness to promote a mechanical bond between the grout and base concrete. After the removal of the deteriorated concrete, proper preparation should provide a dry, clean and sound surface offering a sufficient profile to achieve adequate adhesion. There are many methods of surface preparation such as chemical cleaning, mechanical cleaning and blasting cleaning. Sandblasting uses compressed air to eject the high speed stream of sand onto the surface which needs to be prepared. This method is very effective to process the surface of precast members under industrial conditions. Black Beauty 2050 sand was chosen for sandblasting to prepare the surface in this study. The profiles of the surface before and after sandblasting are shown in Figure F-3.5.

3.2.5 Closure-Pour Materials

The longitudinal joint, which is filled with closure-pour materials connecting the top flange of the adjacent DBT girders, is considered to be the structural element of the bridge deck. It is important for the selected closure-pour material to reach its design compressive strength in a relatively short time for the purpose of accelerated bridge construction. In this study, it was decided to use two grout materials, SET 45 HW (SET) and EUCO-SPEED MP (EUCO), for trial testing (Zhu and Ma 2008). Both of these materials are magnesium phosphate-based materials. The directions for use and

technical data for these two materials were provided. However, all the technical information is based on the grout without aggregate extension. In this study, the compressive strength of the grout without extension and the grout with 60% extension were compared according to ASTM C 109/C 109M – 05 and ASTM C 39/C 39M-05, respectively (Figure F-3.6). The uniform-sized sound 0.25 in. - 0.5 in. round pea gravel, which was thoroughly washed and dried, was used to extend the grouts. The pea gravel was tested with 10% HCL to confirm that it was not calcareous.

The compressive strengths of the grout SET and EUCO were tested and presented in Table F-3.1. It can be seen that both the grout SET and EUCO without extension or with 60% extension reached at least 5570 psi compressive strength within one day. There were no significant differences in terms of setting time between grout without extension and grout with extension. For grout SET, the initial setting time and final setting time were 15-20 minutes and 45-60 minutes, respectively. For grout EUCO, the initial setting time and final setting time were 6-10 minutes and 15-20 minutes, respectively. Since the setting time of grout EUCO is short for the field application, the grout SET was selected in this study.

3.2.6 Testing Plan and Setup

A totally of four slab specimens were made. Each slab specimen consists of two concrete panels connected with an overlapping headed reinforcement and the SET 45 HW extended grout. During the test setup, each panel was placed on the steel I-beam, which was leveled to ensure that the two panels were on the same plane. At the joint zone, the two panels were positioned to satisfy the overlapped length and the spacing of the headed reinforcement (Figure F-3.7-a). The wood form was provided at the bottom and at both ends of the joint to prevent leakage when grouting. After grouting, the slab specimen consisting of 2 panels connected by the joint was ready for testing (Figure F-3.7-b). Since each panel had headed bars and shear keys along two edges, each set of two panels was used to fabricate two test specimens. After completion of testing the first joint, the panels were separated, and then another joint was reassembled by the other two edges to create the second test specimen.

Four slab specimens were tested under different parameters: 1) flexure static (F-S) test; 2) flexure-shear static (FS-S) test; 3) flexure fatigue (F-F) test, and 4) flexure-shear

fatigue (FS-F) test. Figure F-3.8 shows the testing setup and the linear voltage displacement transducers (LVDT) instrumentation for each test. All slab specimens were simply supported with a 72 in. span and the joint zone located in the center of the span. The neoprene pad, with two layers of plastic sheets placed between the wood support and slab bottom, was used at one end; only the neoprene pad was used at the other end. The 10 in. by 20 in. neoprene pad and steel plate were used to simulate the truck tire contact area and the pressure loading. LVDTs were employed to measure the specimen deflection, settlement and curvature. Four LVDTs (Nos. “4”, “5”, “6” and “7” in Figure 3.8) were placed in the joint zone of the slab. LVDTs “4”, “6” and “7” were placed along the centerline of the joint while LVDT “5” was placed at the panel edge off the interface of the joint. In this way, the relative deflection between the two sides of the joint interface can be measured. LVDTs “1”, “2”, “3” and LVDTs “8”, “9”, “10” measured the settlements, if any, of two supports. Two LVDTs were used to measure the average curvature of the joint zone. The DEMEC points and the DEMEC mechanical strain gauge were used to measure the width of crack opening at the joint interface.

The F-S specimen was loaded with two equal loads spaced at 12 in. about the center of the span using Material Test System (MTS) rams until the specimen failed. The joint zone experienced the maximum constant moment without shear. The FS-S specimen was loaded with one load located at 12 in. about the center of the span until the specimen failed. The joint zone experienced the combination of moment and shear. The F-F specimen was loaded with two equal loads spaced at 12 in. about the center of the span. Figure F-3.9 shows the apparatus to apply the fatigue forces to the joint zone of the specimen.

One side of the swivel rod end was screwed to the actuator tightly while the other side was bolted to the spread tube at midspan by 4 steel rods. The spread tube was soldered to two steel hinges, which were located 12 in. away from the middle of the spread tube. The other end of each steel hinge was soldered to the 10 in. by 20 in. steel plate. The use of steel hinges between the spread tube and the steel plates was to eliminate the extra moment applied on the slab specimen produced by the bending of the spread tube. The steel plate and neoprene pad at the bottom of the slab were bolted to the correspondent top steel plate and neoprene pad through the slab by 4 steel rods, which apply the fatigue forces on the slab. The boundary condition was provided by the

steel girder below the slab and by the steel girder above the slab. The two steel girders at each support-end (one below the slab and another one above the slab) were connected by bolts, and the steel girder below the slab was fixed to the strong floor (Figure F-3.9). The FS-F specimen was loaded with two loads spaced at 12 in. about the center of the span. Two loads (P1 and P2) were applied out-of-phase on each side of the joint during the fatigue test. For example, when “P1” reached the maximum force, “P2” was zero. The joint zone experienced the fatigue shear in reversing directions.

The compressive strength of concrete panel $f_c^{'}$ and the compressive strength of grouted joint $f_{cj}^{'}$ at the time of testing for each specimen are shown in Table F-3.2.

3.2.7 Fatigue Loading Determination

FE models of the test specimens (Figure F-3.10) were developed to determine the loadings in fatigue tests and produce the maximum moment or the maximum shear in the joint zone corresponding to the results from previous parametric studies discussed earlier. Figure 3.10-b shows the moment distribution for the model loaded at one pad to produce an average moment along the joint of 10.0 kip-ft/ft. Figure 3.10-c shows the shear distribution and average shear for the same loading. These plots indicate that the moment does not vary significantly from the average or nominal moment as compared to the shear which varies significantly along the joint length. The ratio of average or nominal shear to the peak or maximum shear near the pad load is 3.33/7.3 = 0.46. This ratio was used to determine the pad load in the test specimens required to produce the shear loads resulting from the live load study in Subtask 6.2-A2.

For the F-F specimen, a static loading was applied in several increments up to 22.7 kips in order to produce the maximum positive moment of 7.922 kips-ft per unit length in the joint and to crack the joint. After unloading to zero, a negative static load of -6.2 kips, corresponding to a negative moment of -2.152 kips-ft per unit length, was applied and unloaded to zero.

During the fatigue test, the applied load was cycled between 6 kips corresponding to a positive moment of 2.143 kips-ft per unit length and -1.2 kips corresponding to a negative moment of -0.453 kips-ft per unit length for a total of 2 million cycles at a

frequency of 4Hz. At the end of 0.5, 1.0, 1.5, and 2.0 million cycles, an interim static loading test was conducted. During each of these static tests, the static loading was applied in several increments up to 11.3 kips corresponding to a positive moment of 4.001 kips-ft per unit length after cracking. After unloading to zero, a negative static load of -3.3 kips corresponding to a negative moment of -1.137 kips-ft per unit length after cracking was applied and unloaded to zero. Finally, the slab specimen was loaded to failure.

Figure F-3.11 shows the first few cycles of the fatigue loading history for the FS-F specimen. As discussed earlier, fatigue loads “P1” and “P2” were applied by the two MTS rams having the same frequency but out-of-phase. The slab was under the fatigue loading with the magnitude of “P1+P2” as shown in Figure F-3.11.

The peak P1 is 27.1 kips and the peak P2 is -18.9 kips. Based on the position of the pad load, the nominal shear in the joint at the centerline of the specimen is 1/3 the pad load. Therefore the nominal shear along the length of the joint at the center of the joint associated with P1 is 1.507 kips/ft and the nominal shear at the center of the joint associated with P2 is -1.05 kips/ft. Considering that the ratio of average or nominal shear along the length of the joint to the peak or maximum shear near the pad load is 3.33/7.3 = 0.46, as determined from the finite element analyses discussed above, the maximum shear in the joint associated with P1 is 3.303 kips/ft. This shear is approximately 17% higher than the target shear of 2.826 kips/ft. This target shear is the combination of the fatigue shear of 2.326 kips/ft defined in Section 2.5.10 plus camber leveling shear of 0.5 kips/ft determined from Subtask 6.2-A1.

Using the same considerations, the maximum shear in the joint associated with P2 is - 2.302 kips/ft.

Using the same consideration with the “Average” value of “P1+P2” of 4.10 kips shown in Figure F-3.11 indicates that the camber leveling shear of 0.5 kips/ft was applied at the middle of the joint zone all the time with the fatigue shear oscillating at approximately ± 2.8 kips above and below this average. The target oscillating shear was ± 2.326 kips/ft. Therefore, the loading applied to the FS-F specimen was conservatively high.

Similar to the F-F specimen, an interim static loading test (applying “P1” and “P2” separately) was conducted at the end of 0.5, 1.0, 1.5, and 2.0 million cycles. Again, the specimen was loaded to failure after the fatigue cycles. Also, it should be noted that, due to the shear spans used in the FS-S and FS-F tests, the maximum moment accompanying the maximum shear in the test specimens was higher than the maximum moment accompanying the maximum shear in the analytical models. Therefore, the FS-S and FS-F tests are considered conservative.

Section 2.5.10 of this appendix also includes a discussion of revisions accepted by AASHTO Bridge Committee, Technical Committees T-5 Loads, and T-14 Steel subsequent to panel tests. The revisions consist of inclusion of two levels of fatigue load in Table 3.4.1-1. These are Fatigue I and Fatigue II. Fatigue II retains the current Load Factor of 0.75 and is to be applied to represent an effective stress range caused by the fatigue truck with respect to a large but finite number of stress range cycles. Fatigue I has a Load Factor of 1.5 (or 2 times 0.75) and is to be applied to the stress range caused by the fatigue truck with respect to an infinite number of stress range cycles.

Section 2.5.10 presents factored fatigue loads using the revised Load Factor of 1.5 for Fatigue I of 3.419 kips-ft/ft, -0.568 kips-ft/ft and 4.382 kips/ft for maximum positive moment, negative moment and shear respectively. In addition, the maximum factored fatigue moment would be coincidental with the maximum shear of 4.382 kips/ft is 2.201 kips-ft/ft.

For the F-F test, the Fatigue I moment of 3.419 kips-ft/ft is 60% higher than the maximum 2.143 kips-ft/ft used in the test. Therefore, the F-F test is not adequate to demonstrate infinite life per the accepted AASHTO revisions. For the FS-F test the Fatigue I shear of 4.382 kips/ft is 33% higher than the maximum shear of 3.303 kips//ft used in the test. However, during the FS-F test, moment was cycled between 3.150 and 4.521 kips-ft/ft while the shear was reversed. These moments are 43% and 105% higher than the maximum of 2.201 kips-ft/ft. that would be coincidental with the maximum shear. Therefore, although the shear was low for Fatigue I loading, the flexure was very high. Therefore, in the opinion of the researchers, the FS-F test was a very robust test to demonstrate the viability of the improved longitudinal joint detail.

3.2.8 Moment Capacity and Curvature

Figure F-3.12 shows the curvature-fatigue cycle curves (C-N) for the fatigue tests. The curvature represents the average curvature of the joint zone after a different number of fatigue cycles under a specific loading. For example, the curve labeled with “M=0.5 k-ft/ft” in Figure F-3.12-(a) represents the change of the curvature of the joint zone with numbers of fatigue cycles, which was measured at the loading level corresponding to a moment of 0.5 kips-ft/ft of the joint for the F-F specimen during each of the interim static load tests.

As shown in Figure F-3.12, the curvature increased with the increasing of the joint moment for all specimens. Comparing among different joint moment levels, the impact of fatigue on the curvature is about the same for all specimens. It appears that fatigue loading has no effect on the curvature for the F-F specimen while it increases the curvature for the FS-F specimen. For the FS-F specimen under “P1”, the first set of one-million cycles increases the curvature more than the second set of one-million cycles. For the FS-F specimen under “P2”, however, the first set of 1.5-million cycles have more impact. Damage accumulations due to fatigue loading cycles cease after that point. In general, there is no significant influence of fatigue cycles on the curvature after the first one-million to 1.5-million cycles.

Figure F-3.13 compares the moment-curvature curves between the specimens (F-F and FS-F) subjected to fatigue loading after 2,000,000 cycles with the specimens (F-S and FS-S) subjected to static loading without fatigue cycles. The y axis labeling “Moment/Joint Length” represents the distribution moment along the joint, which the applied moment divided by the length of the joint. Both the F-S specimen and FS-S specimen were loaded with un-cracked section while the F-F specimen and FS-F specimen were loaded with cracked section after 2,000,000 fatigue cycles. As a result, the slope of the curve (stiffness of the slab) for F-S and FS-S is steeper (larger) than the F-F and FS-F at the beginning of the load. After the applied moment exceeds the cracking moment level, the slopes of the two curves are about the same, indicating that the fatigue cycles had no significant effect on the curvature development, as discussed earlier. The Service Load shown in Figure F-3.13-(a) is the maximum positive calculated moment after cracking of 4.001 kip-ft/ft reported in Section 2.6

As shown in Figure F-3.13-(a), when the joint moment reaches about 10.4 kips-ft per unit length, the reinforcement in both specimens (F-F and F-S) is yielded, indicating that fatigue cycles have no significant influence on the yielding load. After yielding of the reinforcement, the F-S specimen shows a larger curvature development than the F-F specimen. The maximum curvature of the F-F specimen is about 50% of the maximum curvature of the F-S specimen. At service loading, the two specimens have essentially the same curvature.

Unfortunately, this kind of comparison cannot be made for flexure-shear tests in Figure F-3.13-(b) because the LVDTs measuring curvature in the FS-S specimen were removed before specimen failure; therefore, the maximum curvature cannot be reported. As shown in Figure F-3.13-(b), for the range of loading for which curvature was measured, there is no obvious flat part of the two curves. The Service Load shown in Figure F-3.13-(b) is the corresponding moment (CM) occurring with the maximum shear is 2.887 kips-ft/ft. after cracking reported in Section 2.5.9

3.2.9 Load Deflection Relationships

Figure F-3.14 compares the load-deflection curves between the fatigue slab after 2,000,000 cycles and the slab under static loading without fatigue cycles. The y axis labeling “Load/Joint Length” represents the nominal distributed load along the specimen, which is the applied load, P, divided by the length of the specimen. Note that the load P is the load applied to one loading pad as shown in Figure F-3.8.

The beam theory (labeled “Theoretical Analysis” in Figure F-3.14) was utilized to predict a load-deflection curve consisting of three parts: before cracking, after cracking until yielding of the reinforcement, and the stage of plastic hinge development at midspan after reinforcement yielding. The deformation capacity of the theoretical analysis was based on crack section property for conservative purpose. Similar to Figure F-3.13, the slope of the curve for F-S and FS-S is steeper than the slope of the curve for F-F and FS-F from the initial loading until cracking load is reached. After cracking, the development of the deflection between static slab and the fatigue slab is the same, and the slopes of the two curves are about the same. This indicates that the fatigue cycles have no significant effect on the deflection in this stage.

The Service Load shown in Figure F-3.14-(a) is the Load/Joint Length of 1.894 kips/ft which corresponds with the maximum positive calculated moment of 4.001 kips-ft/ft after cracking reported in Section 2.6. The Service Load shown in Figure F-3.14-(b) is the Load/Joint Length of 2.306 kips/ft. This Service Load /Joint Length corresponds with the maximum calculated shear near the pad load of 5.056 kips/ft based on analyses using the finite element model shown in Figure F-3.10 and discussed under Subtask 6.2 A3.

After yielding of the reinforcement, the plastic hinge is developed fully at the joint zone of the F-S specimen with large deformation until failure, while the F-F specimen failed without significant development of the plastic hinge. The F-S specimen has 113% load capacity and 112% deformation capacity of the theoretical calculations while the F-F specimen has 101% and 82%, respectively. Under the flexure loading (F-S and F-F), the fatigue cycles have impact on the slab ductility and the development of the plastic hinge after the yielding of the reinforcement. The fatigue cycles prevent the development of the plastic hinge after the yielding of the reinforcement and reduce the ductility significantly.

Under service load, the deflection of the F-F specimen is larger than the F-S specimen. The deflection difference between the F-S and F-F specimen is caused by the un-cracked section property and cracked section property for each slab at the initial loading.

Under the flexure-shear loading (Figure F-3.14-b) both FS-S and FS-F reached the maximum load near the load capacity of the theoretical analysis. Prior to failure, the maximum loads in FS-S and FS-F was 11.2 kips-ft per unit length and 11.6 kips-ft per unit length respectively. The fatigue cycles have no influence on the curvature development before yielding of the reinforcement and the yielding load. However, the deformation capacity in FS-S and FS-F were 77% and 70% of the theoretical value due to the shear failure with limited plastic hinge development.

Figure F-3.15 shows the relative displacement (RD) between the two sides of the joint interface versus fatigue-cycle (N) curves for FS-F under specific loading levels during interim static load tests. For the F-F specimen, the relative displacement of the joint interface is zero under service live load. Figure F-3.15-(a) and Figure F- 3.15-(b)

are the curves for the FS-F specimen under “P1” and “P2”, respectively.

From Figure F-3.15, it can be seen that the relative displacement of the joint interface is dependent upon the applied load. The relative displacement increases with the increasing of the applied load. However, under the same loading level, the curve is very flat. The relative displacement after different fatigue cycles is the same under the same load, so there is no influence of fatigue cycles on the relative displacement under service live load.

3.2.10 Load Crack Width Relationships

During the tests, the cracks at the interface between the grouted joint and the concrete panel were observed and crack widths were measured. The two cracks marked as “14” and “12” shown in Figure F-3.16 are labeled as either “Crack 1” with larger crack width or “Crack 2” with smaller crack width.

Figure F-3.17 (a) and (b) show the load-crack width relationship for the F-S specimen and the FS-S specimen, respectively. The Service Load shown in Figure F-3.17-(a) is the Load/Joint Length of 1.894 kips/ft which corresponds with the maximum positive calculated moment of 4.001 kips-ft/ft after cracking reported in Section 2.6. The Service Load shown in Figure F-3.17-(b) is the Load/Joint Length of 2.306 kips/ft. This Service Load /Joint Length corresponds with the maximum calculated shear near the pad load of 5.056 kips/ft based on analyses using the finite element model shown in Figure F-3.10 and discussed under Subtask 6.2 A3.

The crack width was measured by DEMEC mechanical strain gauges. From Figure F-3.17-(a), it can be seen that the width of the two cracks is developed at a different rate with the increasing of the loading. The width of “Crack 1” grows faster than the width of “Crack 2” due to the reinforcement yielding that is developed at the joint interface of the “Crack 1” location. The crack widths at the Service Load level are relatively small.

In Figure F-3.17-(b), the two cracks are widened at the same rate with the increasing of the loading when the load reaches about 7.4 kips per unit length, the width of “Crack 2” decreases suddenly by 23% due to the flexural-shear crack that developed

across the joint zone, as shown in Figure F-3.18. After the formation of the flexural-shear crack, the two cracks continue to develop with the same rate until the specimen fails. The crack widths at the Service Load level of are relatively small.

Figure F-3.19 shows the crack width-fatigue cycle curve (CW-N) for the fatigue tests representing the maximum crack width at the joint interface after a various number of fatigue cycles under specified loadings.

From Figure F-3.19, it can be seen that the width of the crack at the joint interface is dependent upon the applied load. The crack width increases with the increasing of the loading, however, the curve is very flat under the same loading. So the influence of fatigue cycles on the crack width of the joint interface is negligible under service live load.

3.2.11 Moment-Strain Curve

Figure F-3.20 shows the strain-fatigue cycle curves (S-N) for the fatigue tests representing the reinforcement strain in the joint after a various number of fatigue cycles under service live load. The strain gauge number and the loading are shown in the figure. For example, “2-1” represents the strain gauge #1 at the headed bar #2 and “M = 3 k-ft/ft” means the joint of the slab is subjected to a joint moment of 3 kips-ft per unit length.

From the Figure F-3.20, it can be seen that all the curves are again flat and the variation of the reinforcement strain after different fatigue cycles is not significant. All reinforcement under the loading zone and the longitudinal headed bar experience a very low strain compared with the reinforcement in the joint. Figure F-3.21 shows the moment-strain curves representing the strain values in the joint zone for each slab, which show the similar trends as discussed earlier.

3.2.12 Failure of Specimen

As shown in Figure F-3.22-(a), the failure mode of the F-S specimen is a typical flexure failure. After the headed reinforcement yields, both the concrete in the panel and the grout in the joint crushes. The grout under the reinforcement spalls off along the joint due to the bending of the spliced headed bars. The slab specimen experiences a

ductile failure and spliced headed bars hold the crushed concrete to prevent the separation of the panels.

The failure mode of the FS-S specimen is a typical flexural-shear failure. Figure F-3.22-(b) shows that the shear crack crosses the joint zone when the slab fails. It can be seen that the shear crack is widened from the lower part of the joint interface. Then, it crosses the whole grouted joint and reaches to the top part of the joint interface.

The failure mode of the F-F specimen is a flexure failure. However, by comparing with the F-S specimen, there is little development of plastic hinge at the interface of the joint (Figure F-3.22-c). This confirms that the fatigue cycles inhibit the development of the plastic hinge at the joint zone. The grout in the joint zone is crushed at top. There is a large crack along the interface of the joint at the bottom of the slab. The grout under the reinforcement does not spall off along the joint.

The failure mode of the FS-F specimen is a shear failure. Figure F-3.22-(d) shows the shear cracks in the joint zone when the slab fails. It can be seen that the shear crack is developed from the lower part of the joint interface, then crosses the concrete panel and reaches to the top concrete. It can be seen that there is no spalling along the joint.

3.4 Conclusions

Based on the parametric study and the experimental program, the following conclusions are made:

1. The fatigue loading has little influence on the structure behavior including average curvature of the joint, deflection at midspan, relative displacement of the joint interface as well as reinforcement strain under service live load.

2. The fatigue loading has no effect on the loading capacity of the structure. The slab, after 2,000,000 fatigue cycles, has the same loading capacity as the slab under static load test.

3. The fatigue loading inhibits the development of the plastic hinge under pure-bending load. The fatigue cycles reduce the ductility capacity

significantly.

4. Based on these tests, the improved longitudinal joint detail is a viable connection system to transfer the forces between the adjacent decked bulb tee (DBT) girders.

Table F-3.1. Compressive Strength of Grouts (psi)

Age	Without Extension				With 60% Extension	
	SET		EUCO		SET	EUCO
	Test	Anticipate	Test	Anticipate	Test	Test
3 hour	2319	3000				
1 day	6335	6000	5629	6000	5669	8527
3 day	7350	7000	6262	6500	5963	8626
7 day	8286		6864	7000	5990	8765

Table F-3.2. Compressive Strength of Concrete Panel and Grouted Joint

Specimen	Panel (psi)	Joint (psi)
F-S	7495	5473
FS-S	7495	7295
F-F	5491	7021
FS-F	5491	5829

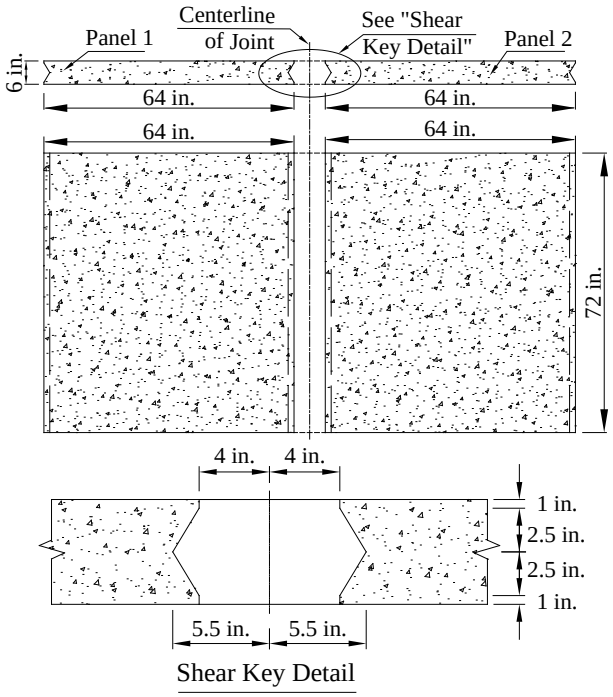

Figure F-3.1. Dimension of Slab Specimen

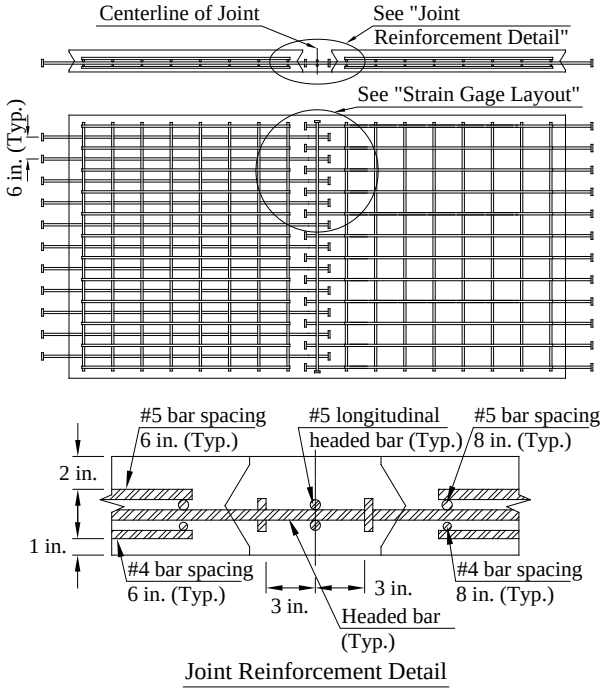

Figure F-3.2. Reinforcement Layout in Slab

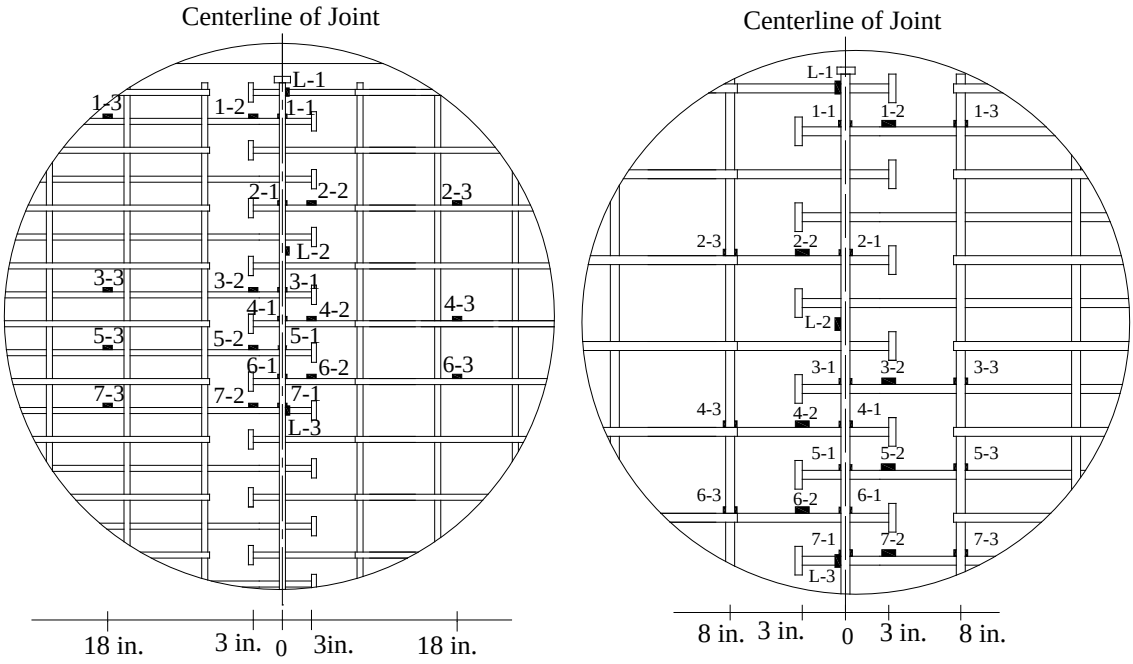

Figure F-3.3. Strain Gage Layout

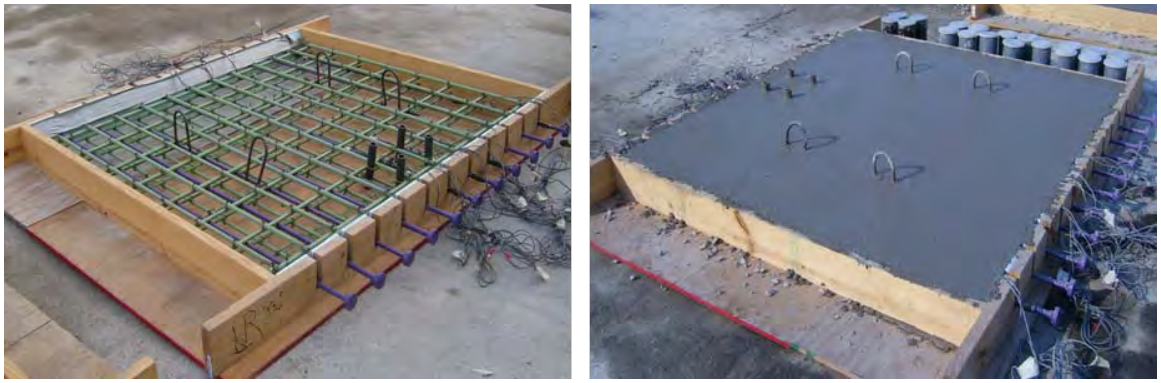

(a): Before Pouring (b): After Pouring

Figure F-3.4. Panel Fabrication

(a): Before Sandblasting *(b): After Sandblasting*

Figure F-3.5. Profile of Joint Surface

(a): Without Extension *(b): With 60% Extension*

Figure F-3.6. Grout Specimen

(a): Before Grouting *(b): After Grouting*

Figure F-3.7. Slab Specimen

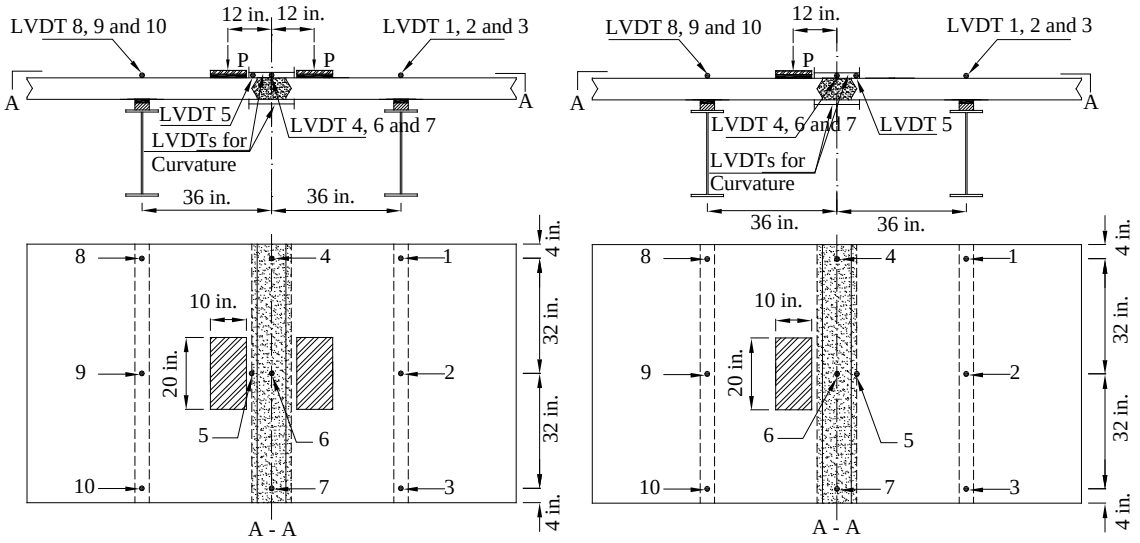

(a) Flexure Static (F-S) Test

(b) Flexure-Shear Static (FS-S) Test

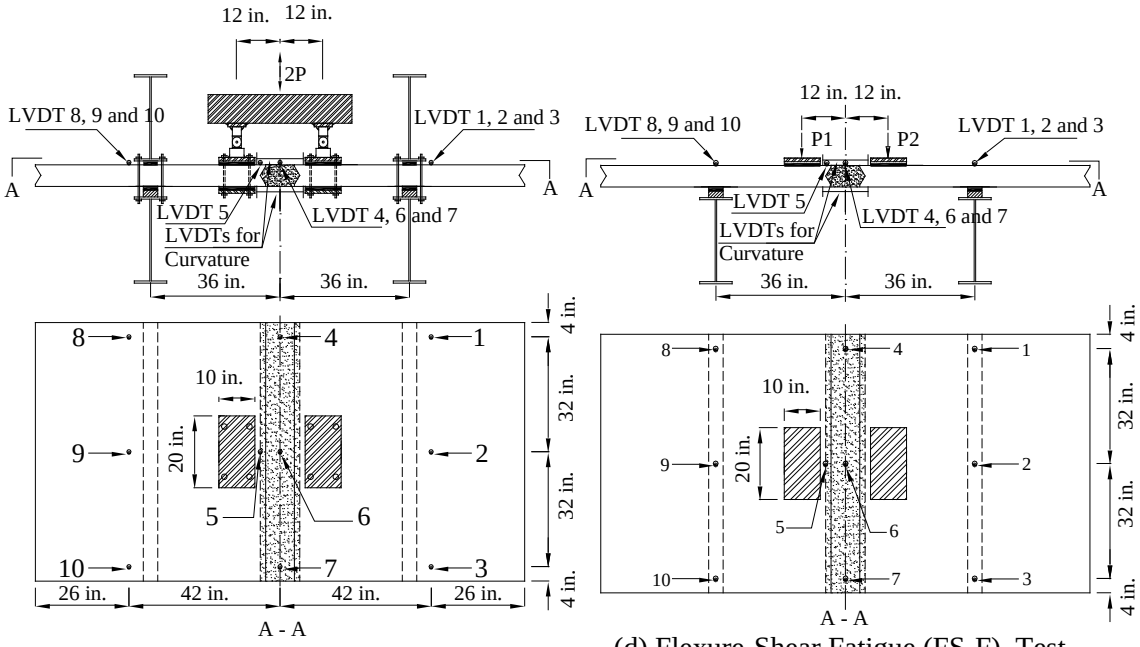

(c) Flexure Fatigue (F-F) Test

(d) Flexure-Shear Fatigue (FS-F) Test

Figure F-3.8. Testing Setup

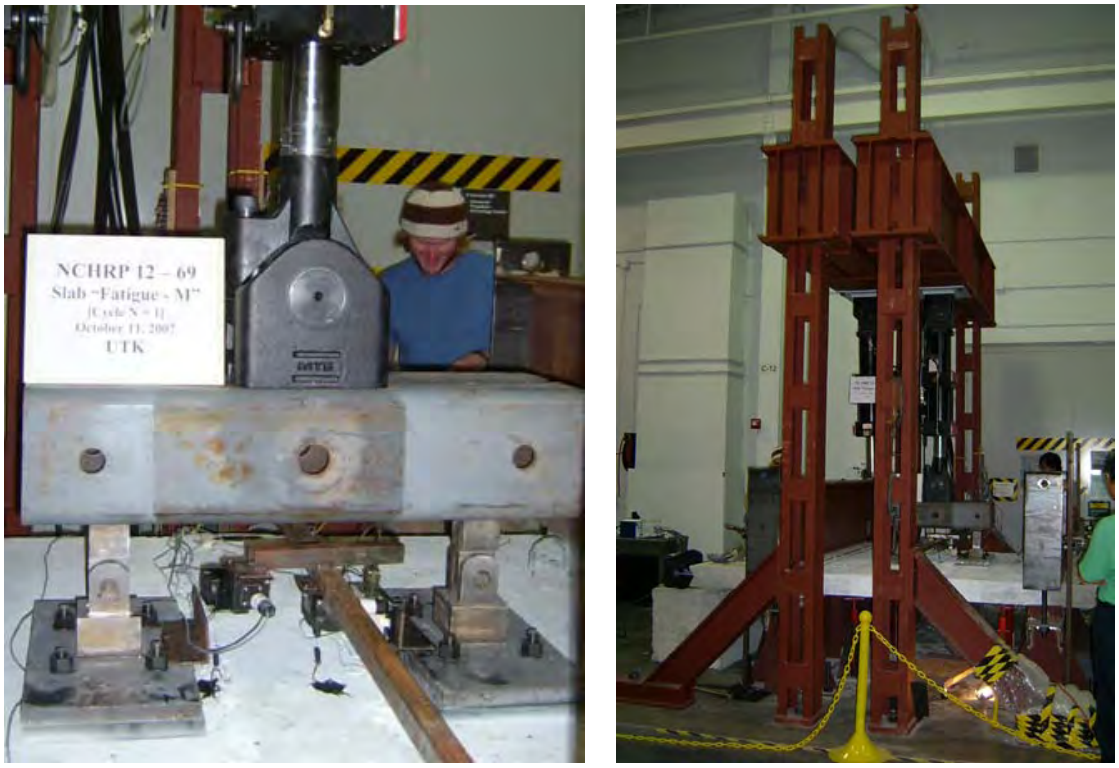

Figure F-3.9. Apparatus Applying Fatigue Forces

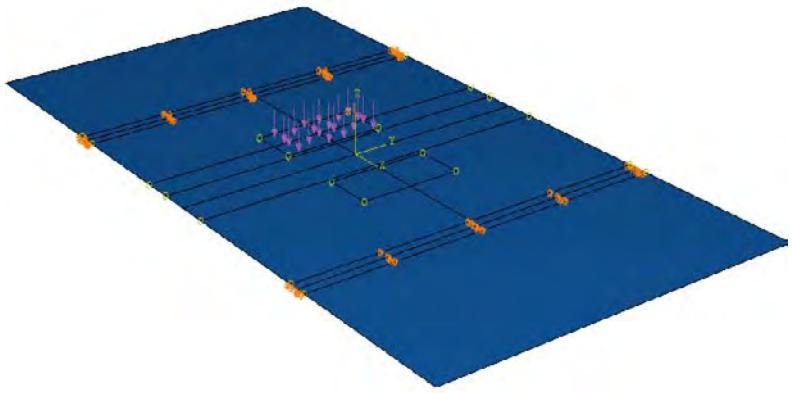

(a) Static Shear Test (FE Model)

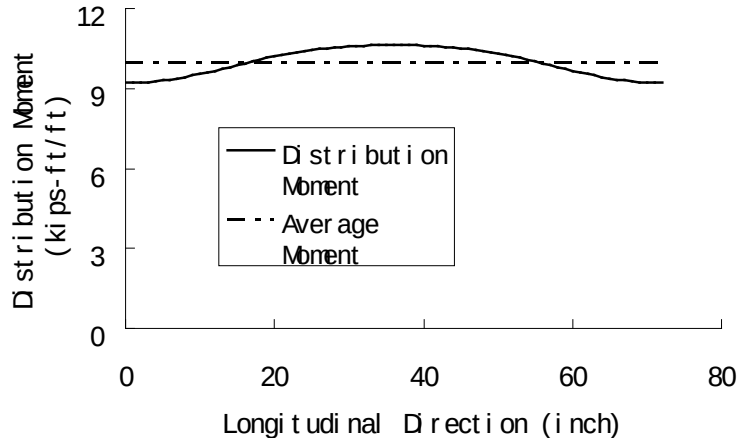

(b) Moment Distribution along Joint

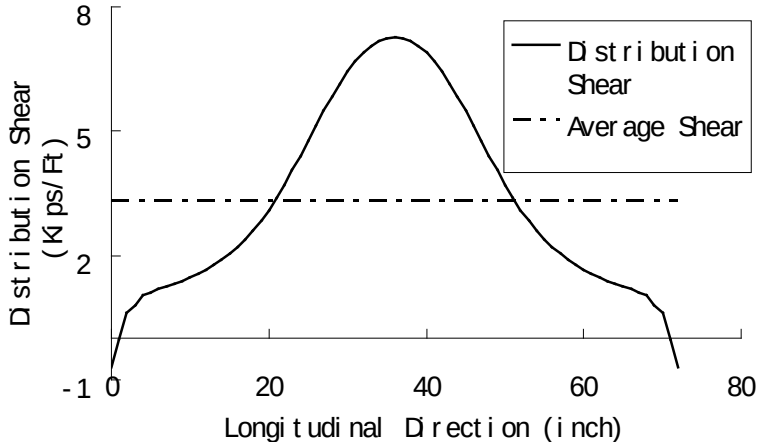

(c) Distribution and Average Shear along Joint

Figure F-3.10 FE Model for Load Determination

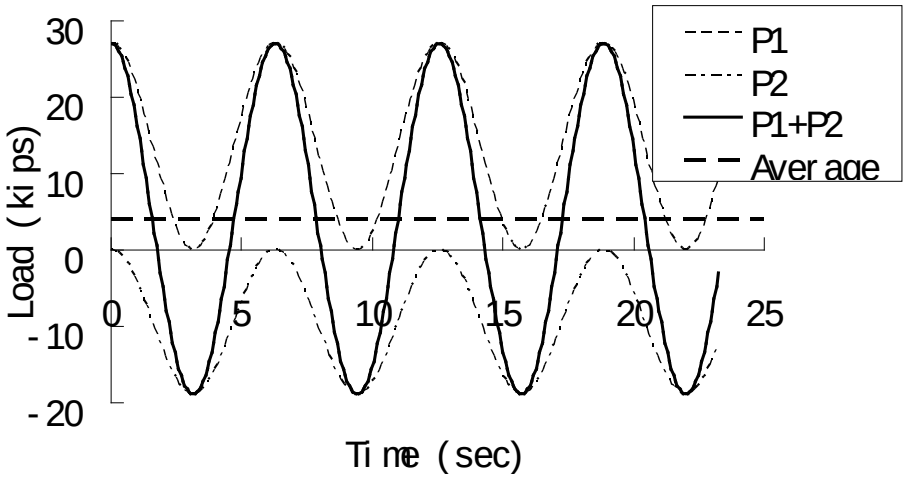

Figure F-3.11: History of Fatigue Loading

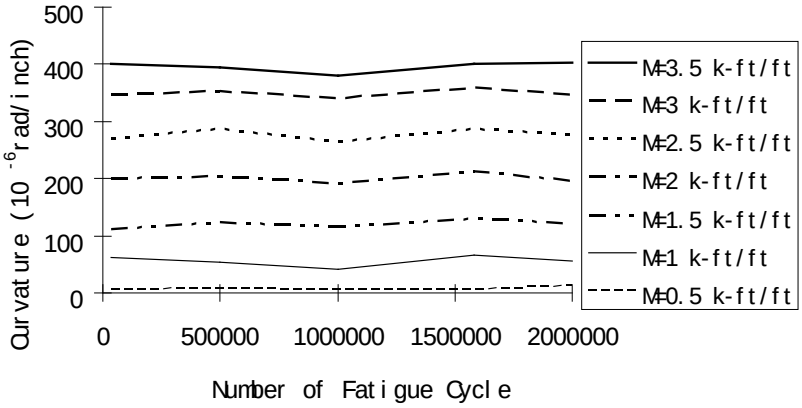

(a) F-F Specimen

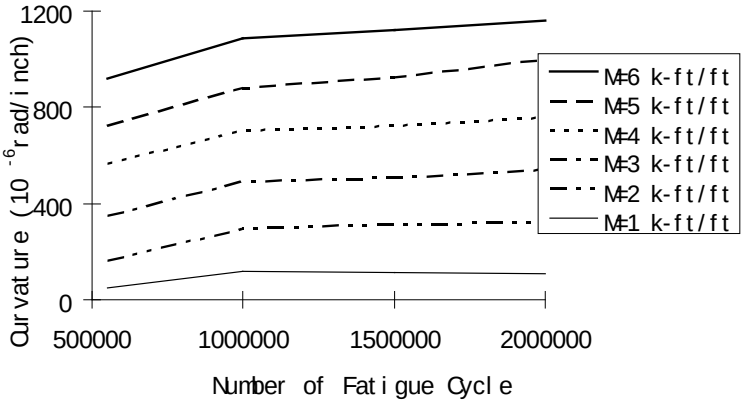

(b) FS-F Specimen under P1

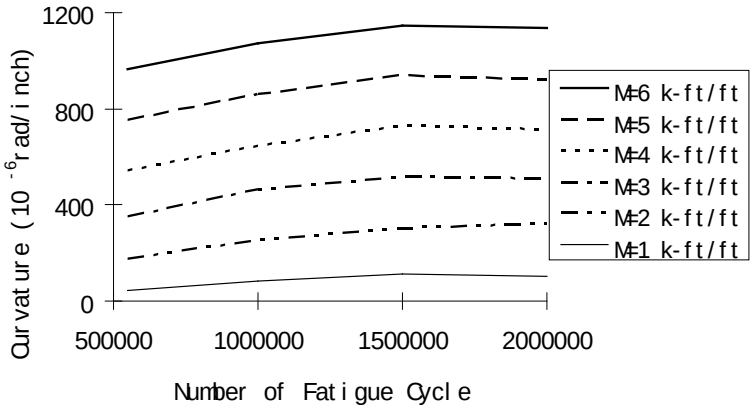

(c) FS-F Specimen under P2

Figure F-3.12. C-N Curve

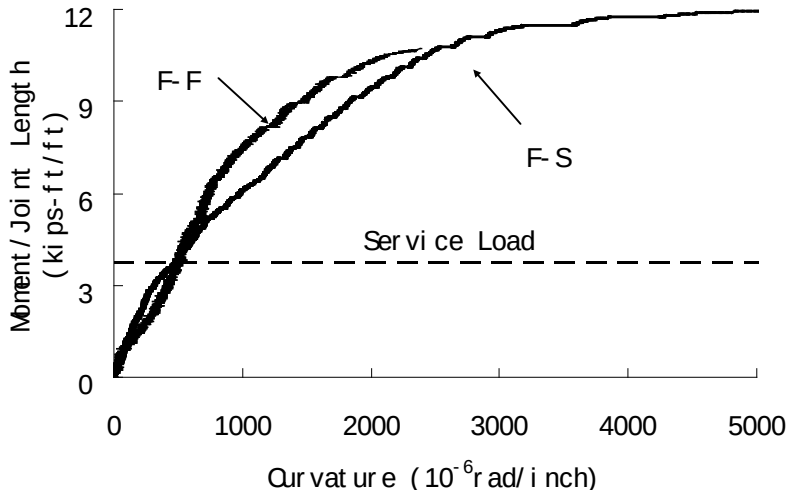

(a) Flexure Tests

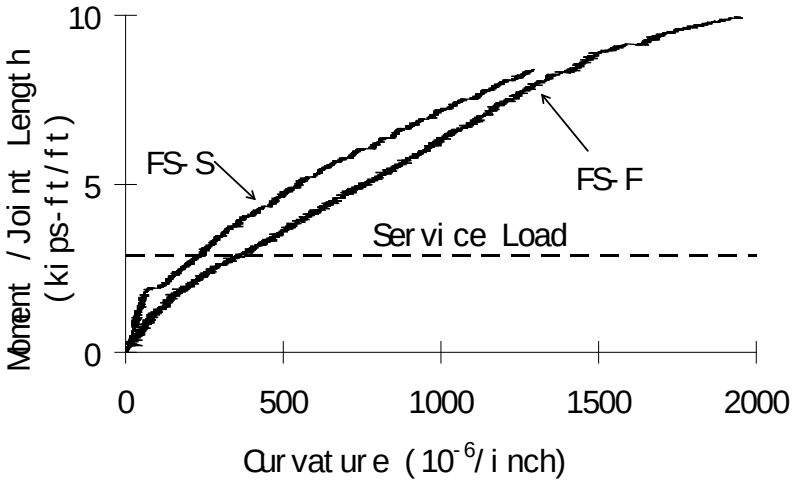

(b) Flexure-Shear Tests

Figure F-3.13. Moment-Curvature Curve

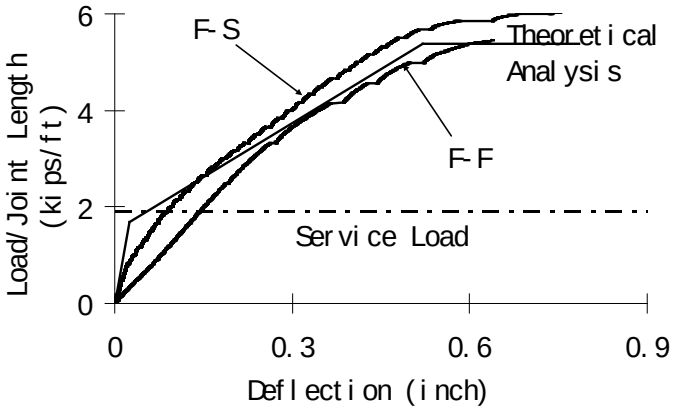

(a) Flexure Tests

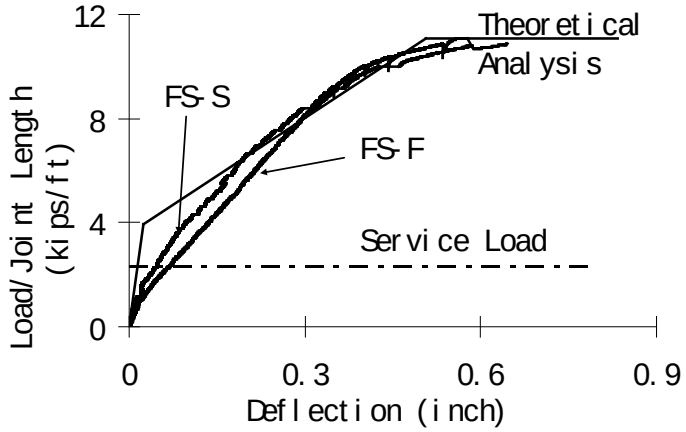

(b) Flexure-Shear Tests

Figure F-3.14. Load-Deflection Curve

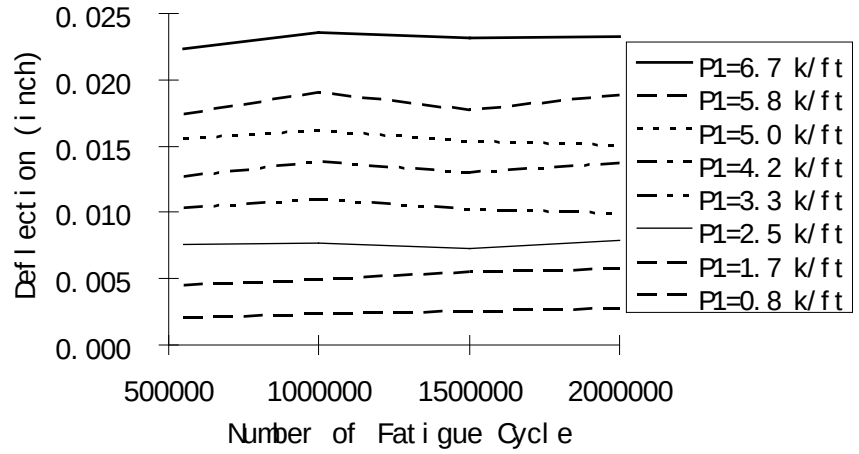

(a) FS-F Specimen under P1

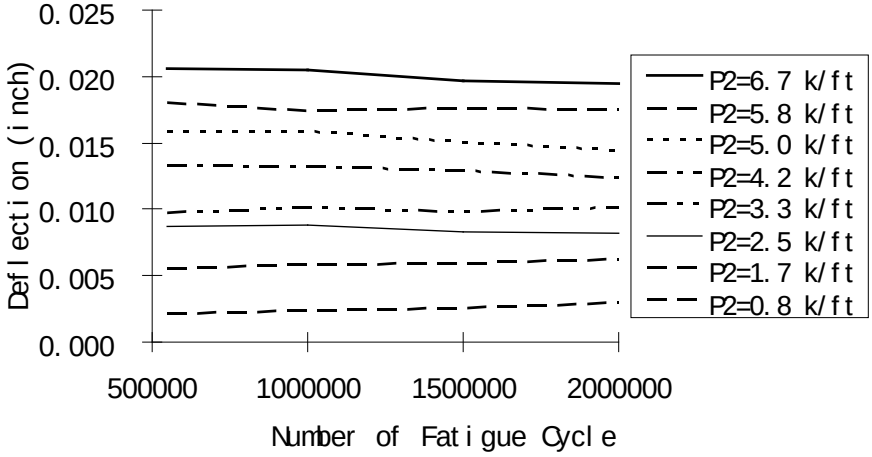

(b) FS-F Specimen under P2

Figure F-3.15. RD-N Curve

Figure F-3.16. Cracks at Interface of the Joint

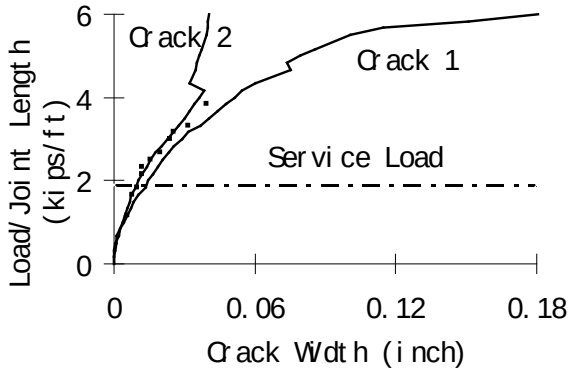

(a) F-S Specimen

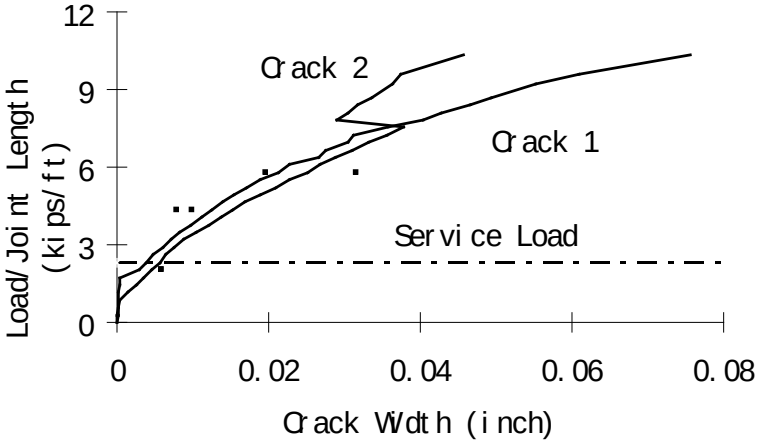

(b) FS-S Specimen

Figure F-3.17. Load-Crack Width Curve

Figure F-3.18. A Flexural-Shear Crack across Joint Zone

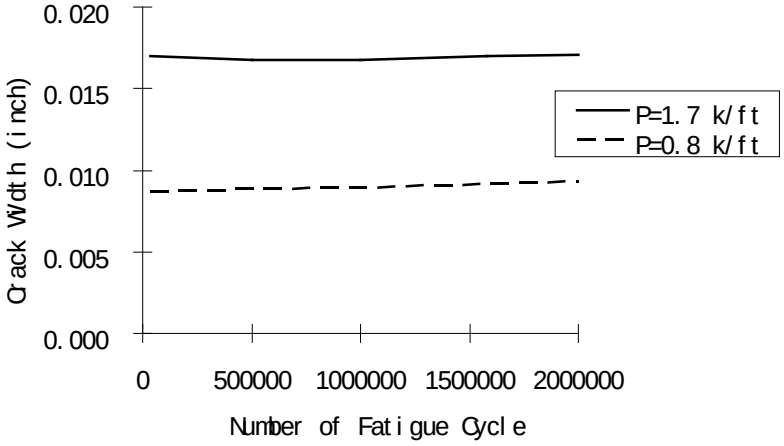

(a) F-F Specimen

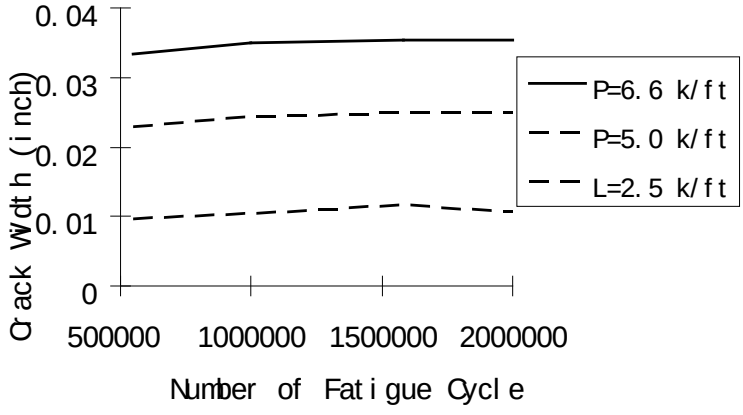

(b) FS-F Specimen

Figure F-3.19: CW-N Curve

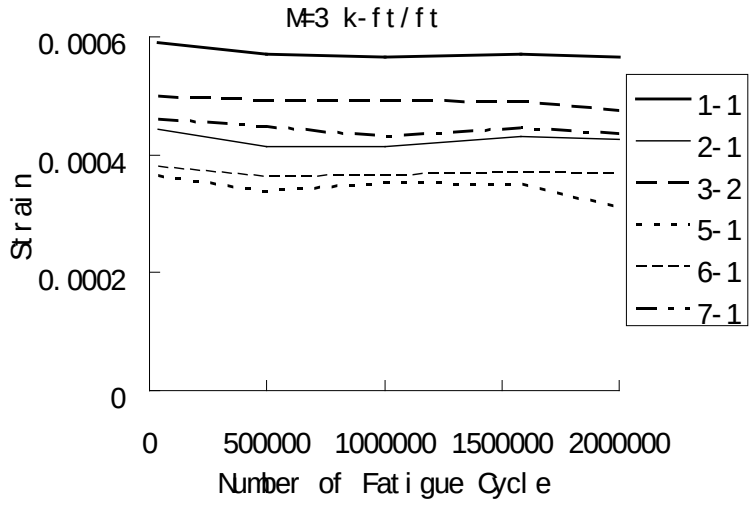

(a) F-F Specimen

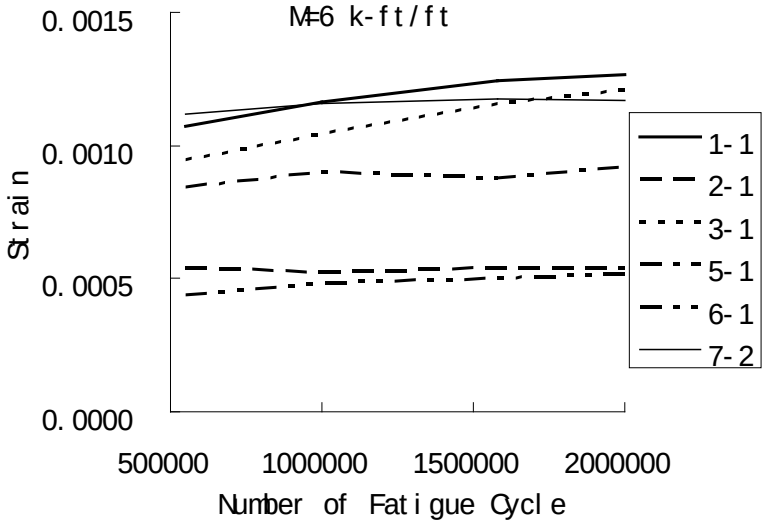

(b) FS-F Specimen

Figure F-3.20. S-N Curve

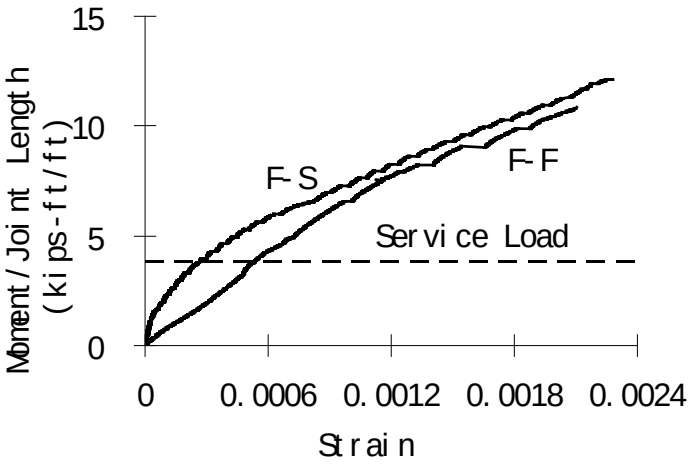

(a) Flexure Tests

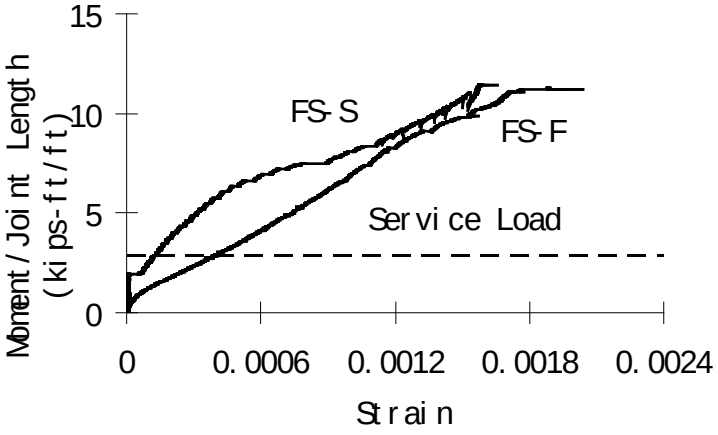

(b) Flexure-Shear Tests

Figure F-3.21: Moment-Strain Curve

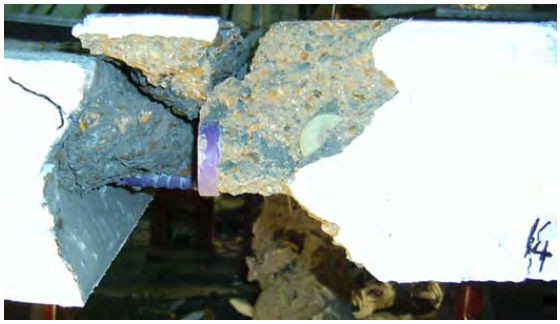

(a) F-S Specimen

(b) FS-S Specimen

(c) F-F Specimen

(d) FS-F Specimen

Figure F-3.22. Specimen Failures

APPENDIX F REFERENCES

AASHTO LRFD (2007). "*Bridge Design Specifications."* Fourth Edition, American Association for State Highway and Transportation Officials, Washington, D.C.

ACI Committee 318 (2005). *Building Code Requirements for Structural Concrete (ACI 318-05)*. Farmington Hills, MI: American Concrete Institute International.

Bentz, E. C., and Collins, M.P. (2000). *Response-2000 Reinforced Concrete Sectional Analysis*. A software downloaded http://www.ecf.utoronto.ca/~bentz/r2k.htm (2006).

Einea, A., Yehia, S. and Tadros, M. K. (1999) "Lap Splices in Confined Concrete" ACI Structural Journal, 96(6), 947-956.

Li, L., Ma, Z., Griffey, M. E., Oesterle, R. G. (2009), "Improved Longitudinal Joint Details in Decked Bulb Tees for Accelerated Bridge Construction: Concept Development," ASCE Journal of Bridge Engineering (companion paper in print).

Li, L., Ma, Z., and Oesterle, R. G. (2009), "Improved Longitudinal Joint Details in Decked Bulb Tees for Accelerated Bridge Construction: Fatigue Evaluation," ASCE Journal of Bridge Engineering (companion paper under review).

Ma, Z. et al (2007), "Field Test and 3D FE Modeling of Decked Bulb-Tee Bridges," ASCE Journal of Bridge Engineering, 12(3), 306-314.

Martin, L.D., and Osborn, A.E.N. (1983), "Connections for Modular Precast Concrete Bridge Decks," Report No. FHWA/RD-82/106, US DOT, Federal Highway Administration

Stanton, J., and Mattock, A.H. (1986) "Load distribution and connection design for precast stemmed multibeam bridge superstructures" NCHRP Rep. 287.

Thompson, M.K., et al. (2006) "Behavior and Capacity of Headed Reinforcement" ACI Structure Journal, 103(4), 522-530.

Zhu, P. and Ma, Z. (2008), “Selection of Closure Pour Materials for CIP Connection of the Precast Bridge Deck Systems,” Proceedings of PCI Concrete Bridge Conference, Orlando, Florida, October.

APPENDIX G

SUBTASK 6.3-C – DESIGN EXAMPLES FOR FUTURE RE-DECKING

Introduction

The objective of Subtask 6.3-C was to demonstrate the design of the interface between deck and girder considering the option of future deck replacement. The interface was designed using the detail discussed in Subtask 6.1-A Full Depth Deck Replacement, which incorporates a debonded joint between the deck and the girder to facilitate deck removal and shear keys with reinforcement for horizontal shear transfer across the interface. The design horizontal shear was based the maximum horizontal shear anticipated for this type of bridge girder as obtained from the parametric studies in Subtask 6.1-B Optimized Girder Study. Two examples are presented. The first considers the optimized section developed in Subtask 6.1-B and the second considers a typical AASHTO type section. These designs demonstrate the maximum reinforcement and shear key geometry required for selected connection details.

Interface Design for Optimized Section

The parametric study conducted on the optimized girder section indicated that the maximum factored horizontal shear stress across the interface between the sub-flange and the upper flange is 186 psi. The purpose of this example is to demonstrate the design of the horizontal shear key under the highest possible interface shear for all feasible bridge configurations using the optimized section. Dimensions of the shear key are shown in Figure G-1. The following steps summarize the design process.

General data:

CIP deck concrete strength	$f'_c = 6000$	psi
Steel yield stress	$f_y = 60$	ksi
ϕ for shear	$\phi_v = 0.9$	
ϕ for bearing	$\phi_b = 0.7$	
Top flange width	$b_v = 42$	in.
Shear key thickness	$t_{sk} = 0.75$	in.

Shear key spacing $s_{sk} = 12$ in.

Factored shear stress $v_{uh} = 186$ psi

Check bearing strength on shear key:

Shear key width $b_{sk} = b_v - 2(2)$

$= 42 - 2(2) = 38$ in.

Bearing strength $v_{nhb} = \dfrac{\phi_b (0.85) f_c' t_{sk} (b_{sk} - t_{sk})}{b_v s_{sk}}$

$= \dfrac{0.7(0.85)(6000)(0.75)(38 - 0.75)}{(42)(12)} = 198$ psi

$v_{nhb} \geq v_{uh}$ OK

Check maximum limit on nominal interface shear resistance:

Maximum resistance $v_{ni} \leq K_1 f_c' \leq K_2$

$K_1 = 0.3$ $K_2 = 1.5$ ksi

$K_1 f_c' = 0.3(6) = 1.8$ ksi $< K_2$

$v_{ni} = K_2 = 1.5$ ksi (acting over the base of the shear key)

Length of shear key $w_{sk} = 0.5 s_{sk} + t_{sk}$

$= 0.5(12) + 0.75 = 6.75$ in

$v_{nhs} = \phi_v \dfrac{v_{ni} b_{sk} w_{sk}}{b_v s_{sk}}$

$= 0.9 \dfrac{(1500)(38)(6.75)}{(42)(12)} = 687$ psi

$v_{nhs} \geq v_{uh}$ OK

Compute required reinforcement:

Required reinforcement $A_{vf,req} = \frac{v_{uh} b_v s_{sk}}{\phi_v f_y}$

$= \frac{(0.186)(42)(12)}{0.9(60)} = 1.74$ in^2/ft

Use 2#5 hairpins at 12 in. spacing as shown in Figure G-2.

$A_{vf,prov} = 4(0.31) = 1.24$ in^2/ft

$< A_{vf,req} = 1.74$ in^2/ft NG

Include reinforcement connecting the sub-flange to the top-flange near the outside tips of the sub-flange (see Figure G-2)

$A_{vf,prov}$ = 4 legs of #5 at 12 in. + 2 legs of #4 at 6 in.

$= 4(0.31) + 2(0.2)(12/6) = 2.04$ in^2/ft

$> A_{vf,req} = 1.74$ in^2/ft OK

It should be noted that the sub-flange is not acting composite with the top flange for transverse bending. However, connecting reinforcement such as shown in Figure G-2 is needed so that the sub-flange can work in parallel with the top-flange for transverse bending moments that put the bottom of the sub-flange in tension. The bars crossing the interface near sub-flange tips will serve as both connecting reinforcement for transverse bending and horizontal shear reinforcement for longitudinal bending.

Interface Design for a Typical AASHTO type section

The purpose of this example is to demonstrate the design of the interface between the two casting stages considering a typical AASHTO type section. Using an AASHTO type section results in a narrow interface between the two casting stages compared to the optimized section developed in this research. For this example, an AASHTO Type II section is considered with top surface width of 12 inches compared to 42 inches for the optimized section used in the example above. Dimensions of the top portion of the section and the shear key are shown in Figure G-3 and G-4. The narrow interface results in high horizontal shear stress demand. Analysis of a bridge with AASHTO Type II section with a span of 74 ft, which is typical for this

section, indicates that the expected horizontal shear stress is 320 psi. In order to accommodate such high shear stress, the shear keys are spaced at a shorter distance than used with the optimized section as shown in Figure G-4. The following steps summarize the design process.

General data:

CIP deck concrete strength	$f_c' = 6000$	psi
Steel yield stress	$f_y = 60$	ksi
ϕ for shear	$\phi_v = 0.9$	
ϕ for bearing	$\phi_b = 0.7$	
Top flange width	$b_v = 12$	in.
Shear key thickness	$t_{sk} = 0.75$	in.
Shear key spacing	$s_{sk} = 6$	in.
Factored shear stress	$v_{uh} = 320$	psi

Check bearing strength on shear key:

Shear key width $b_{sk} = b_v - 2(1)$

$= 12 - 2(1) = 10$ in.

Bearing strength $v_{nhb} = \dfrac{\phi_b (0.85) f_c' t_{sk} (b_{sk} - t_{sk})}{b_v s_{sk}}$

$= \dfrac{0.7(0.85)(6000)(0.75)(10 - 0.75)}{(12)(6)} = 344$ psi

$v_{nhb} \geq v_{uh}$ OK

Check maximum limit on nominal interface shear resistance:

Maximum resistance $v_{ni} \leq K_1 f_c' \leq K_2$

$K_1 = 0.3$ $K_2 = 1.5$ ksi

$K_1 f_c' = 0.3(6) = 1.8$ ksi $< K_2$

$v_{ni} = K_2 = 1.5$ ksi (acting over the base of the shear key)

Length of shear key $w_{sk} = 0.5s_{sk} + t_{sk}$

$= 0.5(6) + 0.75 = 3.75$ in

$$v_{nhs} = \phi_v \frac{v_{ni} b_{sk} w_{sk}}{b_v s_{sk}}$$

$$= 0.9 \frac{(1500)(10)(3.75)}{(12)(6)} = 703 \text{ psi}$$

$v_{nhs} \geq v_{uh}$ OK

Compute required reinforcement:

Required reinforcement $A_{vf,req} = \frac{v_{uh} b_v s_{sk}}{\phi_v f_y}$

$$= \frac{(0.320)(12)(6)}{0.9(60)} = 0.43 \quad \text{in}^2\text{/shear key}$$

Use 1#5 hairpin at each shear key as shown in Figure G-4.

$A_{vf,prov} = 2(0.31) = 0.62$ in^2

$> A_{vf,req} = 0.43$ in^2 OK

This example demonstrates that common AASHTO type sections can be used for decked girders incorporating details for future deck replacement with adequate horizontal shear transfer between the two casting stages.

Conclusions

The examples presented in this study demonstrate that the proposed details for facilitating future deck replacement are adequate for horizontal shear transfer across the interface between the two casting stages. For the optimized section, reinforcement connecting the sub-flange to the top-flange near the outside tips of the sub-flange can be considered as horizontal shear reinforcement if needed. For AASHTO Type II section with narrow top surface, smaller spacing between the shear keys is required

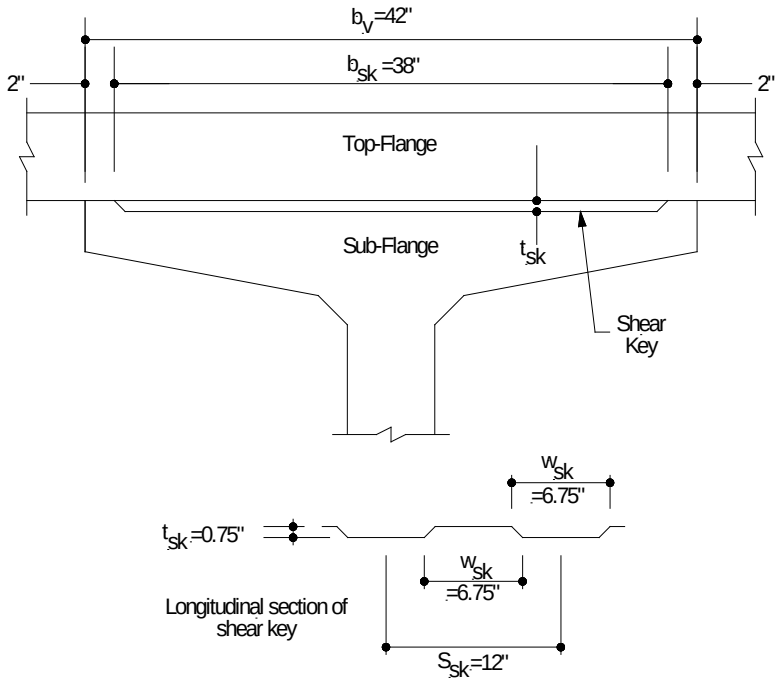

Figure G-1. Shear Key Dimensions for Optimized Section.

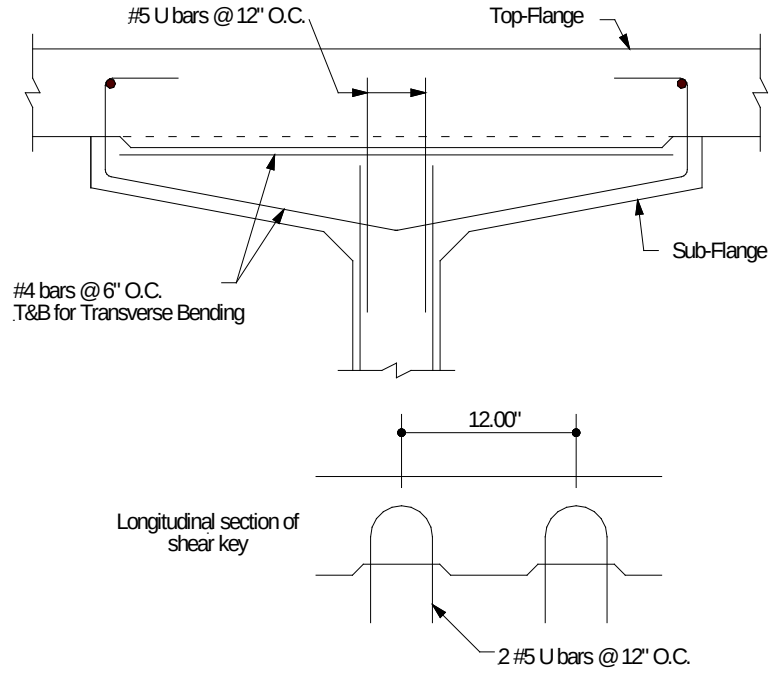

Figure G-2. Horizontal Shear Reinforcement for Optimized Section.

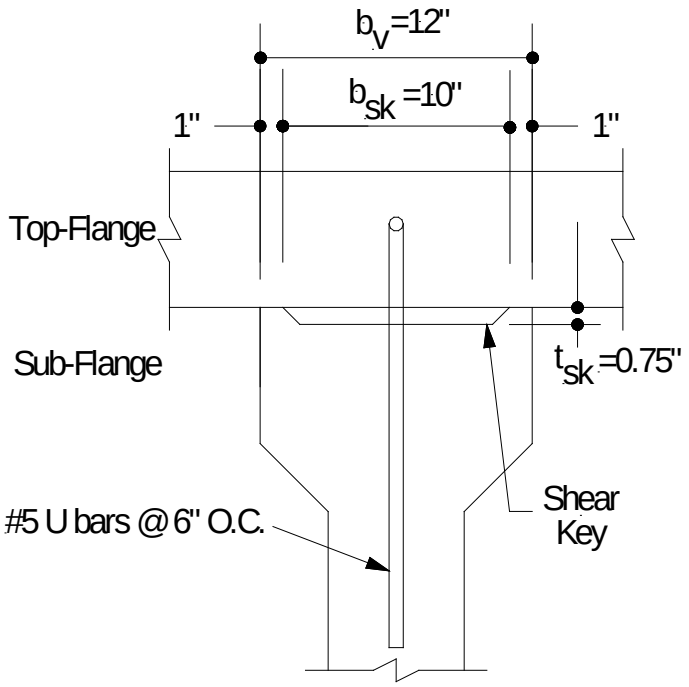

Figure G-3. Shear Key Dimensions for AASHTO Type II Section.

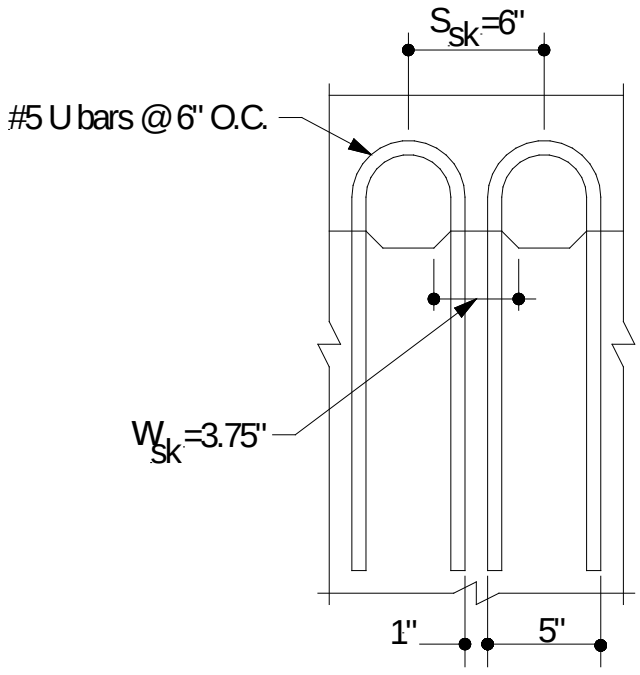

Figure G-4. Horizontal Shear Reinforcement for AASHTO Type II Section.